Human induced pluripotent stem cell-derived cardiomyocytes (hiPSC-CMs) for studying the role of MAP4K4 kinase in cell death

Evie Maifoshie

Imperial College London
National Heart and Lung Institute

A Thesis submitted to
Imperial College London for the degree of PhD

Imperial College London

National Heart and Lung Institute

Word count: 86537

Acknowledgements

This part is for special thanks for very special people, who have been there for me, academically or intimately. Firstly, I would like to express my gratitude to Michael for his efforts in fostering my scientific growth. Sian Harding, I am so grateful for the mental encouragement in every step of the PhD – you are a mother figure! Vania Braga thank you for your advice on experiments and a huge hug and thanks to Lorna Fiedler for her constant advice and mental support – and sorry for the nagging, especially on how to calculate the molarity of a drug. I would like to acknowledge current and past members of the lab for their help throughout the years, specifically Farah Al Beidh, Nasret Harun (my bench buddy), and Michela Noseda. Emma Watson, thank you for being a real person and for your understanding! Last but not least, Martin Spitaler (my Definiens guru) thank you for the timeless discussions/help on image analysis and your enthusiasm, you were like a supervisor to me! Finally, I would like to thank the MRC for the studentship, which made this project possible. I am so grateful I had the chance to pick the brains of so many scientists who have had the patience and time to communicate their ideas and help me develop my skills: Eric Lam, Nigel Gooderham, Veronica Buckle, Francisco Iborra, Alan Clarke and many more to come.

The academic community is small, but I feel very blessed to be surrounded by a significant ($p<0.000001$) number of family and friends. The biggest thanks will go to my cognate family; Mom and Dad you are the best parents in the world and I am so grateful for every sacrifice you made to ensure I receive the best education and reach my potential. I thank you for the endless support and wisdom, which has been conceived as stubbornness throughout the years (Sorry!). I know that we will always argue about our ancestors (Adam and Eve *versus* apes), but I love you and I dedicate the thesis to you!

My very special love and thanks to you: Annie (πουλλίν μου!), my oldest and dearest friend we have been through so much together that I do not know where to start, Maro Pavli (Loubi, Biki, sitaki etc) for putting me under your wings (ξέρεις εσύ...) and for all the fun (especially the hangovers) we had in Cardiff; Evi Goggolidou for all the fun and encouragement; Dimitris Moutaftsis (το καλύτερο Σάμισι στον κόσμο) for all the silly times, sleepovers with Cypriot chickens; Alexandros Floros for your love (even though sometimes είσαι για ξύλο), for learning how to cook for me and for picking me up from the bus stop after all these late nights I had to spend in the lab; Paul Benton (Paulino mou!) for the great scientific and weird non-scientific discussions in a wonderful flat mate and friendship-share I have ever had (which will continue in California one day); Thomas Leja for the abundant overanalytical scientific discussions/teasing and for being that awkward friend version that everyone loves; Vassilako for the games and fun in Leighton Buzzard with the best mom and dad (Dina Spagou and Charis Pavlidis); Estitxu (Angele mou!) for being there (in the gym…) for me;

Sarah(moulini) for your support (I always miss you); and last but not least, my London family (Lea, Magali, Claire, Renaud, Kathy, Matt, Pechlivanis, Sno, Gabrielle, Abdullah, Maria, Michalis, Vorkas, Anita, Florian, Jen and Jessica) for always looking into new ways to boost the economy together! Wherever you are, and no matter how busy our lives will be, I know that we will meet in weddings! I feel so lucky that throughout my academic life I have met wonderful people who left a big-foot-print. Thank you to everyone for carrying me!

Acknowledgements for resources

Images at Fig. 12C were kindly provided with permission by Peter O'Gara, Sian E Handing and Anita L. Alvarez.

Permission from the authors and publishers was acquired for all the images in the Introduction.

Declaration of Originality

This is to certify that to the best of my knowledge, the content of this thesis is my own work. This thesis has not been submitted for any degree or other purposes. I certify that the intellectual content of this thesis is the product of my own work and that all the assistance received in preparing this thesis and sources have been acknowledged.

Evie Maifoshie

Copyright Declaration

‘The copyright of this thesis rests with the author and is made available under a Creative Commons Attribution Non-Commercial No Derivatives licence. Researchers are free to copy, distribute or transmit the thesis on the condition that they attribute it, that they do not use it for commercial purposes and that they do not alter, transform or build upon it. For any reuse or redistribution, researchers must make clear to others the licence terms of this work’

Table of Contents

Acknowledgements **3**

List of Figures **13**

List of Tables **15**

List of Abbreviations **16**

Abstract **22**

1. Introduction **24**

1.1. Heart failure: the socio-economic problem **25**

1.2. Pathobiology of heart failure: a multifaceted problem **28**

1.3. Cell death signalling pathways **32**

1.3.1. Apoptosis 32
1.3.2. Necrosis 37
1.3.2.1. mPTP-dependent necrosis 37
1.3.2.2. Death receptor-dependent necrosis 38
1.3.3. Autophagy 41
1.3.4. Concluding remarks 44

1.4. Endoplasmic reticulum (ER): a link between apoptosis and necrosis **45**

1.4.1. ER stress and UPR signalling 46
1.4.2. ER stress in cardiovascular disease 49
1.4.3. Concluding remarks 50

1.5. Cell death in myocardial infarction and heart failure **51**

1.5.1. Apoptosis in myocardial infarction and heart failure 52
1.5.2. Necrosis in myocardial infarction and heart failure 55
1.5.3. Autophagy in myocardial infarction and heart failure 56
1.5.4. Concluding remarks 57

1.6. The protein kinase complement of the human genome **62**

1.6.1. Classification and mode of action 62
1.6.2. Structure 65
1.6.3. Pharmacological targeting of proteins kinases for the treatment of CVD 67
1.6.4. Mitogen-activated protein kinases (MAPKs) 69
1.6.4.1. ERK1/2 71
1.6.4.2. JNK 71
1.6.4.3. p38 kinase 72

1.6.4.4. ERK5 73
1.6.5. MAPKs in heart function and disease 75
1.6.6. MAPKs in cardiac hypertrophy, chronic heart failure and post-ischaemic remodelling 76
1.6.5.1. ERK1/2 pathway 77
1.6.5.2. JNK pathway 80
1.6.5.3. p38 pathway 82
1.6.7. MAPKs in cardioprotection and myocardial cell death 85
1.6.7.1. ERK1/2 pathway 85
1.6.7.2. JNK pathway 86
1.6.7.3. p38 pathway 88
1.6.7.4. Concluding remarks 90
1.6.8. Protein kinases in cardiac hypertrophy and cell death 91
1.6.8.1. The AGC kinase family of PKC isoforms, PKA and ROCK1 91
1.6.8.2. The Calmodulin/Calcium regulated kinase (CAMK) family 97
1.6.8.3. MAP3K Kinase family 101
1.6.9 Concluding remarks 103
1.7. MAP4K4 and TAK1: "associates" in failing hearts 104
1.8. Induced pluripotent stem cells (iPSCs) and High Content Screening: Novel tools for understanding human pathobiology 107
1.8.1. Differentiation and characterization technologies for ESCs- and iPSCs-derived cardiomyocytes 108
1.8.2. ESCs- and iPSCs-derived cardiomyocytes in disease modelling 110
1.9. The driving forces of High Content Screening: multiplexing and RNAi 113
1.10. The Aim 116
1.10.1. Characterization efforts of hiPSC-CMs from CDI and others 116
1.10.2. Screening shRNAmir constructs for efficient MAP4K4 knockdown in a heterologous system and in hiPSC-CMs 116
1.10.3. Optimize cell death conditions with H_2O_2 ad c_2-ceramide in hiPSC-CMs and deplete MAP4K4 by RNAi 117
2. Materials and Methods 118
2.1. Bacterial culture and DNA purification 119
2.2. Cell culture 121
2.2.1. General procedure 121
2.2.2. Maintenance of HEK293 and HeLa cell lines 121
2.2.3. General culture of hiPSC-CMs 121
2.2.4. Preparing cell culture surfaces 122
2.2.5. Thawing hiPSC-CMs 122

2.2.6. Plating hiPSC-CMs 122
2.2.7. Maintenance of hiPSC-CMs 124
2.3. Cell Death induction with H_20_2 and c_2-ceramide 124
2.4. Transfection 124
2.5. Virus production and titration 125
2.5.1. Cell transfection with lentiviral vectors and virus collection 125
2.5.2. Concentration of viruses with high-speed ultracentrifugation 126
2.5.3. Virus titration 126
2.5.4. Virus transduction of hiPSC-CMs 127
2.6. Immunocytostaining 127
2.7. Proliferation assay 129
2.8. RNA isolation and cDNA synthesis 129
2.9. Quantitative PCR 130
2.10. Fluorescence-Associated Cell Sorting (FACS) 131
2.10.1. Cell Preparation, FACS and collection 131
2.10.2. Cytometer parameters (calibration and gating) 131
2.11. Protein extraction and quantification 131
2.12. Western blotting 132
2.12.1. Preparation of polyacrylamide gels and samples 132
2.12.2. Electrotransfer, blocking and incubating with antibodies 133
2.13. Protein Immunoprecipitation (IP) 133
2.14. Kinase assay 134
2.15. Cell-based assays 135
2.15.1. Lactate Dehydrogenase (LDH) assay 135
2.15.2. Colorimetric aaspase-3 / aaspase-8 assay 135
2.16. Cytotoxicity high-content assays 137
2.16.1. NucView™488 / DRAQ7 137
2.16.2. AnnexinV / DRAQ7 137
2.16.3. Mitochondrial potential assay 137
2.16.4. Fluorescence and high-content microscopy 138
2.17. Bioinformatics analysis 139
2.17.1. High-content image analysis 139
2.17.2. Customized high-content image analysis 139
2.17.3. Statistical analysis 139
3. Results 141
3.1. Characterization of hiPSC-CMs 142
3.1.1. Purity of hiPSC-CMs 142

3.1.2. HiPSC-CMs are refractory to serum-induced proliferation 148
3.1.3. HiPSC-CMs express MAP4K4 mRNA and protein 152
3.1.4. Summary 156
3.2. Screening shRNAmir constructs for efficient MAP4K4 knockdown 157
3.2.1. MAP4K4 knockdown in a heterologous doxycycline-inducible system 157
3.2.2. MAP4K4 knockdown in a heterologous system with a co-transfection strategy 163
3.2.3. MAP4K4 knockdown in hiPSC-CMs 169
3.2.4. Summary 172
3.3. MAP4K4 knockdown in hiPSC-CMs followed by H_2O_2 173
3.3.1. Optimization of cell culture in High-glucose transition medium 173
3.3.2. MAP4K4 knockdown followed by H_2O_2 treatment in HGTM 182
3.3.3. Optimization of cell culture of hiPSC-CMs in LGTM 187
3.3.4. Optimization of H_2O_2 dose in LGTM 191
3.3.5. MAP4K4 knockdown followed by H_2O_2 treatment in LGTM 195
3.3.4. Summary 203
3.4. MAP4K4 knockdown followed by c_2-ceramide conditions 204
3.4.1. Optimization of cell death conditions with c_2-ceramide 204
3.4.2. MAP4K4 knockdown in response to c_2-ceramide 206
3.4.3. Summary 214
4. Discussion and Further Work 215
4.1. Synopsis of key findings 216
4.2. Mechanistic implications 219
4.2.1. H_2O_2 does not activate caspase-3 in hiPSC-CMs 219
4.2.2. MAP4K4 knockdown in hiPSC-CMs is associated with caspase-8 activation in H_2O_2 ... 220
4.2.3. c_2-ceramide activates caspase-3 in hiPSC-CMs 223
4.2.4. MAP4K4 and the mitochondrial death pathway 223
4.3. Technical considerations 227
4.3.1. Dissecting cell death in hiPSC-CMs: considerations for platform refinement 227
4.3.2. Potency and specificity of RNA interference against MAP4K4 228
4.3.3. Suitability of the innocuous vector control 229
4.3.4. Fidelity of hiPSC-CMs: evidence for heterogeneity and immaturity 230
4.4. Further work 233
4.4.1. Unaddressed questions about the MAP4K4/TAK1 signalling axis 233
4.4.2. Pharmacological inhibitors of MAP4K4 or RNAi as a therapeutic strategy 235
4.4.3. Downstream effectors of MAP4K4-dependent signaling 236

4.4.4. Upstream mediators of MAP4K4-dependent signaling 237
4.4.5. Cardiac cell death: critical gaps and further work 239
5. References 241
6. Appendix 282
6.1. Supplementary Material and Methods 283
6.2. Supplementary Figures 286

List of Figures

Figure 1: Cardiovascular diseases statistics.

Figure 2: Heart failure on the rise.

Figure 3: Strategies to increase cardiac muscle cell number.

Figure 4: Illustration of the intrinsic and extrinsic signalling branches of apoptosis.

Figure 5: Schematic illustration of the molecular events of the two signaling pathways leading to necrosis upon cardiac I/R injury.

Figure 6: The different stages of autophagy from initiation, elongation, maturation, and finally lysosome fusion.

Figure 7: ER stress-mediated signal transduction

Figure 8: Dendogram of the seven protein kinase families grouped based on protein sequence homology.

Figure 9: Schematic representation of signal transduction pathways by various kinases.

Figure 10: Schematic representation of the pGIPZ lentiviral shRNAmir vector.

Figure 11: Schematic of cell death assays.

Figure 12: Characterization and purity of the hiPSC-CMs.

Figure 13: Highly prevalent expression of TNNT2 and PLN in hiPSC-CMs.

Figure 14: Heterogeneous hiPSC-CMs comprise a cell mixture of different developmental origins and stages.

Figure 15: hiPSC-CMs are refractory to serum-induced proliferation determined by a multiplex assay of EdU and phospho-H3.

Figure 16: Testing the specificity of the MAP4K4 antibodies in MAP4K4-LF and -SF protein lysates.

Figure 17: hiPSC-CMs express MAP4K4 RNA and protein.

Figure 18: Screening for potent shRNAmir constructs against TAK1.

Figure 19: Screening for potent shRNAmir constructs against MAP4K4.

Figure 20: Investigating potency of shRNAmirs against MAP4K4 in HEK293T^{Dox} cells.

Figure 21: Investigating potency of shRNAmirs on protein levels with a co-transfection strategy system without FACS.

Figure 22: Investigating the potency of shRNAmir constructs with a co-transfection strategy in HEK293T using FACS.

Figure 23: Immunoprecipitation of MAP4K4 from EGFP^{+} and crude lysates to validate protein knockdown by the various shRNAmirs.

Figure 24: Promoter competition effect with the co-transfection strategy.

Figure 25: Titration of viruses on HeLa cells.

Figure 26: Investigating various MOIs for significant MAP4K4 knockdown in hiPSC-CMs.

Figure 27: Time-dependent dose-response of H_2O_2 in hiPSC-CMs.

Figure 28: No Caspase-3 activity was detectable in response to various concentrations of H_2O_2 in hiPSC-CMs.

Figure 29: Caspase-8 activity decreases with increasing H_2O_2 concentration in hiPSC-CMs.

Figure 30: Cytotoxicity measured by LDH assay under H_2O_2 conditions in 0.5% and 2% HGTM.

Figure 31: No caspase-3 activation in response to H_2O_2 in 0.5% or 2%HGTM.

Figure 32: Diminished mitochondrial potential with H_2O_2 in 0.5% or 2%HGTM in hiPSC-CMs.

Figure 33: Schematic timeline of hiPSC-CMs from thawing to screening for cell death.

Figure 34: Cardiac purity of the hiPSC-CMs system under H_2O_2.

Figure 35: DRAQ7 assay of MAP4K4-depleted hiPSC-CMs in the presence of H_2O_2.

Figure 36: Annexin V/DRAQ7 assay to assess cytotoxicity of hiPSC-CMs in LGTM for 4 days.

Figure 37: Cell death assessment of hiPSC-CMs in LGTM with various serum concentrations.

Figure 38: Time-dependent dose-response curve of H_2O_2 in hiPSC-CMs in LGTM.

Figure 39: Caspase-3 was not activated in hiPSC-CMs in response to H_2O_2.

Figure 40: H_2O_2 mediates cell death hiPSC-CMs via the mitochondria.

Figure 41: Cardiac purity of the MAP4K4 knockdown screen in H_2O and H_2O_2 cultures.

Figure 42: MAP4K4 knockdown salvages hiPSC-CMs from cell death.

Figure 43: Images from the DRAQ7 assay.

Figure 44: MAP4K4 knockdown inhibits cell death independent of caspase-3 activation.

Figure 45: MAP4K4 knockdown inhibits mitochondrial potential dissipation in hiPSC-CMs.

Figure 46: MAP4K4 knockdown with sRNAmirs constructs validated by qPCR.

Figure 47: hiPSC-CMs exhibit caspase-3 activation in response to c_2-ceramide at 16h.

Figure 48: Schematic timeline of hiPSC-CMs from thawing to screening with c_2-ceramide.

Figure 49: Cardiac purity of the hiPSC-CMs is high under both treated and untreated conditions and times.

Figure 50: Cell death assessment by DRAQ7 uptake of MAP4K4-depleted hiPSC-CMs under c_2-ceramide conditions at 16h and 36h.

Figure 51: LDH release in MAP4K4-depleted and c_2-ceramide-treated hiPSC-CMs.

Figure 52: Mitochondrial membrane potential of MAP4K4-depleted hiPSC-CMs under c_2-ceramide conditions at 16h and 36h.
Figure 53: Caspase-3 activity is reduced in MAP4K4-depleted hiPSC-CMs in c_2-ceramide-treated conditions.
Figure 54: MAP4K4 signalling axis cartoon with H_2O_2 and c_2-ceramide in hiPSC-CMs.
Figure S1: Health care costs of CHD in Europe and UK.
Figure S2: Strategy for purification of $EGFP^H$ and $EGFP^L$ populations by FACS.
Figure S3: MAP4K4 isoforms.
Figure S4: Sequence alignment of shRNAmirs with the MAP4K4 isoforms.
Figure S5: Caspase-3 activation is not a late event in response to H_2O_2 in hiPSC-CMs.
Figure S6: Algorithm for microscopy-based assays detects both apoptotic and healthy nuclei.
Figure S7: Representative image for diminished mitochondrial potential in the positive control.
Figure S8: Mitochondria of hiPSC-CMs exhibit mitochondria fission with c_2-ceramide.

List of Tables

Table 1: Genetic models implicating cell death regulator genes in cardiac cell death
Table 2: Drug development for kinase targets in cardiovascular disease
Table 3: pGIPZ shRNAmir sequences
Table 4: Terminology and equations for plating hiPSC-CMs
Table 6: qPCR primers
Table 5: Reagents for Immunocytostaining

List of Abbreviations

α-AR, α-adrenergic receptors

αMHC, alpha myosin heavy chain

ACE, angiotensin-converting enzyme

ACTC1, cardiac actin alpha

AIDS, Acquired Immune Deficiency Syndrome

AIF, Apoptosis Inducing Factor

Akt1/2, V-Akt Murine Thymoma Viral Oncogene Homolog or Protein Kinase B

AMPK, AMP-activated protein kinase

ANF, Natriuretic Peptide/Factor

ANT, Adenine Nucleotide Translocator

ARC, Apoptosis Repressor protein with a CARD domain

ARs, adrenergic receptors

AS160, Akt Substrate 160

ASK1, apoptosis signal-regulating kinase 1

ATF4/6, Activating Transcription Factor 4/6

Atg, Autophagy related

ATP, adenosine triphosphate

β-AR, β-adrenergic receptors

βMHC, β myosin heavy chain

BMP, bone morphogenic proteins

c-FLIP, FLICE-(FADD-Like IL-1β-converting enzyme)

c-raf, v-raf-1 murine leukaemia viral oncogene homolog

C2C, c_2-ceramide

Ca^{2+}, calcium

CaMKII, Ca2+/calmodulin-dependent protein kinase II

Caspases, cysteine-dependent aspartate-specific proteases

CASQ, calsequestrin

Cdk9, Cyclin-dependent kinase 9

CGH, Comparative Genomic Hybridization

CHD, coronary heart disease

ChIP, chromatin immunoprecipitation

Chk1, Checkpoint kinase 1

Chk2, Checkpoint kinase 2

CHOP, CCAAT/enhancer-binding homologous protein

CK1, casein kinase 1

CMV, cytomegalovirus

Cn, calcineurin

COPD, chronic obstructive pulmonary disease

CREB, cAMP-responsive element binding protein

CsA, cyclosporine A

CVD, cardiovascular disease

CYLD, cylindromatosis D

CypD, Cyclophilin D

Cyt-c, Cytochrome c

d, day or days

DCM, dilated cardiomyopathy

DISC, Death Inducing Signalling Complex

DOX, doxorubicin

Drp1, dynamin-related protein 1

E, embryonic day

EdU, 5'-ethynyl-2'-deoxyuridine

EGF, epidermal growth factor

EGFP, Enhanced Green Fluorescent Protein

elF2a, elongation factor 2a

EndoG, Endonuclease G

Epac, Exchange protein directly activated by cAMP

ER, Endoplasmic Reticulum

ERK1/2 (or MAPK3), Extracellular Signal-Related Kinase 1

ERK5 (or MAPK7), Extracellular Signal-Regulated Kinase 5

ET-1, endothelin-1

FACS, Fluorescence-activated cell sorting

FADD, Fas (TNFRSF6)-associated via Death Domain

FasL (or CD95), Fas Ligand

FGF-2, fibroblast growth factor-2

FGF-β, fibroblast growth factor-β

Fis1, Fission protein 1

FISH, Fluorescence *in situ* hybridization

Fz, Frizzled

GATA4, GATA binding protein 4

GCK, Germinal centre kinase

gp130, glycoprotein 130

GLUT4, Glucose transporter type 4

GPCRs, G-protein-coupled receptors

Grk2, G-protein-coupled-receptor kinase 2

Grp78, G-Protein Coupled Receptor 78

GSK-3a, Glycogen Synthase Kinase 3 alpha

GSK-3b, Glycogen Synthase Kinase 3 beta

HCM, hypertrophic cardiomyopathy

HCS, High Content Screening

HDAC, histone deacetylase

hESC-CMs, human embryonic stem cells-derived cardiomyocytes

hESCs, human embryonic stem cells

HF, heart failure

HGK, hepatocyte progenitor kinase-like/germinal centre kinase-like kinase

Hsc70, heat shock cognate 70

Hsp20, Heat shock protein 20

HT, High-Throughput

I/R, Ischaemia/Reperfusion

IAP, Inhibitor of Apoptosis

IGF-I, insulin-like growth factor

IKK, IκB kinase

IP3R, 1,4,5-triphospahte receptor

HiPSC-CMs, human induced pluripotent stem cell-derived cardiomyocytes

iPSCs, induced-pluripotent stem cells

Ire1, Inositol-Requiring 1

IRS-1, Insulin Receptor Substrate-1

JAK, Janus kinase

JNK, Jun N-terminal kinase

KO, knockout

LDH, lactase dehydrogenase

LF, Long isoform (of MAP4K4)

LOF, loss-of-function

LTCC, L-type Ca2+ channel

LV, left ventricle or ventricular

LVAD, Left Ventricular Assisted Devices

MAP2K, mitogen-activated protein kinase kinase

MAP3K, mitogen-activated protein kinase kinase kinase

MAP4K, mitogen-activated protein kinase kinase kinase kinase

MAP4K4, HGK/GCK-like kinase, Nck-interacting kinase

MAPK, mitogen-activated protein kinase

MAPK(s), mitogen-activated protein kinase(s)

MCK, Muscle Creatine Kinase

MEF2c, Myocyte Enhancer Factor 2c

MEFs, Mouse Embryonic Fibroblasts

MEK (or MKK), MAPK kinase

MEKK (or MAPKKK), MAPK kinase kinase

MF20, α, β sarcomeric myosin heavy chain

MI, Myocardial Infarction

MINK, mishappen-like kinase 1

MKP, Mitogen-Activated Protein Kinase Phosphatase

MLC2v, Myosin, Light Chain 2 (or Cardiac Ventricular Myosin Light Chain 2)

MLK2/3, mixed lineage kinase 2/3

MnSOD, manganese superoxide dismutase

mPTP, mitochondrial Permeability Transition Pore

mRNA, messenger RNA

MS, Mass Spectrometry

MST2, mammalian sterile 20-like kinase

mTOR, mechanistic target of rapamycin

Myf5, Myogenic factor 5

Myh6, αMHC

MYL2, regulatory light chain 2, ventricular cardiac muscle isoform

MYL7, regulatory light chain 2, atrial cardiac muscle isoform

NA, not applicable

Nec-1, necrostatin-1

NES, Nuclear Export Signal

NFAT, Nuclear Factor Of Activated T-Cells

NFκB, Nuclear Factor κ light-chain enhancer of activated B cells

NGF, nerve growth factor

NLS, Nuclear Localization Signal

NRVCs, neonatal rat ventricular cardiomyocytes

p38, MAPK14

P53 (or TP53), tumour protein p53

PARP-1, poly(ADP-ribose) polymerase-1

PAS, pre-autophagosome

PCD, Programmed Cell Death

PCI, percutaneous coronary intervention(s)

PCSK9, proprotein convertase subtilisin/kexin type 9

PDGF, platelet-derived growth factor

PDGFR, platelet-derived growth factor receptor

PE, phenylephrine

PERK, PKR-like ER kinase

PGC1α, Peroxisome proliferator-activated receptor gamma coactivator 1α

PI, Propidium iodide

PI3K, phosphatidylinositide-4,5-bisphosphate 3-kinase

PKC, protein kinase C

PKG, cGMP-dependent protein kinase

PLN, Phospholamban

PLC, phospholipase C

PPARγ, Peroxisome-Proliferator Activated Receptor γ

PTEN, Phosphatase and TENsin homolog

RIP1 (or RIPK1), Receptor Interacting Protein 1 serine/threonine kinase

RIP3 (or RIPK3), Receptor Interacting Protein 3 serine/threonine kinase

RISK, Reperfusion Injury Salvage Kinase

RNAi, RNA interference

ROCK, Rho-associated kinase

ROS, Reactive Oxygen Species

RT, Room temperature

RyR2, ryanodine receptor 2

SAPK(s), stress-activated protein kinase(s)

SH, short isoform (of MAP4K4)

shRNA, short-hairpin RNA

TAB, TAK1-binding protein

TAC, Transverse Aortic Constriction

TAK1 (or MAP3K7), TGFβ-activated kinase-1

TFG-β, transforming growth factor-β

TG, thapsigargin

TKL, tyrosine kinase-like

TKs, tyrosine kinases

TMRE, potentiometric mitochondrial dye

TNFα, Tumour Necrosis Factor α

TNFR, TNF Receptor

TNNI3, cardiac troponin I

TNNT2, cardiac Troponin T (or Troponin T2)

TNIK, NCK-interacting protein kinase

TRADD (or TNFRSF1A), TNF Receptor superfamily 1A-associated via Death Domain

TRAF, TNF receptor-associated factor

TUNEL, Terminal Uridine Nick-End Labeling

UPR, Unfolded Protein Response

UV, ultraviolet

VDAC, Voltage-dependent Anion Channel

VEGF, vascular endothelial growth factor

VPS34, Vacuolar Protein Sorting gene34

WT, wild type

XBP-1, X-box binding protein-1

XIAP, X-linked IAP

ΔΨm, mitochondrial action potential

Abstract

Kinases comprise universal signalling cascades potentially pivotal to cardiac cell death pathways. Cell death is divided into several modes, chiefly apoptosis and necrosis. Both contribute to the pathophysiology of heart disease, with overlapping signalling pathways of caspase activation and apoptogen release from the mitochondria. This project focuses on the genetic validation of the stress-activated protein kinase, MAP4K4 / HGK, which functions as a control point integrating diverse signals for cardiomyocyte cell death. MAP4K4 and its reported target MAP3K7 / TAK1 appear to operate upstream of JNK in driving cardiac muscle cell death. MAP4K4 is activated in diseased mouse and human myocardium and in cultured rat cardiomyocytes subjected to death signals. Its overexpression in the rodent cardiomyocytes is sufficient to induce cardiomyocyte apoptosis, whereas knockdown of endogenous MAP4K4 using shRNA suppresses it. However, there is no direct or concrete evidence that MAP4K4 has functional importance in a human cardiac muscle cell. Given this unmet need, we deployed shRNAmir-based technology in cardiomyocytes derived from human induced pluripotent stem cells (hiPSC-CMs) to knockdown MAP4K4 and investigate inhibition of cardiac muscle cell death, in response to death-inducing agents (i.e. H_2O_2 and c_2-ceramide). First, we characterized the purity of the proposed human system by cardiac-specific antibodies and confirmed the cells' cardiac identity, with a purity of 95% for the most prevalent marker tested. Then, via a series of optimization efforts using assays for caspase-3 and caspase-8 activities, diminished mitochondrial membrane potential and loss of surface membrane integrity, we developed a short-term maintenance protocol for hiPSC-CMs entailing 2 days in defined (transition) medium prior to death induction. Using this method, the cells were refractory to serum-induced proliferation, thus providing us with conditions under which the cell death assays could be carried out without confounding effects on purity. Prior to phenotypic assessment of MAP4K4 knockdown in hiPSC-CMs, we validated the efficacy of multiple shRNAmirs in a heterologous system. Three potent shRNAmirs were selected for virus production and proven to inhibit MAP4K4 (approximately 60-70%) in hiPSC-CMs. We then defined the conditions for provoking cell death with H_2O_2 and c_2-ceramide, and identified the biochemical responses to each of these complementary death signals. Cell death with various H_2O_2 concentrations at different times was characterized by diminished mitochondrial potential, decreased caspase-8 activity and lack of caspase-3 activation. Cell death with 20μM c_2-ceramide was evident at 16h associated with increased caspase-3 activity. Suppression of MAP4K4 in hiPSC-CMs with the most potent shRNAmir resulted in a 2-fold reduction of death ($p<0.001$) measured by DRAQ7 and 2-fold reduction ($p<0.05$) of cells with diminished mitochondrial potential, compared to the non-silencing control (NSC) upon H_2O_2 treatment. Interestingly, the reduction of cell death was associated with increased caspase-8 activity.

Thus, we prove that MAP4K4 is pro-apoptotic in human cardiac muscle cells, as its knockdown leads to salvage from cell death. This proof-of-concept study will serve as a technical and scientific springboard for later, “higher bandwidth” studies of the entire human kinome or other essential mediators of cardiomyocyte demise.

1. Introduction

1.1. Heart failure: the socio-economic problem

The final pathway of myriad cardiac diseases is the clinical syndrome of heart failure, which arises from diverse genetic and environmental causes, including cardiac structural or functional abnormalities, age, or coexisting systemic conditions (i.e. hypertension, diabetes, renal disease, obesity, high blood pressure). In Europe, diseases of the heart and the circulatory system (cardiovascular disease, CVD) account for 4 million deaths each year (Nichols et al., 2012). Approximately more than a third of Americans suffer from one or more types of CVD, the main forms of which are coronary heart disease (CHD) and stroke (Lloyd-Jones et al., 2009). CHD is the single most common cause of death in Europe accounting for 1.8 million deaths each year, with stroke following in the second place accounting for 1.1 million deaths (Figure 1A).

As the population ages, the prevalence of heart failure will increase, which constitutes a major health problem, not only in terms of decreased life expectancy and quality of life, but also as increased medical costs. As of 2012, 2.4% of the US population suffers from Heart Failure (HF) with prevalence increasing with age; from which 12% are above 80 years of age (Heidenreich et al., 2013). Despite the decline in CVD mortality in developed countries in the last two decades (Fig.1B) due to a combination of prevention and control measures leading to a decline of population-wide risk factor as a result of better treatments (including secondary prevention, heart failure treatment, initial treatment of acute myocardial infarction (AMI) and hypertension treatment), HF mortality is high, with 50% of HF hospitalization not surviving past 3 years (Heidenreich et al., 2013). Figure 2A depicts an increase in the number of PCIs over a 13-year period (1990-2003) in selected countries, but with a stable number of hospitalized patients for HF after AMI (Fig. 2B), from which 44 to 45% die within a year after AMI; a number relatively unchanged for that period (Chen et al., 2013a).

Last but not least, the socioeconomic burden of CVD in the EU economy is estimated to cost almost 196 billion euros a year, with 31% spent on just CHD clinical care. The total health care costs in Europe and UK in 2009 were calculated to be approximately 20 million and 2 million, respectively. Health care costs in Europe (selected countries) and UK are illustrated in Sup. Fig.1 (Nichols et al., 2012). The World Health organization (WHO) in a 2008 statistics report predicted that the four leading causes of death in 2030 would be ischaemic heart disease, cerebrovascular disease (stroke), chronic obstructive pulmonary disease (COPD) and lower respiratory infections (mainly pneumonia). Globally, cardiovascular disease is expected to rise from 17.1 million in 2004 to 23.4 million in 2030, and HF to increase by 23% from 2.42% in 2012 to 2.97% in 2030 (Heidenreich et al., 2013).

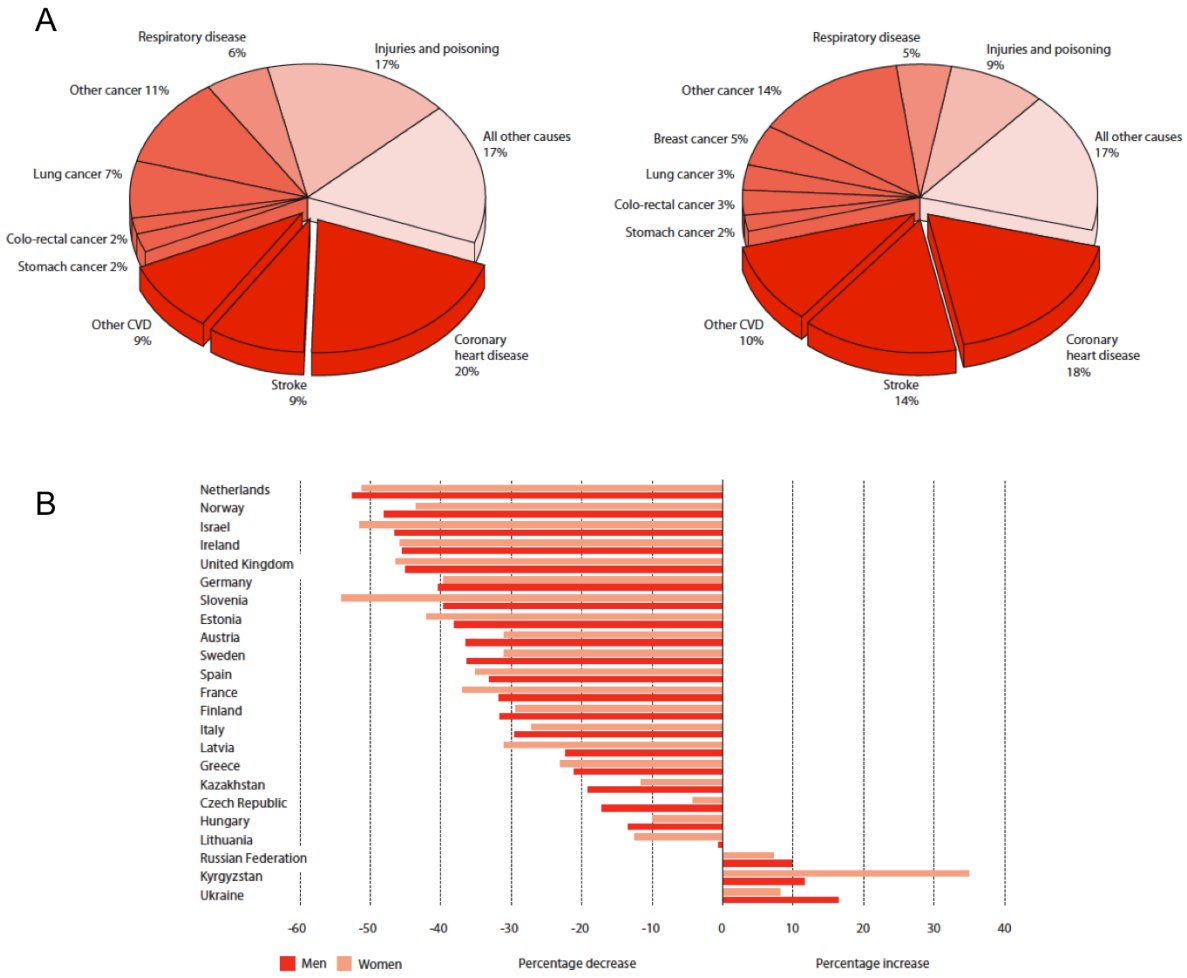


Figure 1: **Cardiovascular diseases statistics (A)** Deaths by cause under 75 years of age in men (left) and women (right). (Data from latest available year can be found in Table 1. in Allender S. et al., 2008) **(B)** Percentage change in CHD death rates, by sex, from selected countries for the period of 1998 to 2008 (Data taken from the Allender S. et al., 2008)

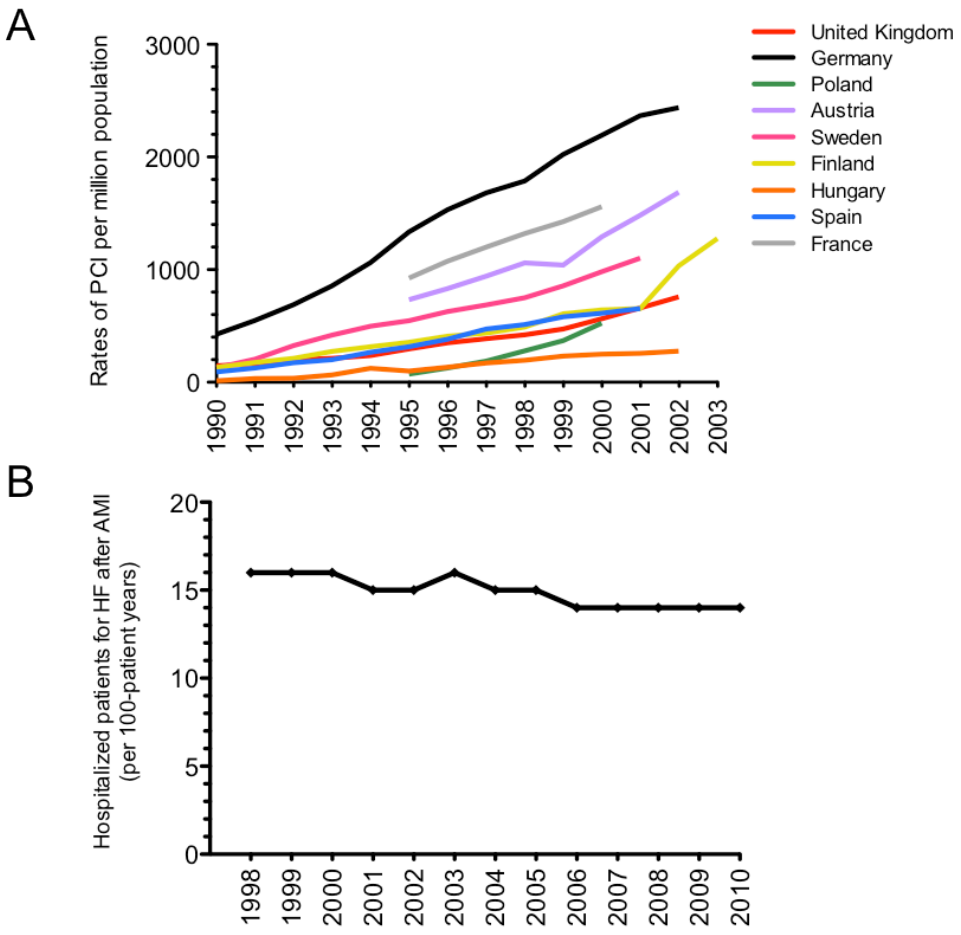


Figure 2: **Heart failure on the rise. (A)** Rates of percutaneous coronary interventions (PCI) from 1990 to 2003 on selected European countries. Data were collected by the European Society of Cardiology from national registries and reports from national cardiology societies and numbers represent crude, non-standardized numbers per million populations (Data from Allender S. et al., 2008). **(B)** Number of hospitalized patients for HF after AMI per 100-patient years. Despite the decline in mortality rates the proportion of patients hospitalized for HF after AMI who died within 1 year of HF hospitalization remain relatively unchanged from 1998 (data not shown) (Chen et al., 2013a).

1.2. Pathobiology of heart failure: a multifaceted problem

Heart failure, regardless of the cause, is characterized by severe left ventricular dysfunction (that can also lead to right-sided ventricular heart failure) that arises through a number of pathophysiological mechanisms. These include: defects intrinsic to cardiac muscle cell contractility (Boudoulas and Hatzopoulos, 2009), defects extrinsic to the cardiac muscle cells, such as excessive myocyte loss unmatched by cell replacement, release of pro-inflammatory cytokines and in the affected area resulting in heart muscle infiltration of immune cells, leading to interstitial fibrosis and cardiac hypertrophy (Dimmeler et al., 2005).

In the case of a myocardial infarction (MI), a common effect of atherosclerosis, the widespread injury and cell death is often exacerbated by reoxygenation following reperfusion that leads to elevated mitochondrial reactive oxygen species (ROS) formation, which cannot be adequately countered by the mitochondria and cytosolic anti-oxidants of the cardiomyocytes (Gustafsson and Gottlieb, 2008). The extra mechanical burden on the remaining ventricular cells, on-going cell death and progressive fibrosis lead to gradual deterioration, electrical instabilities (arrhythmias), ventricular dilation and eventually heart failure (Boudoulas and Hatzopoulos, 2009).

The pathophysiology of CHD arises due to inherent mutations in myofibrillar genes (most commonly *MYH7*, *MYBPC3*, *TNNT2*, and *TNNI3*) that give rise to human birth defects and abnormalities of the adult human heart (Olson et al., 2004). These mutations can lead to hypertrophic cardiomyopathies characterized by increased cardiac mass due to left ventricular wall thickening that can produce enlarged and disarrayed cardiomyocytes (also known as myocyte disarray) (Seidman and Seidman, 2001).

Just as the developing heart is prone to abnormalities, the adult heart is also susceptible to defects that impinge on cardiac muscle's growth and contractile function, such as hypertension, aortic stenosis, cardiac arrhythmias and valve dysfunction. These can provoke pathological hypertrophy, traditionally thought of as an adaptive response to injury or cardiomyocyte loss. Prolonged hypertrophy that is accompanied by the activation of the foetal cardiac gene program can result in diastolic and systolic heart failure, cardiac arrhythmias and sudden death. Presenting commonly as spontaneous adult cardiac hypertrophy ("hypertrophic cardiomyopathy") are mutations of contractile and structural proteins (e.g. myosin heavy chains, myosin binding proteins) that are part of the contractile apparatus that is involved in biomechanical force production (Olson et al., 1998; Seidman and Seidman, 2001). Other mutations (e.g. dystrophin, cardiac actin, desmin, titin) (Seidman and Seidman, 2001) are a common cause of dilated cardiomyopathy characterised by an increase in ventricular size, thinning of the ventricular walls and cardiac conduction abnormalities (Chien, 2000; Dalloz et al., 2001; Li et al., 1999; Olson et al., 2004). In many of the above cases, mutant genes encode

poison protein peptides as a result of missense mutations, deletions and splice defects. Cardiac hypertrophy classified as “physiological” develops in healthy individuals after exercise or pregnancy and is characterized by a benign increase in the heart mass not associated with cardiac damage (Bernardo et al., 2010).

While some stress signals (in both inherited and acquired conditions) trigger cardiac hypertrophy, which can progress to left ventricular dilatation and eventually heart failure, others instigate cardiac dilatation and heart failure without causing intermediate hypertrophy (Olson et al., 2004). The balance between cell survival and apoptosis appears crucial in the transition of hypertrophy to ventricular dilatation. Consequently, suppressing apoptosis and promoting cell survival are attractive strategies for the treatment of heart failure, dilated cardiomyopathies and remodelling after a MI (Olson et al., 2004).

Current therapies for hypertension, heart failure and cardiomyopathies involve the use of angiotensin-converting enzyme (ACE) inhibitors, angiotensin-II receptor antagonists, beta- and calcium channel blockers to provide some improvement of symptoms relief of myocardial workload and protection from progressive dilatation (LV remodelling). Furthermore, thrombolytic drugs are used within hours in patients who have had a MI to dissolve clots and prevent the onset of secondary attacks. Recent developments prefer the use of percutaneous coronary intervention (PCI) as it results in improved overall outcome including the reduced risk of stroke that exists with thrombolytic drug therapy. In addition, aspirin and statins are used as prophylaxis to lower cholesterol and prevent atherothrombosis (Bonow et al., 2011; p487-514). Together, these advances have improved the clinical outcomes in patients with acute MI resulting in increased life expectancy and quality of life.

On the other hand, current drugs and therapies cannot restore the dead myocardium to a living state. Since it is widely agreed that the human myocardium is incapable of robust regeneration after injury - as opposed to the regenerative response in organisms such as zebrafish and newts - clinicians have turned their hopes to tissue repair, by (i) autologous adult progenitor cells that are resident in the mammalian myocardium, or (ii) exogenous progenitor cells found in the bone marrow with the reported potential to differentiate into cardiomyocytes and/or supportive cell types (endothelial and smooth muscle cells) (Boudoulas and Hatzopoulos, 2009; Segers and Lee, 2008). The clinical promise for these cell types already in clinical trials, as well as for pluripotent stem cells not yet in human studies (notably, embryonic stem cells and induced pluripotent stem cells), would be to rescue cardiac muscle cell number by cardio-myogenesis and neovascularization. (Dimmeler et al., 2005). As each approach has its hurdles (Dimmeler et al., 2005; Mummery et al., 2010; Segers and Lee, 2008), the present challenges to cell therapy include optimizing the choice or “cocktail” of cells favouring heart function improvement, optimizing the delivery method for such cells, increasing clinical

compliance of culture reagents for expanding autologous stem cells *ex vivo* to minimize health risk issues.

Complementary methods to enhance cardiac muscle cell number would include inciting the controlled proliferation of resident cardiomyocytes (Mercola et al., 2011), which normally occurs at vanishingly low levels in the adult heart (Bergmann et al., 2009; Mollova et al., 2013), and to inhibit cardiomyocyte cell death by enhancing cell survival (Fig. 3) (Chiong et al., 2011). Conversely, and perhaps more safely and feasibly, one might focus on pharmacological inhibition of cardiac muscle cell death, i.e. to salvage jeopardized myocardium by 21st century means.

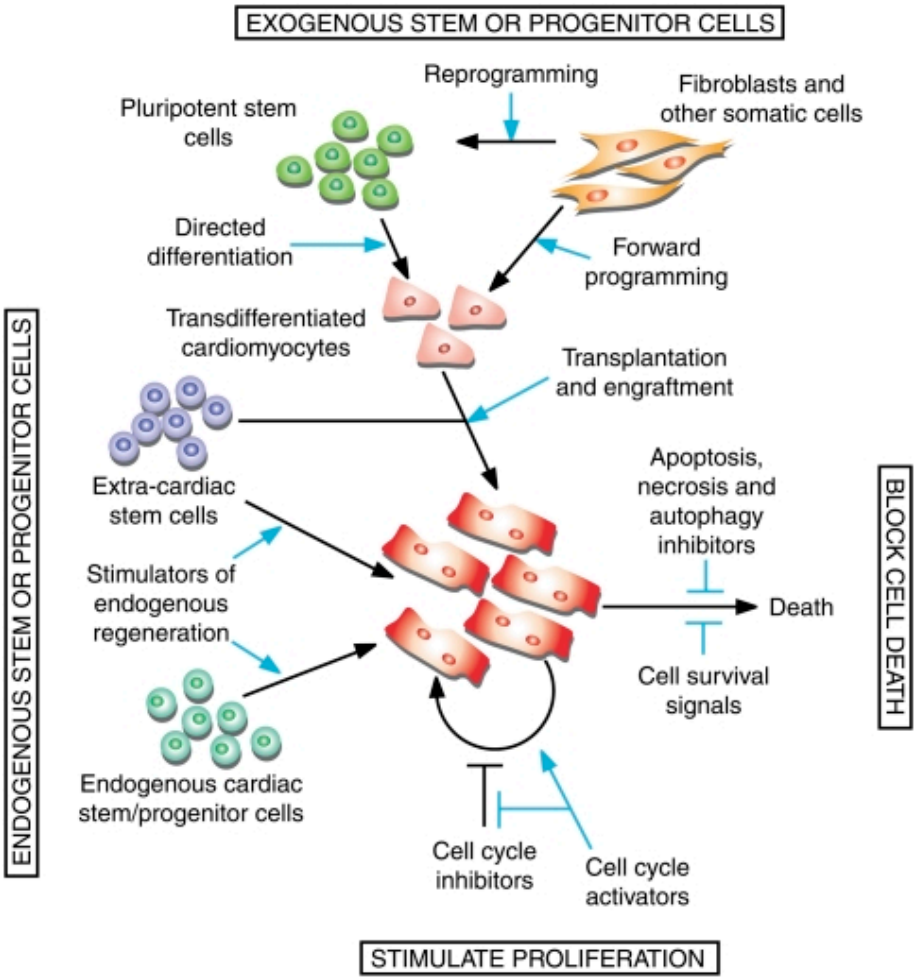


Figure 3: **Strategies to increase cardiac muscle cell number.** In principle, the heart's inability to replace cardiomyocytes after their loss in various ischaemic and non-ischaemic cardiomyopathies can be improved by the four strategies depicted above, such as (i) reactivating cell division of pre-existing cardiomyocytes or stimulating proliferation and differentiation of multipotent stem cell progenitors that reside in the heart, (ii) inhibiting cell death by the use of various pharmacological inhibitors and (iii) by cell therapy approaches using ex vivo stem cell progenitors from the heart of other organs or, in the future, even derivatives cardiomyocytes from ESCs or iPSCs. Challenges to regeneration of the heart also include inflammation, fibrosis, and the lack of neovascularization and blood supply. Image taken with permission from (Mercola et al., 2011).

1.3. Cell death signalling pathways

Multiple diseases, such as stroke, diabetes, heart failure and neurodegenerative diseases are characterized by excessive cell death unmatched by cell replacement. Cell death is divided into at least three main types: apoptosis, necrosis and autophagy. Autophagy is an intracellular recycling process initiated in response to cellular stress, nutrient limitation, damaged organelles or accumulation of protein aggregates that contributes to cardiac cell death in some circumstances (Pattingre et al., 2005; Rothermel and Hill, 2008), but is not well understood. On the other hand, apoptosis and necrosis are widely reported types of cell death, based initially on morphological differences that are based mechanistically on distinct, but convergent, signalling pathways. In heart disease, all types contribute towards the pathophysiology of the disease and their signalling pathways are relevant for future therapeutic strategies (Scarabelli and Gottlieb, 2004; Whelan et al., 2010). This overall introduction will be followed by the signalling events that characterize each mode of cell death and their contribution to the development of heart disease.

1.3.1. Apoptosis

Apoptosis is an evolutionary conserved mechanism of programmed cell death (PCD) as a counterbalance to cell proliferation (Riedl and Scott, 2009; p3-24), with an important role in development and homeostasis. The process was first described in *C. elegans* with genetic approaches that led to the discovery of anti-apoptotic and pro-apoptotic genes (Yin and Dong *et al.,* 2009). Apoptosis can be triggered by different stimuli and is classified into two central pathways: the extrinsic pathway, which utilizes cell surface receptors and the intrinsic pathway entailing mitochondria and endoplasmic reticulum (ER). Central to both pathways are specialized enzymes called caspases (from **c**ysteine-dependent **asp**artate-specific prote**ases**), which in the absence of a stimulus exist as inactive zymogens referred to as pro-caspases (reviewed in Riedl and Scott, 2009; p3-24). Understanding this machinery both is essential to understand the potential molecular targets of cardiac death signals and to devise potential molecular indicators of cardiac cell death.

In the **extrinsic** (death receptor, caspase-8/10-dependent) pathway, so-called death ligands bind to cell surface receptors to initiate a signalling cascade of programmed cell death. Death ligands can be found in the form of integral membrane proteins on the surface of neighbouring cells (e.g. FasL) or as soluble extracellular proteins (e.g. tumour necrosis factor-α [TNFα]). Ligand binding leads to activation of initiator caspases by their recruitment to the receptors, leading ultimately to downstream activation of effector/executioner caspases by proteolytic cleavage. Ligand binding induces the recruitment of adaptor proteins, such as Fas-associated via death domain (FADD), which interacts with pro-caspase-8 to form the death

inducing signalling complex (DISC). Dimerization of pro-caspase-8 in the complex, results in its activation, which then proteolytically cleaves and activates effector pro-caspase-3 (Fig. 4).

In contrast to the extrinsic pathway that transmits a specialized set of extracellular death stimuli from the cell membrane to intracellular compartments, the **intrinsic** (Bcl2-inhibitable, mitochondrial) pathway relies on an intermediary mitochondrial response through a variety of Bcl-2 family proteins, responding to a range of extracellular and intracellular stimuli (e.g. loss of survival factors, toxins, DNA damage, hypoxia, radiation and oxidative stress). The Bcl-2 family of pro-apoptotic proteins (i.e. Bax, Bak; and BH3-domain only members: Bid, Bam, Bim, Bmf, Noxa, Puma, Bnip3 and Bnip3L) and anti-apoptotic (i.e. Bcl-2, Bcl-x_L) proteins unites the extrinsic and intrinsic death signalling pathways, which formerly were seen as wholly separate. A common signal transducer or key point of convergence is BH3-interacting domain death agonist (Bid), which is cleaved by caspase-8/10, whereupon its C-terminal portion (tBid) translocates into the outer mitochondrial membrane (Wei et al., 2000). Bax, a prerequisite for the intrinsic signalling pathway together with Bak, is activated through a conformational change and also inserted into the outer mitochondrial membrane forming a conductance channel for release of apoptogens (Cytochrome c [cyt-c]) (Crow et al., 2004; Suzuki et al., 2000). The precise mechanism by which cyt-c and other apoptogens are released is not completely understood, but it has been proposed that interactions among the three proteins (Bim, Bad and Bax) lead to the opening of the mitochondrial permeability transition pore (mPTP) (Belzacq et al., 2003; Cheng et al., 2003; Marzo et al., 1998; Shimizu et al., 1999). Released cytochrome c binds to released apoptosis activating factor-1 (Apaf-1), along with ATP, recruiting homo-oligomers of pro-caspase-9 into a complex called the apoptosome, which subsequently activates downstream caspases (Acehan et al., 2002; Yu et al., 2005) (Fig. 4).

Apoptosis is held in check by “mitochondrial gatekeepers” anti-apoptotic Bcl family proteins, Bcl-2 and Bcl-x_L, that act as antagonists of pro-apoptotic proteins, as well as by other endogenous inhibitors. Bcl-2 and Bcl-x_L are constitutively localized on the outer mitochondrial membrane, nuclear envelope and endoplasmic reticulum. One postulated mechanism for the death antagonist activities of Bcl-2 and Bcl-x_L is via interactions with Bax and Bak, or indirectly by preventing BH3-only proteins binding to Bax and Bak (Crow et al., 2004; Kim et al., 2006; Whelan et al., 2010). Evidence consistent with this model support that expression of Bcl-x_L inhibits the apoptotic phenotypes that are induced by truncated tBid, such as loss of mitochondrial membrane potential, release of cytochrome c, cell shrinkage and nuclear condensation (Chen et al., 2001b). Bcl-2, as a death antagonist, is suggested to bind to pro-apoptotic factors or by binding to proteins, such as voltage-depended anion channel (VDAC), that block the formation of the pore for cyt-c release (Imahashi et al., 2004; Shimizu et al., 1999). Furthermore, cells treated with a broad kinase inhibitor (i.e. staurosporine) underwent apoptosis and showed an elevation of cyt-c in the cytosol that corresponded to decreased

levels of cyt-c in the mitochondria. The efflux of cyt-c from the mitochondria was prevented when Bcl-2 was overexpressed (Yang, 1997). However, Bcl-2 has a more general role in cardiomyocyte homeostasis and its survival effect is not limited to its anti-apoptotic function. In support of this notion, cardiac-specific overexpression of Bcl-2 minimized I/R injury due to reduced acidification and reduced rate of ATP consumption (Imahashi et al., 2004), indicating cardioprotection through modulation of metabolism.

With regards to caspase inhibition, the best-illustrated mammalian inhibitors belong to the inhibitor-of-apoptosis (IAP) family. In most cell types, X-linked IAP (XIAP) directly binds to caspases to inhibit their catalytic activity. IAPs utilize their E3 ubiquitin/ligase activity to target caspases (i.e. caspase-7, caspase-3) for proteasome degradation as a safety mechanism to prevent transient or accidental cyt-c leakage from eliciting a full apoptotic response. To achieve biologically sufficient activation of caspase-9, for example, a significant loss of mitochondrial membrane potential leads to release of mitochondrial Smac/DIABLO and Omi/HtrA2 apoptogens that then bind to IAPs (c-IAP1, c-IAP2, XIAP), displacing caspases, and thereby neutralizing caspase inhibition (Du et al., 2000). IAPs can also bind procaspase-9 to directly inhibit apoptosome formation. In addition, Omi/HtrA2 uses its serine protease activity in a caspase-dependent mechanism to irreversibly inactivate XIAP (Verhagen et al., 2000; 2002).

The need for Smac/DIABLO and Omi/HtrA2 in the execution of apoptosis underscores that cyt-c release alone is inadequate to complete the death circuit, and that it may be necessary to eliminate inhibitory mechanisms. In contrast to just apoptosis, cIAPs also play a critical role in the regulation of cell death that occurs by the death receptor activation (Whelan et al., 2010). Mice with a cardiac IAP-2 transgene displayed a reduction in infarct size and a decreased number of TUNEL-positive cardiomyocytes (Chua et al., 2007). cIAP-1 and -2 utilize their ubiquitin ligase activity to catalyse the ubiquitination of RIP1 kinase and TNF receptor-associated factor 2 (TRAF2), both of which are part of complex I formed by the binding of TNF to TNFR1. Polyubiquitinated RIP1 and TRAF2 are then used to recruit and activate TGF-β-activated kinase-1 (TAK1) through TAK-1 binding protein (TAB2/3). The downstream effect is the activation of survival genes (Whelan et al., 2010), though TAK1 can drive cardiomyocyte death in other settings (Zhang et al., 2000).

Another potential inhibitor c-FLIP [FLICE-(FADD-Like IL-1β-converting enzyme)-inhibitory protein], which is enriched in striated muscle (Shu et al., 1997), binds to pro-capase-8 to prevent DISC formation. Interestingly, c-FLIP exists in two isoforms, where only the long isoform is inhibitory at high concentrations (Peter, 2004), but low concentrations result in pro-caspase-8 activation (Whelan *et al.,* 2010). This bifunctional dose-dependent role resembles the stimulation of cyclin-depended kinases by low concentrations of their inhibitors, through facilitated assembly of active complexes (Cheng et al., 1999; LaBaer et al., 1997). Inhibition of the extrinsic pathway by the short isoform of FLIP occurs by occupying FADD and pro-

caspase-8 to preclude DISC complex (Whelan *et al.,* 2010). In contrast to the inhibitors that block either the extrinsic or intrinsic pathway, **A**poptosis **R**epressor protein with a **C**ARD domain (ARC), which is expressed in cardiac and skeletal myocytes, exerts an inhibitory effect on both intrinsic and extrinsic pathways (Nam et al., 2004) (Fig. 4). ARC engages with the death domains of Fas and FADD to inhibit Fas-FADD binding and DISC assembly, as well as antagonizing the intrinsic pathway by ARC-Bax complex formation to inhibit Bax activation and translocation to the mitochondria (Nam et al., 2004). In addition, knockdown of ARC triggers spontaneous Bax activation and apoptosis (Nam et al., 2004). ARC protein levels decrease in response to death stimuli in an MI model as a result of protein destabilization mediated by the ubiquitin-proteasomal pathway (Nam et al., 2007).

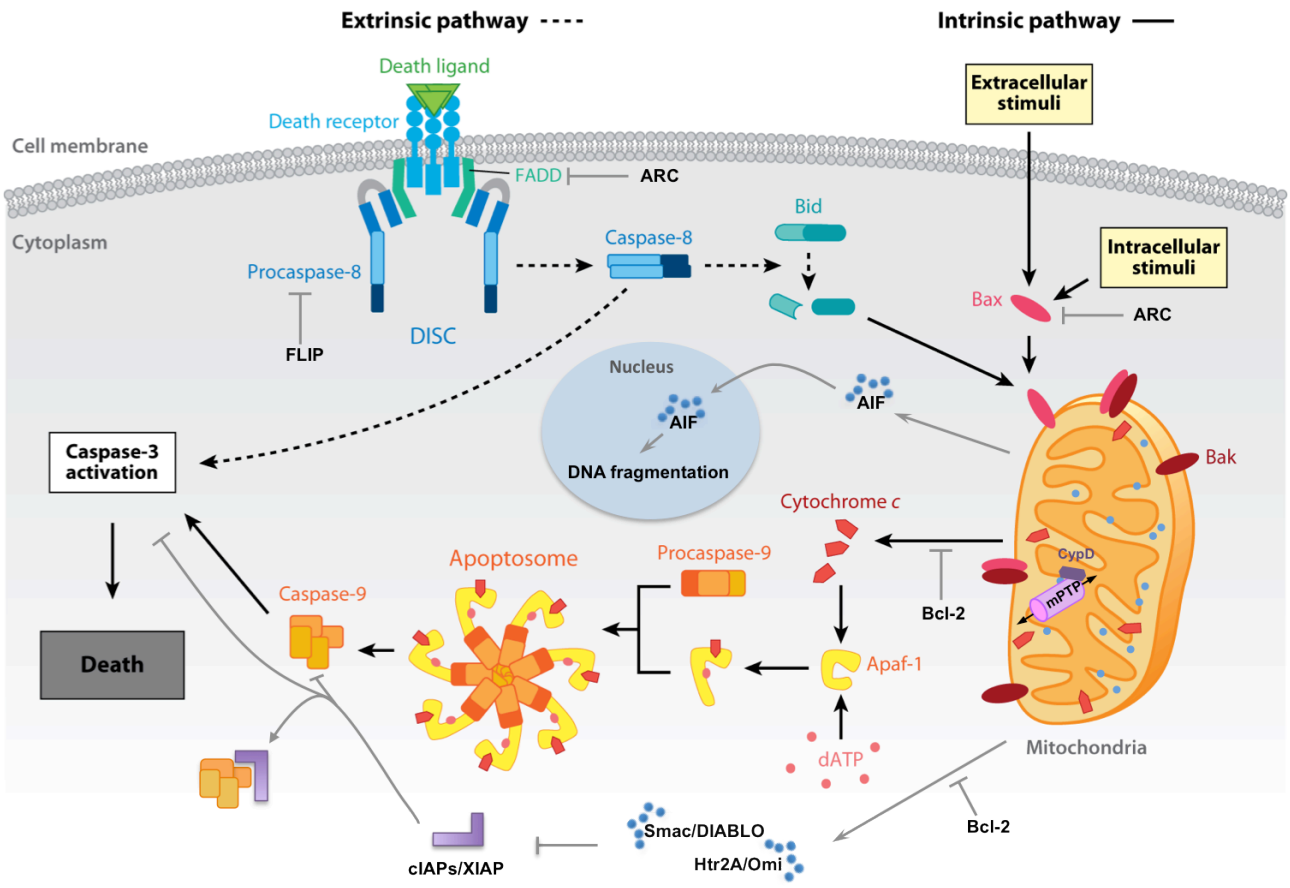


Figure 4: **Illustration of the intrinsic and extrinsic signalling branches of apoptosis.** In the extrinsic pathway, ligand binding induces recruitment of adaptor proteins and subsequent activation of procaspase-8. Mitochondria, as an integral organelle of the intrinsic pathway, hold signal proteins in its internal membranes and space that are released in response to various stimuli via the Bid/Bax/Bak proteins. Cyt-c apoptogen release accounts for the activation of pro-caspase-9 by stimulating its binding on Apaf-1, which along with ATP, ends in the formation of the apoptosome. Both pathways converge on the activation of pro-caspase-3 that will subsequently target cytoskeletal proteins and other enzymes. AIF presumably translocates in the nucleus from the mitochondria to induce large-scale DNA fragmentation. Under non-stimulatory conditions, apoptosis signalling is held in-check by caspase inhibitors (IAPs), such as XIAP, that is relieved by the release of apoptogens such as Omi/HtrA2 and Smac/DIABLO. Apoptosis repressor with a CARD (ARC) domain, expressed preferentially in striated muscle antagonizes both pathways, by binding to Bax to inhibit its conformational translocation on the mitochondrial membrane, and by binding to FADD on the death receptors. Subsets of stimuli promote the release of Ca^{2+} from ER to the cytoplasm and opening of mPTP, which leads to apoptogen release. Image taken with permission from (Whelan et al., 2010) and further adapted.

1.3.2. Necrosis

The alternative scheme of cell death is called necrosis and is an important component to MI and stroke. The quintessential features of necrosis are the depletion of ATP and loss of plasma membrane integrity, resulting in a swollen appearance in contrast to the shrunken phenotype of apoptotic cells. Necrosis, similar to apoptosis, is characterized by two branches: (i) the mitochondrial branch that involves the opening of mPTP (Whelan et al., 2010), and (ii) the regulated death-receptor signalling branch that involves TNF ligand binding.

1.3.2.1. mPTP-dependent necrosis

The most obvious connection between necrosis and prolonged myocardial ischaemia, with or without reperfusion, is the mechanism of mPTP opening (Whelan et al., 2010) (Fig. 5). mPTP is a voltage-dependent high-conductance anion channel (VDAC) for small molecules (up to 1.5kDa) regulated by adenine nucleotide (ADP/ATP) translocators (ANTs), members of the pro- and anti-apoptotic Bcl-2 protein family and cyclophilin D (*PPIF*: gene, CypD: protein; also known as cyclophilin F) (Kokoszka et al., 2004). However, the identity and regulatory importance of mPTP protein components remains controversial.

Mitochondria are the most abundant organelles in cardiomyocytes, ensuring a highly efficient localized ATP delivery system for ion homeostasis, contraction and metabolism, to meet the high energy demand of the beating heart (Gustafsson and Gottlieb, 2008). They provide ATP for the cells through oxidative phosphorylation of the electron transport chain complexes. As a by-product of this activity, mitochondria are a major source of reactive oxygen species (ROS). In the context of I/R, high oxygen concentrations lead to increased oxygen uptake by the respiratory chain, thus yielding higher, than physiologic, levels of ROS (Gustafsson and Gottlieb, 2008). The high density of mitochondria in cardiomyocytes can result in significant increased levels of superoxide, quickly converted into hydrogen peroxide, that cannot exceed detoxification by antioxidant systems (i.e. MnSOD, glutathione peroxidase). This results in oxidative modification of mitochondrial proteins and a series of molecular events, culminating in mitochondrial dysfunction and cell death (Gustafsson and Gottlieb, 2008).

Intracellular generation of ROS causes a collapse of $\Delta\Psi_m$ and action potential destabilization that is linked to mPTP opening. Under normal conditions, the inner mitochondrial membrane is impermeable and tightly regulated to maintain pH gradient and membrane action potential. In I/R, a drop in pH gradient due to a decrease in ATP/ADP ratio leads to a collapse of the proton gradient and opening of mPTP (Fig. 5). Indeed, inhibition of pore opening is cardioprotective, as demonstrated by several mPTP inhibitors (e.g. cyclosporine A) where cell death and infarct size was reduced in an *ex vivo* model of hypoxia/reoxygenation (Clarke et al., 2002). Furthermore, CypD-deficient mice, whose mitochondria are more resistant to mPTP opening in response to Ca^{2+} and oxidative stress

stimuli, show a high resistance level to I/R cardiac injury (Baines, 2007; Baines et al., 2005; Nakagawa et al., 2005) compared to wild type littermates; CypD-deficient mice were still sensitive to apoptotic stimuli, such as TNFα and staurosporine treatment (Baines et al., 2005).

In the case of the role of VDAC and ANTs for the function of mPTP, evidence is controversial. Co-immunoprecipitation studies and other evidence (Halestrap et al., 2009) are consistent with the model where CypD binds to the ANT and in response to stress triggers a conformational change for pore opening. However, Kokoszka and colleagues showed that the mPTP from mitochondria isolated from mice with genetic ablation of ANT1 and ANT2 could still be inhibited by cyclosporine A (CsA), but where more sensitive to calcium overload and cell death compared to the controls. Furthermore, no difference in cell death sensitivity was observed between controls and ANT-deficient mitochondria treated with TNFα and soluble FasL ligand (Kokoszka et al., 2004). Along this line of evidence, cardiac mitochondria isolated from wild-type, *Vdac1-, Vdac3-,* and *Vdac1-Vdac3*-null mice exhibited pronounced Ca^{2+}-induced swelling compared with wild type, that was still inhibited with CsA (Baines, 2007). So far, more work is required to elucidate the crucial components of mPTP and its role in conjunction with the Bax/Bak apoptosis-dependent mitochondrial pore and the release of apoptogens. Indeed, Bax and Bak are required for mPTP-dependent cell death by facilitating the permeability of the outer mitochondrial membrane (Karch et al., 2013).

1.3.2.2. Death receptor-dependent necrosis

The second branch of necrosis involves the activation of death receptors via TNF signaling, that can result in survival, proliferation or cell death, and is implicated in diseases, such as malaria, Acquired Immune Deficiency Syndrome (AIDS) and cancer (Whelan et al., 2010). Treatment of cells with the TNF pro-inflammatory cytokine alone does not promote cell death, since both survival and death mechanisms are activated. However, when survival mechanisms are inhibited, TNF can induce apoptosis, and when caspases are inhibited (e.g. with a pan-caspase inhibitor), TNF can elicit necrosis (Whelan et al., 2010). Many of the TNF-induced cellular responses are mediated by either one of the two receptors of the TNF-receptor superfamily, TNFR2 or TNFR1, the latter receptor mainly activated to achieve apoptosis or necrosis (Liu, 2005). These dual effects may underlie the discouraging results of general TNFα antagonists in early clinical trials (Feldman et al., 2000; Mann et al., 2004) for heart failure pushing towards the requirement of selective inhibitors against TNFR1 alone (Mann, 2005). In addition cardiac overexpression of TNFα led to the development of dilated cardiomyopathy (Kubota et al., 1997a). Binding of TNF to TNFR1 stimulates the formation of either of two complexes (complex I or complex II) with the recruitment of various adaptor proteins and serine/threonine kinase RIP1.

Complex I comprise the adaptor TRADD protein, RIP1 kinase, TRAF2 and inhibitors of apoptosis c-IAP1 and -2. RIP1 and TRAF2 become K63-polyubiquitinated by the E3-ubiquitin ligase activity possessed by c-IAP1/2. Polyubiquitinated RIP1 and TRAF2 recruit and activate TAK1 kinase via its binding protein TAB1 (Whelan et al., 2010). TAK1 kinase, a member to the MAPKKK cascade, phosphorylates the Inhibitor of NFκB (IκBα, IκBβ or IκBε) as part of the NFκB/IκB (IKK) complex to promote the nuclear translocation of the NFκB transcription factor to stimulate the expression of multiple survival genes (Tanaka et al., 1999). IKKs comprise a complex of IKKα, IKKβ and a regulatory subunit IKKγ (NEMO) (Ea et al., 2006). Interestingly, polyubiquitinated RIP1 recruits IKK through binding to NEMO via its polyubiquitin chains (Devin et al., 2001; Ea et al., 2006). Mutations of NEMO were shown to abolish IKK activation (Ea et al., 2006). Similarly, cells lacking TAK1 expression following TNFα stimulation undergo rapid RIP1-mediated cell death (Çöl Arslan et al., 2011). In summary, complex I regulates cell survival, but complex I can transition to complex II to promote cell death (Fig. 5).

The events for the transition of multiprotein complex I to II towards cell death signaling are the following. Complex I becomes dissociated by the TNFR1 and is internalized in the cytosol by endocytosis. RIP1 is deubiquitinated by CYLD (cylindromatosis), a K63-specific de-ubiquitinase, and stimulates recruitment of FADD-pro-caspase-8 complex (Chan et al., 2003; Wang et al., 2008). Unless pro-caspase-8 is inhibited, complex II will stimulate apoptosis. Caspase-8 targets RIP1 for C-terminal cleavage (Chan et al., 2003), obstructing RIP1 to signal necrosis or survival via NFκB (Fig. 5). However, pharmacological or genetic inhibition of pro-caspase-8, leads to recruitment of RIP3 into a complex with RIP1 (RIP1/RIP3), where both kinases undergo activating phosphorylation (He et al., 2009; Lin et al., 1999). The molecular interplay between apoptotic and necroptotic signals is reinforced by evidence from the RIP3-caspase-8 and RIP1-FADD double knockout mice, where embryonic lethality caused by caspase-8 and FADD-deficiency is rescued by loss of RIP3 or RIP1 (Feoktistova et al., 2011).

In summary, the kinase activities of both RIP1 and RIP3 are critical for necrosis (He et al., 2009; Holler et al., 2000), but identification of downstream mechanism of regulated necrosis remain unclear and are required to further define the connections to the mitochondrial pathway. One possible way by which RIP3 may stimulate necrosis is through activation of metabolic pathways and increase of ROS levels. Furthermore, it is worth noting that so far pathway dissection of TNFα-induced programmed necrosis was studied in inflammatory, cancer cells and fibroblasts. However, the role TNF cytokine in cardiomyocytes seems to generate apoptotic signals via caspase-8 receptor, that are diminished with Bcl-2 overexpression (Haudek et al., 2007). With these in mind, it is important to delineate the role of RIP1-RIP3 axis in programmed necrosis in the context of cardiac muscle cell death.

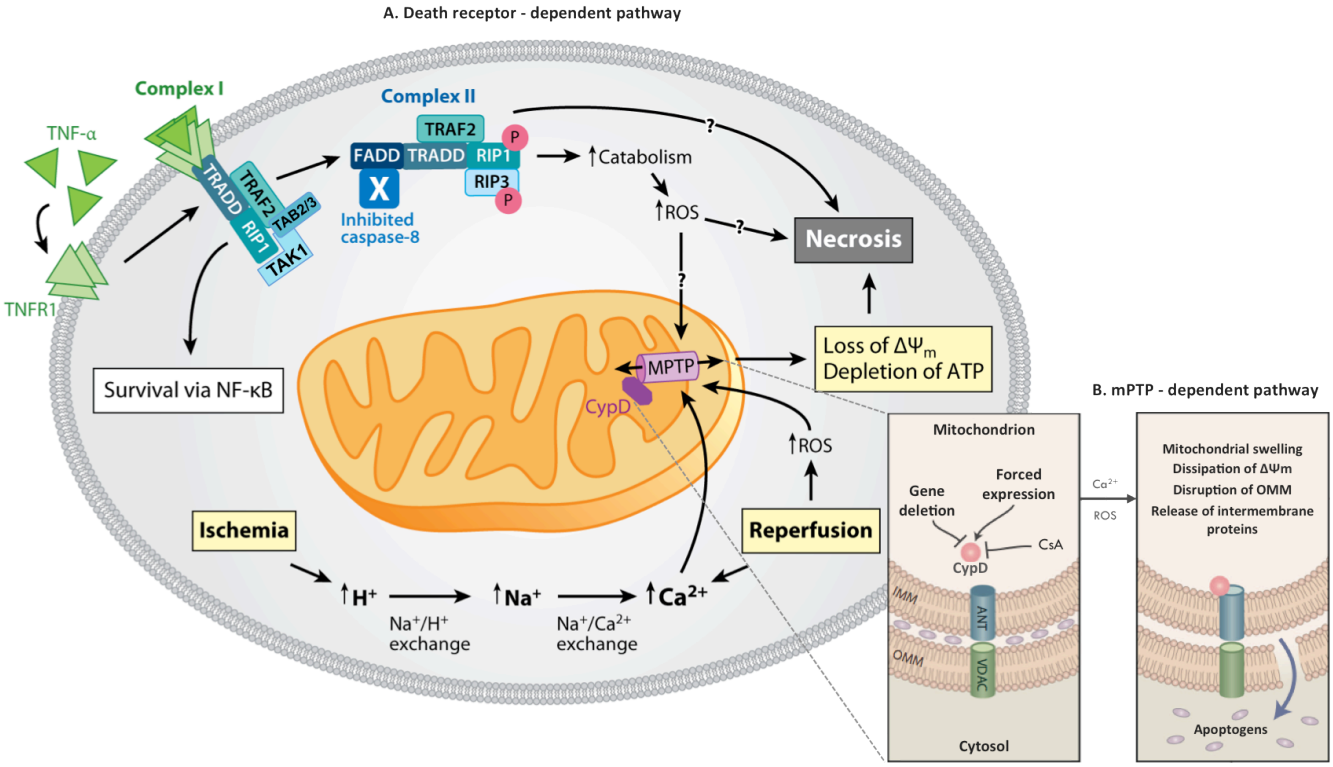


Figure 5: **Schematic illustration of the molecular events of the two signaling pathways leading to necrosis upon cardiac I/R injury.** ***(A) Death receptor-dependent necrosis.*** Information about necrosis is limited into the formation of either TNFR1-complex I promoting cell survival or complex II signalling cell death. Multiprotein complex I comprise of TNFR1, TRADD, RIP1, TRAF2, and cIAP1/2. One model proposes that TNFR1-TRADD-RIP1 are linked via their death domains. cIAP1/2 polyubiquitinates at K63 residues of RIP1 and TRAF2, so that they recruit TAK1 kinase via TAB2/3 binding proteins, which in turn will turn-on survival genes via NFκB activation or IKK inhibition. Complex II as a mediator of cell death will first be dissociated from TNFR1 by endocytosis. De-ubiquitination of RIP1 by CYLD (not shown) will lead to recruitment of FADD-pro-caspase-8 via DD interactions. If pro-caspase-8 is activated, RIP1 is cleaved by caspase-8 and rendered inactive to signal necrosis or survival. In the case of pro-caspase-8 inhibition, RIP1 recruits RIP3 instead ensuing a series of phosphorylation events probably by activating catabolic pathways and increasing ROS. ***(B) mPTP-dependent necrosis.*** During ischaemia, depletion of ATP sensitizes mPTP opening, an event that occurs upon reperfusion when mitochondria resume respiration and generate action potential. With reperfusion, the mitochondria become overloaded with Ca^{2+} and Reactive Oxygen Species (ROS) leading to events, such as dissipation of mitochondrial membrane potential ($\Delta\Psi_m$), mitochondrial swelling, disruption of the outer mitochondrial membrane and release of inter-membrane apoptogens that mark irreversible cell death. Cyclophilin D (CypD or *ppif*) has an essential role in protein folding and is involved in the regulation of mPTP. Loss-of-function studies of CypD in mice showed resistance to necrotic cell death induced by ROS and Ca^{2+} overload (Nakagawa *et al.,* 2005; Baines *et al.,* 2005). Mice overexpressing CypD in the heart showed mitochondrial swelling and spontaneous cell death, whereas CypD null mice were protected from I/R-induced cell death (Baines *et al.,* 2005). Images combined from (Schneider, 2005; Whelan et al., 2010) and permission was acquired from the publisher and authors.

1.3.3. Autophagy

Autophagy is a complex orchestration of gene machinery that is initiated in response to the lack of nutrients, cellular stress, ROS, protein aggregation or damaged organelles. Autophagy is a mechanism to tolerate starvation with the mammalian target of rapamycin (mTOR) being the core sensor of nutrient availability (Gottlieb et al., 2010). When mTOR is activated, it stimulates protein synthesis and suppresses the degradation by inhibitory phosphorylation of autophagy-related (Atg) proteins (Whelan et al., 2010). Conversely, autophagy is activated when mTOR is inhibited. Other regulators of autophagy are the AMP-activated protein kinase (AMPK), which can override suppression of mTOR. AMPK activation activates a gene regulatory cascade of multiple autophagy-related (Atg) proteins leading towards the formation of a phagophore that will attach and enclose its targets (i.e. a protein aggregate or a damaged organelle) to form a double-membrane autophagosome (Gottlieb et al., 2010) (Fig. 6).

In summary, following AMPK activation, BH3-only protein Beclin1 and vacuolar protein sorting gene34 (VPS34), a class I PI3-kinase, will trigger the activation of two ubiquitin-like signalling events consisting of multiple Atg proteins. Atg7, an E1-like enzyme, activates Atg12 into a ubiquitin that will in turn activate Atg10, an E2-like enzyme, and subsequently lead to the formation of Atg5/Atg12 complex. This will then assemble with Atg16 homodimer and form the phagophore membrane structure. The formation of the phagophore is a prerequisite for the second ubiquitin-like pathway, which involves the cleavage of Atg8 (also termed LC3) by a cysteine protease Atg4 (Gottlieb et al., 2010). Atg4 is a direct target for oxidation by hydrogen peroxide and appears to upregulate autophagy in the presence of oxidative stress (Gottlieb et al., 2010; Scherz-Shouval et al., 2007). Cleavage of LC3 exposes a terminal glycine residue that is now termed as LC3-I. Another form of LC3, LC3-II, is a result of reaction with phospatidylethanolamine by Atg7 E2-like enzyme. This sequence of events gives rise to the autophagosome (Fig. 6).

Beclin 1, the mammalian yeast orthologue Atg6, was an early-characterized protein with a central role in autophagy. Beclin 1 is important for autophagic protein localization in the pre-autophagosome (PAS) for vesicle-trafficking processes and depends on the interaction and regulation by multiple proteins (comprehensive review by (Kang and Izumo, 2000)). Disruption of the beclin 1 - Bcl-2 complex by mutations in the BH3-only domain results in the stimulation of autophagy. However, its relationship between Bcl-2 and Bcl-x_L is complicated since Beclin 1 cannot neutralise Bcl-2 anti-apoptotic action, whereas Bcl-2 and Bcl-x_L reduces the autophagic activity of beclin 1 (Maiuri et al., 2007; Pattingre et al., 2005). Interestingly, inhibition of autophagy can be achieved with ER-localized, but not mitochondrial-localized Bcl-2. Beclin 1 interaction with these anti-apoptotic proteins is inhibited by tBid, Bad and BNIP3. Moreover, pro-apoptotic proteins such as BNIP3, Bad, Noxa and PUMA all induce autophagy and may

function as competitive inhibitors of Beclin 1-Bcl-2/ Bcl-x_L interactions (Sinha and Levine, 2008). Recent studies describe a new mechanism of Beclin 1 action via a complex formation with PI3K, Vps34, Vps15 and Atg14L, the latter of which localizes to ER and mediates the localization of the complex to the ER important for the induction of autophagy (Matsunaga et al., 2010). The same authors also knocked-down Atg14L causing a defect in autophagosome formation. Rubicon, another protein that localises to in a subpopulation of UVRAG-Atg14L-Beclin 1 complexes, was shown to localise at the lysosome and its knockdown caused enhancement of mature autophagy and lysosome trafficking (Matsunaga et al., 2009). The role of Rubicon as an inhibitor of autophagy is reinforced by an independent study in which forced expression of Rubicon impaired autophagosome maturation, lysosomal structure formation and overall downregulated autophagy (Zhong et al., 2009).

The next important (maturation) step in the life of the autophagosome is the fusion with the lysosomes (Fig. 6). Lysosomes along with lysosomal hydrolases, such as cathepsin D, are increased in cells that undergo autophagy, even though an increase in lysosomal markers is not indicatory of autophagosome-lysosome fusion. Catabolic reactions are important in the process of late autophagy as amino acids, free fatty acids and carbohydrates are exported into the cytosol after the degradation of the contents and the shrinkage of lysosomes. An additional type of autophagy (termed macroautophagy) is mediated by chaperones, where heat shock cognate 70 (Hsc70) binds to the target protein and escorts it to the lysosome (Whelan et al., 2010).

Thus, in contrast to necrosis and apoptosis, autophagy is a survival mechanism of an intracellular recycling process that provides energy to the cells in times of nutrient deprivation. There has been considerable debate whether autophagy is an independent form of cell death, as the autophagic morphology can be associated with cell death, but not causally connected (Whelan et al., 2010). The clearest evidence for this proposition is the genetic analysis of PI3K-expressing, atg-mutants and other mutants of Drosophila's salivary glands (Berry and Baehrecke, 2007). In this setting, caspases are active and combined inhibition of both caspases and autophagy supressed gland degradation. Significantly, inhibition of caspase activity did not suppress Atg-1-induced cell death (Berry and Baehrecke, 2007). However, the study proves apoptosis and autophagy cooperatively contribute to the clearance of salivary gland cells during development, without however showing a unique molecular signature or whether autophagy feeds into existing forms of cell death, such as apoptosis or necrosis. Finally, more work needs to be carried to determine the overlap of autophagy with other forms of cell death.

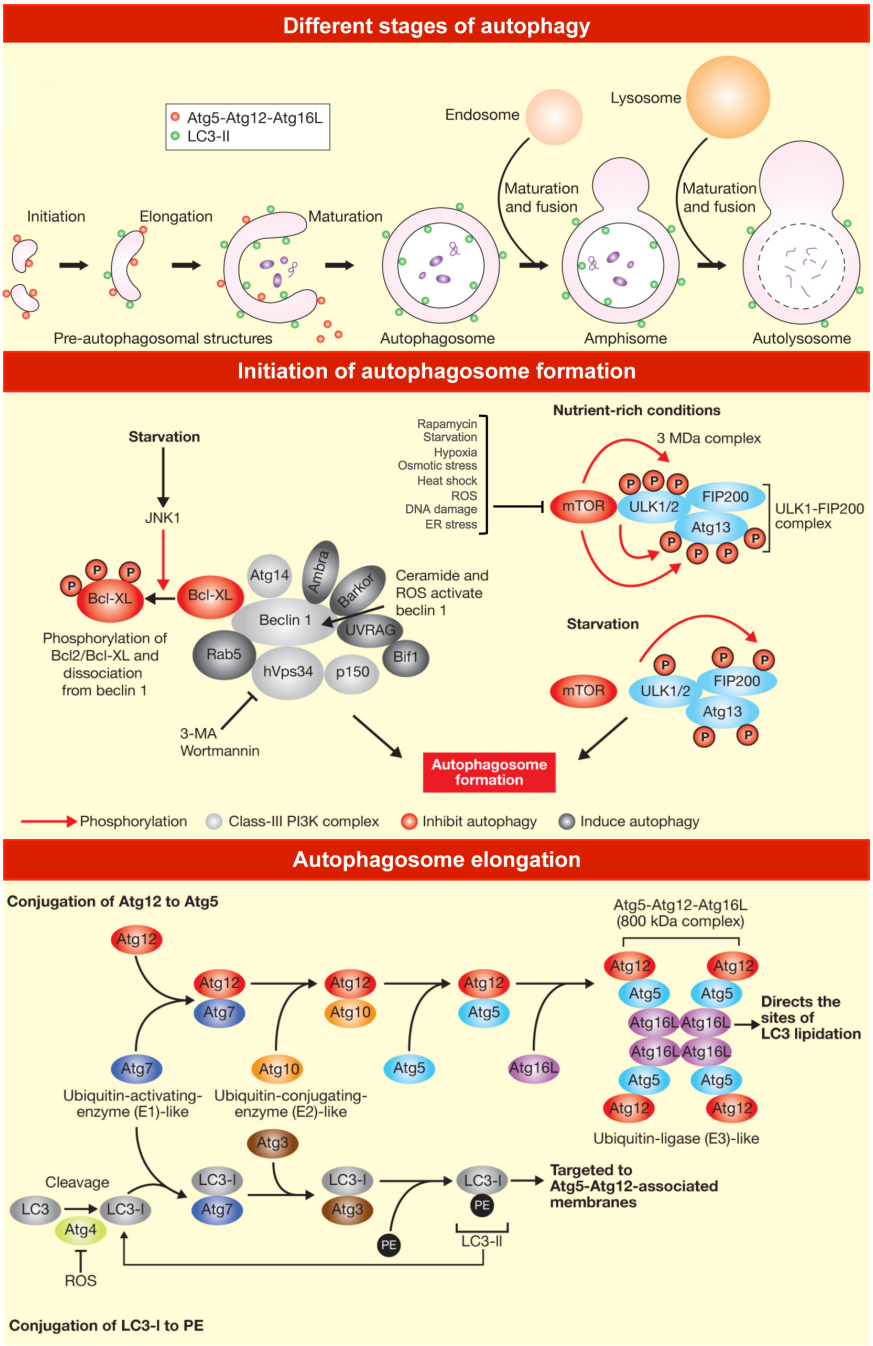


Figure 6: **The different stages of autophagy from initiation, elongation, maturation, and finally lysosome fusion.** (Top panel) Under starvation conditions phosphorylation of Bcl-x_L leads to the dissociation from the Beclin 1 complex that consists of many proteins. mTOR is inhibited under the same conditions, that normally inhibits by phosphorylation ULK1/2 and Atg13 proteins, leading to the formation of the autophagosome (Middle panel). The elongation of the autophagosome will involve two ubiquitin-like modifications (i.e. activation of the complex by E1-like and E2-like enzymes, Atg7 and Atg10 respectively) that will consequently consist of multiple Atg proteins with ubiquitin-ligase (E3)-like activity. At the same time, LC3 will be cleaved by Atg4 (inhibited by ROS) to form LC3-I and later LC3-II that will bind to PE, a process that requires Atg7 and Atg3 activities. LC3-II will be targeted at the Atg5-Atg12-associated membranes (bottom panel). Image adapted with permission from (Ravikumar et al., 2009).

1.3.4. Concluding remarks

In summary, as viewed presently, cell death undoubtedly involves crosstalk between various signalling pathways, such as caspase-dependent signaling for apoptosis, RIP kinases and mPTP/CypD for necrosis, whereas the predominant mechanism executing cell death is dependent on cell context and stimulus (Crow et al., 2004). From this perspective, apoptosis and necrosis, are not dichotomous Platonic entities, but rather highly overlapping because of the shared use of caspases and mitochondrial release of apoptogens. In the future, it will be important to establish death assays that can be used: (i) to determine the relative contribution of caspase activity and apoptogen release in I/R in an animal setting, and (ii) to enable robust high content genetic screens for the development of predictive *in vitro* models of heart disease at the most fundamental level, the cell level (Scarabelli and Gottlieb, 2004).

1.4. Endoplasmic reticulum (ER): a link between apoptosis and necrosis

Calcium signalling homeostasis is critical for normal cell functioning and aberrant ER calcium regulation, normally a case with MI, can interfere with protein folding, due to the calcium-dependent nature of many chaperones (i.e. Grp78, Grp94 and calreticulin) (Xu et al., 2005). In ischaemia/reperfusion (I/R) injury, calcium can activate calcium-dependent enzymes including protein kinases, phosphatases, endonucleases and proteases called calpains, all of which can feed forward into apoptotic and mitochondrial cell death (Xu et al., 2005).

Excessive and prolonged ER stress triggers cell death in the form of apoptosis. One molecular signature of ER-mediated apoptosis is the transmission of signals by BH3-only proteins. Certain death stimuli increase the concentration of Ca^{2+} in the cytoplasm, a process controlled by Bax and Bcl-2 via interactions between Bcl-2 and 1,4,5,-triphosphate receptor (IP3R) that works as an ER calcium-release channel. CCAAT/enhancer-binding homologous protein (CHOP) is a pro-apoptotic transcription factor that can mediate transcriptional induction of Bim and translocation to the ER membrane, under ER stress conditions (Minamino et al., 2010). CHOP also represses anti-apoptotic Bcl-2 and Bnip3 proteins in cardiomyocytes (Minamino et al., 2010). PUMA, a pro-apoptotic member of the Bcl-2 family, was induced in mouse hearts in response to ER stress. Calcium overload in isolated mitochondria from the heart has been shown to also mediate cyt-c release (Logue et al., 2005). A second ER death signature is the activation of pro-caspase-12, which activates pro-caspase-9 independently of the formation of the apoptosome. This means of pro-caspase-9 activation is a way of crosstalk into the intrinsic pathway of apoptosis independently of the mitochondria (Foo et al., 2005). However, the relevance of caspase-12 activation to ER-induce apoptosis is a matter of question in humans since some populations carry an inactive protein due to nonsense mutations (Xu et al., 2005). Human caspase-4, one of the closest paralogs of rodent caspase-12, may be ascribed with the functions of the rodent caspase-12 as it is associated with the ER, but it is also a proinflammatory caspase responsible for cytokine proteolytic activation rather than involved in apoptotic events. Nevertheless, knockdown of caspase-4 with RNAi in human neuroblastoma cells partially reduced cell death that was induced with thapsigargin (inhibitor or endoplasmic/sarcoplasmic reticulum Ca^{2+} ATPases [SERCAs], which pump Ca^{2+} into the ER), a reduction of which did not occur with UV and DNA-damaging reagents that induced mitochondrial cell death. In HeLa cells, however, caspase-4 knockdown had little effect on apoptosis implying a tissue-specific relevance of the protein (Xu et al., 2005).

Other members of the cysteine protease family besides caspase-12 associated with the ER are the calpains, which are non-caspase Ca^{2+}-dependent cysteine proteases. The first line of evidence suggesting a role in cell death comes from loss-of-function mutations in calpain

orthologues (CLP-1, TRA-3) in *C. elegans*, where cell death mediated by Na^+- and Ca^{2+}-channel opening (Whelan et al., 2010). The conventional calpains (forms m- and μ-) are implicated in degrading a diverse array of substrates, such as desmin, PKCα and multiple pro-caspases (Patterson et al., 2011). Bax (Wood et al., 1998) and Bid proteins are also cleaved by calpains (Chen et al., 2001b) with their activity enhanced, while cleaved Bcl-2 is converted into to a pro-apoptotic form. Since, elevated cytosolic calcium is generally associated with necrosis and I/R, it is worth noting that calpains can be activated under these conditions without caspase activation in adult rabbit hearts (Chen et al., 2001b). Given these observations, calpains and caspases work cooperatively to transduce apoptosis, but also independently of each other. However, a major question is whether these or other proteases play a role in the execution of necrosis similar to the role of caspases in apoptosis (Whelan et al., 2010).

Furthermore, mitochondria play a role in regulating calcium homeostasis and can capture Ca^{2+} to buffer the cytosolic levels and to prevent depletion by the ER. A subset of stimuli originating outside the ER, such as oxidative stress, can alter intracellular Ca^{2+} signalling leading to the development of cardiac hypertrophy and subsequently heart failure (Chakraborti et al., 2007; Foo et al., 2005). Increased cytoplasmic Ca^{2+} concentrations overload the mitochondrial matrix which lead to depolarization of inner mitochondrial membrane, mitochondrial swelling causing rupture of the outer mitochondrial membrane, mitochondrial permeability transition pore (mPTP) opening and apoptogen release (Foo et al., 2005). However, the role of mPTP opening in response to Ca^{2+} remains to be elucidated, as most experimental evidence come from *in vitro* work with isolated mitochondria; an effect not demonstrated in isolated cardiac myocytes (Gustafsson and Gottlieb, 2008). A recent study by Chen and colleagues reports the dual role of a pro-apoptotic protein, Nix/BNip3L, in mitochondrial and ER-directed cell death in cardiomyocytes. Mitochondrial-localized Nix/BNip3L induced cell death via Bax/Bak activation, whereas ER-localized Nix/BNip3L promoted mPTP-dependent (caspase-independent) necrosis that was inhibited by the knockdown of CypD, the identical mediator being essential in both contexts (Chen et al., 2010) of both mitochondrial and endoplasmic triggers.

1.4.1. ER stress and UPR signalling

A basic role of the endoplasmic reticulum (ER) is to facilitate protein and phospholipid synthesis, glycosylation, and maturation of newly synthesized proteins. A disruption of these processes may affect ER homeostasis and accumulation of misfolded proteins can elicit a reverse translocation into the cytoplasm to be degraded via the 26S proteasome (Logue et al., 2005). A second major role of ER is to function as stores of intracellular calcium (Ca^{2+}), a

critical messenger involved in intracellular signal transduction for cardiac muscle contraction (Chakraborti *et al.,* 2007). ER stress triggers the unfolded protein response (UPR) to maintain homeostasis. The UPR is a signal transduction group of proteins that increase ER-resident chaperones Grp78 and Grp94 to inhibit protein translation and accelerate the degradation of unfolded proteins (Minamino et al., 2010).

The UPR signal transduction events that restore homeostasis of the ER involve many kinases downstream of the ER lumen (Fig. 7) (Xu et al., 2005). Certain UPR stress sensors (i.e. Ire1, PKR-like ER kinase [PERK] and ATF6) occupy the ER membranes with their C-terminus facing the cytosol and their N-terminus in the lumen, providing a bridge between the two compartments. The N-termini of these proteins are anchored to Grp78 to prevent their activation, but when misfolding occurs Grp78 releases the proteins, which oligomerize in ER membranes. Upon removal of Grp78, PERK oligomerizes and autophosphorylates its kinase domain to inactivate downstream eIF2α to switch off mRNA translation and reduce the ER protein load. However, ATF4 transcription factor gains a selective advantage over mRNA translation as it regulates the promoter of other UPR genes. Knockout studies of *perk* and knock-in of a dominant-negative eIF2α that cannot become activated both display ER stress hypersensitivity. An alternative UPR proteins with a Ser/Thr kinase domain that oligomerizes, Ire1, binds TRAF2 to signal downstream kinases implicated in immunity and inflammation, such as Ask1, which activates JNK and NF-κB and c-Jun (AP-1) kinases that promote expression of alarm genes encoding mediators of host defence (Xu et al., 2005). Furthermore, the intrinsic ribonuclease activity of Ire1 renders it competent to translate and produce XBP-1 bZIP-family transcription factor that promotes the reverse transport of misfolded proteins from the ER to the cytosol. A different mechanism of protein activation occurs when Grp78 is released from the N-terminus of ATF6, which then translocates to the Golgi apparatus. ATF6 is cleaved by resident proteases to release it to the cytosol for regulating expression of UPR genes (Fig. 7). ATF6 is also a feed-forward mechanism for increasing transcription of XBP-1 that will then be processed by Ire1 to produce XBP-1 protein (Xu et al., 2005).

The initial ER response is normally adaptive, but if remains unresolved, it can promote apoptosis (Xu et al., 2005). The UPR is fundamental (following section) in the development and progression of cardiovascular diseases including cardiac hypertrophy, heart failure, I/R, hypoxia, atherosclerosis, and cardiotoxicity as a result of cancer therapy, as well as other diseases like neurodegeneration and diabetes.

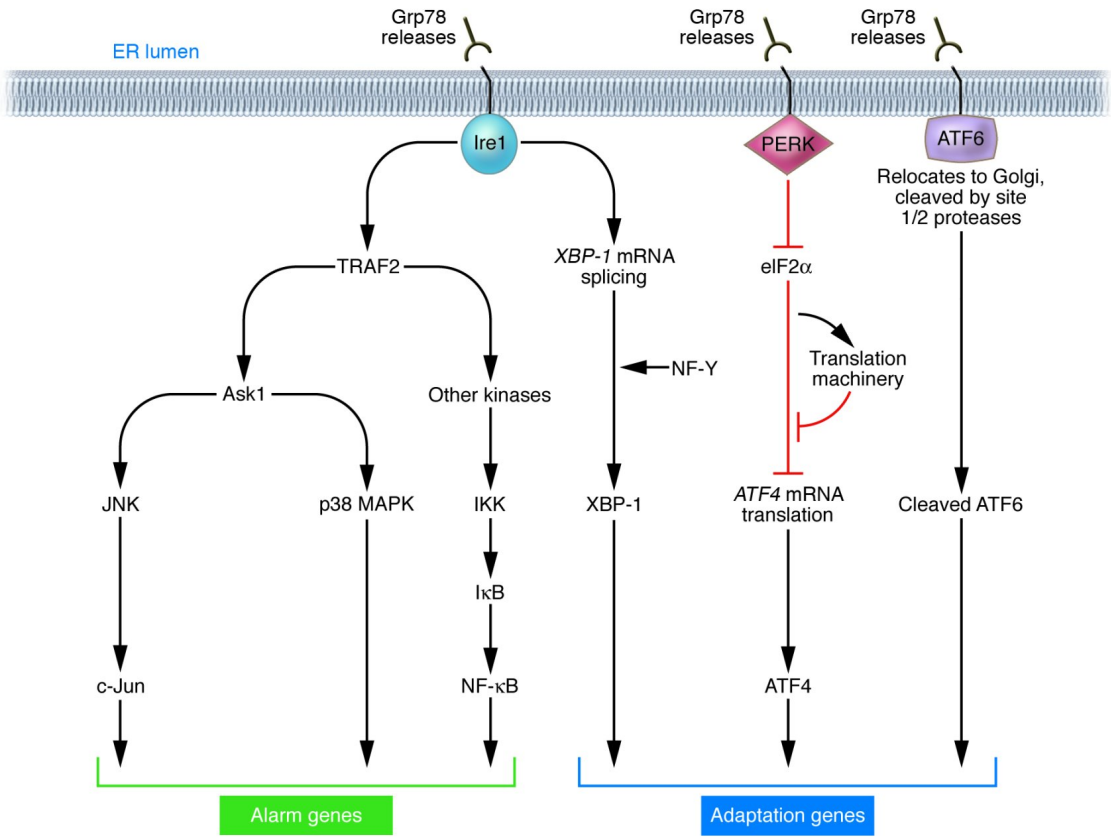


Figure 7: **ER stress-mediated signal transduction.** Protein folding perturbation leads to the release of Grp78 and Grp94 proteins that trigger the release of Ire1, PERK and ATF6 from the ER lumen membranes. Ire1 oligomerization will bind TRAF2 for activation of downstream kinases, such as Ask1, JNK, and NFκB and transcription factors like c-Jun. Alternative mechanisms include the upregulation of XBP-1 mRNA for restoring protein folding and ATF6 activated by cleavage of proteases in the Golgi apparatus for the control of UPR gene expression and to further promote the transcription of XBP-1 mRNA. Image was taken with permission from (Xu et al., 2005).

1.4.2. ER stress in cardiovascular disease

The ER environment can be experimentally perturbed by substances (i.e. dithiothreitol, SERCA inhibitors: thapsigargin [TG] or tunicamycin [TU], adriamycin), which can impair the protein folding process by altering the redox ER state, glycosylation process and calcium levels. Pathophysiological stimuli that can activate the ER in cultured cardiomyocytes are oxidative stress, hypoxia (Terai et al., 2005), TNFα and angiotensin II (Okada et al., 2004).

Indeed in failing hearts of patients there are increased levels of spliced XBP1 and GRP78, suggesting an involvement in the pathophysiology of heart failure. The same patients also have increased levels of ATF4 and CHOP with ubiquitinated protein aggregates suggesting impaired protein quality control in human failing hearts (Minamino et al., 2010). In addition, cardiac-specific deposition of β-amyloid aggregates was shown to activate the UPR in mouse transgenic hearts. In fact, mice that received TAC had elevated levels of GRP78 and CHOP. An interesting observation is that UPR was activated in both hypertrophic and human failing hearts, whereas CHOP mediated apoptosis without activation of JNK or caspase-12. These findings are consistent with UPR activation in hearts subjected to pressure overload. However, ER-initiated apoptosis via CHOP is activated in failing mouse hearts under conditions of pressure overload (Okada et al., 2004). A caution of note, is that Terai *et al.* showed coincidental CHOP upregulation with the timing of apoptosis appearance with TUNEL staining, a marker of DNA fragmentation, but with no evidence of caspase-3 activation. In the cited study, upregulation of ER chaperones, CHOP and DNA fragmentation was observed in isolated adult rat cardiomyocytes treated with angiotensin II, and additional caspase-3 cleavage with treatment by pharmacological inhibitors (TG and TU) (Okada et al., 2004). In a different model of ER stress-mediated cell death, hypoxia-induced CHOP expression was associated with caspase-12 activation in neonatal rat cardiomyocytes that was significantly suppressed by AMPK inhibition (Terai et al., 2005). Neonatal rat ventricular cardiomyocytes subjected to hypoxia for 16h also exhibited increased XBP1 mRNA and protein upregulation (Thuerauf et al., 2006).

In the case of MI, sudden burden of ROS and proinflammatory kinases can potentially induce the adaptive and pro-apoptotic pathways of UPR. Cardiomyocytes near the MI zone, but not in distal areas, exhibited increased expression of chaperone GRP78 (Thuerauf et al., 2006). A model of tamoxifen-induced cardiac-specific ATF6 expression was shown to exhibit enhanced functional recovery as well as reduced levels of cell death. In addition, ATF6 inhibition by an inhibitor reduced cardiac function after M/I (Minamino et al., 2010). This finding illustrates a cardioprotective role of ATF6 in I/R injury. PUMA, a pro-apoptotic member of the Bcl-2 family, was also induced in neonatal rat cardiomyocytes when treated with SERCA inhibitors that block ER protein glycosylation. Knockdown of PUMA with shRNA attenuated ER-mediated cell death after treatment with TG or TU as assessed by TUNEL and TO-PRO-3 (IP

equivalent) staining, and attenuated release of cyt-c from the mitochondria. A decrease in cleaved caspase-3 was also observed in puma$^{-/-}$ cardiomyocytes treated with TG compared to puma$^{+/+}$ controls (Nickson et al., 2007).

1.4.3. Concluding remarks

As presented by the studies above, UPR signalling of ER stress is tightly linked to the activation of apoptotic cell death machinery implicated in the development of ischaemic cardiomyopathies, cardiac hypertrophy and heart failure. The principal challenge for blocking cell death caused by UPR proteins is the same concept for direct inhibition of cell death machinery: universal signalling involved in natural homeostasis, not just in disease. In addition, blocking a single death pathway emanating, or not, from the ER may be inadequate to inhibit cell death and preserve survival. Further studies of genes involved in ER-mediated cell death are required to fully validate the possible drug targets and to understand their position next to alternative death mechanisms in the heart.

Thus far, we have discussed the universal signalling pathways in apoptosis, necrosis, autophagy and ER-induced cell death, considered for the most part generically. The following section is devoted to the more specific role of these cell death modes and their machinery in the context of MI and cardiac hypertrophy.

1.5. Cell death in myocardial infarction and heart failure

The most common form of heart disease is MI and the optimal treatment is immediate mechanical reperfusion (balloon angioplasty, stents). The ischaemic phase deprives the myocardium from oxygen, nutrients and survival factors and can result in the accumulation of waste products (Gustafsson and Gottlieb, 2008; Whelan et al., 2010). Reperfusion, that is the reintroduction of oxygenated blood into the diseased myocardium, results in oxidative stress (i.e. ROS accumulation) and increased cytosolic and mitochondrial Ca^{2+} efflux, which translate to molecular events described above (e.g. mPTP opening, caspase activation, caspase inhibitor inactivation), overall leading to cardiac cell death, inflammation and heart failure.

The human events of a clinical MI are modeled in animals by permanent surgical coronary occlusion and by coronary occlusion followed by reperfusion (I/R), each leading to increased cell death in myocytes and non-myocytes within the ischaemic zone by apoptotic, necrotic and autophagic mechanisms (Whelan et al., 2010). The concept of cell death leading to progressive deterioration in heart function was supported by observations of apoptotic cardiomyocytes (measured by techniques that detected DNA fragmentation or "laddering") (Narula J et al., 1996, Olivetti et al., 1997). However, establishing the relative contributions of apoptosis and necrosis, both in spatial and temporal manner, in human tissues or animal models has always been a major challenge. Part of the problem is mainly methodological where techniques cannot distinguish between the two (Scarabelli and Gottlieb, 2004). Gottlieb was the first to show that reperfusion injury, but not ischaemia alone, in cardiomyocytes induced apoptosis measured by the presence of DNA fragmentation, thus exhibiting apoptosis as a specific feature of reperfusion (Gottlieb et al., 1994). Similarly, caspase-3 activity and DNA fragmentation were more prevalent in cardiomyocytes from patients who died of HF than those with sudden cardiac arrest (Kytö V et al., 2004, Fiedler et al., 2004). In fact, the severity of ATP shortage caused by ischaemia seems to be pivotal in establishing the mode of cell death. Severe depletion of ATP did not exhibit features of nuclear condensation and DNA fragmentation, whereas less severe depletion of ATP was sufficient to initiate apoptosis, suggesting that ATP is required to execute apoptosis (Leist et al., 1997). In conclusion, cardiac myocyte death during MI is usually completed within 24h by necrosis in contrast to modest but chronic levels of cell death during HF (Wencker et al., 2003).

The following section discusses the mechanisms and significance of cell death and the machinery involved in the infarct zone and in heart failure during post-infarct remodeling. The focus of the next section is to elude the functional significance of cardiomyocyte apoptosis and necrosis in pathology of MI and the development of heart failure.

1.5.1. Apoptosis in myocardial infarction and heart failure

The involvement of caspases in cardiomyocyte apoptosis is widely accepted during embryonic heart development (Whelan et al., 2010), as well as having a mechanistic role in the pathology of dilated lethal cardiomyopathy (Wencker et al., 2003). Caspase-deficient mice (of caspases 3, 8 and 9) exhibited cell death abnormalities, indicating an important role of caspases in apoptosis (Kuida et al., 1998). Genetic ablation of caspase-8 resulted in defective heart muscle development (Varfolomeev et al., 1998), and mice with ablation of caspase-3 and -9 had profound developmental defects in the central nervous system with decreased apoptosis (Wang and Lenardo, 2000). Isolation of fibroblasts from caspase-$8^{-/-}$ mice exhibited death-receptor-mediated apoptosis (Varfolomeev et al., 1998).

One of the most influential studies uses a conditionally active caspase-8 exclusive to the myocardium. Mice carried a cardiac-specific transgene of pro-caspase-8 fused with a module that could confer catalytic activity by proximity with similar chimeric molecules, upon administration of a small synthetic dimer acting as a physical bridging mechanism. Activation of this caspase transgene *in vivo* resulted in massive cardiac cell apoptosis, which was markedly reduced by the administration of a pan-caspase inhibitor (Wencker et al., 2003). One key limitation of the study was the use of desmin as a marker for TUNEL-positive cardiomyocytes: a protein also expressed in smooth muscle. In neonatal and adult rat cardiomyocytes, overexpression of caspase-1 induced cardiomyocyte apoptosis via activation of caspases-3 and -9 that was prevented with a broad-spectrum caspase inhibitor (Merkle et al., 2007), but not with caspase-8-specific inhibition. This suggests that caspase-1 is uniquely involved in the activation of the intrinsic pathway, and not in the extrinsic pathway. Similarly, deletion of endogenous caspase-1 ameliorated post-infarction HF assessed by echocardiographic analysis. In addition, treatment of rodents with poly-caspase inhibitors reduced infarct size by 21-52% followed by I/R, which was accompanied by decrease in cardiac dysfunction and cardiomyocyte apoptosis (Whelan et al., 2010).

A significant reduction in infarct size was also present in (*lpr* [lymphoproliferation]) mice lacking Fas and in isolated Langerndoff-perfused hearts from the *lpr* mouse, demonstrating that Fas is directly involved in cell death after MI (Jeremias et al., 2000). Interestingly, death-induced ligands were secreted from perfused hearts suggesting an additional trigger in post-ischaemic myocardial cell death (Jeremias et al., 2000). Furthermore, adenoviral overexpression of FasL resulted in marked apoptosis in primary neonatal rat cardiomyocytes and intact adult rat myocardium (Lee et al., 2003). In the same study, *lpr* mice subjected to I/R exhibited smaller infarcts and apoptosis compared to wild-type mice (Lee et al., 2003), suggesting that Fas is a critical mediator in I/R in *vivo*. Similar to Fas signalling for pathogenesis, one might expect involvement of the TNF pathway in the setting of MI. When left ventricular infarct size was accessed 24h after coronary occlusion in mice lacking one or both

TNF receptors (TNFR1, TNFR2), investigators found that double-deficient mice had a greater infarct and increased apoptosis (not necrosis) compared to WT controls and mice lacking TNFR1 or TNFR2 alone (Kurrelmeyer et al., 2000). These data suggest that both TNFR1 and TNFR2 have a cytoprotective role and a single gene deletion is insufficient to abrogate survival. An additional explanation is the opposing roles of TNFR1 and TNFR2 in cell survival, with TNFR1 having a pro-apoptotic role and TNFR2 a pro-survival role (Hamid et al., 2009).

The intrinsic pathway also has a central role in MI, with evidence coming from transgenic models. Mice with a germline deletion of pro-apoptotic Bax showed a reduction in infarct size and in cardiac dysfunction following both I/R in perfused hearts and permanent coronary occlusion in intact mice. In the same way, cardiac-specific human Bcl-2 overexpression (under the control of muscle creatine kinase [MCK] promoter) reduced infarct size and cardiac dysfunction, reduced cardiomyocyte apoptosis assessed by TUNEL staining following I/R (Brocheriou et al., 2000). A better model for cardiac-specific expression of Bcl-2 (under the αMHC [*Myh6*] promoter) showed increased functional recovery in perfused hearts accompanied by decrease in lactate dehydrogenase (LDH) release from transgenic hearts. Infarct sizes were significantly smaller by 20% compared to non-transgenic control mice and had fewer TUNEL-positive myocytes showing resistance in apoptosis. Trasgenic animals also exhibited decreased levels of AIF protein in the mitochondrial fraction (Imahashi et al., 2004) and protection from I/R injury measured by decreased LDH release (Chen et al., 2001c).

Finally, permanent coronary occlusion and I/R stimulates large numbers of cell death in both myocytes and non-myocytes within the ischaemic zone. According to a non-human primate model and human HF patients, apoptosis predominates in non-myocytes in the heart (Park et al., 2009; Gelpi et al., 2011) and cellular disruptions of interactions between myocytes and non-myocytes can play an important role in the pathogenesis of HF. In fact, non-myocytes might be more susceptible to apoptosis, because of low levels of Apaf-1 in myocytes (Potts *et al.,* 2005). Primary neonatal cardiomyocytes with low levels of Apaf-1 were insensitive to cyt-c release in the cytoplasm and were sensitized by inhibition of XIAP or restoration of Apaf-1 levels. Along this line of evidence, cardiomyocytes are in a strict control of caspase-9 activation by endogenous XIAP as a consequence of low Apaf-1 activity (Potts *et al.,* 2005). However, the study did not determine whether the low levels of Apaf-1 had a direct effect on caspase-3 activation. For instance, UCF-101 (a small molecule inhibitor of serine protease activity) when used in two independent rodent models showed a significant reduction in infarct size following I/R and cardiac dysfunction, which was accompanied by reduction of IAP loss, thus decrease in downstream caspase-9 and -3 activities (Bhuiyan and Fukunaga, 2007; Liu et al., 2005a). This inhibitor is a cell-permeable compound against pro-apoptotic Omi/HtrA2 that pocesses a serine protease activity for irreversible inactivation of IAPs and apoptosis induction.

At the same time, caspase activation plays a role towards the development of HF. Failing hearts of transgenic mice with a modified allele of conditionally active caspase-8 for expressing low levels of caspase-8 (Wencker et al., 2003) exclusive to the myocardium demonstrated very low, but sustained, levels of apoptosis (0.08-0.25%) compared to the controls (0.001-0.002%). These transgenic mice at approx. 8-9 weeks developed lethal dilated cardiomyopathy with increase mortality rates at 2-6 months of age, suggesting that low absolute levels of cardiomyocyte apoptosis play a role in the pathogenesis of heart failure. Likewise, abrogation of dilated cardiomyopathy was accomplished by the administration of a pan-caspase inhibitor (Wencker et al., 2003). In another study, transgenic mice with cardiac-specific expression of caspase-1 displayed significant cardiomyocyte hypertrophy after 4 months of age and homozygous caspase-1-null mice displayed reduced cardiomyocyte hypertrophy in comparison with wild-type mice (Merkle et al., 2007).

Cardiac-specific overexpression of Gαq (under the αMHC promoter) resulted in cardiac hypertrophy associated with activation of the fetal gene program and heart failure (D'Angelo et al., 1997). Gαq is a subunit of heterotrimeric Gq protein dissociated upon interaction of Gq with an agonist-occupied receptor (i.e. type 1 angiotensin II, α_1-adrenergic and endothelin [ET] receptor) used for downstream activation of protein kinase C. In the same Gαq hearts, a BH3-like protein Nix/Bnip3L (BCL2/adenovirus E1B 19kDa interacting protein 3-like) was transcriptionally activated, which when overexpressed as a transgene results in massive cardiomyocyte apoptosis and animal death. Conversely, a splice variant of Nix/Bnip3L (sNix) protected against apoptotic peripartum cardiomyopathy in Gαq transgenic females, with diminished cardiomyocyte apoptosis, improved cardiac function and attenuated early death (Yussman et al., 2002). Germline ablation of Bnip3, a closely related BH3-like protein, demonstrated diminished apoptosis post I/R and inhibited late ventricular remodelling. As expected from the loss-of-function study, forced cardiac expression of Bnip3 increased cardiomyocyte apoptosis in unstressed mice leading to progressive LV dilatation, while conditional Bnip3 overexpression exacerbated apoptosis and increased infarct size prior to coronary ligation (Diwan et al., 2007). An anti-apoptotic splice variant of Bnip3 (Bnip3Δex3) was also identified in cardiomyocytes that was defective for mitochondrial targeting due to a frame-shift mutation in the mitochondrial transmembrane domain (Gang et al., 2011). Bnip3Δex3 when co-expressed with Bnip3 in ventricular myocytes suppressed loss of mitochondrial potential and cell death (Gang et al., 2011). Together, these results identify Bnip3 as a major mediator of apoptosis and cardiac remodelling under baseline conditions and post-ischaemic myocardium.

1.5.2. Necrosis in myocardial infarction and heart failure

At present there is no precise connection between necrotic signalling (RIP1-RIP3 signalling axis) and the events during I/R, but cardiomyocytes might be more susceptible into necrotic mechanisms in I/R that coincide with hypoxia following ischaemia, anaerobic metabolism and intracellular acidosis, all events that contribute to the opening of mPTP. Mice null for CypD exhibit reduced infarct size following I/R and cells lacking CypD are resistant to calcium-induced and oxidative stress-induced cell death, but still respond to apoptotic stimuli (Baines et al., 2005). Similarly, mice overexpressing CypD exhibit mitochondrial swelling as assessed by electron microscopy and increased cell death in response to hydrogen peroxide assessed by PI staining (Baines et al., 2005). Along the RIP1/RIP3 signaling axis, a small-molecule inhibitor called necrostatin-1 (nec-1) that inhibits RIP1 kinase activity reduced infarct size following I/R independent of CypD and mPTP opening (Lim et al., 2007; Smith et al., 2007).

As for a possible mechanistic role of on-going necrosis in chronic heart failure, the evidence is sparse. An early study that used molecular probes to distinguish between necrosis and apoptosis based on the cleavage pattern of DNA in patients with idiopathic and ischaemic heart failure suggests that myocyte necrosis is even more prevalent than apoptosis, with both presumed to be contributing to the evolution of cardiac failure (Guerra et al., 1999). A recent, more convincing study provides molecular evidence that myocyte necrosis is associated with heart failure as a result of Ca^{2+} overload (Nakayama et al., 2007). The authors used transgenic inducible mice in which the β2a subunit of the L-type Ca^{2+} channel (LTCC) was overexpressed (as it enhances open channel probability) via a cardiac-specific promoter, where increased activity was controlled with doxycycline withdrawal. The LTCC is the primary source for Ca^{2+} influx in cardiac myocytes with an increased overall activity in heart failure. Hearts from low- and high-expressing LTCC mice became hypertrophic by 4 months of age with focal and interstitial fibrosis and increased cardiomyocyte cell death associated with Ca^{2+} overload. When verapamil (LTCC inhibitor) was administrated, histopathology was reduced. Other evidence in this study that further reinforce the role of necrosis as a contributing factor to HF are: (i) lack of caspase-3 activation, (ii) lack of increased TUNEL staining, (iii) inability of cardiac-specific Bcl-2 expression to prevent HF (Chen et al., 2001c), and (iv) block of Ca^{2+} influx-induced necrosis and HF with genetic ablation of CypD.

In summary, the pathophysiology of MI and the development of dilated cardiomyopathy and heart failure are plausibly a combined result of increased apoptosis and necrosis, both of which have been investigated chiefly as independent pathways in heart disease.

1.5.3. Autophagy in myocardial infarction and heart failure

Autophagy is induced in the settings of coronary occlusion, I/R, in failing human hearts and in cardiomyopathies (Knaapen et al., 2001; Kostin et al., 2003; Matsui et al., 2007; Tannous et al., 2008). Autophagy was induced by ischaemia and enhanced by reperfusion in the mouse heart, but the mechanisms by which autophagy was induced was distinct between the two phases. Ischaemia-induced autophagy was accompanied by AMPK activation, similar to the case of permanent coronary occlusion, which was inhibited by transgenic cardiac overexpression of dominant-negative AMPK (Matsui et al., 2007). Autophagy was further enhanced by reperfusion in the mouse heart depicted by an increased LC3II/LC3I ratio. In contrast, autophagy during reperfusion was independent of AMPK activation and accompanied by Beclin 1 upregulation, which was decreased in beclin$^{+/-}$ mice. Furthermore, I/R injury in beclin$^{+/-}$ showed a marked decrease in the infarct size compared to WT animals with decreased numbers of TUNEL-positive cells in the ischaemic region (Matsui et al., 2007). The limitations of this study were that the ischaemic zone was assessed with TUNEL staining that addresses DNA fragmentation as late-stage apoptosis with no overlapping caspase activity marker and/or cardiomyocyte marker. Similarly, pre-treatment of mice with a small molecule activator of AMPK (A-769662) showed a better recovery of left ventricular contractile function, decreased necrosis and smaller infarcts following I/R (Kim et al., 2011). This cardioprotection effect was not present in mouse hearts with a genetically inactivated AMPK form, indicative of the specificity of the AMPK inhibitor (Kim et al., 2011).

Human failing hearts exhibit increased number of autophagosomes suggesting increased autophagy (Hein et al., 2003; Kostin et al., 2003), but the question in this setting is whether increased autophagy is cardioprotective or has a deleterious role in heart failure. Several *in vivo* studies addressed this question. Atg5-deficient adult hearts (Cre recombinase expressed from MLC2v promoter) after transverse aortic constriction (TAC) had an increased number or TUNEL-positive cardiomyocytes, but with no evidence for activation of pro-apoptotic caspases-3 and -9 (Nakai et al., 2007). The hearts however, had increased levels of caspase-12 (endoplasmic reticulum stress-induced apoptosis), proteasome activity, protein synthesis and proteasome-dependent degradation and precipitated left ventricular enlargement and cardiac dysfunction (Nakai et al., 2007). Embryonic deletion of Atg5 showed no abnormalities at birth, but upon hemodynamic stress mice developed cardiac enlargement and failure (Whelan et al., 2010). Another study used WT and beclin$^{+/-}$ mice to examine the role of autophagy in heart failure induced by pressure overload (Zhu et al., 2007). Upon pressure overload in WT left ventricles there was an increase in cardiomyocyte autophagy as demonstrated by a cardiac-specific LC3-GFP reporter and increased level of lysosomal markers (i.e. Cathepsin D). Heterozygous disruption of Beclin 1 decreased cardiomyocyte

autophagy and diminished pathological remodelling. Conversely, overexpression of Beclin 1 heightened autophagic activity and exacerbated pathological remodelling (Zhu et al., 2007).

The mechanism by which inhibition of Beclin 1 leads to decreased autophagy associated with diminished pathological remodelling and decreased infarcts in I/R remains largely unknown. A recent study suggests that I/R by left coronary artery ligation markedly impaired autophagosome clearance assessed by the LC3-GFP construct (Ma et al., 2012). I/R injury provoked an increase in Beclin 1 abundance and a decrease in LAMP1 and LAMP2 (lysosomal proteins), that was associated with ROS generation and was prevented with the use of a ROS scavenger. This impaired autophagosome clearance caused cardiomyocyte death because of ROS accumulation measured by a potentiometric mitochondrial dye (TMRE), which was inhibited by treatment with cyclosporine A (CypD inhibitor) (Ma et al., 2012). This is the first study that attempts to answer the assumption that death is the result of excess autophagy. Therefore, based on these data, beclin$^{+/-}$ mice may have a better outcome because they clear autophagosomes more efficiently via enhanced lysosome fusion rather than a reduction in autophagosome formation.

1.5.4. Concluding remarks

Cell death undoubtedly entails a complex system of signalling and effector cascades that together play a major role in the pathology of MI and heart failure syndrome. Deletion of various protein components of death pathways, in different genetic and cell culture models, led to exacerbation or attenuation of apoptosis, necrosis or autophagy (Table 1). However, a limitation is that, in many studies, only one pathway is considered at any one time. In the future, it will be prudent to consider the multiple different component of cell death, that is apoptosis, necrosis, autophagy, and ER-mediated cell death.

Caspases, and other proteins, have long been considered for therapeutic intervention. However, direct targeting of caspases along with other proteins central to cell death, is not therapeutically viable because (i) caspase activation is associated with homeostatic functions other than cell death (Condorelli et al., 2001; Fujita et al., 2008; Nhan et al., 2006), and (ii) caspases are hotspots for destruction of cells with acquired mutations that can result in the expansion of a tumour mass. An attractive alternative for inhibiting cell death is by targeting kinases that work as upstream mediators of the cell death machinery, many of which have a direct role in cardiac muscle cell death and the development of cardiac pathology.

Table 1: Genetic models implicating cell death regulator genes in cardiac cell death

Gene	Disease Model	Phenotype	Reference
Caspase-1	*Casp1*$^{-/-}$	Reduced cardiomyocyte hypertrophy, increase survival, rescued decline of left ventricular function after MI	(Merkle et al., 2007)
	YVAD inhibitor	Attenuation of ischaemia-induced myocardial dysfunction (contractility improvement)	(Pomerantz et al., 2001)
Caspase-3	*Myh6-Casp3*	Nuclear and myofibrillar damage; increased infarct size with MI and decreased survival	(Condorelli et al., 2001)
Caspase-8	*Casp8*$^{-/-}$	Embryonic lethality (E11-E12.5), impaired cardiac muscle development and haematopoietic cell development; MEFs resistant to death-receptor-induced apoptosis	(Varfolomeev et al., 1998)
	Myh6-FKBP-Casp8 (conditionally active)	Massive cardiomyocyte apoptosis and death; low levels of casp-8 activity lead to sustained but low levels of apoptosis in mice that developed lethal DCM; abrogated with a pan-caspase inhibitor	(Wencker et al., 2003)
mPTP/CypD	CsA or SfA	Cell death inhibition (LDH release), improved left ventricular developed pressure (LVDP)	(Clarke et al., 2002)
	PPIF$^{-/-}$	Isolated mitochondria resistant to mPTP opening in response to Ca^{2+} and oxidative stress; mice resistant to I/R injury, but sensitive to apoptotic stimuli	(Baines, 2007; Baines et al., 2005; Nakayama et al., 2007)
VDAC	*Vdac1*$^{-/-}$ *Vdac3*$^{-/-}$ Double KO	Isolated cardiac mitochondria exhibit Ca^{2+}-induced swelling, no difference in cyt-c release, caspase cleavage in response to Bax and Bid compared to WT controls	(Baines et al., 2007)
TNFα	*Myh6-Tnf*	Higher heart weight–to–body weight ratio, reduced ejection fraction, cardiac inflammation, cardiomyocyte cell death,	(Kubota et al., 1997a)

		increased ANF mRNA	
	Myh6-Tnf	Spontaneous death of weaning mice, diffuse cardiac inflammation, and interstitial edema (severe myocarditis)	(Kubota et al., 1997b)
Nix/BNip3L	Tet-off ER-targeted Nix	Hearts were protected against cell death in *PPIF*$^{-/-}$ background; Bax/Bak-independent and mPTP-dependent cell death	(Chen et al., 2010)
	Tet-off Mitochondria-targeted Nix	Hearts were not protected against cell death in *PPIF*$^{-/-}$ background; Bax/Bak- and caspase-dependent apoptosis	
	Myh6-sNix	**Protection against peripartum cardiomyopathy in Gaq transgenic females**	(Yussman et al., 2002)
			(Diwan et al., 2007)
Bnip3	*Bnip3*$^{-/-}$	Diminished apoptosis in I/R, preserved LV systolic performance and diminished LV dilatation	
	Myh6-Bnip3	Increased apoptosis in unstressed mice leading to progressive LV dilatation; conditional overexpression exacerbates apoptosis and infarct size	
ATF6	*Myh6-ATF6-MER; Myh6-caATF6*	Better functional recovery (increased LVDP); reduced cell death (TUNEL-positive cardiomyocytes)	(Martindale et al., 2006; Toko et al., 2010)
	Myh6-dnATF6	LV dilatation, reduced fractional shortening and HF	(Toko et al., 2010)
PUMA	shRNA	Attenuation of ER-mediated cell death in response to TG or TU, measured by DNA fragmentation and cyt-c release	(Nickson et al., 2007)
	puma$^{-/-}$	Decrease in caspase-3 activation in cardiomyocytes treated with TG	
FasL (*CD95*)	*CD95*$^{-/-}$	Reduction in cell death from isolated hearts (in MI and Langendorff perfusion)	(Jeremias et al., 2000)

	CD95 OE	Increased cell death in NRVCs and in adult cardiomyocytes *in vivo*	(Lee et al., 2003)
TNFR1	*TNFR1*$^{-/-}$ *TNFR2*$^{-/-}$ Double KO	Increased infarct size in double KO compared to WT or single KO mice after MI with accelerated apoptosis	(Kurrelmeyer et al., 2000)
Bax	*Bax*$^{-/-}$	Decreased CK release, caspase-3 activity and infarct size after I/R from isolated hearts	(Hochhauser et al., 2003)
Apaf-1	Low levels of Apaf-1	Insensitive NRVCs to cyt-c release; sensitized by inhibition of XIAP or restoration of Apaf-1 levels	(Potts et al., 2005)
IAP Omi/HtrA2	Small molecule inhibitor against Omi/HtrA2	Reduction in infarct size and cardiac dysfunction in two independent rodent models following I/R; reduction in IAP loss; decrease in casp-9 and casp-3 activities	(Bhuiyan and Fukunaga, 2007; Liu et al., 2005a)
FADD	*FADD*$^{-/-}$	Embryonic lethality (E9–E12.5), impaired cardiomyogenesis and abdominal hemorrhage	(Yeh et al., 1998)
Bcl-2	*Myh6-Bcl2*	Increased functional recovery and decreased LDH release after I/R; decreased infarct sizes by 20% with fewer TUNEL-positive cardiomyocytes; decreased levels of mitochondrial AIF	(Chen et al., 2001c; Imahashi et al., 2004)
XIAP	*XIAP*$^{-/-}$	Isolated NRVCs die rapidly with cyt-c release	(Potts et al., 2003)
cFLIP	*casper*$^{-/-}$	Embryonic lethality, impaired heart development, increased FasL and TNF-induced apoptosis	(Yeh et al., 2000)
ARC	*nol3*$^{-/-}$	Larger infarcts after I/R; mice developed DCM after TAC	(Foo et al., 2007)
Nec-1	Small molecule inhibitor	RIP1 kinase inhibition; reduction of infarct size following I/R	(Lim et al., 2007)

LTCC	*Myh6-tTA* x Tet responder *Myh6-β2a*	Development of cardiac hypertrophy with interstitial fibrosis; increased cardiomyocyte cell death after Ca^{2+} overload	(Nakayama et al., 2007)
	LTCC inhibitor	Ca^{2+} influx-induced cell death and cardiomyopathy was prevented	

1.6. The protein kinase complement of the human genome

Kinases are enzymes that comprise universal signalling cascades that couple extracellular and intracellular inputs to diverse effector pathways of cell growth, survival, differentiation, apoptosis and chromosome integrity (Grueneberg *et al.,* 2008). The protein kinase complement (known as the kinome) has been catalogued in 2002 with 518 putative protein kinase genes and 106 protein kinase pseudogenes (Manning et al., 2002). Pseudogenes are defined as non-functional sequences of DNA derived from tandem duplication of functional gene sequence with ensuing loss of function (Balakirev and Ayala, 2003). Using genomic sequence analysis and chromosomal mapping the authors ascribed 244 kinases to disease loci or cancer amplicons (Manning et al., 2002). Nearly 60 years ago, the regulation of kinases has been described by reversible phosphorylation. Since then a considerable interest has been growing in the role of phosphorylation in regulating protein function with kinases involvement in homeostasis and disease. In the following sections I will introduce the mechanism of action of various kinases in myocardial disease, in relation to myocardial cell death, and their role as putative therapeutic targets.

1.6.1. Classification and mode of action

Proteins kinases form highly interactive networks to achieve their function in cells and as can be seen from the main dendogram (Fig. 8) they are divided in multiple families. Kinases are grouped together based on the sequence similarity of their kinase domains between different kinases that were derived from public sequences and gene prediction methods (Fig. 8) (Manning et al., 2002). In summary, the seven main families are: AGC family that comprises protein kinases A, G and C; CAMK family that contains Ca^{2+}/CAM-dependent PK; CK1 family – casein kinase 1; CMGC family that contains CDK, MAPK, GSK3 and CLKs; STE family that activates the MAPK family; the tyrosine kinases (TKs); and finally the tyrosine kinase-like (TKL) kinases (Manning et al., 2002). Most kinases, and other protein substrates, are modulated by autophosphorylation and phosphorylation by other kinases as a common form of signal transduction, modifications reversed by phosphatases. The second classification method is based on the type of the residues they phosphorylate. The two main classes are tyrosine kinases (TKs) and serine/threonine kinases where the catalysis process involves the transfer of a phosphate group from ATP onto the hydroxyl group of tyrosine or serine/threonine residues, respectively.

Diverse cellular processes depend on the signalling events of phosphorylation and dephosphorylation where protein kinases are regulated by secondary messengers (e.g. cyclic AMP, Ca^{2+}, hormones, neurotransmitters) in response to growth factors and under stress

conditions. Kinases act as cell surface trans-membrane receptors activated by ligand binding (receptor TKs) or other stimuli or as intracellular signal mediators launching a chain of kinase activation leading to gene transcription and functional changes (Kyriakis et al., 2012). Activation of receptor TKs is connected to intracellular events leading to the activation of phospholipase C, protein kinase C (PKC), mitogen-activated protein kinase (MAPK), and phosphatidylinositol 3-kinase (PI3K). One mechanism by which MAPKs ensure the specificity of action and the prevention of crosstalk between related upstream components is through interaction with docking domains of other kinases, scaffold proteins and transcription factors (Sharrocks et al., 2000). Another mechanism of how specificity is achieved by phosphorylation of the residues that flank the phospho-acceptor sites. However, some proteins (i.e. JunB) contain docking sites, but lack phospho-acceptor residues, which can act to recruit kinases (i.e. JNK) for trans-phosphorylation of other proteins (i.e. JunD). Thus, docking domains can serve for the formation of signalling complexes to enhance their own regulation or to bind to other transcriptional regulatory proteins found onto promoters (Sharrocks et al., 2000). Additionally, regulation of some kinases is facilitated by an auto-inhibitory domain ("on-site" repressor), which secures the activity of the functional domain (e.g. kinase domain) in an "off" state, thus interfering with its function (i.e. ligand binding, enzymatic activity or subcellular localization). Binding of a second molecule on the domain can reverse auto-inhibition (Kyriakis et al., 2012; Pufall and Graves, 2002).

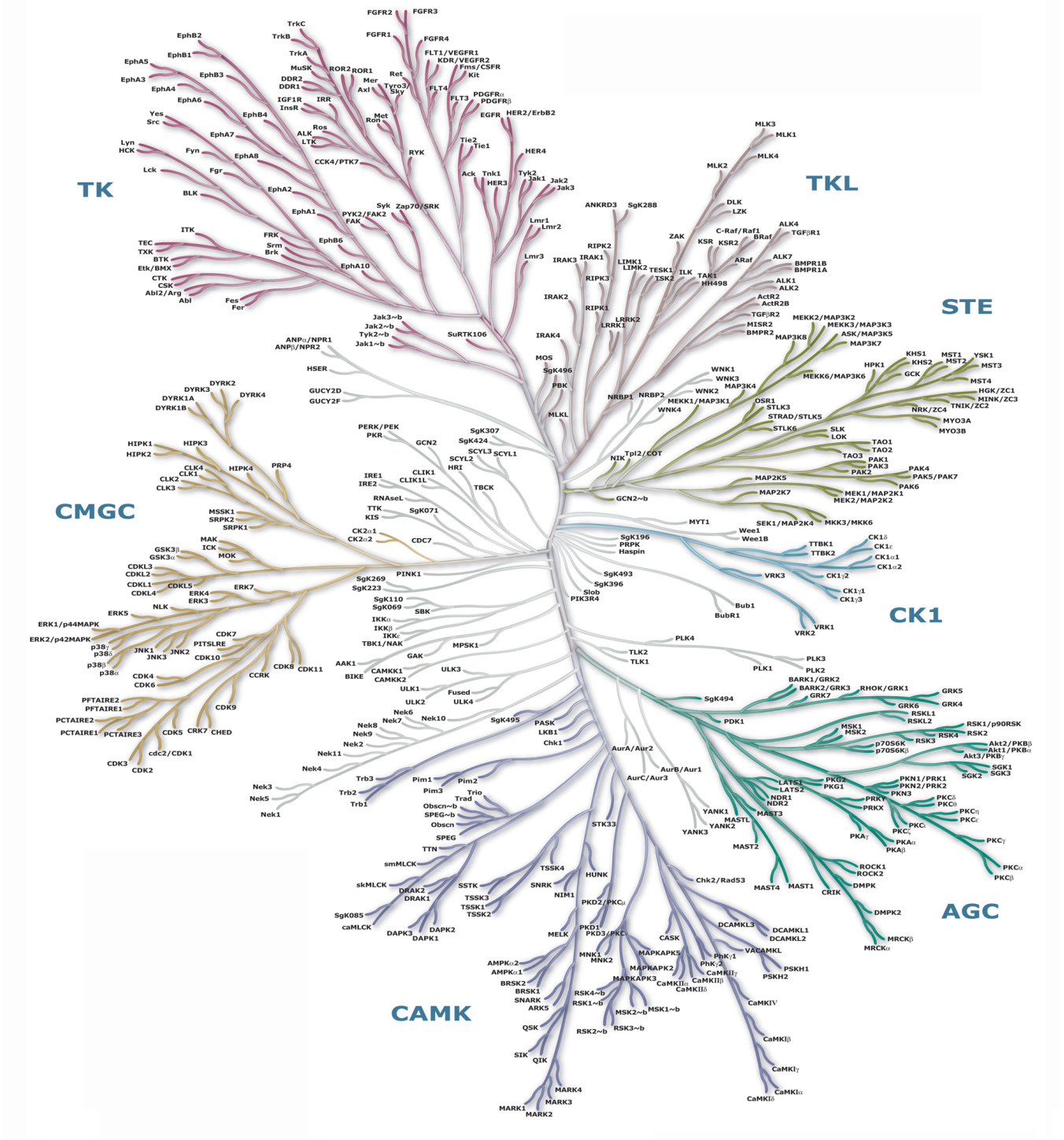


Figure 8: **Dendogram of the seven protein kinase families grouped based on protein sequence homology.** These are: the AGC family that comprises protein kinases A, G and C; CAMK family that contains Ca^{2+}/CAM-dependent PK; CK1 family – casein kinase 1; CMGC family that contains CDK, MAPK, GSK3 and CLKs; STE family that activates the MAPK family; the tyrosine kinases (TKs); and finally the tyrosine kinase-like (TKL) kinases family. Illustration reproduced courtesy of Cell Signaling Technology, Inc., taken with permission from (Manning et al., 2002); Reprinted with permission from AAAS.

1.6.2. Structure

Although kinase families have certain structural differences between them, they have a similar general structure of the ATP-binding pocket. The ATP-binding site consists of five areas: the sugar region, adenine region, hydrophobic pocket, hydrophobic channel and phosphate binding region (Engh and Bossemeyer, 2002; Shchemelinin et al., 2006). ATP comprises of two halves: the adenine region and the triphosphate, each requiring a distinct environment for binding. The triphosphate surface binds to a cluster of invariantly conserved kinase residues (Lys, Asp and Asn) directly involved in the enzymatic catalysis. In the active form of a protein, the ATP phosphates also interact with the sugar backbone (not conserved across the kinome, but conserved within the same family). The adenine-binding interactions, on the other hand, are much less conserved. The adenine region is hydrophobic where at least two key hydrogen bonds are formed of the N-1 and N-6 amino groups of the adenine ring with the NH and carbonyl groups of the adenine hinge region of the protein kinase. The ATP-binding site provides a surface area that engulfs the nucleotide, whereas adjacent sites allow the binding of molecules larger than adenosine (also known as the hydrophobic pocket and the hydrophobic channel), which can vary considerably within the kinase family and play a role in inhibitor selectivity (often called the “gatekeeper” residue) (Engh and Bossemeyer, 2002). An example of such inhibitor is dasatinib (Lombardo et al., 2004). Allosteric binding sites can also be found in pockets remote of the ATP binding site, into which when inhibitors bind can change conformation of the catalytic domain, rendering it inactive. Examples of inhibitors binding to these remote allosteric binding sites are targeting Akt1 and Akt2 (Li et al., 2009b), Chk1 (Converso et al., 2009) and MEK (Tecle et al., 2009).

The ATP-binding site is exploited by kinase inhibitors indicative of the steric interference with ATP binding as a major mechanism for kinase inactivation and is important in inhibitor selectivity and binding affinity (Shchemelinin et al., 2006). That is, small molecule inhibitors act in competition with ATP. The ATP binding site has been aggressively targeted for drug development – typically starting with a high-throughput screen of a compound library that contain structures conforming to size, polarity and other criteria allowing them to fit into the ATP binding site – rather than the protein-substrate binding site, since the latter approach is more chemically challenging. However, despite the fact that various methodologies for detecting kinase inhibition in compound screening are based on radioactive- or fluorescently-labelled phosphates or peptides, are considered the gold-standard in drug development, a major concern of targeting kinases via the ATP binding pocket is its similarity across kinases — the challenging but potentially surmountable issue of adequate kinase selectivity (Anderson et al., 2006).

Drugs that bind to substrate interaction sites, as an alternative to the ATP binding pocket offer another selectivity route (termed allosteric inhibition) (Engh and Bossemeyer, 2002).

However, interruptions of high-avidity protein interactions with a small molecule are difficult to achieve. Peptides have been made available that have high affinity and specificity, but cannot cross cell membranes similar to monoclonal antibodies, thus are not orally bioavailable. Increased specificity can be also achieved by an inhibitor that binds both the ATP binding and the protein substrate pocket (Anderson et al., 2006) or by interruption of secondary messengers (such as Ca^{2+} for CaMKII). Interruption of a kinase's localization, for example disrupting the membrane targeting function of a kinase for regulation of membrane-bound substrates, but not cytosolic substrates, might block only a subset of its function, and remains another novel approach of kinase targeting (Churchill et al., 2005; Dorn and Mochly-Rosen, 2002). This could be particularly attractive for targeting mutant kinases that lead to the development of genetic cardiomyopathies, similar to the stabilization, thus inhibition, of the inactive state of BCR-ABL by the binding of imatinib (Gleevec™) to the distorted ATP binding (Kerkela et al., 2006).

Antisense technology (RNAi) is another powerful tool for kinase inhibition by selective and complementary binding to the kinase's mRNA of interest with minimal off-target effects. One excellent example of this specificity of shRNAmir sequences can be found in the current thesis, where MAP4K4 inhibition is achieved and a lack of inhibition of its structural homologues TNIK and MINK kinases – something impossible with current pharmacological inhibitors – is demonstrated. Antisense technology offers excellent tools for pathway dissection in high-content cell-based screens for the discovery of refined drug targets, such as MAP4K4, and is discussed below.

1.6.3. Pharmacological targeting of proteins kinases for the treatment of CVD

Most clinically validated drugs for cardiovascular disease target G-protein-coupled receptors (GPCRs) localized in the cell membrane. Protein kinases, localized in the cytoplasm, are found downstream from the GPCRs and are rapidly emerging as promising drug targets in cardiovascular disease (Anderson et al., 2006). There are several reasons for the preference of the kinome as a drug development platform: their biochemistry is well known and based on the conserved three-dimensional structure of their kinase domain, and they can be effectively targeted by small-molecule inhibitors to precisely influence their diverse biological responses (Anderson et al., 2006; Grueneberg et al., 2008). Immunosuppressant drugs, cyclosporine (a potent inhibitor of calcineurin and CypD) and rapamycin (inhibitor of mTOR kinase) are used for the treatment of solid tumours, and Gleevec (inhibitor of ABL protein kinase) for the treatment of chronic myelogenous leukaemia (Cohen, 2002) are examples of kinase-targeted drugs with many others. Few kinase inhibitors for cardiovascular disease are currently in phase I/II clinical trials against ROCK, PKCδ, PI3K and p38, with many others in a preclinical stage (Table 2).

While GPCRs have a hierarchical position in signal transduction, inhibition at the level might not be optimal, as it cannot select between the beneficial and harmful effects in disease (Anderson et al., 2006). Inhibitory drugs might achieve superior biological specificity to a downstream kinases, such as MAPKs, something that remains to be seen in clinical practice. But, why is there so much interest for emerging therapies in myocardial disease using pharmacological inhibitors of protein kinases? What is the evidence that MAPKs have a pathophysiological role in heart diseases?

Table 2: Drug development for kinase targets in cardiovascular disease
(Adapted based on (Anderson et al., 2006)

Target	Compound	Indication	Most advanced stage of testing
p38 MAPK	VX-702[a]	Acute coronary syndromes	Phase II
PI3K	TG100-115[b]	Acute myocardial infarction	Phase I/II
PKCδ	KAI-9803[c]	Myocardial infarction, adjunct to angioplasty	Phase II
ROCK	Fasudil	Angina	Phase II[d]
p38 c-raf	Semapimod	Congestive heart failure	Preclinical[e]
CaMKII[f]	KN-93	Arrhythmia/Heart Failure	Preclinical
Cdk9	EXE-8647[g]	Acute cardioprotection	Preclinical
Chk2	NA	Cardiovascular disease	Preclinical
Grk2[h]	M119	Heart failure	Preclinical
HDAC kinase[i]	Trichostatin A MPT0E014	Heart failure/Fibrosis	Preclinical
HGK[j]	Compound 1 Compound 2	Cardiomyocyte survival	Preclinical
JAK2	AG490 (Tyrphostin)[k]	Heart failure	Preclinical[k]
JNK	JNK9395	Ischemia reperfusion injury	Preclinical
PKC ε	Activator Peptide (ψεRACK)[L]	Cardiovascular disease	Preclinical
PKC[m]	LY333531 (Ruboxistaurin) Ro-32-0432 Ro-31-8220	Heart failure	Preclinical[m]
PKCβ	LY379196	Heart failure	Preclinical[m]

Notes: [a]An oral p38 MAPK inhibitor (Vertex Pharmaceuticals Inc., Cambridge, MA). [b]PI3K-selective inhibitor (TargeGen Inc., San Diego, CA). [c]A PKCδ inhibitor (KAI Pharmaceuticals Inc., South San Francisco, CA). [d]Approved for the treatment of cerebral vasospasm in Japan. [e]Phase II for inflammatory disease. [f]End-stage human heart failure (dilated and ischaemic cardiomyopathy) where inhibition of CaMKII acutely improved contractility (Sossalla et al., 2010). [g]Discovered by Exelixis Inc in a high-throughput screen and is currently the most selective inhibitor against Cdk9 (Krystof et al., 2010). [h]Utility as a biomarker in heart failure (Johnson & Johnson). M119 inhibits GRK2 binding to $\beta G\beta_1\gamma_2$ subunit (Bonacci et al., 2006) and halted HF progression in mice (Casey et al., 2010) [i]Trichostatin A (TSA) attenuated cardiac hypertrophy by suppressing autophagy (Cao et al., 2011) and MPT0E014 had anti-fibrotic activity in rat hearts (Kao et al., 2013). [j]Pfizer compounds (Guimarães et al., 2011) and others currently being investigated in Prof. Michael D Schneider's lab. [k]Selective inhibition used for cancer treatment; patent by Daniel L. Beckles. CEP-701 (lestaurtinib) is currently in Phase I/II trials for patients with acute monocytic leukemia. [L]Activator peptide combined with δV1-1 (PKC δ inhibitor in isolated perfused hearts showed greater cardioprotection after I/R compared to each treatement alone (Inagaki et al., 2003). [m]Broad-activing PKC inhibitors (Liu et al., 2009b).

1.6.4. Mitogen-activated protein kinases (MAPKs)

MAPKs are involved in signalling pathways that primarily respond to mitogens and stress stimuli, the latter subfamily therefore also known as stress-activated protein kinases (SAPKs). They are implicated in cell division, differentiation, apoptosis, gene expression and metabolism. Perturbed regulation of MAPKs leads to deregulated signal transduction prominent in cancer, diabetes, and inflammatory and cardiovascular disease. They are activated by dual phosphorylation of conserved Thr/Tyr residues and target Ser/Thr residues of kinases, other substrates and scaffold proteins (Kyriakis et al., 2012). Their activity can be counter-regulated by dual-specificity protein phosphatases (MKPs) (Owens and Keyse, 2007).

The kinase signal transduction kinase hierarchy encompasses mainly three-tiered kinase cascades: upstream MAP kinase kinase kinase (MAPKKKs or MAP3Ks, e.g. MEKK1, TAK1 and ASK-1), downstream MAP kinase kinases (MAPKKs or MAP2Ks, e.g. MKK4, MKK7, MKK3 and MKK6) and terminal MAPKs or SAPKs, (e.g. ERK, JNK and p38). A MAP3K phosphorylates and activates a MAP2K, which in turn phosphorylates and activates a MAPK. From this point onwards, MAPKs phosphorylate non-kinase substrates, such as transcription factors or other kinases known as MAP kinase-activating protein kinases (MAPKAPKs). Frequently, a MAPKKK kinase (MAPKKKK or MAP4K) activates the MAP3Ks, both of which can be linked to the plasma membrane (Qi and Elion, 2005). A simplified schematic representation of the signal transduction kinase pathways is depicted in Figure 9.

MAP3Ks have large regulatory domains with functions of ubiquitination, autoinhibition and oligomerization and are typically activated by interactions with small GTPases, such as Rho and Ras regulators. MAP2Ks have smaller regulatory domains activated by dual phosphorylation of a conserved TxY motif in the activation segment (Kyriakis et al., 2012). Mammalian MAPK modules associate with numerous scaffolding proteins and regulate their activity and localization, thus affecting gene transcription programs of inflammation, apoptosis, growth and differentiation (Morrison, 2012; Qi and Elion, 2005).

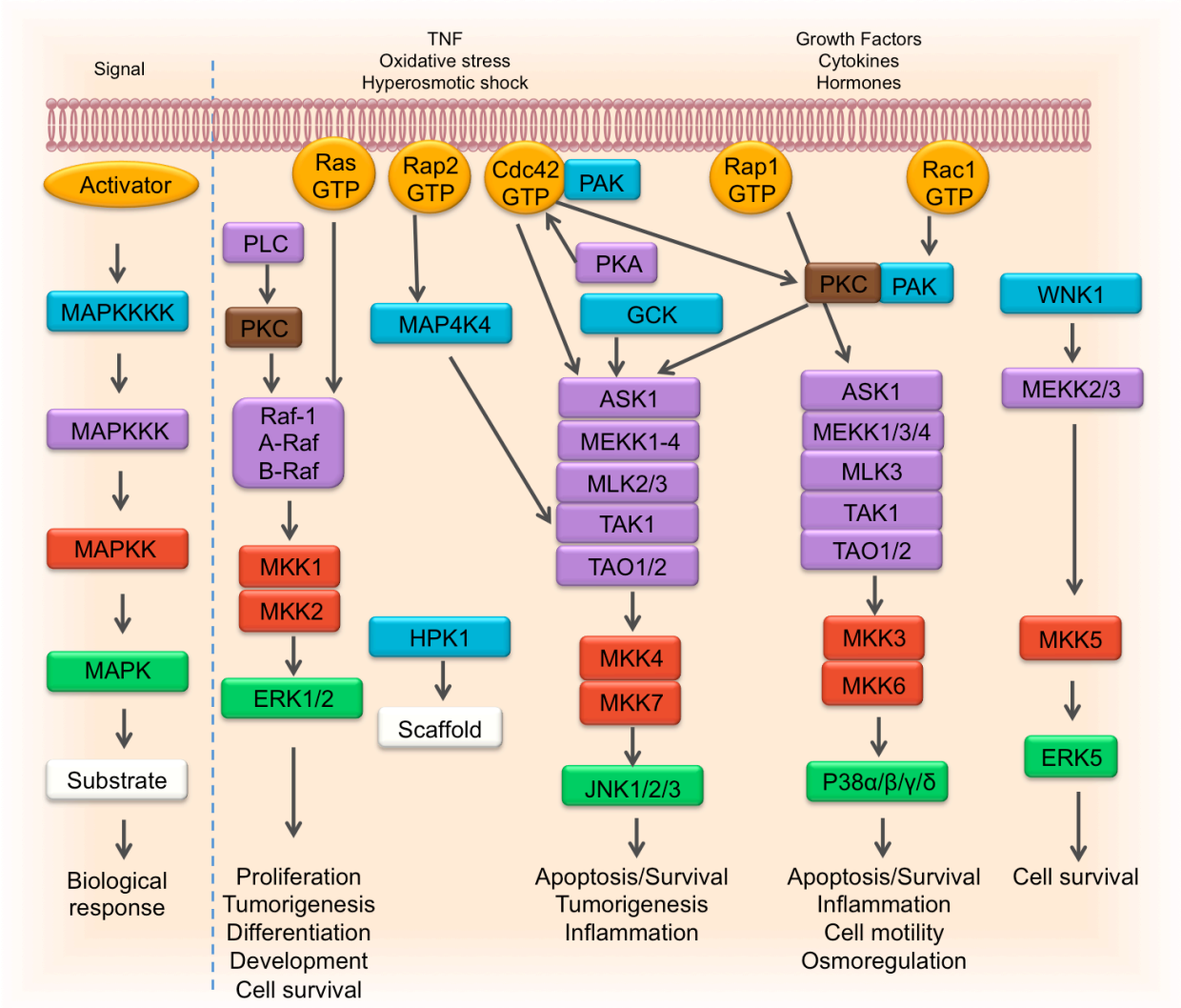


Figure 9: **Schematic representation of signal transduction pathways by various kinases.** The signal transduction pathway activated depends on cell type and stimuli (extracellular or intracellular). The three MAPK signalling pathways result in the activation of SAPKs, such as ERK1/2, JNK1/2/3, p38α/β/γ/δ, or ERK5 leading to a biological response that can be proliferation, apoptosis, differentiation, cell motility, osmoregulation and metabolism. Rap2-GTP has been shown to interact with MAP4K4 through its C-terminal citron homology domain (CHD). This interaction has enhanced MAP4K4-induced JNK activation (Machida et al., 2004).

1.6.4.1. ERK1/2

The Ras-Raf-MEK-ERK1/2 pathway is the founding or prototypic MAPK cascade, in which Ras acts as a molecular switch between tyrosine kinase (TK) receptors and downstream kinases MEK1/2 and ERK1/2 (Kyriakis et al., 2012). Ras is a small GTP-binding protein that induces activation of downstream Raf (a MAPKKK), which translocates from the membrane to the cytosol to activate MEK1 (MAPKK1) and ERK1/2. Ras mutations are frequently found in human tumours, thus classified as a proto-oncogene (Shih and Weinberg, 1982). The signal to ERK1/2 can also be transmitted via the phospholipase C (PLC) or the PI3K/Akt pathway. Active ERK is then released from MEK and can dimerize and translocate into the nucleus, where in turn it can phosphorylate many substrates including transcription factors. Alternatively, active ERK in the cytoplasm can phosphorylate kinases and cytoskeletal proteins (Ramos, 2008).

The pathway can be activated by mitogenic stimuli growth factors like EGF and PDGF, by insulin, or cytokines like interleukin-1β (IL-1β) (Wan et al., 2006; Yu et al., 2008) and cytokine transforming growth factor-β (TGF-β) (Ieda et al., 2009; Matsumoto-Ida et al., 2006), to modulate cell cycle progression, proliferation, cytokinesis, transcription, senescence, cell death, differentiation, migration, GAP junction formation, actin and microtubule networks, and cell adhesion (Ramos, 2008). ERK1 and ERK2 are required for immune system development, memory formation and heart development and aberrations in the signalling are a characteristic in a wide range of pathologies, such as cancers, diabetes and cardiovascular disease (Ramos, 2008).

ERK1/2 has many known targets, such as NFκB, AP-1, Myc, Ribosome S6 kinase (RSK), Bcl-2 and cytoskeletal scaffold protein known as paxillin (Roskoski, 2012). ERK1 and ERK2 are nearly 85% identical and ubiquitously expressed (although with variable tissue abundance). ERK1 null mice have a normal phenotype, whereas ERK2 null mice die at E6.5 and E8.5, demonstrating that both proteins are not completely redundant functionally. Knockout studies demonstrate importance of ERK1 in T cell responses, whereas of ERK2 in mesoderm differentiation, apoptosis and placenta formation (Agrawal et al., 2006; Yao et al., 2003). In the heart, this pathway is critically involved in cardiac development and hypertrophy, as discussed in detail in section 7.5.

1.6.4.2. JNK

JNK was discovered as a second MAPK subfamily through its ability to phosphorylate the transcription factor c-Jun at two sites upon UV radiation (Hibi et al., 1993). JNK is involved in proliferation, apoptosis, differentiation, cell motility, metabolism and cytokine production (Rose et al., 2010). Deregulation of JNK is described in neurological disorders, liver disease, obesity, diabetes, atherosclerosis, cancer and cardiac diseases. Robust activation of JNK occurs as a result of different stimuli, such as inflammatory cytokines, heat shock,

hyperosmolarity, I/R, UV, oxidative and ER stress, and DNA damage, and to a lesser extent by growth factors. MEKK1, MEKK2 and MEKK3 are MAP3Ks that stimulate JNK activation, as well as mixed lineage kinase 2 and 3 (MLK2, MLK3) (Kyriakis et al., 2012). MKK4 and MKK7 act downstream of MAP3Ks, to phosphorylate, thus activate, a Thr-Pro-Tyr motif of JNK. Substrates of JNKs involve nuclear, cytoplasmic and scaffolding proteins. JNK has the ability to shuttle between nucleus and cytoplasm to exert its effects depending on the stimuli and cell type (Weston and Davis, 2007).

There are three separate *JNK* genes (*JNK1*, *JNK2* and *JNK3*), all of which are alternatively spliced, producing 10 different JNK protein sequences in all, with more than 80% overall homology (Rose et al., 2010). JNK1 and JNK2 are ubiquitously expressed, whereas the pattern of JNK3 expression appears highest in the heart, brain and testis (Weston and Davis, 2007). Gene knockout studies have shown specific roles for different JNK kinases *in vivo*. Mice with disruption of *Jnk1*, *Jnk2* and *Jnk3* by homologous recombination are viable, but exhibit apoptosis and immune response defects (Weston and Davis, 2007). Distinct from this, the disruption of the upstream JNK-activating kinases MKK4 or MKK7 causes embryonic lethality, and disruption of both genes prevented JNK activation (Tournier et al., 2001). Fibroblasts isolated from $JNK1^{-/-}JNK2^{-/-}$ mice exhibit decreased proliferation and resistance to stress (UV)-induced apoptosis, via a defect in mitochondrial signalling and failing to release cyt-c (Tournier et al., 2000). Treatment of the cells with tumour necrosis factor (TNF), however, activates only MKK7. Gene-knockout studies of MKK7 demonstrate that this kinase is essential for TNF-stimulated JNK activation, whereas deficiency of MKK4 causes only a partial reduction in JNK activation. Together, these data suggest that dual phosphorylation (on Tyr and Thr) by both MKK4 and MKK7 is required for JNK to be activated in full (Tournier et al., 2001).

In the heart, JNK is activated by mechanical overload or I/R injury (Bogoyevitch et al., 1996; Ramirez et al., 1997; Wang et al., 1998a) and has a role in the heart related to hypertrophy, heart remodelling and cardiac muscle cell death (Wang et al., 2007) (see section 6.6 and 6.7).

1.6.4.3. p38 kinase

p38 is the third major MAPK, originally isolated as a phosphorylated protein from stimulated macrophages, and was described as inhibiting the production of proinflammatory cytokines (Han et al., 1994). Four different isoforms of p38 have been identified; the prototypic p38α (reffered to as just p38), p38β, p38γ (ERK6 or SAPK3) and p38δ (or SAPK4). The first two isoforms are ubiquitously expressed, while p38γ is primarilly present in skeletal muscle and p38δ in the lung, kidney, pancreas, small intestine and testis (Ono and Han, 2000). Thus, only p38α and p38β are thought to be directly relevant to cardiomyocytes and other cells of the heart. All isoforms share more than 60% overall sequence homology and more than 90%

identity within the kinase domains, but display kinetic differences in the level of activation (Coulthard et al., 2009b). p38 kinase responds to UV radiation, heat, osmotic shock, pathogens, growth factors and inflammatory cytokines. Knocking out p38 leads to embryonic lethality because of placental and erythroid differentiation defects, whereas mice lacking any other p38 isoform appear phenotypically normal, demonstrating functional redundancy of the three β, γ, and δ isoforms in embryonic development (Coulthard et al., 2009a).

The canonical pathway for p38 activation is formally similar to the JNK and ERK1/2 pathways: a number of upstream MAP3Ks including MEKK1-4, TAK1 and ASK activate MKK3, MKK6 and possibly MKK4 at the MAP2K level. However, in addition, “non-canonical” p38 activation occurs via TAB1 protein (De Nicola et al., 2013), previously mentioned as complexed with TAK1 via a necrosis-mediated death receptor pathway. Once activated, p38 functions in the nucleus and the cytoplasm by targeting transcription factors or cytoplasmic proteins, respectively. p38 is involved in numerous biological roles, such as promoting expression of proinflammatory cytokines (interleukins; IL-1β, IL-6, TNFα, adhesion proteins; VCAM-1), regulating proliferation, differentiation, cell growth and senescence; processes deregulated in chronic inflammatory conditions, tumorigenesis, Alzheimer’s and CVD (Rose et al., 2010).

In the heart, p38 reportedly regulates a cardiac gene program for the development of myocyte hypertrophy, inflammation, metabolism, contractility, proliferation and cell death, though with significant controversies as to how p38 leads to cardiac pathologies (Wang et al., 2007) (see section 6.6 and 6.7).

1.6.4.4. ERK5

The final classic MAPK and least studied among the four is ERK5, involved in both growth and stress signalling responses (Wang et al., 2007). This kinase was discovered using a yeast two-hybrid screen using MEK5 mutants as bait (Zhou et al., 1995), while at the same time a second group used a PCR strategy to clone novel MAPKs (Lee et al., 1995). ERK5 is most abundant in the heart, skeletal tissue, placenta and kidney among adult human tissues. The most distinguishing feature is its length of 816 amino acids, more than twice the size of other MAPKs, due to a large C-terminal extension. The gene undergoes alternative splicing to generate four species: ERK5α, ERK5β, ERK5c and ERK5-T, the former being most abundant. ERK5β and ERK5c splice variants were found to utilize the C-terminus, which contains a putative nuclear localization signal allowing activation of MEF2c (Yan et al., 2001). In contrast, the N-terminus is important for the cytoplasmic targeting required for association with MEK5 (Yan et al., 2001). ERK5-T was shown to interact with itself and ERK5, in stimulated and unstimulated cells, functioning as negative regulator of ERK5α by preventing its nuclear localization (McCaw et al., 2005).

A variety of growth factors (EGF, NGF, VEGF, FGF-2), serum, hyperosmotic stress, oxidative stress and UV have been shown to induce ERK5 activity. The best-studied MAP3Ks shown to activate ERK5 are MEKK2 and MEKK3, via activating MEK5. Other kinases and transcription factors in the nucleus are targeted substrates for ERK5, while scaffold proteins also influence its activity. Biological roles of ERK5 are survival, differentiation, proliferation and growth.

Global deletion of ERK5 resulted in embryonic lethality (E9.5-E10.5) due to cardiac development defects, defects in placental angiogenesis, extra-embryonic and embryonic vasculature (Regan et al., 2002). In a separate study, conditional ablation in adult tissues including the heart, brain and lung resulted in acute haemorrhages, vascular leakage and vascular defects. Endothelial-specific ablation triggered cardiovascular defects (not observed with cardiomyocyte-specific ERK5 inactivation) and consequently early embryonic lethality (Hayashi et al., 2004). This is indicative that the primary cause of embryonic lethality after germline deletion was vascular defects, not the concurrent heart malformations. The same study also demonstrated that ERK5 delivers a survival mechanism in endothelial cells via MEF2C as substrate (Hayashi et al., 2004). Mice with a cardiomyocyte-specific deletion of ERK5 demonstrated decreased hypertrophic growth and fibrosis and increased apoptosis with upregulated levels of p53 and Bad proteins. Silencing of ERK5 using a pharmacological inhibitor in NRVCs attenuated hypertrophy (Kimura et al., 2010; Tatake et al., 2008). Thus, ERK5 has a pro-hypertrophic and anti-apoptotic role in the heart.

1.6.5. MAPKs in heart function and disease

MAP kinases are ubiquitously expressed and their specific heart roles has been an intensive focus for more than a decade, with recognizable functions in cardiac development (review by (Rose et al., 2010)) and at different stages of heart disease progression, such as hypertrophy, dilated cardiomyopathy and I/R injury. Significant insights into their *in vivo* function in cardiac physiology and pathology, their regulatory mechanisms and potential downstream targets have been revealed from engineered animal models and kinase-specific inhibitors (Wang et al., 2007). Below is an overview of the recent advances in the field of MAPK pathways in cardiac protection and pathology, highlighting some controversies, outstanding issues and future research directions (Wang et al., 2007). The following section will focus on the role of MAPKs and of their upstream mediators (MAP2Ks, MAP3Ks and MAP4Ks) in cardiomyocytes though it is fully appreciated that fibroblasts and other heart cells also contribute to the pathological manifestations of heart failure. The following text is divided into two major sections describing in detail the involvement of MAPKs (i.e. ERK1/2, JNK and p38) in (i) cardiac hypertrophy and chronic heart failure, and (ii) in cardioprotection and cardiac muscle cell death. Following this, I will present in a similar manner the role of kinases upstream of the MAPKs, finally focusing on evidence around MAP4K4.

1.6.6. MAPKs in cardiac hypertrophy, chronic heart failure and post-ischaemic remodelling

As mentioned earlier, cardiac hypertrophy *without* dysfunction can be an initial compensatory mechanism to external stressors (helping correct the increase in wall stress dictated by the law of Laplace), evolving into more severe hypertrophy *with* contractile dysfunction if the pathobiological signals persist (Bernardo et al., 2010). These stressors for pathological cardiac hypertrophy – as well as physiological cardiac hypertrophy – elicit intracellular signalling pathways involving MAPKs. MAPK signalling is initiated in cardiomyocytes from G-protein-coupled receptors (GPCRs) (e.g. angiotensin II, ET-1, α and β adrenergic receptors [ARs]) and from receptor tyrosine kinases (RTKs) (e.g. insulin-like growth factor [IGF-I], TGF-β and fibroblast growth factor [FGF-β], glycoprotein 130 [gp130], platelet-derived growth factor [PDGF] receptor) (Bueno and Molkentin, 2002).

Several growth factors and RTKs are implicated in the pathogenesis of cardiac hypertrophy and heart failure. Early studies found elevated serum IGF-I levels in cardiac hypertrophy in both rodents and humans (Li et al., 1997; Serneri et al., 1999), but without the activation of hypertrophy gene markers (i.e. collagen III, ANF, α-skeletal actin) in response to pressure overload induced by TAC (Tanaka et al., 1998). Treatment of mice with IGF-I with LV dysfunction after MI showed significant improvement in the cardiac output (i.e. ejection fraction) compared to the untreated controls, suggesting a beneficial effect (Duerr et al., 1995). In addition, transgenic mice overexpressing IGF-IR displayed cardiac hypertrophy without any evidence of cell death and fibrosis (McMullen et al., 2004); an effect prevented by a dominant-negative PI3K mutant. Taken together, IGF-I plays a role in physiological rather than pathological hypertrophy. Indeed, elevated serum levels of IGF-I were found in competitive swimmers and in rodents that underwent chronic exercise (Koziris et al., 1999; Yeh et al., 1994). Furthermore, local (pericardial) IGF-I signalling seems to be regulated differently from the systemic IGF-I system since pericardial IGF-I serum levels were increased in HF patients, whereas the plasma IGF-I levels were not; indicating a compensatory mechanism for LV dysfunction (Abe et al., 2006).

TGF-β mRNA levels are elevated during the transition of cardiac hypertrophy to HF in both rodents and humans (Hein et al., 2003; Takahashi et al., 1994; Villarreal and Dillmann, 1992; Zhang et al., 2000). Cardiac-specific overexpression of PDGF resulted in cardiac hypertrophy with sex-dependent differences; where only females exhibited severe dilated cardiomyopathy with HF and sudden death (Pontén et al., 2003). However, both sexes had phenotypes of altered vasculature implicating PDGF in fibrosis and heart vascularization (Pontén et al., 2003). In addition to its role in immunity, gp130, a common signal transducing subunit of cytokine receptor complex has been implicated in HF. Constitutive expression of gp130 lead to ventricular hypertrophy (Hirota et al., 1995), while mice with cardiac-specific

dominant-negative gp130 blunted cardiac hypertrophy without increased apoptosis after TAC (Uozumi et al., 2001). Contrary, ventricular-specific (i.e. *MLC2v* promoter) knockout mice of gp130 display rapid onset of apoptosis and dilated cardiomyopathy (Hirota et al., 1999). The discrepancies between the two studies can be explained by (i) the differences in the methods for applying pressure overload (i.e. TAC induces stronger pressure compared to constriction of the abdominal aorta) and (ii) the type of model (i.e. dominant-negative vs. null mice).

GPCRs are another class of receptors that regulate chronotropy, inotropy and cardiac growth and are important in the pathophysiology of cardiac hypertrophy and HF. GPCRs are transmembrane receptors that upon extracellular ligand binding undergo a conformational change and coupling of their intracellular domain with a G-proteins (themselves classified into fours families based on their a subunits; Gs, Gi, Gq, and Gα) with the simultaneous conversion of GDP to GTP (Chen and Rockman, 2008). There are three families of regulatory molecules involved in the desensitization of a GPCR response and these are second-messenger regulated kinases (PKA, PKC), G-protein-coupled receptor protein kinase (GRKs) and arrestins. Arrestins serve as scaffold molecules for internalization of receptors and GPCR-mediated cell signalling. β-ARs are the predominant type in the heart muscle and abnormal signalling results in abnormal contractility (Chen and Rockman, 2008). α-ARs are also found in the heart muscle, but at a smaller ratio compared to β-ARs, which respond to norepinephrine and phenylephrine (PE) to mobilise Ca^{2+} via the PKC/PLC pathway. Several transgenic models have been developed to elucidate the mechanistic role of β-ARs (Engelhardt et al., 1999; Liggett et al., 2000; Rohrer et al., 1996; Sheridan et al., 2000) and α-ARs (Akhter et al., 1997; Milano et al., 1994; Vecchione et al., 2002) in HF.

The various receptors introduced above transmit signals into intracellular pathways to mediate responses of hypertrophy, cell death, extracellular tissue remodelling, and inflammation. The following section focuses on the involvement of various MAPK signalling axes in cardiac hypertrophy leading to HF, followed by their involvement in cardiac muscle cell death.

1.6.5.1. ERK1/2 pathway

Many studies implicate the Ras/Raf/MEK1/ERK1/2 pathway in the development of cardiac hypertrophy. Two early studies used transgenic mice with cardiac-specific overexpression of a constitutively activated Ras (H-Ras^{V12}). In one, homozygous mice displayed cardiac muscle hypertrophy associated with cardiomyocyte hypertrophy, up-regulated atrial natriuretic factor (ANF), and disarrayed myofibrils (Tanaka, 1995). In the other, transgenic Ras hearts developed hypertrophy with postnatal lethal heart failure (Zheng et al., 2004). Isolated adult ventricular cardiomyocytes had depressed calcium transients with

reduced RNA levels of phospholamban (PLN) and sarco-endoplasmic reticulum Ca^{2+}-ATPase (SERCA) 2a, and reduced phosphorylated PLN protein. Overall these Ras-induced contractile defects were not attributed to decreased L-type channel activities or disruption of the sarcomere, but rather to suppressed SR calcium uptake. Mice also displayed myofilament disarray and interstitial fibrosis (Zheng et al., 2004).

While both studies used the same H-Ras^{V12} coding sequences, they used different promoters (MLC-2v and αMHC, respectively), perhaps explaining the milder cardiac hypertrophy in the first study versus lethal cardiomyopathy in the second. This can be attributed to the different strength of the promoters leading to dose-dependent effects of Ras signalling. Another key difference in the design of the studies is their use of a simple transgene for active Ras (Tanaka, 1995), versus excision of a stop signal by *cre* recombination under MLC-2v control to achieve the tissue specificity (Zheng et al., 2004). Excess Ras activity led to the development of cardiac pathological changes such as reduced cardiac output and electrophysiological abnormalities associated with altered ion channel proteins and expression of genes involved in the hypertrophy program.

Upregulated levels of human c-H-*ras* RNA were found in patients with hypertrophic cardiomyopathy (HCM) as a secondary result of mutations in βMHC (Kai et al., 1998). Likewise, increased Ras/Raf/MEK/ERK1/2 activity has been a biological similarity between patients of Costello, Cardio-facio-cutaneous (CFC), Noonan and LEOPARD syndromes, all of which exhibit cardiac defects and develop hypertrophic cardiomyopathy (Kai et al., 1998). These patients carry mutations in all c-*Ras* genes – or other gene mutations (i.e. *SHP-2*, *PTPN11*) – that is however unclear how the activity of the pathway is affected as various mutations exists that increase or decrease Ras signalling (Gelb, 2006). Furthermore, a proportion of Noonan and LEOPARD patients develop HCM ascribed to missense gain-of-function mutations of *RAF1,* which encodes the Ser/Thr kinase that activates MEK1/2 (Pandit et al., 2007). Similarly, cardiomyocyte hypertrophy was provoked *in vitro* in neonatal ventricular rat cardiomyocytes (NVRCs) by constitutively active MEK1, while the dominant-negative form attenuated the response to agonists like ET-1, PE and isoproterenol (Ueyama et al., 2000). However, unlike the Ras transgenic models, MEK1 overexpression in the heart led to compensated cardiac hypertrophy without signs of fibrosis or dysfunction (Bueno and Molkentin, 2002), suggesting that cardiac pathology induced by Ras activation is not explained exclusively by MEK1/2. Technically, the discrepancies between the two studies (Ueyema vs. Bueno) can be attributed to the strength of the promoter regulating constitutively active MEK1.

Conversely, mechanical unloading by left ventricular assist devices (LVAD) reverses cardiac hypertrophy, associated with decreased ERK activity (Flesch et al., 2001). Indeed, complementary to the gain-of-function approaches above, cardiac hypertrophy and fetal gene induction in response to pressure overload were attenuated by inhibition of the ERK pathway

using dominant-negative Raf (Harris et al., 2004). Likewise, cardiac-specific Raf-1 knockout mice demonstrated left ventricular dysfunction and heart dilatation, but without cardiac hypertrophy (Yamaguchi et al., 2004). Although both groups found apparent lack of hypertrophy, there was a significant increase in the cardiomyocyte apoptosis associated with Raf inactivation (Harris et al., 2004; Yamaguchi et al., 2004), consistent with the partial resistance of NRVCs to apoptotic stimuli conferred by adenoviral expression of constitutively active MEK1 defined by TUNEL staining and caspase-3 activity (Bueno et al., 2000). These observations suggest that Raf-1 promotes cardiomyocyte survival through a MEK/ERK1/2-independent mechanism. Similar to the phenotype observed in c-raf-1 KO animals, mice with cardiac-specific deletion of *SHP2* gene exhibit dilated cardiomyopathy without hypertrophy after pressure overload and Shp2-null cardiomyocytes have diminished ERK activity (Kontaridis et al., 2008).

Interestingly, left ventricular dysfunction and apoptosis in Raf-1 KO hearts were rescued by inactivation of a second gene, for apoptosis signal-regulating kinase 1 (ASK1). A variety of stress stimuli activate ASK1 (e.g., TNFα, ROS and Fas), which in turn phosphorylates both MKK4/7 and MKK3/6, the activators of JNK and p38, respectively. Raf-1 appears to bind ASK1 and suppresses its apoptotic activity (Chen et al., 2001a). Proteomic analysis of Raf-1 signalling complexes suggests that Raf-1 also blocks apoptosis by suppressing the dimerization and phosphorylation of the activation loop of mammalian sterile 20-like kinase (MST2) (ONeill et al., 2004).

In the heart ERK1/2 activation was induced, in part, in response to IGF-1 and cardiotrophin-1 (CT-1) with anti-apoptotic effects (Párrizas et al., 1997; Sheng et al., 1997) and via GPCRs (in response to PE, angiotensin-II, and endothlin-I). β-ARs (β1 and β2), activated by β-adrenergic agonists, associate with arrestins leading to receptor internalization and ERK1/2 activation via direct interaction (Cervantes et al., 2010; Noma et al., 2007). β-ARs which have dentrimental effects when activated in failing hearts, utilise β-arrestin to activate ERK – independently of the classical mode of α-AR activation (that is via PKA and PKC) – via EGFR transactivation. This mode of ERK actvity is thought to be cardioprotective (Noma et al., 2007).

Likewise, treatment of α-ARs and angiotensin receptors with pharmacological blockers (Xiao et al., 2001b; Yue et al., 2000) and ROS scavengers (Xiao et al., 2001a) have been shown to prevent ERK activation and cardiomyocyte hypertrophy. ERK1/2 was shown to target specific downstream targets involved in cardiac hypertrophy by an autophosphorylation mechanism at Thr188 site of ERK1/2. Phosphorylation at this side required phosphorylation of the TY motif, dimerization and binding of ERK1/2 to Gβγ subunits. (Lorenz et al., 2009). ERK1/2 autophosphorylation at Thr188 was observed in hypertrophic mouse hearts induced by TAC, human failing hearts, and isolated NRVCs treated with angiotensin-II (Lorenz et al., 2009). Moreover, the temporal and spatial patterns of ERK1/2 activation were agonist-

dependent. Epinephrine treatment (targeting both α- and β-ARs) induced transient cytosolic ERK1/2 phosphorylation, while phenylephrine (α-AR-specific agonist) induced prolonged nuclear accummulation (Cervantes et al., 2010). However, blocking β-ARs by blockers and by using β-AR-null cardiac fibroblasts prevented nuclear translocation of the α1-AR-induced ERK1/2 activation, that was shown to be dependent on arrestin recruitment (Cervantes et al., 2010). In light to this evidence, ERK1/2 activation is a result of crosstalk between α- and β-ARs and arrestin recruitment – even thought the exact binding mechanisms of ERK to arrestin remains to be elucidated.

In summary, ERK1/2 can be activated via classic receptor tyrosine kinases and GPCRs and play a significant role in cardiac hypertrophy and protection to cell death. In general, the Ras/Raf/MEK/ERK1/2 pathway is regarded as pro-hypertrophic and pro-survival, but not a necessary component for the development of cardiomyocyte hypertrophy (Rose et al., 2010).

1.6.5.2. JNK pathway

The evidence around JNK's role in cardiac hypertrophy, compared to ERK1/2, is less consistent and therefore more confusing. Early studies in cultured NRVCs used overexpression of a constitutively active MKK7, leading to the over-activation of JNK (but not ERK1/2 or p38) and the characteristic features of hypertrophy (e.g., increased cell size and elevated ANF) (Wang et al., 1998a). Conversely, dominant-negative MKK4 blocked ET-1-induced JNK activity (with no effect on ERK1/2 and p38) and abrogated the hypertrophic response (Choukroun et al., 1998). Furthermore, delivering the dominant-negative MKK4 adenovirus to rat hearts inhibited cardiac hypertrophy following pressure overload, as determined by echocardiographic parameters and lack of ANF expression (Choukroun et al., 1999). In these animals, c-Jun activity was decreased compared to the littermate controls and these findings would suggest that JNK has a pro-hypertrophic role in the heart.

However in later studies, cardiac-specific deletion of MKK4 exacerbated pathological cardiac hypertrophy and apoptosis in response to pressure overload and chronic β-adrenergic stimulation, whereas MKK4 was dispensable for exercise-induced physiological hypertrophy (Liu et al., 2009c). In support of this anti-hypertrophic role of JNK, tamoxifen-inducible activation of JNK in the adult heart by a constitutive form of MKK7 caused progressive lethal cardiomyopathy shown by the fetal gene expression program and morphological changes, but without hypertrophy itself, i.e., without a net increase in cardiac mass or myocyte cross-sectional area (Petrich et al., 2004; 2003). Additionally, disruption of JNK1 or JNK2 activity in the adult myocardium by a dominant-negative mutant of JNK1 and JNK2 expressed from the αMHC promoter contributed significantly to hypertrophy, that was exacerbated in double knock-out mice lacking JNK1/2 (Liang et al., 2003). This body of work suggests that MKK4/JNK1/2 axis is essential to prevent maladaptive hypertrophic remodeling and is required for

cardiomyocyte survival, whereas diminished JNK activity renders the hearts more susceptible to growth. Deletion of JNK was accompanied with an increase in fibrosis flowing pressure overload (Tachibana et al., 2006) and chronic treatment (for 20 weeks) of a cardiomyopathy hamster model with a JNK inhibitor exhibited increased apoptosis and cardiac fibrosis associated with LV chamber dilatation (Kyoi et al., 2006).

The postulated anti-hypertrophic role of JNK is partly attributed to the inhibition of NFAT nuclear translocation in cardiomyocytes. NFAT is a nuclear transcription factor positively regulated by calcineurin in response to elevated calcium. Activation of calcineurin leads to the dephosphorylation of NFAT localized in the cytoplasm facilitating its nuclear translocation (Liang et al., 2003). Inhibition of JNK (by dominant-negative JNK1/2) leads to the enhancement of nuclear localization and activity of NFAT both *in vivo* and *in vitro* (Liang et al., 2003; Liu et al., 2009c). The fact that JNK inhibition caused enhanced stimulus-induced cardiac hypertrophy and nuclear localization of NFAT suggests that JNK's anti-hypertrophic role derives from this negative regulation of the Calcineurin-NFAT growth-inducing pathway in the heart. In another investigation, mice with deletion of *Jnk1*, *Jnk2* or *Jnk3* each displayed hypertrophy similar to WT littermates after pressure overload (TAC), though *Jnk*$1^{-/-}$ mice uniquely showed severe cardiac apoptosis, inflammation and dysfunction (Tachibana et al., 2006).

Furthermore, two studies report conflicting result about the role of MEKK1-JNK signalling in response to pressure overload, one suggesting a pro-hypertrophic role while the second suggests a protective anti-hypertrophy role. Minamono *et al.,* demonstrated that MEKK1 is required in ESC-derived cardiomyocytes for JNK activation and subsequent c-Jun phosphorylation induced by oxidative stress and that cardiac-specific G_q requires *MEKK1* for cardiac enlargement, ANF induction, and mechanical dysfunction (Minamino et al., 2002). Following pressure overload, *Mekk1*$^{-/-}$ mice showed decreased levels of JNK activity, and cytokine induction compared to the controls, though not interference with cardiac hypertrophy, and at two weeks showed even greater apoptosis, inflammatory infiltration, and mechanical impairment (Sadoshima et al., 2002).

In summary, while most *in vitro* studies support the pro-hypertrophic role of JNK, the majority of *in vivo* studies do not concur with these conclusions. Some differences between studies may relate to the differences in biology and time-course between cell culture and whole-animal experiments, but also the use of germline mutations, versus cardiomyocyte-restricted ones. An anti-hypertrophic role of JNK could involve the NFAT-calcineurin mechanism alredy discussed, or potentially the requirement of JunD, a transcription factor substrate shown to prevent cardiomyocyte hypertrophy in response to both PE and pressure overload in cell culture and animal models (Hilfiker-Kleiner et al., 2006; 2005). Thus, distinct from its ambiguous role in hypertrophic growth per se, JNK may have a role in pathological remodelling.

1.6.5.3. p38 pathway

As with JNK, p38 was concluded to promote cardiac growth and hypertrophy in cell culture, results that could not be extrapolated to the intact heart given the lack of a hypertrophic effect in mice. Thus, the implication of p38 and its upstream regulators (MKK3, MKK6) as mediators of cardiac hypertrophy have been mostly acquired from culture of NRVCs. Inhibition of this pathway by p38 inhibitors (SB203580, SB202190) or by dominant-negative p38 showed inhibition of myocyte growth in response to hypertrophic agonists, such as PE and ET-1 (Nemoto et al., 1998; Wang et al., 1998b). Overactivation of p38 by overexpressed MKK6 or by activating mutations in MKK6 and MKK3, induced hypertrophic changes like augmented cell size, promoter activities of ANF and α-skeletal actin measured by luciferase assay and enhanced sarcomere organization in response to PE (Wang et al., 1998b; Zechner et al., 1997). Thus, cardiomyocyte hypertrophy is mediated by p38, but suppressed by JNK.

Furthermore, whereas mutationally activated MKK6 caused hypertrophy, the corresponding mutation of MKK3 showed chiefly an additional increase in apoptosis that was increased by co-expression of p38α and suppressed by dominant-negative p38α. Regardless of the suggested difference in isoform function, the main thrust of studies, with some exceptions (Choukroun et al., 1998), support the hypothesis that p38 plays a causative role in hypertrophy, at least in NRVCs. However, cardiac muscle cell hypertrophy and apoptosis were later shown to result from distinct members of the p38 kinase family, with p38β having a role in inducing a hypertrophic response, whereas p38α increasing apoptosis (Wang et al., 1998b).

Having in mind the limitations of using *in vitro* cultures as a model of investigating pathological adult hypertrophy, targeted activation of p38 was studied in mouse myocardium by a gene-switch transgenic approach with activating mutations of MKK6 and MKK3 specifically expressed in ventricular myocytes. Both transgenic lines resulted in depression of systolic contractility and compromised diastolic function and died prematurely from HF, but did not exhibit significant hypertrophy on an organ level revealed by echocardiography. MKK3 transgenic hearts showed extensive interstitial fibrosis, ventricular wall thinning and heterogeneous myocyte atrophy (Liao et al., 2001), whereas MKK6 transgenic hearts had mild myocyte hypertrophy. The severity of the MKK3 transgenic mice can be explained by the preferential activation of p38α through dual-phosphorylation by MKK3, leading to increased cell death (Wang et al., 1998b).

Conversely, cardiac-specific expression of dominant-negative mutants of p38 α and p38 β led to cardiac hypertrophy 7 days after TAC, but with resistance to cardiac fibrosis (Zhang et al., 2003). Examined cardiac tissue showed typical myocyte enlargement with preserved

myofibrillar structure, and gene expression revealed increased in *ANF* and reduced *SERCA*. Moreover, transgenic mice with cardiac-specific dominant-negative p38α, MKK3 and MKK6 exhibited progressive cardiac hypertrophy with increased cardiac dilatation at baseline and exacerbated hypertrophy following TAC, angiotensin-II, isoproterenol and phenylephrine infusion (Braz et al., 2003). Mechanistically, p38 was shown to negatively regulate the nuclear shuttling of NFAT transcription factors, thus antagonising Calcineurin signaling. This was demonstrated by increased in luciferase activity in cardiac extracts collected from double transgenic mice carrying an NFAT-luciferase-reporter (containing nine repeats of the NFAT-binding site upstream to the αMHC promoter) and dominant-negative p38α. This suggests that inhibition of p38 enhances NFAT transctriptional activity. Furthermore, genetic disruption of Calcineurin *Aβ* rescued the hypertrophic cardiomyopathy observed in the dominant-negative p38 mice (Braz et al., 2003; Molkentin, 2004). In a loss-of-function investigation, cardiac-specific deletion of p38α did not alter pressure overload-induced hypertrophy, compared to the wild-type animals, but caused significant cardiac dysfunction and heart dilatation in banded mice accompanied by increased apoptosis and fibrosis (Nishida et al., 2004). Taken together, these findings indicate that p38 is not involved in promoting cardiac hypertrophy, but plays an important role in cardiac cell death and pathological remodelling, conclusions similar to those for JNK.

By contrast, p38 may make a clearer contribution in «physiological» hypertrophy in response to exercise. This is suggested by deletion of ASK1 (MAP3K5), an upstream activator of both JNK and p38, and is shown more directly by conditional knockout of p38 in the myocardium, which the authors attribute to an increase in Akt activity. The result was increased hypertrophy without fibrosis (Taniike et al., 2008). Converesely, dominant-negative p38 trangenic animals did not experience an increase in cardiac hypertrophy after swimming (Watanabe et al., 2007a). Loss of regulatory protein 14-3-3 resulted in increased p38 activity associated with maladaptive hypertrophy with increased apoptosis and fibrosis in response to exercise. Regression of cardiac hypertrophy was shown with a p38 MAPK inhibitor (FR-167653) (Watanabe et al., 2007a).

While gain- and loss-of-function studies overule the hypothesis where p38 activity is sufficient to promote cardiac hypertrophy *in vivo*, upstream activators of p38 are involved in the hypertrophic process (Rose et al., 2010). For example oestrogen is shown to have protective effects on the myocardium mediated partly via p38 signaling (Babiker et al., 2006; Satoh et al., 2007). Administration of oestrogen blocked cardiac hypertrophy and dilatation and improved contractility in response to pressure overload and activation of Gq. This was associated with decreased ASK1 and its downsteam effectors JNK and p38. Eostrogen-treated cultured cardiomyocytes, were in fact more resistant to angiotensin-II-induced apoptosis (Satoh et al., 2007).

Similar to JNK, p38 appears to play a role in cardiac remodelling after injury. Restrictive cardiomyopathy with interstitial fibrosis after targeted activation of p38 in the myocardium was shown to induce the release of cytokines, TNFα and IL-6, an event that was blocked with the a p38 inhibitor (Li et al., 2005). Deletion of p38γ and p38δ impaired the immune response of macrophages and dendritic cells by blocking ERK1/2 activation, suggesting that both p38 isoforms are key components of the immune system and of cross-talk between ERK1/2 and p38 cascades (Risco et al., 2012). Furthermore, DNA microarray of animals with cardiac-specific p38 overexpression revealed upregulated genes related to fibrosis and inflammation (Tenhunen et al., 2006). p38 was activated via a TGF-β1/TAK1-dependent manner in the non-infarcted area of the rat's left ventricle after MI, accompanied by upregulation of ANF and β-MHC, suggesting a role in cardiac remodeling (Matsumoto-Ida et al., 2006). An activating TAK1 mutant in mouse myocardium was sufficient to induce cardiac hypertrophy, fibrosis, severe myocardial dysfunction, apoptosis and early lethality, and in this gain-of-function study p38 was the chiefly activated terminal MAPK (Zhang et al., 2000).

Notwhithstanding the controversy among studies with regard to the role of p38 in cardiac hypertrophy, it is clear that activation of p38 in the heart has dentrimental effects on cardiac function. Therefore, p38 induction is more closely related to pathological hypertrophy rather than the physiological or compensatory hypertrophy, with chronic levels of p38 activity in the injured myocardium contributing towards maladaptive cardiac remodelling (i.e. contractility and extracellular matrix [ECM] effects).

1.6.7. MAPKs in cardioprotection and myocardial cell death

Cardiomyocyte cell death, unmatched by cell replacement, is the first step following compensatory mechanisms of macrophage infiltration and cardiac remodelling (i.e. fibrosis, ECM changes) that can lead to progressive deterioration of heart function leading to end-stage heart failure (Bing, 1994). This concept was supported by pathologists' findings of sporadic cardiomyocyte drop-out/cell death in failing dilated human hearts (Narula et al., 1996; Olivetti et al., 1997), analogous to DNA fragmentation and caspase-3 activity. Interestingly, this was more prevalent in patients who died from heart failure than those who died with acute MI (Kytö et al., 2004). Central to myocardial cell death or cardioprotection are the terminal MAPKs, which receive signalling cues from upstream kinases, and will be the focus of the following section, taking account of genetically engineered animal models that recapitulate the features of the human disease.

1.6.7.1. ERK1/2 pathway

ERK1/2 signalling has been identified as one of the major components of the Reperfusion Injury Salvage Kinase (RISK) pathway. The RISK term has been given to both Akt and ERK1/2 pro-survival kinases, which confer cardioprotection when activated at the time of reperfusion. The RISK pathway now includes additional cardioprotective kinases, such as PKCε, GSK3β and PKCδ. Blockade or deletion of cardiac ERK1/2 rendered the heart more susceptible to failure after long-term pressure overload (14-weeks) that was associated with increased levels of TUNEL staining after 1 week of TAC, which remained elevated even after 14 weeks (Purcell et al., 2007). MEK1 transgenic mice, similar to MEK1-infected cardiomyocytes *in vitro*, were also partially resistant to I/R-induced cell death and no signs of cardiomyopathy and lethality up to 12 months. These mice showed elevated phosphorylation levels of ERK1/2 (Bueno et al., 2000). While MEK1 transgenic mice were better protected from injury and death in response to I/R, this effect was lost in *Erk2* heterozygous ($Erk2^{+/-}$) gene-targeted mice that showed enhanced infarction areas and TUNEL staining. These results demonstrated that ERK2 specifically has a role in preventing myocardial apoptosis (Lips et al., 2004). Further, the cardioprotective role of ERK1/2 has been studied in relation to doxorubicin (DOX), a chemotherapeutic agent known to induce myocardial damage including cardiomyopathy. While the cardiotoxicity mechanism of doxorubicin is unknown, administration of drugs that increase ERK1/2 and Ras activity prevented DOX-induced cardiotoxicity and the progression of systolic/diastolic dysfunction (Su et al., 2006). However in this study they have not shown evidence of activation of p38 or JNK.

While much work has been carried out to identify the cardioprotective kinases feeding into ERK1/2 activation, much less is known about the mechanism(s) by which ERK1/2 exerts protection. ERK1/2 was shown to have a role in cGMP-dependent protein kinase (PKG)-

mediated cardioprotection in isolated adult cardiomyocytes in I/R, where inhibition of PKG with drugs or siRNA led to decreased levels of cell death and infarct size. Inhibition of PKG showed elevated levels of phospho-ERK1/2, phospho-GSK3β and phospho-Akt, associated with Bcl-2 upregulation and Bax downregulation (Das et al., 2008). Furthermore, ERK1/2 has been proposed to exert its cardioprotective effects via activating phosphorylation of GATA4 directly, which in turn activates pro-apoptotic proteins such as Bcl-x_L in NRVCs in response to the α_1-AR agonist PE (Aries et al., 2004; Liang et al., 2001). However, this does not hold to be true in adult cardiomyocytes, where GATA4 acts as a survival factor and is not required for α_1-AR signalling (Huang et al., 2008). Rather, in adult cardiomyocytes, IL-10 prevented TNFα-induced apoptosis by upregulation of ERK1/2, most likely by blocking IKK phosphorylation, thus NFκB activation (Dhingra et al., 2009). Cardioprotection can also be independent of Raf-MEK-ERK1/2 signalling, since Raf directly interacts with both pro-apoptotic kinases Ask1 and Mst2 *in vitro* and *in vivo* (Chen and Sytkowski, 2005; Chen et al., 2001a). Ablation of Ask1 on c-raf-1 knockout mice rescued apoptosis, dilatation, and lethality, protection that was independent of ERK1/2 activity (which remained unchanged in the ERK1/2 knockout and c-raf-1 knockout mice) (Yamaguchi et al., 2004).

In summary, the evidence suggests a cardioprotective role for the Raf-MEK1-ERK1/2 signalling branch via multiple downstream targets, but still with no delineation of the specific contribution of each kinase.

1.6.7.2. JNK pathway

A dichotomy between the protective and pathological roles of JNK is evident in most cell types, including cardiomyocytes; thus, the role of JNK in cardioprotection remains unclear. Studies have shown activation of JNK in both the ischaemic phase and in reoxygenation upon reperfusion (Fryer et al., 2001; Knight and Buxton, 1996; Yin et al., 1997), and the use of JNK-selective inhibitors reduced infarct size and apoptosis in the setting of I/R (Ferrandi et al., 2004; Milano et al., 2006). JNK activity sits upstream of numerous proteins with a detrimental role in myocardial injury, such as β-ARs (Remondino et al., 2003), Rho-kinase (Zhang et al., 2009b), PKCβ (Kong et al., 2008), MAP4K4 (Xie et al., 2007) and PARP-1 (Song et al., 2008). Furthermore, JNK, among other MAPKs, was shown to co-localise with cardiac mitochondria, an effect greatly increased in PKCε transgenic mice where the PKCε-JNK complex was present (Baines et al., 2002). Sustained JNK activation resulted in activation of pro-caspase-9 and pro-caspase-3 as well as interacting with pro-apoptotic proteins such as Bax and Bad (Aoki, 2002; Baines et al., 2002). It has been also shown to mediate Apoptosis Inducing Factor (AIF) translocation from the mitochondria to the nucleus (Song et al., 2008; Zhang et al., 2009b); thus possibly involved in caspase-independent cell death.

The complexity of the system with JNK is best exemplified by evidence from the Molkentin group. Activation or inhibition of JNK was associated with enhanced cardiomyocyte survival (Kaiser et al., 2005): $JNK1^{-/-}$ and $JNK2^{-/-}$ or dominant-negative JNK1/2 transgenic mice, with decreased JNK activity, exhibited decreased cell death *in vivo* after I/R injury. Interestingly, transgenic MKK7 mice with sustained JNK activation were significantly protected in I/R. Between the two models of decreased and sustained JNK activation differences were observed in phosphorylation of Bad at S^{112} (Kaiser et al., 2005) suggesting that the role of Bad is not determining the survival of myocytes. In addition, pharmacological inhibition of JNK following 4h reoxygenation after 12h hypoxia *in vitro* led to increased apoptosis, associated with decreased Akt and c-Jun phosphorylation, suggesting that the cardioprotective effect of JNK was due to Akt activation (Shao et al., 2006). Inhibition of JNK using selective pharmacological inhibitors against JNK, but not p38, and dominant-negative and constitutively active mutants of MKK4 demonstrated that JNKs, but not p38, positively regulate Akt after hypoxia/reoxygenation. In addition, dual JNK/p38 inhibition with non-selective drugs enhanced I/R injury, whereas selective p38 inhibition had an opposite effect, suggesting that JNK has predominantly a pro-survival signalling role over pro-death one. These results are in agreement with ablation of MEKK1 in ESC-derived cardiomyocytes, where no activation of JNK was observed in response to oxidative stress (hydrogen peroxide). Furthermore, MEKK1-JNK activation was shown to negatively regulate TNFα production via repressing its promoter, an opposing function to p38 that promotes TNFα production. Thus, the discrepancy for JNK's pro-survival versus pro-apoptotic role (Kaiser et al., 2005) could be underlined in the opposing functions to other MAPKs (i.e. p38) (Minamino et al., 1999) and the functional dichotomy of TNFα in cell death and survival. In support of this pro-survival role, JNK1-null mice display increased cell death that led to decreased fractional shortening 3 days after TAC (Tachibana et al., 2006). ASK1-null mice also displayed decreased JNK activity following Ang-II infusion that was associated with decreased TUNEL staining, whereas activation of ASK1 in WT mice had an opposite effect (Izumiya et al., 2003).

In short, the role of JNK pathway in cardioprotection remains controversial, perhaps reflecting the complexity and multistage signalling with other pathways (e.g. ASK1, p38). One of the most promising leads toward reconciling these disparate views is evidence that JNK1 is a "conditional survival kinase," protecting the mouse heart from brief ischemia (5 min) but not from extended ischemia (20 min) more closely resembling human MI (Wei et al., 2011). The suggested mechanism for this time-dependent switch in JNK function is inactivation of the pro-survival kinase Akt by JNK, only after extended ischemia (Wei et al., 2011).

1.6.7.3. p38 pathway

As is common to the other protein kinases discusses, studies have been published with contradictory evidence on the role of p38 in cardioprotection versus myocardial cell death. The complexity of its role is exemplified by the confounding factor that p38 consists of four isoforms, of which p38α is best recognised of its cardiovascular importance. Clearly this isoform is of greatest developmental relevance, as evident from homozygous p38α knockout mice with a phenotype of embryonic lethality: knockouts of other isoforms result in a near-normal adult phenotype (Denise Martin et al., 2012). Shortly after its identification, it was demonstrated that p38 was robustly activated by both ischaemia and I/R in isolated rat hearts, whereas reperfusion injury was needed for activation of JNK (Bogoyevitch et al., 1996). The activation of p38 was rapid and transient in duration after the induction of ischaemia, with a number of studies indicating that its activation during ischaemia and I/R leads to increased injury and apoptosis (Kaiser et al., 2004; Ma et al., 1999; Mackay, 1999). Dominant-negative p38 mutants overexpressed in NRVCs reduced apoptosis in response to 2-deoxyglucose, whereas wild-type p38 overexpression enhanced cell death (Kaiser et al., 2004). Similarly, overexpressing MKP-1 - a phosphatase that inactivates p38 – partially protected mice from I/R (Kaiser et al., 2004). A selective p38 inhibitor also protected myocytes against extended ischaemia *in vitro* (Mackay, 1999). Furthermore, in mice undergoing coronary artery ligation, a novel drug delivery system using the p38 kinase inhibitor SB203580 delivered on microparticles by direct cardiac injection resulted in p38 inhibition, improved cardiac function, reduced fibrosis, minimal tissue inflammatory response (i.e., TNFα, infiltration), and reduced levels of superoxide (Sy et al., 2008).

p38α and p38β isoforms have differential roles during ischaemia, where p38β may be the isoform that imparts cardioprotection (Liu et al., 2010). To understand the isoforms and their mechanism of activation during MI, a combination of chemical genetic approaches have been used. A study by the Marber group attempted to solve the controversy regarding the mechanism of p38 activation in MI by the use of non-selective pharmacological inhibitors such as SB203580. What they have done is create mice in which the p38α alleles were targeted to substitute the gatekeeper threonine residue that is critical for binding SB203580. Mice homozygous for this substitution and treated with the inhibitor failed to prevent the activating phosphorylation of p38α or to reduce the infarction area by MI. In contrast, wild type and knock-in mice treated with the inhibitor BIRB796, which does not rely on the gatekeeper residue, both responded with less p38-activating phosphorylation and infarction. Thus, during I/R, the p38α isoform is the dominant contributor to ischaemic injury, and its inhibition is cardioprotective (Kumphune et al., 2010). In addition, inhibition of p38α correlated with downregulation of activating phosphorylation of heat shock protein-27 (Hsp27) and of TAB1. Autophosphorylation

of p38α occurs by direct interaction with TAB1, and not with p38β, and interference of this interaction abolishes p38α's cardiac toxicity (De Nicola et al., 2013).

Mechanistically, other studies have investigated how inhibition of p38 is cardioprotective. One study proposed that inhibition of p38 following ischaemia led to decreased size of MI injury by promoting myocytes proliferation (Engel et al., 2006). Others have shown that p38 activity is important in TNFα-mediated apoptosis (Dhingra et al., 2009; Minamino et al., 1999) as a result of ROS production, and in mitochondrial-mediated cell death that was associated with increased phosphorylation of VDAC-1 (Schwertz et al., 2007). Phosphorylation of VDAC-1 was inhibited in the presence of a p38 inhibitor. However, the role of VDAC-1 in mPTP-mediated cell death was shown to be redundant; thus the functional importance of this finding remains relatively unexplained. In addition, chronic induction of p38 also plays a role in cardiac contractility after injury, as it phosphorylates various downstream proteins involved in mechanotransduction, such as α-tropomyosin, NCX1 and SERCA (Andrews et al., 2003; Liao et al., 2002; Menick et al., 2007).

Similarly, p38 inhibition by RWJ67657 reduced cardiac remodelling following MI (Liu et al., 2005b; See et al., 2004). Long-term inhibition of p38 by SB239063 – for 9 weeks beginning 7 days after MI – led to reduced levels of cytokine production without affecting cardiac function and cardiac remodelling (Frantz et al., 2007). This finding is in contrast to the significant reduction in fibrosis and hypertrophy following IR and long-term p38 inhibition with RWJ67657 (Kompa et al., 2008). Despite the utilization of different rodent models (rat vs. mouse), the main discrepancies can be explained by the use of different p38 inhibitors. This intensifies the point for complete characterization of the mode of action for each pharmacological inhibitor. In this case, one might have a more direct anti-apoptotic mechanism, whereas the other inhibits post-infarct cardiac remodelling important in the development of dilated cardiomyopathy and heart failure.

In conclusion, p38 inhibition by various pharmacological and genetic interventions is cardioprotective with beneficial effects on cardiac remodelling and cardiac contractility. However, whether cardioprotection is a result of direct inhibition of cell death signalling or quite indirect through inhibition of cardiac contractility defects or ECM remodelling remains a promising area for future exploration. Currently, a p38α/β inhibitor is being tested in Phase I/II clinical trials for coronary heart disease (clinical trial identifier; NCT00291902), congenital cardiomyopathy (NCT02057341) and MI (NCT01043991) (Denise Martin et al., 2012).

1.6.7.4. Concluding remarks

Whereas the role of JNK in cardioprotection remains controversial but with many studies supporting a pro-apoptotic role, p38 activation is more clearly associated with increased cell death in MI and ERK1/2 activation with cardiac survival. Apart from acute effects on cell death, it is important to acknowledge that each of these MAPKs has a role in post-ischaemic cardiac remodelling, associated with the development of a dilated phenotype leading to heart failure. The multiple functions at different stages of disease (ischaemia, reperfusion, remodelling, and heart failure) are likely a main underlying reason for discrepancies among studies and highlight the difficulty of delineating, for example, whether ECM deposition is a specific and direct result of MAPK activation or is secondary to hypertrophy caused by MAPK-independent pathways. Thus, it is important to delineate the kinases' direct effect on cardiac cell death signalling components and pathways versus secondary maladaptive mechanisms that contribute to the former.

1.6.8. Protein kinases in cardiac hypertrophy and cell death

Besides the role of JNK, p38 and ERK1/2 in cardiac hypertrophy and apoptosis, multiple upstream kinases have been described with related or interconnected functions. Below is a brief overview of key examples of kinases feeding into MAPKs with a role in cardiac hypertrophy and cell death.

1.6.8.1. The AGC kinase family of PKC isoforms, PKA and ROCK1

Protein kinase C (PKC) isoforms

The protein kinase C (PKC) family comprises Ca^{2+} and/or lipid-activated Ser/Thr kinases that function downstream of membrane-associated signal transduction pathways. There are 10 PKC isozymes/isoforms, which are classified by their activation characteristics. The Ca^{2+}- and lipid-activated isozymes are PKCα, PKCβI, PKCβII and PKCγ, while the novel isozymes (PKCε, PKCθ, PKCη, and PKCδ) and atypical enzymes (PKCζ and PKCλ) are Ca^{2+}-independent but depend on distinct lipids for their activation. PKCs are the terminal effector molecules for the subset of seven-membrane-spanning-domain (heptahelical) GPCRs that are coupled to the Gq class of heterotrimeric G proteins. Although PKC isoforms function in the cytosol or the nucleus, they also have a membrane translocation mechanism to regulate substrate access through docking complexes. PKC activity is measured by the relative amounts of soluble (supernatant) and particulate (sediment) PKC, that is synonymous of PKC translocation from cytosolic to membranous structures (i.e. nucleus or perinucleus) (Dorn and Mochly-Rosen, 2002). Tha activity of any given isoform depends upon its cellular localization its expression level, and its phosphorylation status (Dorn and Force, 2005). PKCα, β, ε and ζ are highly expressed in fetal and neonatal hearts and decrease in the adult ones, while some PKC isoforms increase during transition to heart failure in humans. Several studies addressed the intracellular mechanisms downstream of PKC activation and their emerging role as mediators of hypertrophic stimuli. Neurohormones and mechanical stress converge on PKC activation, which in turn can cause cardiac myocyte hypertrophy or apoptosis. Some PKC isozymes (PKCα, β, ε, λ and ζ) have a more central role in the development of cardiac hypertrophy, and others (PKCδ and θ) are pro-apoptotic.

PKCα

PKCα, a conventional isoform of the protein kinase C family, is the predominant subtype expressed in the mouse, human and rabbit hearts (Liu and Molkentin, 2011). PKCα activation is synonymous to the translocation from diffuse cytosolic locations to the perinucleus (Dorn and Mochly-Rosen, 2002). As mentioned above, PKCα is highly expressed in fetal and neonatal hearts, but least expressed in the adult ones. PKCα is the least-studied of the cardiac PKCs as,

unlike PKCδ and PKCε, it is not regulated in acute myocardial ischaemia, but is associated with cell hypertrophy and dilated cardiomyopathy following ischaemic injury (Dorn and Force, 2005). PKCα is upregulated in failed hearts compared to normal ones and is more evident in cardiomyocytes from failed hearts localized to intercalated disks (Bowling et al., 1999). Genetic analysis of PKCα in the mouse myocardium suggests a functional involvement as a regulation of cardiac contractility. In general, PKCα$^{-/-}$ and dominant-negative PKCα-carrying mice showed an increase in cardiac contractile function that is associated with protection of the adult heart from dilated cardiomyopathy after I/R and β-adrenergic stimulation. PKCα$^{-/-}$ mice had an increased contractility in response to β-adrenergic stimulation caused by PKCα deletion and protected mice against heart failure induced by pressure overload (Braz et al., 2004). Isolated cardiomyocytes from PKCα-deficient mice and or transduced with a dominant-negative PKCα displayed enhanced contractility, Ca^{2+} transients and Ca^{2+} loading in the SR compared to PKCβγ$^{-/-}$ and wild-type animals (Braz et al., 2004; Liu et al., 2009b). PKCα$^{-/-}$ mice were less susceptible to heart failure following pressure overload post MI injury, whereas PKCβγ$^{-/-}$ mice were more susceptible to heart failure when stressed. These observations correlated well with the effects of cardiac-specific overexpression of PKCβ in mice versus PKCα. PKCβ-expressing mice showed no pathology at baseline with increased function following I/R, while PKCα-expressing mice showed reduced contractility (hypocontractility) and manifested signs of cardiac hypertrophy (Braz et al., 2004). Mechanistically, changes in PKCα activity affects PLN phosphorylation (at Ser^{16}). Cardiac-specific knockout of PKCα resulted in hyperphosphorylation of PLN, whereas PKCα transgenic mice exhibited reduction in PLN phosphorylation (Braz et al., 2004). PLN is an inhibitor of SERCA-2 that regulates Ca^{2+} loading of the SR and alters the Ca^{2+} transient, thus its hyperphosphorylation in PKCα knockout mice explains the enhanced Ca^{2+} loading of SR and the reduction in left-ventricular chamber dilatation development (Braz et al., 2004). A pharmacological inhibitor against PKCαβ, ruboxistaurin, which has been through late-stage clinical trials for diabetic macular edema, was originally reported to be selective for PKCβ. Later ruboxistaurin was shown to augment cardiac contractility in PKCβγ$^{-/-}$ mice but not PKCα$^{-/-}$, indicative of specific effects on PKCα only. Indeed, administration of the drug in WT and PKCβγ$^{-/-}$ mice that have been under pressure overload for 10 weeks prevented death, reduced ventricular dilatation, fibrosis and pulmonary edema, and enhanced ventricular performance (Liu et al., 2009b).

PKCβ and PKCε

While PKCβI and βII are low in the mouse, rabbit and human myocardium, these forms are abundant in human and rat cardiomyocytes. PKCβ is also restricted to emrbyonic and neonatal cardiac myocytes, but is upregulated in adult cardiomyocytes under hypertrophic stimuli and in human failing hearts (Ferreira et al., 2011). Upregulation of PKCβII is associated

with increase of ANF and βMHC fetal gene program in cultured mouse cardiomyocytes and in adult cardiac myocytes under hypertrophic stimuli and in human failing hearts (Ferreira et al., 2011). Activated PKCβI is translocated from a punctuated structure in the cytosol into the nucleus, whereas PKCβII is translocated from cytosolic fibrillar structures to the perinucleus and plasma membrane (Dorn and Mochly-Rosen, 2002).

PKCβI and βII isoforms are both upregulated in failed hearts compared to non-failed left ventricles and in cardiomyocytes from the same hearts (Bowling et al., 1999). Transgenic mice with cardiac-specific overexpression of PKCβII exhibit left ventricular hypertrophy and fibrosis with decreased left ventricular performance. Ventricular hypertrophy was marked with the up-regulation of βMHC, ANF and collagens (IV and VI) (Wakasaki et al., 1997). A second study used a temporal transgenic system for PKCβ expression with αMHC-tTA (doxycycline-inducible trans-activator) and a CMV-PKCβ with a tTA-responsive promoter. Sustained activation of PKC in the absence of a stimulus was sufficient to induce concentric cardiac hypertrophy associated with impaired diastolic relaxation, whereas expression in newborns caused sudden death because of calcium transient relaxation defects (Bowman et al., 1997). In the hypertensive rat model treatment with a PKCβII-specific inhibitor (bIIV5-3) prolonged their survival by suppressing fibrosis, inflammation and delayed the onset of cardiac dysfunction from compensated cardiac hypertrophy. The inhibitor was found to improve calcium handling and enhanced contractility in isolated rat cardiomyocytes and isolated rat hearts, respectively. However, PKCβ KO mouse hearts responded to hypertrophy normally to PE or TAC. These studies suggest PKCβII is sufficient to produce cardiac hypertrophy in the hypertensive rat model, but is not necessary for normal hypertrophy in response to adrenergic stimulation or pressure overload.

PKCε translocates from the nucleus to cross-striated structures and intercalated disks of cell-cell contact areas (Dorn and Mochly-Rosen, 2002). PKCε was shown to be activated during transition from compensated hypertrophy to heart failure in a hypertensive-induced rat model with induction of inflammatory response, fibrosis, and ventricular dysfunction, whereas its inhibition by a selective inhibitor (εV1-2) abrogated this pathological phenotype (Inagaki et al., 2008). Transgenic mice with cardiac-specific overexpression of consitutively active PKCε developed cardiac hypertrophy without heart failure associated with increase in βMHC expression with normal *in vivo* cardiac function. This was also synonymous with increase in the membrane/cytososol ratio of PKCε in the whole heart, though without clarifying if this a cardiomyocyte-specific event (Takeishi et al., 2000). Cardiac-specific overexpression of the PKCε-specific inhibitor (εV1-2) at low levels led to increased cardiomyocyte size with impaired left ventricular function, whereas higher levels caused lethal dilated cardiomyopathy. Enhancement of PKCε translocation via cardiac-specific overexpression of an activator peptide selective for PKCε (ψεRACK) resulted in normal contractile function, decreased cardiomyocyte

size and hypertrophic remodeling (Mochly-Rosen et al., 2000). However, the latter evidence was restricted βMHC upregulation. Furthermore, PKCε has a role in chronic immune response as shown in an allograft transplantation mouse heart model. Delivery of the inhibitor εV1-2 significantly improved the beating of the heart during and post transplantation, reduced the infiltration of macrophages and T cells into the cardiac grafts and abolished the pro-fibrotic cytokines TGF-β and monocytes (Koyanagi et al., 2007). In contrast, systemic (germline) knockdown of PKCε in mice subjected to TAC caused cardiac hypertrophy similar to WT animals, but with increased interstitial fibrosis and enhanced expression of collagens Iα1 and III associated with diastolic dysfunction and no effect on apoptosis. The lack of PKCε was also associated with upregulation of PKCδ and activation of p38 and JNK. These data suggest that PKCε is not required for pressure overload-induced hypertrophy (Klein et al., 2005).

Although PKCε activation is detrimental in this hypertension-induced heart failure, the same isozyme was activated prior to MI, with a cardioprotective role (Inagaki et al., 2005). Activator ψεRACK delivered in the heart before ischaemia conferred cardioprotection against I/R. Continuous delivery of ψεRACK in isolated perfused hearts before being subjected to ischaemia reduced the incidence of lethal arrhythmia during I/R. Similarly in a porcine model of I/R, intracoronary injection of ψεRACK during the first 10min of ischaemia reduced infarct size by 20% and resulted in fewer cases of ventricular fibrillation during I/R due to reduced ventricular tachyarrhythmia (Inagaki et al., 2005). Furthermore, acute activation of PKCε by infusion of ψεRACK activator peptide protected the heart from ischaemia by 60%, measured by MCK release from the hearts (Chen et al., 2001c).

In adult rat ventricular cardiomyocytes, β-adrenergic stimulation using isoproterenol induced apoptosis associated with membrane translocation of PKCε, but not of PKCα or δ. Inhibitor εV1-2 significantly blocked the translocation and enzymatic action confirmed by a kinase assay, that overall inhibited isoproterenol-induced apoptosis shown by TUNEL assay. PKCε inhibition was found to enhance ERK1/2 activity that was Akt-independent, suggesting that PKCε promotes apoptosis by inhibiting ERK1/2 (Shizukuda and Buttrick, 2001). The distinct roles of PKCε in cardiac hypertrophy and in I/R make an interesting case of the distinct roles a kinase can have in cardiac pathology.

PKCδ and PKCθ

Upon cell stimulation, PKCδ activation is related as translocation from the nucleus to fibrillar structures (Dorn and Mochly-Rosen, 2002). PKCδ is a critical mediator of post-ischaemic cardiomyocyte necrosis and contractile dysfunction in rats, mice and pigs. In the heart, PKCδ has a role in I/R linked with its translocation to the mitochondria and inhibition of its mitochondrial translocation with a selective inhibitor protects the heart from I/R injury (Churchill et al., 2005; Kostyak et al., 2006).

Opposed to the cardioprotection effect of PKCε activation in the heart, PKCδ activation demonstrated an opposing effect of cardiac damage (Chen et al., 2001c). Moreover, acute inhibition of PKCδ by a selective inhibitor (dV1-1) protected the isolated hearts from ischaemic damage measured by the release of CK. PKCδ inhibition with inhibitory peptide (KID1-1) also reduced infarct size in adult and aged rat hearts (Kostyak et al., 2006). A separate study investigated the PKCδ-associated alternations in the proteome of cardiac tissue in mice with genetic ablation of PKCδ and found a metabolic shift from glycolysis to fatty acid oxidation (Mayr et al., 2004). Sustained cardiac-specific activation of PKCδ in the heart resulted in the upregulation of fetal βMHC with hearts showing impaired systolic and diastolic functions from ischaemia. In the setting of acute ischaemic injury followed by reperfusion, mouse hearts with sustained PKCδ activation also had increased infarct size compared to the control transgenic littermates (Chen et al., 2001c). In older mice, sustained activation of PKCδ led to increase in cardiac mass with a normal response to cardiac adrenergic stimulation (Chen et al., 2001c). PKCθ isoform is also expressed in cardiac muscle and is rapidly activated after pressure overload. Gene ablation of PKCθ in whole animals led to the development of left ventricular dilatation and reduced cardiac function combined with hypertrophy, cardiac fibrosis and ECM remodelling (Paoletti et al., 2010). A PKCδ inhibitor (KAI-9803) was used to limit total infarct size in acute MI in a human clinical study (DELTA MI) to evaluate safety, tolerability and activity in patients (Bates et al., 2008).

Protein Kinase A (PKA)

PKA is a cAMP-dependent kinase that is the terminal effector molecule of membrane receptors coupled to G_s or G_i heterotrimeric G proteins (Dorn and Mochly-Rosen, 2002). β-ARs activate G_s, which in turn activate PKA by stimulating adenylyl cyclase for increasing cAMP formation. Conversely, receptor-mediated activation of G_i (i stands for inhibitory) inhibits PKA activity by diminishing cAMP formation by adenylyl cyclase. Ubiquitous signal transduction as such has critical cardiac functions, such as modulating heart rate, vascular tone and cardiac output (Dorn and Mochly-Rosen, 2002). The pathway is important in the sympathetic response of the cardiovascular system by stimulating calcium flux through the L-type calcium channels via phosphorylation of the β2 modulatory subunit of the channel at three consensus-phosphorylating sites. It also phosphorylates the ryanodine receptor (RyR), troponin I (TnI), and cAMP-responsive element binding protein (CREB). The activation of PKA increases the rate of cardiac muscle contraction, but in heart failure the myocardium is desensitized to β-adrenergic stimulation leading to impaired cardiac contraction. This can lead to left ventricular hypertrophy, dilated cardiomyopathy, and heart failure (Ruehr et al., 2004). β_1-adrenergic stimulation is also linked to apoptotic heart cell death through a PKA-independent mechanism via Ca^{2+}/calmodulin-dependent kinase II (CaMKII) (discussed below).

Rho-associated coiled coil kinase 1 (ROCK-1)

Rho-associated coiled-coli kinases (ROCKs) were initially identified as effectors of Rho GTPases with critical roles in mediating stress fibre formation, smooth muscle contraction, cell adhesion, cell motility and cell death. ROCK1 is a direct cleavage substrate for active caspase-3, the latter of which is the biochemical hallmark of apoptosis and is associated with heart failure. Cleaved ROCK1 was found in heart failure patients, which was absent in normal hearts and in a cohort of patients with left ventricular assist devices. ROCK1 cleaved product was present in murine cardiomyocytes treated with doxorubicin, whereas loss-of-function studies with siRNA decreased apoptosis (with inhibition of caspase-3 activation) induced by c_2-ceramide. Furthermore, germline genetic ablation of ROCK1 in mice reduced apoptosis in response to pressure overload, associated with activation of PTEN and subsequent inhibition of PKB/Akt survival pathway (Chang et al., 2006). Furthermore, ROCK1$^{-/-}$ mice were used to investigate the role of the kinase in cardiac hypertrophy. ROCK1 deletion did not impair compensatory cardiac hypertrophy induced by pressure overload or G_q, however the mice exhibited reduced interstitial fibrosis associated with reduced expression of ECM proteins (Zhang et al., 2006), most likely associated with decreased apoptosis in the heart (Chang et al., 2006). A novelty application based on the blockade of apoptosis is the use of a ROCK1 inhibitor (Y-27632) in dissociated embryonic stem cells for increasing cloning efficiency (sub-cloning) following gene modifications and for increasing post-recovery after thawing (Watanabe et al., 2007b). Currently, Fasudil, a potent ROCK1 inhibitor and vasodilator is used for the treatment of cerebral vasospasm (intense vasoconstriction of the larger conducting arteries surrounded by a clot) and was demonstrated to be effective for the treatment of pulmonary hypertension (Doggrell, 2005).

1.6.8.2. The Calmodulin/Calcium regulated kinase (CAMK) family

AMP-activated protein kinase (AMPK)

The AMP-activated protein kinase is an evolutionary conserved energy sensor activated by raising levels of AMP coupled with decreasing levels of ATP. Historically, AMPK pathway was viewed primarily as a regulator of energy balance in the cells, however it has become apparent that is involved in the fundamental energy regulation of the whole body by responding to hormones, nutrients, and oxidative stress. AMPK is connected to cellular processes of autophagy, metabolism and cell polarity (Shirwany and Zou, 2010). As mentioned earlier, AMPK can override mTOR suppression of autophagy and can activate PGC1α, which is a key transcriptional regulator of mitochondrial biogenesis (Gottlieb et al., 2010). In recent years it has emerged that AMPK can modulate cardiac hypertrophy. Constitutive activation of AMPK by mutations in *PRKAG2* encoding for the g2 regulatory subunit causes familial hypertrophic cardiomyopathy with electrophysiological abnormalities (Arad et al., 2002). In cultured NRVCs, activation of AMPK by metformin and AICAR drugs attenuated protein synthesis induced by PE treatment, as was shown by increase in phosphorylation of other kinases involved in protein synthesis and cardiac myocyte enlargement (Chan et al., 2004). Furthermore, ^{31}P NMR spectroscopy was used in rat hearts with pressure overload-induced hypertrophy to show increased AMPK activity (Tian et al., 2001). However to determine whether AMPK alone can exert pressure overload-induced cardiac hypertrophy, a specific AMPK activator (AICAR) was administered in rats with TAC. Long-term AMPK activation attenuated protein synthesis in the rat heart and blocked cardiac hypertrophy AMPK-infected NRVCs (Li et al., 2007). AMPK activity is also elevated during cardiac ischaemia and this is likely to compensate by upregulation of GLUT4 translocation (glucose transporters) to the plasma membrane (Tian et al., 2001). Isolated mouse hearts with a direct activation of AMPK by a small molecule activator (metformin) showed better recovery of left ventricular contractile function and smaller infarct sizes following I/R, evidence of a cardioprotective effect (Kim et al., 2011). Integral to the AMPK pathway is an upstream Ser/Thr kinase termed LKB1, which directly phosphorylates AMPK *in vitro*. Cardiac-specific deletion of LKB1 demonstrated cardiac dysfunction with left ventricular hypertrophy and collagen remodelling. Similarly, TAK1 is also connect to AMPK signalling, where a dominant-negative mutant of TAK1 prevented metformin-induced phosphorylation of AMPK and inhibited LKB1 activation in cultured cardiomyocytes (Xie et al., 2006), suggesting that LKB1/AMPK signalling depends on TAK1. Currently, the AMPK activator drug metformin is a widely prescribed oral anti-diabetic drug for the inhibition of hepatic gluconeogenesis, with unknown mechanism of action.

Calcium/Calmodulin-Dependent kinase II (CaMKII)

CaMKII is a major activator kinase of a number of Ca^{2+} homeostatic proteins and a gene transcription regulator. It shares many substrates with PKA downstream of the β_1-adrenergic receptors. Notably these substrates are central to the regulation of calcium (i.e. PLN, RyR, Cn) and to the development of cardiac hypertrophy (i.e. NFAT, MEF2). Sympathetic stimulation of the cardiac β_1-adrenergic receptors induces positive inotropic and chronotropic effects (increase contractile force and heart rate, respectively) in a PKA-dependent or independent manner. A solid body of evidence has emerged around CaMKII confirming the following: (i) that CaMKII activity is increased in cardiac hypertrophy and in failing myocardium of mice and patients, (ii) CaMKII overexpression induces myocardial hypertrophy, arrhythmias (Sag et al., 2009), heart failure and exacerbates apoptosis (iii) inhibition of CaMKII by drugs, inhibitory peptides and gene ablation improves myocardial hypertrophy, protects the myocardium against cell death in I/R (Yang et al., 2006; Vila-Petroff et al., 2007; Ling et al., 2009), and reduces arrhythmias (Zhu et al., 2003; Ling et al., 2009). In contrast to the last point, knockout of CaMKIIδ, the most prominent cardiac isoform, induced comparable increases with the WT animals in cell size, HDAC phosphorylation and hypertrophic gene expression following TAC. What was interesting was that CaMKIIδ deficiency ameliorated phenotypic changes associated with the transition of heart failure, such as chamber dilation, ventricular dysfunction, apoptosis and fibrosis (Ling et al., 2009).

The role of PKA in activation of CaMKII is evident in a series of studies. Firstly, phosphorylation of PLN was present in both PKA-targeting and CaMKII-targeting residues in β-adrenergic-stimulated perfused rat hearts (Kuschel et al., 1999). Experiments with a PKA inhibitor further supported that PKA activation is required for phosphorylation of PLN (Ferero et al., 2007). A similar effect was observed with the phosphorylation of RyR2 receptor, which was prevented by treatment with a PKA inhibitor (Said et al., 2002). A second indirect mechanism that supports the role of PKA in the activation of CaMKII is via the activation of protein phosphatase-1 inhibitor-1 (I-1) by PKA at Thr^{35} or suppression at Ser^{67} or Thr^{75}. Activation of I-1 leads to inhibition of protein phosphatase-1 (PPI). Knockout of I-1 led to increased CaMKII-phosphorylated RyR2 at Ser^{2815} and hypophosphorylation of PLN at the PKA-targeting residues (El-Armouche et al., 2008). Thus, activation of CaMKII might be dependent on PKA, but phosphorylation of their respective targets could be regulated independently.

CaMKII can also be activated in response to β-adrenergic stimulation in a PKA-independent manner. Chronic and acute β_1-adrenergic stimulation of adult cardiomyocytes both increased the contraction amplitude, but with mechanistic differences. Acute effects were mediated via PKA, whereas chronic effects required CaMKII in a PKA-independent manner, shown by the use of CaMKII inhibitors and a dominant-negative CaMKII mutant (Wang et al., 2004). Sustained activation of CaMKII was concomitantly obvious in the phosphorylation

pattern of PLN, as a shift from the PKA to CaMKII site, suggesting that sustained CaMKII activation leads to desensitization of PKA activity (Wang et al., 2004). A separate study also addressed the independence of CaMKII from PKA activation in the role of apoptotic cell death: β_1-adrenergic-induced apoptosis was resistant to PKA inhibition, but cardiac myocytes were completely protected when CaMKII activity was inhibited (Zhu et al., 2003). Alternatively, Epac protein acts in a separate mechanism for CaMKII activation independent of PKA in isolated adult rat cardiomyocytes (Grimm et al., 2010). Knockdown of Epac1 blocks hypertrophic changes induced by β-adrenergic stimulation *in vivo* and in neonatal cardiomyocytes (Métrich et al., 2008).

Lastly, it is worth mentioning the CaMKII negatively regulates calcineurin-NFAT signalling in cardiac myocytes (MacDonnell et al., 2009). Pathological hypertrophy is induced by increases in intracellular Ca^{2+} when systolic wall stress is increased. Elevated Ca^{2+} binds to calmodulin (CaM) and activates calcineurin phosphatase and CaMKII. Calcineurin dephosphorylates the transcription factor NFAT (nuclear factor of activated T cells), which activates anti-apoptotic and hypertrophic genes. Dominant negative CaMKII expressed in NRVCs and adult feline ventricular cardiomyocytes increased NFAT in the nucleus, whereas a constitutively active CaMKII had an opposite effect in addition to increased TUNEL and caspase-3 activity. Calcineurin was also phosphorylated in constitutively active CaMKII-infected NRVCs and feline hypertrophied hearts (MacDonnell et al., 2009).

In conclusion, CaMKII is part of a multifunctional signalling cascade in the heart, activated by β-adrenergic stimulation and targets cytoplasmic proteins involved in the regulation of Ca^{2+}, where overexpression can cause heart failure and increased apoptosis, so inhibition or gene ablation of CaMKII is cardioprotective.

Protein kinase D (PKD)

The importance of protein kinase D (PKD) in cardiac pathology is a fairly recent development. PKD activation promotes diacylglycerol (DAG) biogenesis in response to various stimuli, such as hormones, oxidative stress and growth factors. PKD is recruited to the plasma membrane where it phosphorylates PKC (commonly PKCε isoform) that is also recruited by DAG. Activated PKD can accumulate transiently to the nucleus after undergoing autophosphorylation and respectively regulate 14-3-3 and other proteins (Avkiran et al., 2008). The kinase phosphorylates downstream effector molecules that regulate gene transcription, Golgi vesicles formation and transport, cell migration and survival. Deregulated PKDs are linked to cardiac hypertrophy and inhibition by PKD-selective drugs are proven powerful tools for treating cardiac disease (Fu and Rubin, 2011).

In mammals there are three widely expressed member of the PKD family (PKD1, PKD2 and PKD3), all of which are associated with organelle surfaces, such as plasma and Golgi

membranes and mitochondria. All isoforms are detected in adult mouse, rat, rabbit and human hearts (Avkiran et al., 2008). PKD1 is the main isoform expressed in adult rat ventricular cardiomyocytes and PKD3 is prominently detected in early and late stages (E10-E16.5) of embryonic cardiogenesis (Ellwanger et al., 2008; Oster et al., 2006). PKD is activated in response to norepinephrine and PE via α_1-adrenoreceptors, and in response to ET1 and angiotensin-II in neonatal and adult ventricular cardiomyocytes (Haworth, 2000). In many cases, PKD activation was inhibited by PKC inhibition highlighting the critical role of PKC isoforms in PKD function (Harrison et al., 2006). PKD interacts and phosphorylates Troponin I myofilaments to regulate contraction (Haworth, 2000; Haworth et al., 2004) and as a mediator of histone deacetylase isoform 5 (HDAC5) kinase (Harrison et al., 2006).

CaMKII signals to nuclear-localized HDAC5, which appears to function as a negative regulator of cardiac remodeling and hypertrophy through association with myocyte enhancer factor-2 (MEF2). Interaction of HDAC5 with MEF2 represses the expression of MEF2-dependent muscle-specific pro-hypertrophic genes (Vega et al., 2004). MEF2 is a common endpoint for hypertrophic signalling, also triggered by calcineurin (van Oort et al., 2006). PKD facilitates the binding of 14-3-3 proteins and induces the nuclear export of HDAC5 exposed to hypertrophic stimuli. HDAC5 is also directly phosphorylated by PKD to stimulate its nuclear export and stress signals, like ET1 and PE, neutralize the repressive function of HDAC via PKC-mediated PKD phosphorylation of HDAC5 leading to its nuclear export (Harrison et al., 2006; Vega et al., 2004). This disrupts its interaction with MEF2 and allows the expression of pro-hypertrophic genes (Vega et al., 2004). Recently it has also been shown that deletion of PLCε protects mouse cardiac myocytes from stress-induced cardiac hypertrophy that is concomitant with decrease of nuclear PKD. Furthermore, PKD was found to be part of a multicomponent complex containing PLCε, Epac, PKCε and Ryr2 required for PKD activation (Zhang et al., 2013).

A significant increase in PKD activity was observed in spontaneously hypertensive heart failure (SHHF) rat model, which was exacerbated in response to TAC-induced pressure overload (Harrison et al., 2006). Cardiac-specific overexpression of a constitutively active PKD transgene led to pathological cardiac hypertrophy in mice with ventricular chamber dilatation, contractile dysfunction and wall thinning (Harrison et al., 2006), whereas conditional PKD1 knockout showed diminished fibrosis and improved cardiac function after TAC or adrenergic stimulation (Fielitz et al., 2008). In conclusion, PKD regulates fundamental processes in the heart, such as contraction and cardiac hypertrophy and is an emerging clinical target of heart failure.

1.6.8.3. MAP3K Kinase family

TAK1

Transforming growth factor β activated kinase-1 (TAK1), or else known as MAP3K7, has been extensively studied in various models and has emerged as a key regulator of signal transduction in cascades of differentiation, development, cell death and survival. As described earlier, TAK1 is an important component of multiple cell membrane receptor complexes, such as TNFR1 and Toll-like receptors (TLR), resulting in the activation or inhibition of NFκB signalling. In summary, stimulation of TNFR1 leads to the activation ubiquitin ligases of TRAF2 and TRAF5, which in turn promote the polyubiquitination of RIP1. The polyubiquitinated RIP1 then recruits a kinase complex that consists of TAK1 and TAK1-binding proteins TAB2 or TAB3. The polyubiquitin chains of the complex also recruit IKK by binding to an essential regulatory subunit NEMO, allowing TAK1 to phosphorylate and thus activate IKK. Subsequently, IKK phosphorylates IκB for inhibitory degradation via the proteasome. This allows the cytoplasmic-to-nuclear translocation of NF-κB for the activation of genes that mediate immune and inflammatory responses, cell death or survival. Among the most well studied activators of NFκB are IL-1β and TNFα, or c_2-ceramide (a downstream product of TNFα) (Adhikari et al., 2007).

Activation and function of TAK1 was shown to be important in T cell development and function (Wan et al., 2006), in thymocyte development (Liu et al., 2006) and in dendritic cell survival (Wang et al., 2012a). Furthermore, inhibition of TAK1 was shown to promote cell death in *KRAS*-dependent colon cancers (Singh et al., 2012), whereas when TAK1 was specifically deleted in hepatocytes lead to the spontaneous development of hepatocellular carcinoma that correlated with increased JNK activity (Nikolaou et al., 2012). JNK activation was TAK1-dependent in monocytes isolated from the bone marrow of mice. TAK1 deficient monocytes showed increased cell death phenotype that could be rescued by retroviral expression of TAK1 (Lamothe et al., 2013). Recently, it has also been shown that double epithelial-specific $Tab1^{-/-}$ $Tab2^{-/-}$ knockouts mice had the same phenotype as $TAK1^{-/-}$ mice, both showing increased cell death, inflammation and ROS accumulation (Omori et al., 2010).

In a cardiac setting TAK1 activation can be JNK-dependent via MAP4K4 (see section 7) or p38-dependent via the expression of TGF-β in cardiac hypertrophy (Zhang et al., 2000). TAK1 was activated in the adult mouse myocardium 7 days after TAC, and an activating TAK1 mutant was sufficient to produce increased phosphorylated p38 levels with mice developing cardiac hypertrophy, fibrosis and increased cell death (Zhang et al., 2000). We and others (Chen et al., 2000) have seen activation of TAK1 in NRVCs in response to hydrogen peroxide and c_2-cermide, even though at different concentrations. In addition, JNK activation in NRVCs

was dependent on the MAP4K4-TAK1 axis and resulted in cardiac muscle cell death (see section 7).

1.6.9 Concluding remarks

The role of various MAPKs and upstream kinases in the development of heart failure following dilated cardiomyopathy and/or I/R is evident from many studies. PKC isozymes (PKCα, β, ε, λ and ζ), AMPK and PKD have a more central role in the development of cardiac hypertrophy and heart failure, some (CaMKII, ROCK1) have an integral role in cardiac apoptosis while others (PKCδ, PKCθ) are pro-apoptotic – even though their roles are overlapping with kinases and other targets not described here. However, besides the availability of pharmacological inhibitors targeting kinases in cancer, only few have moved to clinical trials for the treatment of cardiovascular diseases (most are still at the preclinical stage), in part because industry would criticize the lack of direct evidence that the kinases have a similar effect in a humanized cardiac setting, even if they were proven to be activated in human heart disease. Similarly, MAP4K4 (also known as HGK/NIK), the central kinase of this thesis, is involved in human cardiac muscle cell death with unpublished evidence from various animal *in vivo* and *in vitro* experiments (see Section 7, below). The aim of my project was to validate the role of MAP4K4 in a humanised setting and for this purpose we used human induced pluripotent stem cell-derived cardiomyocytes (hiPSC-CMs).

1.7. MAP4K4 and TAK1: "associates" in failing hearts

Mitogen-activated protein kinase kinase kinase kinase-4 (MAP4K4, ZC1, HGK, HGK/GCK-like kinase or NIK) is an upstream member of the MAPK superfamily that clusters into the GCK subfamily along with its close relatives TNIK and MINK. It is the mammalian orthologue of yeast serine/threonine kinase Ste20 and of the *Drosophila* kinase *Misshapen* (*msn*). MAP4K4 contains two consensus SH3 binding motifs (574-579, 611-616aa), both of which interact with the adapter protein Nck, which is thought to be involved in actin cytoskeleton regulation, affecting cell motility and shape. Unlike the long isoform (LF), a short isoform (SF) of human MAP4K4 (HGK) was shown to have a deletion in the proline-rich region lacking the SH3 binding motifs. Differential expression of the two isoforms, but equal ability to activate JNK, suggests tissue-specific regulatory functions most likely associated with their underlying distinct ability to interact via the SH3 domain with adaptors and cytoskeletal proteins (involved in membrane trafficking) (Yao et al., 1999). In Drosophila, *msn* is required for dorsal closure with the subsequent activation of JNK module (Su et al., 1998) in the embryo and mediates epithelial planar cell polarity in eyes and wings (Paricio et al., 1999). Genetic and biochemical analysis of *msn* mutants indicates action of *msn* downstream of the Frizzled (Fz) transmembrane receptor, independent of JNK activation (Paricio et al., 1999).

MAP4K4 and its reported target, Ste11-related kinase TAK1 or MAP3K7, are activated in diseased human myocardium, in mouse myocardium and cultured cardiomyocytes by diverse stress signals (Xie et al., 2007). MAP4K4 is highly enriched in heart muscle and was first implicated in signalling by TNFα and other inflammatory cytokines for the activation of the terminal MAPK, Jun N-terminal kinase (JNK) (Yao et al., 1999), but not the extracellular signal-regulated kinase p38. The best-characterized activating target of MAP4K4 is TAK1, necessary for the downstream activation of JNK as shown by the kinase-negative TAK1 mutant (Yao et al., 1999). *Msn* in *Drosophila* and its MAP4K4 mammalian orthologue in human cancer cell lines were demonstrated to target the α-helix of Smad1 proteins for phosphorylation, which was inhibited by siRNA knockdown of *Msn* or MAP4K4 respectively (Kaneko *et al.,* 2011). This study demonstrates that MAP4K4 can switch off Smad proteins and control their availability to transduce TGF-β/BMP signals (Kaneko *et al.,* 2011) in various cancers. In fact, MAP4K4 is upregulated in many types of cancer and is significantly associated with larger tumour size (Liang et al., 2008; Liu et al., 2011) and worsened overall prognosis. Inhibition of MAP4K4 by knockdown was associated with reduced cell proliferation, increased apoptosis, and decreased cell motility and migration, an effect mediated through JNK pathway (Collins *et al.,* 2006). Furthermore, the MAP4K4 gene was shown by genome-wide bioinformatics to have six p53-binding sites, and upregulation of MAP4K4 is likely one of the ways through which JNK activation is p53-dependent in cancer (Miled *et al.,* 2005).

The scientific evidence for MAP4K4 that implicates the kinase as integral to cell death pathways in the heart and its importance in cardiac muscle cell death include: (i) activation in failing human hearts, (ii) activation in genetic and pathobiological mouse models of cardiac cell death, (iii) gain-of-function studies in mouse myocardium, and (iv) gain-of-function mutations, dominant-negative mutations, and RNA interference in cultured NRVMs (Xie et al., 2007). Activation of endogenous MAP4K4 was present in diseased human myocardium of patients with dilated cardiomyopathy (DCM), ischaemic cardiomyopathy (ICM) and adriamycin-induced cardiomyopathy, which overlapped with increased caspase-3 activation. In cell culture experiments, MAP4K4 was activated in response to diverse cardiac cell death signals, such as anti-cancer agent doxorubicin, hydrogen peroxide (H_2O_2) and c_2-ceramide (a TNFα-mediator).

The functional consequences of MAP4K4 *in vivo* were evident by the use of αMHC-MAP4K4 and αMHC-Gq mice compared to non-transgenic littermates. A 25-copy αMHC-Gq line, which induces mild hypertrophy on its own and confers apoptotic predisposition, was sufficient to activate MAP4K4, but only mice co-inheriting both transgenes died prematurely, with dilated cardiomyopathy, fibrosis, apoptosis, severely diminished systolic function, and death by 3 months of age. αMHC-MAP4K4 mice did not show any elevated apoptosis, dysfunction or mortality.

The functional role of MAP4K4 was tested in NRVMs by forced expression of catalytically active vs. catalytically inactive constructs. Active MAP4K4 increased the proportion of apoptotic cardiomyocytes 4-fold by 24hr, whereas the catalytically inactive forms induced apoptosis by 36hr, most likely occurring by GCK-like other kinases that weakly activate JNK activation. MAP4K4 induced dissipation of mitochondrial transmembrane potential, suggestive of an effect on apoptosis via the intrinsic pathway, and induced the activation of pro-caspase-3 and pro-caspase-8.

The effect of MAP4K4 was suppressed, even though incompletely, by Bcl-2. Inhibition of MAP4K4 by dominant interfering mutants of the kinase or by RNA interference (shRNA) attenuated H_2O_2- and c_2-ceramide-induced apoptosis by 50-60% assessed by DNA hypodiploid with flow cytometry and by caspase-3 and caspase-8 colorimetric assays. Furthermore, co-infection of MAP4K4 with a dominant-negative TAK1 mutant blocked the activation of JNK and subsequently suppressed MAP4K4-induced apoptosis, suggesting that TAK1 is essential for the death “spiral” activation in cardiomyocytes (Xie et al., 2007).

A question of great importance to industry and clinicians is whether MAP4K4 is essential in human cardiomyocytes. While most human clinical trials of pharmacological inhibitors depend on preclinical data from animal models, only about 20% of the clinical trials passing through Phase I safety testing in humans make it successfully through Phase III to receive approval for clinical use (Magnus, 2010). One of the reasons for this is the lack of a humanized model of many diseases, such as cardiac and neurodegenerative diseases, equivalent to the

easy use of human T cells and B cells in culture. Traditionally, for the collection of human cardiac tissue, patients would be required to sign a consent form explaining the potential risks of such procedures; the quantity and timing of availability are limited. This restricts the utility of tissue from diseased donors towards the characterization of disease and the development of pharmacological treatments. For this reason, scientists have turned their hopes to human embryonic stem cells and human induced pluripotent stem cell (hiPSC) technology, to explore disease mechanisms, define novel therapeutic molecular targets, advance the process of drug discovery, and accelerate proof-of-concept studies for drug development (Inoue and Yamanaka, 2011). This paradigm shift is central to the current thesis: is suppression of MAP4K4 or TAK1 able to confer protection from cell death in hiPSC-CMs similar to the functions demonstrated to date in rat and mouse ventricular myocytes?

1.8. Induced pluripotent stem cells (iPSCs) and High Content Screening: Novel tools for understanding human pathobiology

Undoubtably, science's golden standard in disease modelling is the use of various *in vivo* models (including non-vertebrate and vertebrates), having anatomical and physiological fidelity to the human organ, complemented by dominant-negative, constitutively active and knockdown cell culture models. However, the main limitations of working with animal models include increased expenses for maintenance of animal colonies, highly skilled personnel for reproducibility of various surgical procedures, time, and difficulties in studying the simultaneous roles of various kinases in any one clinical setting. For these reasons, scientists have turned their efforts towards the deconvolution of the kinome's complexity with the use of high-throughput technologies such as phosphoproteomics, microarrays, whole-genome and epigenome sequencing and high-content microscopy. The opportunity to use such technologies could not come at a better time: the era of human tissue modelling "in a dish" by the use of induced pluripotent stem cells (iPSCs).

In 2006 the field of developmental biology was catapulted forward by a startling experiment of reprogramming technology. Shinya Yamanaka, the 2012 Nobel Laureate of Medicine, was able to show that somatic cells (and more specifically skin fibroblasts) can be reprogrammed into a pluripotent state through ectopic expression of a cocktail of reprogramming factors (e.g. OCT3/4, SOX2, KLF4, c-MYC, NANOG, and LIN28) only present in embryonic stem cells (Takahashi and Yamanaka, 2006). Adult cells could be reprogrammed "backwards" to become stem cells, circumventing the use of human embryos, and then to differentiated "forward" into any human cell type (i.e. hepatocytes, neurons, cardiomyocytes). Since almost a decade ago, scientists have managed to convert various adult cell types (other than skin fibroblasts) to iPSCs and then to patient-specific adult cells. Nowadays, iPSC-derived cells are considered the "Holy Grail" in the study of human disease, in the discovery of novel therapeutic molecular targets and for cell therapy applications as a form of personalized medicine.

Ten years since Yamanaka's breakthrough, the scientific community has been flooded with papers describing: (i) advances in reprogramming technology (reviewed in (Robinton and Daley, 2012) to circumvent issues of genomic integration, such as episomal vectors (Yu et al., 2011) or others (Anokye-Danso et al., 2011), for efficient reprogramming and successful derivation of iPSC lines (Dick et al., 2011; Rais et al., 2013), (ii) the differences between iPSC cells and embryonic stem cells, (iii) the biological characteristics and similarities of iPSC-derived adult cells to the equivalent human cell types, (iv) their suitability/safety in cell therapy applications, using refined analysis in a genome- and epigenome-wide level (Robinton and Daley, 2012) and (v) characterization of various disease models and investigation of biological

mechanisms for identification of suitable drug targets, and even (vi) correcting single-gene mutations that cause diseases like cystic fibrosis and thalassemia for future cell transfusion therapies (Chang and Bouhassira, 2012; Hanna et al., 2007; Somers et al., 2010; Wang et al., 2012b).

1.8.1. Differentiation and characterization technologies for ESCs- and iPSCs-derived cardiomyocytes

Various differentiation protocols have been developed leading to the expansion of various tissue progenitors and cardiomyocytes. The most widely used method of embryoid body (EB) formation via the hanging drop, the forced aggregation and the suspension culture techniques. Later monolayer and other differentiation protocols with enhanced mesodermal lineage differentiation were developed to produce more homogenous (pure) population of cardiomyocytes with or without antibiotic selection (Lian et al., 2012). Slowly the ESC and iPSC culture moved away from animal derived cells (xeno-free environments) (Ludwig et al., 2006) under defined growth factor conditions (Brons et al., 2007; Yang et al., 2008b; Yao et al., 2006), for the potential development of clinically relevant pluripotent cell lines that could be, in principle, be used for transplantation to restore the function of the damaged heart.

For the continued development of the field of regenerative medicine towards clinically-relevant cell populations, scientists needed to find ways to validate that their technologies and methodologies continue to: (i) support the passage of pluripotent ESCs and iPSCs in an undifferentiated state and (ii) support their differentiation into the three developmental lineages (ectoderm, endoderm and mesoderm). Similarly, central to the differentiation efforts of pluripotent stem cells towards a specific lineage, in the current case mesoderm and cardiac lineage, would be the use of techniques such as immunofluorescence, flow cytometry, and microarrays and/or real-time PCR. Other techniques, such as Fluorescence *in situ* Hybridization (FISH) or Comparative Genomic Hybridization (CGH) would be used to ensure karyotype stability and electrophysiological studies to exhibit the nature and maturity of the differentiation products (e.g. ventricular, atrial or nodal subtypes of cardiomyocytes). In general, depending on the developmental lineage of interest and the nature of the final differentiated cell product, different RNA and protein markers as well as specialized techniques would be used to prove their resemblance of the equivalent human cells.

Scientists use various assays to validate the development of mutation-free fully reprogrammed iPSC cell lines and their corresponding differentiation populations. Differentiated cardiomyocytes are assessed by light microscopy for spontaneous beating, thus easily detected in culture as beating EBs or beating areas in monolayer differentiation approaches (Muller et al., 2000). EB aggregates can be dissociated and plated on extracellular matrices like gelatin to measure their action potential morphologies (i.e. nodal, atrial or ventricular subtypes)

using patch clamp electrophysiology. Beating areas in differentiation EB cultures are normally visible four days after plating (Mummery et al., 2012). In addition, the differentiation efficiency of each method is estimated by the expression of cardiac RNA and protein markers. Cardiomyocytes are normally phenotypically assessed with qPCR and immunocytostaining (measured by microscopy or flow cytometry) against late structural proteins, such as Troponins. All of the differentiation efforts from pluripotent ESCs or iPSCs so far yielded a mixture of atrial, nodal and ventricular cell types, that more closely resemble a fetal cardiac phenotype (Willems et al., 2009). Nowadays, scientists have achieved increased efficiency of cardiomyocyte differentiation yielding 80-90% pure cardiomyocytes (compared to maximum 5-10% achieved traditionally via the EB method) using defined growth factor conditions or pharmacological inhibitors (Chen et al., 2008; Leschik et al., 2008; Lian et al., 2012; Willems et al., 2009; 2011; Xu et al., 2008; Yang et al., 2008b). A recent publication utilizes a growth factor-defined and serum-free system that can yield 0.8-1.3 million cardiomyocytes per cm^2 or virtually pure cardiomyocytes after 14d without cell sorting or selection (Lian et al., 2012).

So far the pluripotent-derived cardiomyocytes (from both ESCs and iPSCs) resemble immature human fetal cardiomyocytes (Willems et al., 2009) by multiple criteria, such as contractile protein expression and myofibrillar structure (Lundy et al., 2013), electrophysiology (Binah et al., 2007; Zhang et al., 2009a), calcium handling (Binah et al., 2007; Dolnikov et al., 2006) and force generation (Dolnikov et al., 2006; Kita-Matsuo et al., 2009). Currently a huge interest is drawn towards the maturation of pluripotent-derived cardiomyocytes and two studies have shown that prolonged cell culture of both ESC- ad hiPSC-CMs (80-120 days) results into the maturation to a more adult-like phenotype based on RNA expression and structural/contractile properties (Babiarz et al., 2012; Lundy et al., 2013). Other maturation efforts involve the use of T3 hormone (Lee et al., 2010) or overexpression of calsequestrin (CSQ) a Ca^{2+}-handling protein (Liu et al., 2009a) that was absent in pluripotent-derived cardiomyocytes (Dolnikov et al., 2006).

1.8.2. ESCs- and iPSCs-derived cardiomyocytes in disease modelling

Despite the importance of iPSCs in disease modelling and the hype about their future use in the clinic, the more immediate value of iPSCs may be found in their differentiated products employed in cell-based assays for small molecule drug discovery and predictive, even personalised, toxicology efforts. In the field of cardiac research, ESCs and iPSC cell lines have accelerated our understanding of the developmental cues towards mesoderm and cardiomyocyte differentiation that finally yielded high-purity cultures of human cardiomyocytes (Hattori et al., 2009; Khan et al., 2013; Laflamme et al., 2007; Lundy et al., 2013; van Hoof et al., 2010; Zandstra et al., 2003). For obvious reasons, human cardiomyocytes are clinical relevant as they resemble closely aspects of human biology in comparison to myocytes from animal models. Toxicology assessment (developmental, hepatotoxicity and cardiotoxicity) is a major challenge in predicting accurately adverse drug reactions and industry has taken up the opportunity to generate large genetically diverse libraries of iPSC lines for preclinical human trials in order to reflect the diversity of drug responses (Anson et al., 2011). Disease-specific iPSCs are also important for building such profiles, but more important their derivatives can potentially be used to identify specific patient populations who would respond favourably or adversely to a drug (Itzhaki et al., 2011; Ma et al., 2013).

To strengthen the case, cardiotoxicity remains the foremost cause for drug withdrawal from the market, thus demonstrating the need for more predictive preclinical testing (Rana et al., 2012). Despite the extensive efforts to identify the toxicity profile *in vitro*, up to 40% of drugs tested in clinical trials are abandoned because of unanticipated adverse side effects. Drug-induced cardiotoxicity can be of two forms: biochemical or electrophysiological. Electrophysiological toxicities arise when compounds affect ion channels or transporters and increase the chances of patients developing arrhythmias (Anson et al., 2011). The most common example is the prolongation of the QT interval representing the ventricular action potential and several drugs have been withdrawn because of such effects (Anson et al., 2011; Rana et al., 2012). At the same time, anthracyclines, anti-inflammatory and anti-HIV drugs, while not withdrawn, carry safety warnings (Rana et al., 2012). HiPSC-CMs, even though they exhibit embryonic electrophysiological properties and action potentials, express many of ion channels present in the adult human heart (Anson et al., 2011) and can be used to screen much earlier in the drug discovery pipeline for arrhythmogenic side-effects. Biochemical cardiotoxicity is less understood, but can be exhibited by various drugs (e.g. chemotherapeutic agents) through mechanisms that potentially include increasing the generation of ROS. Kinase inhibitors used for the treatment of cancer can provoke cardiotoxicity, since many of the same kinases have an important function in the heart (Anson et al., 2011; Cheng and Force, 2010). In this situation, MAP4K4 makes an excellent target for drug development since inhibition of MAP4K4 would lead to decreased cell motility and decreased cell death of cardiomyocytes.

Furthermore, hiPSC-CMs can be employed for the detection of more clinically relevant and sensitive death assays, such as release of cardiac Troponins, rather than the more generic markers like LDH release and decreased ATP (Anson et al., 2011).

Returning to the problem of the drug discovery pipeline, the major reasons for the high attrition rates of drug compounds in the clinic are lack of efficacy and safety (approx. 30% each) (Kola and Landis, 2004). Such failures demonstrate the demand for more predictive animal models, where possible, and the development of paradigms and proof-of-concept experiments that are more predictive much earlier in the drug discovery process. This can explain the prevailing view in the 1990s that quick reductionist measurements in simple homogeneous solution assays (biochemical screening) did not have the desired impact on generating of novel investigative drugs (Taylor L., 2007). Alternative paradigms generating deep functional information include cell-based high-content (HCS) and –throughput (HT) imaging screens.

High content screening (HCS), an automated image-based approach that can measure multiplex phenotypes in cell-based assays, is an engine for driving high-throughput lead discovery. The advantages of HCS lie within its letter, “C” meaning: (i) ***content***, which is the extraction of fluorescence intensities within digitized cell images that can be translated in a number of biological phenotypes, and (ii) ***context***, which is the multi-parametric interrogation of a cell system for simultaneous collection of information to assess true target function in various biological states (Nichols, 2007; p379-414).

HCS was developed to meet the needs of scientists in both basic biomedical science and early drug discovery. High-content image screens are important in two aspects: (i) target identification aiming for a comprehensive functional characterization of the tested genes, while at the same time screen for multiple biological parameters to extract a detailed phenotype and mechanism of action, (ii) lead optimization, which encompasses activities ranging from improvement of compound potency and efficacy, optimization of physical properties, compound metabolism and toxicology issues; all in cellular and subcellular features in individual cells, defined cellular populations and subpopulations of interest. The HCS assays to be established will depend on the read-out (or metric) (e.g. increased/decreased proliferation/cell death/hypertrophy/migration) in the model of interest (cardiomyocytes, neurons, hepatocytes etc). In the case of cardiotoxicity, the interest is to minimize cell death. The next significant aspect is to develop multiplex assays that are robust (regarding signal-to-noise and dynamic range) and are able to differentiate the signalling pathways of cell death (i.e. apoptosis, necrosis, autophagy, ER-stress, senescence). Two recent examples of HCS investigated cardiomyocyte proliferation in mouse ESC-CMs (Uosaki et al., 2013) and NRVCs (Eulalio et al., 2012), respectively, manipulated by a chemical compound or a miRNA library, and using high-content microscopy as the readout.

Finally, the driving force of HCS for cellular phenotype identification to characterize target proteins (i.e. MAP4K4) in an academic environment – upstream of lead optimization - is the use of RNAi technology that has become a field in own right. This is the opportunity to introduce the importance of RNAi technology in HCS.

1.9. The driving forces of High Content Screening: multiplexing and RNAi

RNAi is entrenched in preclinical drug discovery and since the first RNAi-based screen initiated in *C. elegans*, to identify genes for cell division (Fire et al., 1998), there has been a breakthrough in the number of screens that followed. HCS has predominantly been a driving force for the discovery of cancer therapeutics due to the abundance and easy handling of tumour cell lines, but nowadays since the development of iPSCs, it is being used as a functional genomics tool in neurons (Lu and Palacino, 2013), cardiomyocytes(Eulalio et al., 2012), and other differentiated adult cell types, to investigate signalling pathways in cell death, differentiation, migration and proliferation.

The full power of HCS is explored by combining high-throughput inhibitory RNA (RNAi) with high content read-outs (Sachse *et al.,* 2008; p145-185). Inhibitory RNA (RNAi) was first applied to *C.elegans* as a revolutionary tool to silence specific individual genes (Fire et al., 1998) , and is now exploited in organisms ranging from Drosophila to human. It is used for studying fundamental problems in signal transduction and cell physiology, through suppression of gene expression. Naturally occurring RNAi involves double-stranded RNAs that direct sequence-specific gene silencing at the translational level, after they have been processed by nuclear enzymes (Echeverri and Perrimon, 2006). In mammalian cells, the most commonly used experimental systems are (i) synthetic siRNAs (short dsRNAs) or (ii) vector-based short hairpin RNAs (shRNAs) that can be co-expressed with a fluorescent marker (Echeverri and Perrimon, 2006) and modified with flanking microRNA sequences to enhance effectiveness (Silva et al., 2005).

Multiple pathways can be activated by distinct modes of action from a single agent and these are relevant to apoptosis and necrosis (Sachse, 2008; p145-185). Most of the genetic studies on cancer cells depend on monitoring caspase activation, which is the biochemical hallmark of apoptosis, and on proteins that are activated in response to stress (e.g. p53 activation in response to DNA damage, cleaved PARP-1). Potentiometric dyes (e.g. Mitotracker^{TM} Red) that are sensitive to the loss of mitochondrial membrane potential are used to monitor mitochondrial cytotoxicity (Sachse, 2008; p145-185). Lastly, the most vigorous cell-based assays have been built around a viability assay that is a combination of Annexin V/Hoechst nuclear dye, measuring a proportion of live/dead cells, respectively. Disadvantages associated with the last two assays are lack of sensitivity and specificity, respectively.

High-throughput HCS for cell death commonly depend on measuring caspase activation, but this is limited by: (i) caspase activation being non-synonymous with cell death (e.g. in differentiation of ESCs (Fujita et al., 2008) and sub-lethal caspase-3 activation (Chang et al., 2006) in heart failure) and (ii) the existence of caspase-independent cell death. To this end, a

robust HCS is the one that can multiplex endpoints of different pathways or integrate two or more endpoints in the same pathways.

The emergence of RNAi just as genome-sequencing efforts were reaching completion, prompted investigators to explore RNAi as a new functional genomics tool (Sachse, 2008; p145-185). The two most powerful applications of RNAi are in direct loss-of-function (LOF) screening and modifier screens. Modifier screens are particularly powerful in identifying genes and pathways that, when silenced, can either suppress or enhance the phenotype of interest (Echeverri and Perrimon, 2006). This principle has been applied in the context of *in vitro* tumour transformation assays to identify novel tumour suppressors (Kolfschoten et al., 2005; Westbrook et al., 2005) and genes that induce differentiation in cancer stem cells (Wurdak et al., 2010). Recently, a functional miRNA screen was performed on NRVCs to determine miRNAs triggering proliferation in adult cardiomyocytes (Eulalio et al., 2012). The screen identified 204 miRNAs that significantly increased proliferation more than twofold, from which two were selected for downstream testing *ex vivo* in adult cardiomyocytes. A very high-bandwidth approach for the use of RNAi has been the use of genome-scale shRNA libraries in selection-based screens using FACS based on a fluorescent reporter or a receptor ligand. This systematic approach has been carried out in K-*ras*-transformed tumour cells to identify genes required for Ras-mediated gene silencing (Gazin et al., 2007), and in tumour cell lines for the identification of genes that affect cell survival and proliferation (Moffat and Sabatini, 2006; Schlabach et al., 2008; Silva et al., 2008). The pool format libraries allows for the identification of genes based on a survival or differentiation phenotype by simultaneous gene silencing, where each cell is targeted by a single shRNA. Deconvolution of the shRNAs is carried out by barcode microarrays or shRNA sequencing, after a selection pressure is applied. By contrast to the pool knockdown strategy, typically for simple endpoints, the predominant advantage of HCS is the extraction of precise information on cellular events (Echeverri and Perrimon, 2006).

For the HCS in hiPSC-CMs, we plan to utilize the kinome-wide shRNAmir library developed by Stephen Elledge and Gregory Hannon (Silva et al., 2005), whose specifications allow: (i) optimal small RNA performance due to the shRNAmir design that mimic the naturally-occurring knockdown cell machinery (i.e. microRNAs), (ii) higher shRNA expression level due to its regulation from a eukaryotic pol II promoter and (iii) an EGFP protein as a marker for DNA integration after successful lentiviral transduction. The shRNAs will be delivered in a lentivirus form for maximal delivery and stable expression (Cao *et al.,* 2009). With this in mind and for the purpose of knocking down MAP4K4 in hiPSC-CMs we have selected three out of six shRNAmirs after a series of conclusive experiments showing inhibition of MAP4K4 RNA and protein level. We are using hiPSC-CMs in a humanized high-content microscopy platform to investigate – early in the preclinical drug portfolio – the role of MAP4K4 in cell death (as a

proof-of-concept) towards the development of pharmacological inhibitors against the kinase in the setting of MI, and later in cardiac hypertrophy.

1.10. The Aim

MAP4K4 is a novel kinase with involvement in cardiac muscle cell death with evidence from: (i) failing human hearts, (ii) genetic and pathobiological mouse models of cardiac cell death, (iii) gain-of-function studies in mouse myocardium, (iv) gain-of-function and dominant-negative mutations, and (vi) RNA interference in cultured NRVMs. However, there is presently no concrete evidence that these or other death-associated kinases have functional importance in a human cardiac muscle cell. Given this unmet need, the aim of this project was to deploy shRNAmir-based technology in hiPSC-CMs and hypothesized that knockdown of MAP4K4 will result in inhibition of cardiac muscle cell death in response to death-inducing agents (i.e. hydrogen peroxide and c_2-ceramide).

1.10.1. Characterization efforts of hiPSC-CMs from CDI and others

For the purpose of this study we used induced pluripotent stem cell-derived cardiomyocytes (iPSC-CMs). We chose commercially available hiPSC-CMs, because of the high purity of cardiomyocytes (opposed to other available systems at the time) as it confers versatility for using both whole-well-based and high-content cell-based assays. In addition, these cells are commercially available to industry and other institutions with continuous efforts towards characterization and disease modeling. hiPSC-CMs from CDI have been extensively characterized using microarrays (Babiarz et al., 2012), whole-cell patch clump electrophysiology (Ma et al., 2011) and a combination of flux analysis and mitochondrial function toxicity profiling techniques (Rana et al., 2012). The purity of the system was also defined with immunocytofluorescence against the cardiac TNNT2 or α-actin with purity shown to be above 95% (Ma et al., 2011).

Our main interest was to determine the purity of the hiPSC-CMs system based on multiple structural proteins, which we have done using immunofluorescence and high-content microscopy. In addition we wanted to know how much the cells would proliferate in various serum concentrations, and finally to determine whether MAP4K4 was expressed in hiPSC-CMs, which later would be inhibited to investigate its role in cardiac muscle cell death.

1.10.2. Screening shRNAmir constructs for efficient MAP4K4 knockdown in a heterologous system and in hiPSC-CMs

For the knockdown of MAP4K4 we have chosen shRNAmirs in lentiviral vectors that belong to the second-generation shRNA expression library (Silva et al., 2005), where the silencing of these constructs is designed to mimic a natural microRNA primary construct. Additional advantages of these shRNAmirs involved the availability of a fluorescent protein

(EGFP) that offers real-time tracking of EGFP-positive and –negative cells in high-content screening. Prior to phenotypic assessment of MAP4K4 knockdown in hiPSC-CMs there is a requirement to validate the knockdown efficacy of the shRNAmirs on the protein of interest.

In this chapter I will describe the (i) the initial screen for selecting three shRNAmirs and (ii) the downstream experiments to validate the efficacy of shRNAmirs on RNA and protein level, all of which were carried out in a heterologous cell system using HEK293T cells. In summary, cells were transfected, sorted at different time-points (24-96h) and knockdown efficiency was investigated with qPCR. For all the experiments a negative control vector was used known as the non-silencing vector (NSC) where the sequence does not map anywhere on the human genome, and a positive control against GAPDH. Later, virus was produced and the knockdown efficacy of the three shRNAmirs was tested at various MOIs on hiPSC-CMs.

1.10.3. Optimize cell death conditions with H_2O_2 ad c_2-ceramide in hiPSC-CMs and deplete MAP4K4 by RNAi

Reactive Oxygen Species (ROS) (or oxidative stress) are generated from a variety of cellular processes in mammalian cells and are important features of cardiovascular diseases. H_2O_2 as an active ROS and ceramides as molecular species of structural cell membrane components play a major role in I/R and in cell signalling. Ceramides are characterised by a long-chain sphingoid backbone that consists of 2 to 28 carbon atoms (Morales et al., 2007). The fatty acid chain of ceramide is an important determinant of its biological effect. While those with C16 and C24 fatty acids are the most common ceramides, they exhibit negligible solubility in water, thus C2 and C6 ceramides are most frequently used in experimentation. Similarly, myocardial H_2O_2 content was increased (>250%) within 30min of ischaemia and in the early phase of reperfusion (600%). MAP4K4 kinase activity was increased in patients with ischaemic cardiomyopathies (Xie et al., 2007) and in NRVCs in response to H_2O_2 ad c_2-ceramide. Ceramide induced a 20-fold increase in hypodiploid cardiomyocytes at 2h, which was attenuated by co-infecting the cells with either dominant-negative kinase-deficient TAK1 (K63W) or dominant-negative kinase-deficient MAP4K4 (MAP4K4 KR). Similarly, knockdown of MAP4K4 by adenoviral delivery of shRNA directed against this kinase resulted in reduction of c_2-ceramide-induced cell death by 54% as measured by the percentage of hypodiploid cells.

With these in mind I aimed to investigate the effect of knockdown of MAP4K4 on cell death induced by H_2O_2 or c_2-ceramide in hiPSC-CMs. Initially, I optimized the conditions under which hiPSC-CMs undergo cell death for a variety of outputs, including measuring caspase activities, LDH release and loss of mitochondrial potential. Next, knockdown of MAP4K4 was achieved with lentiviral transduction under baseline and agonist-treated conditions to investigate a rescue phenotype from cell death.

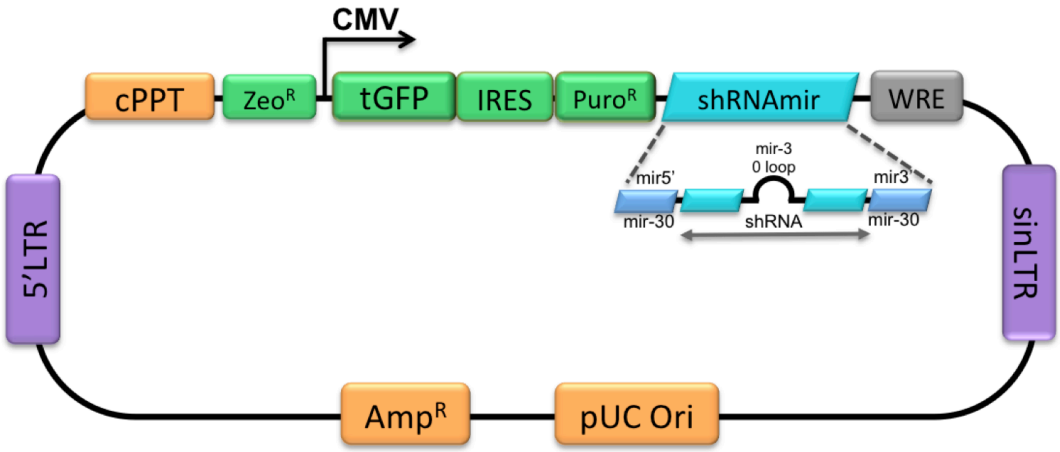
2. Materials and Methods

2.1. Bacterial culture and DNA purification

The GIPZ Lentiviral™ shRNAmirs (Thermo Scientific™) for MAP4K4, TAK1 and, GAPDH genes (RHS4371) and non-silencing (NSC) control (Fig. 10) were purchased as a stock of transformed *E.coli* cryopreserved in glycerol and stored at -80^{o}C (Table 3). Individual constructs were amplified by scraping the stocks with a pipette tip and placing in LB Lennox (low-salt) broth (EMD Millipore 71751) supplemented with 25μg/mL Zeocin (Life Technologies R250-05) and 100μg/mL ampicillin (Sigma-Aldrich A9393) antibiotics. Cultures were grown at 37^{o}C, with continuous shaking at 220rpm. Due to the tendency of viral vectors to recombine, the incubation times for the bacterial cultures were for a maximum of 18h. For the purification of the DNA plasmids, bacterial cultures were collected by centrifugation at 4000g for 10min, and purified using the Plasmid Maxi kit (Qiagen 12163), following the manufacturer's instructions (Qiagen 12163). DNA was quantified on a NanoDrop 1000 Spectrophotometer (Thermo Scientific) and used for downstream applications including transfection and virus production.

Table 3: pGIPZ shRNAmir sequences

Gene	Sense Sequence	Antisense Sequence	Product code
MAP4K4	CAGTGAAGTTTCTCCGTTA	TAACGGAGAAACTTCACTG	V2LHS_173825
	CAAGTTAGAATCCAGCTTA	TAAGCTGGATTCTAACTTG	V2LHS_202781
	GCTTACATCTCCAGAGAAA	TTTCTCTGGAGATGTAAGC	V2LHS_201856
	AGATAAATATGCTAAAGAA	TTCTTTAGCATATTTATCT	V2LHS_68219
	TCACCAAGGATGTAGTTCT	AGAACTACATCCTTGGTGA	V3LHS_375570
TAK1	CGCCCTTCAATGGAGGAAA	CGCCCTTCAATGGAGGAAA	V2LHS_201612
	CCTTTGGAGTTGTTTGCAA	TTGCAAACAACTCCAAAGG	V2LHS_201931
	CGTGTGAACCATCCTAATA	TATTAGGATGGTTCACACG	V2LHS_202210
	AGCTTTTAGATGAAAACAA	TTGTTTTCATCTAAAAGCT	V3LHS_370924
	AGAGTGAATCTGGACGTTT	AAACGTCCAGATTCACTCT	V3LHS_370925



Vector Element	Utility
CMV	RNA polymerase II promoter
cPPT	Central Polypurine Tract; Helps translocation into the nucleus of non-dividing cells
WRE	Enhances stability and translation of transcripts
tGFP	Turbo Green Fluorescent Protein; Marker to track shRNAmir expression
IRES	Internal Ribosome Entry Site; For co-expression of heterologous genes, in this case tGFP and Puro^R, by CMV promoter
Puro^R	Puromycin mammalian selectable marker
shRNAmir	Second-generation shRNA contained within the backbone of the primary miR-30 miRNA, to mimic the endogenous mammalian miRNA biogenesis pathway
Amp^R	Ampicillin bacterial selectable marker
Zeo^R	Zeocin bacterial selectable marker
pUC Ori	Bacterial high-copy origin of replication and maintenance of plasmid in *E.coli*
sinLTR	3' Self inactivating Long Terminal Repeat
5'LTR	5' Long Terminal Repeat
RRE	Rev Response Element; Transport to the cytoplasm for translation and virion packaging

Figure 10: **Schematic representation of the pGIPZ lentiviral shRNAmir vector.** Vector features or elements and their utility are depicted in the table.

2.2. Cell culture

2.2.1. General procedure

All cells and cell culture reagents (falcon tubes, solutions, and media) were handled under sterile conditions in biological safety cabinets. Media were aliquoted and frozen at -20°C for long-term storage and thawed overnight at 4°C when needed. Defined HyClone™ Fetal Bovine Serum (FBS) was obtained from Thermo Scientific (SH30070.03), aliquoted and stored at -80°C. Powdered reagents were always sterile-filtered after reconstitution with 0.2µm filter units. All solutions were stored at 4°C for a maximum of one month, whereas medium was kept for maximum 2 weeks. All cell cultures were maintained in 95% air and 5% carbon dioxide (CO_2) at 37°C.

2.2.2. Maintenance of HEK293 and HeLa cell lines

Early passage (P3-P10) Lenti-X HEK293T cell line (Clontech 632180) was used for transfection and virus production. Lenti-X HEK293T cells were maintained in DMEM (Life Technologies 61965-026) supplemented with 10% (v/v) FBS (growth media). Cells were maintained by sub-culturing at approximately 80% confluency. Cells were removed by trypsinisation, using 2ml 0.25% Trypsin/EDTA (Life Technologies 25200056source) per 75cm^2 and incubating at 37°C for 2min. Trypsin was inactivated by addition of 8ml growth media and collected by centrifugation at 250g for 5min. Cells were re-suspended in 10ml fresh growth media, from which the cell suspension was divided into vented T75 (Corning® 430641) or -T150 (Corning® 430825) cell culture flasks (Corning®) and, made up to 12ml and 25ml volume, respectively, with growth media. HeLa (ATCC® CCL-2™) cell line was maintained in Eagle's Minimum Essential Medium (ATCC® 30-2003) and sub-cultivated at 1:4 ratio following a similar procedure.

2.2.3. General culture of hiPSC-CMs

For the purpose of this study, iCell cardiomyocytes were purchased from Cellular Dynamics International (CDI CMC-100-110-001). HiPSC-CMs were derived from induced pluripotent stem cells through proprietary differentiation and purification protocols. The cells are a mixture of atrial, nodal and ventricular-like myocytes that are spontaneously electrically active. Cells were received in 1ml cryovials as cryopreserved single-cell suspensions and immediately placed for long-term storage in a dry-air freezer (-150°C). When thawed, hiPSC-CMs were seeded in Plating Medium for 2 days and maintained in Maintenance Medium for a total period of 8 days. Media was then replaced with DMEM (Life Technologies 61965026 or

10567014) supplemented with 2% (v/v) FBS (or other amounts stated appropriately) to minimise effects of potential cell death inhibitors or enhancing survival agents present in Maintenance Medium prior to experiments. Experiments were carried out thereafter in the same media. HiPSC-CMs were maintained in culture for less than 2 weeks without appreciable loss of purity. Cells were thawed in 24-well plates (Greiner 662960) for the collection of RNA and in µClear™ half-area 96-well plates (Greiner 675090) for cell death assays.

2.2.4. Preparing cell culture surfaces

HiPSC-CMs were plated on artificial substrate Collagen Type I (BD 354249). Collagen stock was prepared in 500ml of distilled water (Life Technologies, 15230001) supplemented with 0.02N Glacial Acetic Acid (Fischer-Scientific, A/0400). The stock was membrane-filtered (0.2µm) and stored at 4^{o}C for maximum one month. Prior to thawing hiPSC-CMs, half-area 96-well plates and 24-well plates were coated with 50µl or 250µl of stock collagen solution respectively and left under sterile conditions at RT for 1h. Wells were washed 3X with 1X PBS (Life Technologies 14190-144) to remove unbound collagen, and plates were left to air-dry under the hood for 30min prior to use.

2.2.5. Thawing hiPSC-CMs

The iCell cryovial was placed in a 37^{o}C water bath (without submerging the cap) and held stationary (no swirling) for 4min. The cryovial was removed from the waterbath, submerged into 70% ethanol and the contents transferred into a 50ml centrifuge tube using a 1ml pipette. The cryovial was rinsed with 1ml of RT Plating Medium to recover residual cells. To minimize osmotic shock and increase cardiomyocyte viability the 1ml was added drop-wise over 90sec (approx. one drop every 4-5sec) to the thawed cardiomyocytes and the 50ml tube was swirled gently after addition of each drop. Next, 8ml of Plating Medium was added in a drop-wise fashion over 30-60 seconds. Another 7ml was added over the next 30sec seconds. For the accurate assessment of viable cell number and correct seeding, hiPSC-CMs were gently mixed using a 10ml pipette and quantified via the trypan blue excretion method (where only live cells exclude the dye, thus dead cells stain positive) using the Vi-CELL® cell viability analyser (Beckman Coulter 731050). A positive control for trypan blue excretion was not used.

2.2.6. Plating hiPSC-CMs

Using the Plating Efficiency control metric found on the Certificate of Analysis (CoA) the following calculations were carried out to obtain the Target Plating Density and the Total Plating Volume using the Viable Cell Count (Table 4). The Plating Efficiency for the lot used in this study was 53%. The desired cell number per well for death assays and RNA collection was 10000 (µClear™ half area 96-well half area plates) and 120000 (24-well plates) per well,

respectively. For the calculations the following characteristics were taken into account and are explained in detail below (Table 4).

Table 4: Terminology and equations for plating hiPSC-CMs

Characteristics	Description
Viable Cell Count	The total number of viable cells after counting of the single-cell suspension post thaw.
Viable Cell Density	The number of viable cells per ml after cell counting of the single-cell suspension post thaw.
Seeded Cell Count	The total number of viable cells added to the cell culture well to achieve the plated cell count (or density).
Plated Cell Count / Target Plating Density	The number of viable cells that have firmly attached to the cell culture well after 48h. $Target\ Plating\ Density = \frac{Desired\ Cell\ Number\ per\ well}{Seeding\ volume\ per\ well\ (ml)}$
Plating Efficiency	A quality control metric determined for each lot of iCell cardiomyocytes, found on the Certificate of Analysis (CoA) with each shipment. $Plating\ Efficiency = \frac{Plated\ Cell\ Count}{Seeded\ Cell\ Count} x\ 100$
Total Plating Volume	The volume of Plating Medium required bringing the thawed cell suspension to the Target Plating Density. $Total\ Plating\ Volume = \frac{Actual\ Volume(ml) x\ Viable\ Cell\ Density\ \left(\frac{cells}{ml}\right) x\ Plating\ Efficiency}{Target\ Plating\ Density\ (\frac{cells}{ml})}$

2.2.7. Maintenance of hiPSC-CMs

Cells were cultured in 120µl of Plating Media for 48h post-thaw and replaced with Maintenance Medium for a further 48h. Wells were washed to remove non-adherent cells and debris by gently pipetting the medium up and down (approx. 3 times). Maintenance Medium was then aspirated and cells were replenished with 120µl fresh Maintenance Medium, and every 2 days thereafter. Cells were cultured in Maintenance Medium (MM) until the application of cell-based assays.

2.3. Cell Death induction with H_20_2 and c_2-ceramide

HiPSC-CMs were treated with H_2O_2 (Sigma-Aldrich H1009) and c_2-ceramide (Sigma-Aldrich A7191) at various concentrations with cell-culture grade distilled H_2O and DMSO as vehicle controls (VC), respectively. The original stock of H_2O_2 was 9.8M, which was first diluted to 20mM in water and then in medium. Serial dilutions of H_2O_2 were prepared and added onto the cells within 10min. Treatments with H_2O_2 were carried out in DMEM (Life Technologies 61965026 or 10567014) and with c_2-ceramide in DMEM (Life Technologies 10567014) both supplemented with 2% (v/v) FBS. For the initial optimisation, various serum concentrations were used and are stated in the appropriate sections.

2.4. Transfection

For testing efficiency of MAP4K4 shRNAmir constructs in knocking down MAP4K4 mRNA, Lenti-X HEK293T cells were used. Cells were seeded 24h prior to transfection in 60mm x 15mm culture dishes (Corning 430166) at ~70000 cells/cm^2 (or $1.5x10^6$ per / dish). For successful transfection of DNA into cultured cells, the ratio of FuGENE® 6 Transfection Reagent (Promega E2692) to DNA (µg) used was 3:2. FuGENE® 6 was left at RT for 10min prior to mixing with 100µl serum-free DMEM medium and incubated for 10min at RT. The DNA plasmid mixture (MAP4K4 DNA plasmid with pGIPZ shRNAmir or NSC plasmid) was prepared in eppendorf tubes to contain equal µg amounts of DNA (MAP4K4 DNA plasmid with each shRNAmir or NSC plasmid), added to the FuGENE® 6-containing medium. The transfection mixture was incubated at RT for 20min. In each dish, the transfection mixture was added drop-wise throughout the entire surface to ensure even distribution. Cells were cultured at 37°C and collected at consecutive time-points: 24h, 48h, 72h or 96h by the method of trypsinisation and centrifugation (described at 2.2.2). Prior purification of EGFP-positive cells via FACS, cell suspensions were re-suspended in growth medium [DMEM with 2% (v/v) FBS].

2.5. Virus production and titration

The most knockdown-efficient three out of six shRNAmirs were packaged into viral particles for downstream transduction of non-replicating hiPSC-CMs. The following section describes how lentiviruses were prepared, purified and titrated using a 2nd generation packaging system, the vectors for which were kindly provided by Prof. Didier Trono. Lentiviral work was carried out in a Bio-safety Level II cell culture cabinet.

2.5.1. Cell transfection with lentiviral vectors and virus collection

Extra-pure plasmid DNA was isolated from the 2nd generation packaging vectors pSPAX2 (Addgene 12260) and pMD2.G (Addgene 12259) using the Endo-Free Maxiprep kit (QIAGEN 12632). Early passage (P3-P5) Lenti-X HEK293T cells (Clontech 632180) were seeded in the morning (Day 1) at a density 8.33x10^5 cells/cm^2 in 10cm^2 dishes to achieve approx. 80-90% confluency at the time of transfection. For each virus 4X 10cm^2 dishes were seeded. The same day in the afternoon HEK293FT cells were transfected with the DNA plasmid mixture. For the transfection of each dish, the packaging plasmids were mixed in a sterile eppendorf tube with the corresponding shRNAmir lentiviral vector in the following ratio: 6µg shRNAmir to 3µg pMD2G to 4.5µg pSPAX2. Fugene® 6 (67.5µl) was added into 580µl serum-free DMEM (Life Technologies 61965-026) minus the volume of the DNA mixture to be added and left for 5min at RT, where the DNA mixture was added and left for an additional 30min at RT. The transfection mixture (160µl) was drop-wise added over the entire surface of the cells and placed in the 37^{o}C incubator. The next morning (Day 2) the medium was removed (approx. 8-12h after transfection) and replenished with 6ml of fresh DMEM medium supplemented with 10% (v/v) FBS. To rapidly test for sufficient virus production, 20µl of the supernatant was collected and tested with the Lenti-X GoStix (Clontech 631244) according to the kit's instructions. The Lenti-X GoStix are designed to qualitative confirm the presence of the lentivirus within a usable concentration range by detecting the lentiviral p24 protein, similar to an ELISA assay. Supernatant was collected 36h after transfection (24h after media change) (Day 3) and filtered with a 0.45µm filter units (Corning 430773) to remove cell debris. The supernatant was stored at 4^{o}C overnight, whereas HEK293T were replenished with additional 6ml of growth medium and placed at 37^{o}C. The next day (Day 4) the second supernatant was harvested, similarly filtered and pooled together with the first supernatant.

2.5.2. Concentration of viruses with high-speed ultracentrifugation

The viral particles were concentrated in a sucrose cushion by ultracentrifugation at 82700xg (or 26000rpm) for 2h at 4°C using the Beckman SW32Ti (swinging bucket) rotor with a capacity of six tubes. Conical bottom ultracentrifugation tubes (Beckman 358126) were autoclaved the previous day and filled with 24ml of virus-containing supernatant. The supernatant was underlayed with 4ml of 20% (v/v) sucrose solution in water by slowly pipetting to the bottom of each conical tube with a 5ml pipette. Before the centrifugation, the tubes were weighed and balanced to the closest 0.1 degree (100µl ~ 0.1g). After centrifugation the supernatant was decanted and the remaining liquid drained by resting the tube on a paper towel for 5min. The viral translucent pellet was re-suspended by addition of 200µl of serum-free DMEM and enclosing the tube in a screw-cap 50ml falcon tube. The viral pellet was vortexed every 20min at low speed and was kept at 4°C in-between vortexing steps, for a total of 2h. Finally, 15µl aliquots were prepared for long-term storage at -80°C. Freeze-thaw cycles were avoided and minimized to less than two to maintain virus transduction efficiency. All steps were carried out under sterile environment.

2.5.3. Virus titration

Each virus preparation was titrated to determine the concentration of the stock (transforming units (TU)/ml) and calculate equal Multiplicity of Infection (MOI) for hiPSC-CMs. For the titration, HeLa cells were used, as they have more similar transduction efficiency to rat neonatal rat ventricular cardiomyocytes (NRVCs) than HEK293T cells and might better reflect transduction efficiency in hiPSC-CMs. HeLa cells were seeded in 24-well plates at 40000 cells/cm^2 24h prior to viral infection. A ten-fold serial dilution of the lentiviral preparation in 1X serum-free DMEM supplemented with 8µg/ml Polybrene (Merck Millipore TR-1003-G) was prepared in 96-well plates. The highest concentration was prepared by addition of 10µl virus to 90µl media, with the consecutive transfer of 20µl to 80µl media between each dilution series. At the same time, the medium of the 24-well plates was removed and replaced with 250µl of serum-free DMEM supplemented with 8µg/ml Polybrene. 25µl of each viral dilution was transferred to the cells and left for 24h at 37°C. Two extra wells were used for counting HeLa cells at the time of transduction, required for the calculation of the transduction efficiency. The next day, HeLa cells were collected by trypsinisation and the proportion of EGFP-positive population analysed by Flow Cytometry. To calculate the biological titre (TU/ml or transducing units) the following formula was used:

$$\frac{TU}{\mu l} = \frac{(P * N)/(100 * V)}{DF}$$

Where:

P = % $EGFP^+$ cells

N = number of cells at time of transduction

V = volume of virus added to each well

DF = dilution factor (1 for undiluted, 10^{-1} for diluted 1/10, and so on)

2.5.4. Virus transduction of hiPSC-CMs

For the transduction of hiPSC-CMs multiple MOIs were tested (10, 20 and 50) with most efficient knockdown of MAP4K4 achieved at MOI50. This concentration was therefore used in further experiments for investigating the effect of MAP4K4 knockdown on cell death. Transduction of hiPSC-CMs in 24-well plates (for harvest of RNA) with shRNAmir-carrying virus was carried out as described for transduction of HeLa cells. For the transduction of hiPSC-CMs in half-area 96-well plates, a master mix of each virus was prepared in serum-free DMEM supplemented with 8µg/ml Polybrene, of which 50µl was added onto the cells for 8h. Virus-containing medium was removed and replaced with 120µl of MM, in which cells were maintained for 36h.

2.6. Immunocytostaining

HiPSC-CMs were immunolabeled with cardiac-specific antibodies at the corresponding concentrations (Table 5). Immunocytostaining was carried out by fixing the cells by addition of 4% (w/v) PFA in 1X PBS for 15min and washing 3X with 1X PBS. Cells were permeabilised with 0.2% (v/v) Triton-X in 1X PBS for 15min and non-specific binding sites blocked with 4% (v/v) Donkey serum (Jackson Immunoresearch 17000121) in 0.02% (v/v) Triton-X in 1X PBS at RT. The primary antibody was incubated at final concentrations of 1µg/ml to 2µg/ml in the blocking buffer (4% Donkey serum in 1X PBS) (Table 5) at 4°C overnight. The next day cells were washed 3X with 1X PBS and incubated with the secondary antibody at 2.5 to 3.5µg/ml in blocking buffer in the dark for 1h at RT. Cells were then washed 3X with 1X PBS and incubated for 5min in 5µg/ml (200nM) DAPI in 1X PBS. Cells were washed once and imaged immediately, or stored overnight at 4°C protected from light by wrapping in foil. All incubations steps were carried out with gentle shaking using a table orbital shaker at 40rpm.

Table 5: Reagents for Immunocytostaining

Reagents	Species raised, Antigen	Conjugate	Company	Product code	Final Concentration	Isotype
Cardiac-specific Antibodies						
Troponin 2 (1C11)	Mouse IgG1	Biotin	Abcam	ab105441	2µg/ml	[B]
Troponin 2 (1C11)	Mouse IgG1	NA	Abcam	ab8295	2µg/ml	[E]
Troponin I	Goat IgG (polyclonal)	NA	Santa Cruz	sc-8118	2µg/ml	[G]
Phospholamban (clone 2D12)	Mouse IgG2a	NA	Enzo Life Sciences	ALX-804-093-R100	1µg/ml	[A]
MLC2v	Mouse IgG2a	ATTO®647N	Synaptic Systems	310111AT1	1µg/ml	[A]
MLC2a	Mouse IgG2b	NA	Synaptic Systems	311011	2µg/ml	[D]
Sarcomeric myosin (clone MF-20)	mouse IgG2b	NA	R&D	IC4470F	2µg/ml	[C]
α-actinin (clone EA-53)	mouse IgG1	NA	Sigma-Aldrich	A7811	2.5µg/ml	[E]
βMHC	Rabbit IgG (polyclonal)	NA	Abcam	ab46936	2µg/ml	[F]
Isotype controls						
Isotype [E]	Mouse IgG1 k	NA	Abcam	ab18448	2µg/ml	
Isotype [C]	Mouse IgG2B	NA	R&D	MAB004	2µg/ml	
Isotype [D]	Mouse IgG2b	NA	Santa Cruz	sc-3879	2µg/ml	
Isotype (MG2a-53) [A]	Mouse IgG2a k	NA	Abcam	ab18414	1µg/ml	
Biotin Isotype (clone MOPC-21) [B]	Mouse IgG1 k	NA	BioLegend	400104	2µg/ml	
Polyclonal isotype (Protein G purified) [F]	Rabbit IgG	NA	Abcam	ab27472	2µg/ml	
Polyclonal isotype (Protein G purified) [G]	Goat IgG	NA	Santa Cruz	sc-2028	2µg/ml	
Secondary Antibodies						
Mouse 488	Donkey	NA	Jackson ImmunoResearch	715-546-150	2.5µg/ml	
Rabbit 647	Donkey	NA	Jackson ImmunoResearch	711-606-152	3.5µg/ml	
Rabbit 488	Donkey	NA	Jackson ImmunoResearch	711485152	2.5µg/ml	
Mouse 647	Donkey	NA	Jackson ImmunoResearch	715-606-150	3.5µg/ml	
Goat 647	Donkey	NA	Jackson ImmunoResearch	705495147	3.5µg/ml	
Rat 647	Goat	NA	Cell Signalling	4418	3.5µg/ml	
APC	Mouse	Streptavidin	eBioscience	174317	1µg/ml	
FITC	Mouse	Streptavidin	eBioscience	114317	0.5µg/ml	

2.7. Proliferation assay

To determine the percentage of proliferating hiPSC-CMs, we used the Click-iT© EdU HCS Assay (Life technologies C10351) as an alternative to the traditional method for detecting and quantifying DNA by BrdU. HiPSC-CMs, HeLa and mouse SP clones were seeded in 96-well plates in triplicate. Positive controls (SP clones and HeLa cells) were serum-starved for 48h and 24h respectively, while the hiPSC-CMs were cultured for 48h in various serum concentrations (0.5, 2, 5 and 10%) and in the absence of serum. In the last 6h of the 48h period cells were incubated with EdU, fixed and permeabilised. The working EdU solution (Component A of the kit) was prepared in complete medium was at 5mM (2X EdU) from a 10mM stock. EdU was added into each well at a final concentration of 5μM and the plates were incubated under normal cell culture conditions for 6h. A negative control for the hiPSC-CMs was included that was not treated with EdU (data not shown). After EdU incubation the medium was removed and 200μl of 4% (v/v) PFA in 1X PBS was added for 15min at RT. Fixative was removed and each well was washed twice with 1X PBS. Cells were permeabilised with 0.2% (v/v) Triton-X-100 in 1X PBS for 15min at RT. The Click-iT© reaction cocktail (Reaction components found within the manual) was prepared immediately before use in 1X Click-iT© EdU Buffer as per manufacturer's instructions. The permeabilisation buffer was removed, wells were washed twice in 1X PBS and 100μl of Click-iT© reaction cocktail was added per well. Plates were incubated for 30min at RT, protected from light. The reaction cocktail was removed and cells were washed once with 100μl of Click-iT© Reaction Rinse Buffer (Component F). At this stage antibody labelling against Phospho-H3 Ser^{10} (Millipore, 06-570) was performed. Cells were blocked in 4% (w/v) BSA in 1X PBS, supplemented with 0.02% (v/v) Triton-X-100 for 1h at RT. The primary antibody was incubated for 2h at RT under gentle agitation, washed twice in 1X PBS and incubated with the secondary antibody (Life Technologies, 4412) for 1h at RT. Nuclei were counterstained with 5μg/ml DAPI for 5min at RT. The plate was visualised by the Cellomics® High Content Screening platform under the green emission filter (for the detection of phospho-H3) and under the far-red emission filter (for EdU).

2.8. RNA isolation and cDNA synthesis

For all RNA isolations from FACS-sorted HEK293 cells and hiPSC-CMs the PureLink® RNA Micro Scale Kit (Life Technologies 12183016) was used. The final elution volume was 13μl with 2μl dead-volume. Further purification of RNA (removal of contaminating DNA) was carried out within the isolation columns using the DNase treatment components provided with the kit. RNA was quantified on the NanoDrop 1000 instrumentation and was subsequently used for cDNA synthesis. For the conversion of RNA to cDNA, the High

Capacity cDNA transcription kit (ABI 4368814) was used for conversion of 500µg of RNA in a final volume of 20µl. The minimum amount of RNA used in 20µl of reaction volume was 200µg. The reaction mixture contained the following components; 2µl of 10X RT Buffer, 0.8µl of 25X (100mM) dNTP Mix, 2µl of 10X RT Random Primers, 1µl of MultiScribe Reverse Transcriptase and 1µl of RNase Inhibitor made up to a final volume of 10µl with nuclease-free water. cDNA was added in a final volume of 10µl to bring the total reaction volume to 20µl. The thermal cycler conditions for the conversion of RNA to cDNA were: 25^{o}C for 10min, 37^{o}C for 120min and 85^{o}C for 5min. cDNA was stored at -20^{o}C and thawed on ice when required for quantitative PCR (qPCR). A negative control for each cDNA synthesis was carried out without the presence of RNA.

2.9. Quantitative PCR

Quantitative PCR reactions were prepared in MicroAmp™ Optical 384-Well plates (Life Technologies 4309849) for all genes using standard inventoried Gene Expression Assays (Table 6) that span exon-exon boundaries for cDNA transcripts unless otherwise stated. A single-well reaction mixture consisted of 7.5µl of 2X TaqMan Gene Expression Master Mix (Life Technologies 4369016), 0.75µl of 20X TaqMan Gene Expression Assays (Table 6) with 20ng cDNA in a final reaction volume of 15µl. A Master Mix was prepared each time without the cDNA, the latter of which was added to each well last. The qPCR plates were run under the Standard Mode of the Thermal Cycler Protocol at 50^{o}C for 2min, 95^{o}C for 10min, 40 cycles at 25^{o}C for 15sec and 60^{o}C for 1min using an Applied Biosystems (ABI) 7500 Real-Time PCR System. Large Ribosomal Protein (RPLP0) gene was used as the endogenous reference control in all experiments.

Table 6: qPCR primers

Gene	Expression Assay
MAP4K4	Hs00377415_m1
TAK1	Hs01105682_m1
MINK1	Hs01093259_m1
TNIK	Hs00323234_m1
RPLP0	Hs99999902_m1
GAPDH	4333764F

2.10. Fluorescence-Associated Cell Sorting (FACS)

2.10.1. Cell Preparation, FACS and collection

For MAP4K4 knockdown experiments, HEK293 cells were collected by trypsinisation and centrifugation for 5min at 200g on a standard bench-top centrifuge. Trypsin-containing medium was discarded and replaced with FACS Buffer (2% (v/v) FBS, 15mM HEPES pH 7.0, 1mM EDTA) supplemented with and 100 μ g/ml Deoxyribonuclease (DN*ase*) I (Sigma-Aldrich D4527) in 1X PBS to preserve cell viability and prevent clumping. Cell suspensions were kept on ice and passed through a 40µm nylon mesh filter immediately prior to sorting. To exclude dead cells, 2µl of Sytox Blue Dead Cell Stain (Life Technologies S34857) was added for 5min prior to sorting (Life Technologies). Negative unstained controls were used in every experiment and purity was confirmed after sorting by re-analysing a small fraction of the sorted population. For RNA collection, $6x10^5$ cells were collected in RNA*later* (Life Technologies AM7021) and samples and were kept on ice until all samples were purified. RNA samples in RNA*later* were centrifuged at 4500g for 8min and re-suspended in the Lysis Buffer provided with the PureLink® RNA Micro Scale Kit. For protein isolation, $1.5x10^6$ cells were sorted in FACS Protein Buffer (2% (v/v) FBS in 1X PBS with 15mM HEPES). Samples were centrifuged at 250g for 5min immediately and suspended in 100-200 µl of Protein Lysis Buffer for protein extraction and quantification.

2.10.2. Cytometer parameters (calibration and gating)

Cell suspensions of Lenti-X HEK293T cells were purified by FACS (FACSAria II, BD) where debris and doublets were excluded using the forward scatter (FSC, a measure for particle size) and Side Scatter (SSC, a measure for particle complexity and density). Dead cells were excluded on the basis of their emission spectrum (480nm) when excited with 405nm Violet laser light. The EGFP-positive population was identified by gating above the unstained EGFP-negative population on a FITC/negative fluorescence channel histogram using an excitation 488nm Blue laser and for detection a 561nm emission filter. At least 20000 events were recorded for each FACS-sorted population.

2.11. Protein extraction and quantification

For protein extraction, one PhosSTOP phosphatase inhibitor cocktail tablet (Roche 04906845001) and one cOmplete EDTA-free protease inhibitor tablet (Roche 04693159001) were freshly added per 10ml of protein Lysis Buffer (complete Lysis Buffer), which was stored on ice until required. Complete Lysis Buffer was aliquoted and stored at -20^{o}C. Cells were collected by centrifugation at 250g for 5min, and 100-400µl of complete Lysis Buffer

added. The cell suspension was transferred into 1.5ml eppendorf tubes and lysed by placing on ice for 30min with regular vortexing. The cell lysate was centrifuged at 12000g for 10min at 4°C to pellet insoluble cell debris and the supernatant was transferred into a fresh eppendorf tube. Protein extracts were stored at -80°C and thawed on ice for protein quantification and Western blot applications. Total protein was quantified using the BCA protein assay kit (Pierce 23225) using a 1:8 dilution of the stock protein. The BCA assay was carried out on a 96-well plate format using a series of pre-diluted BSA standards (Pierce 23208) at 125, 250, 500, 750, 1000 and 1500µg/ml to generate a standard curve. After mixing the protein extracts with the BCA diluent solution (10mM TrisHCl, 0.01mM EDTA) according to the manufacturer's protocol, the plate was incubated at 37°C for 30min. For the extraction of protein from 96-well plates used for the normalization of colorimetric cell assays (LDH, caspase-3, caspase-8), the MicroBCA Protein Assay kit (Pierce 23235) was used similarly, with the exception of an extended incubation time of 2h. In both assays, the absorbance was measured at 562nm on a Paradigm plate reader (Molecular Devices). Total protein concentration was calculated from the standard curve slope (y=ax+b).

2.12. Western blotting

The following protocol describes the entire process of the Western blot procedure carried out for the characterization of hiPSC-CMs and the investigation of the efficacy of shRNAmirs in knocking down MAP4K4. The different steps include sample preparation for loading into gels, preparation and running of SDS-PAGE gels, the transfer of proteins from the gel onto the membrane and detection of specific proteins.

2.12.1. Preparation of polyacrylamide gels and samples

Polyacrylamide gels (for Sodium Dodecyl Sulphate Polyacrylamide Gel Electrophoresis (SDS-PAGE)) were prepared as shown in *Supplementary Materials and Methods*. For the separation of both MAP4K4 and TAK1, 10% polyacrylamide gels were used. The gels were placed in the running chamber, which was filled with 1L of 1X Running Buffer. The combs were removed and the wells were flushed with Running Buffer to remove excess polymerised acrylamide. Samples were prepared by mixing equalised total protein extracts with 4X Laemmli loading buffer to a final volume of 25µl. Proteins were denatured at 95°C for 5min and loaded into each lane. Electrophoresis was carried out at 90-120V between 1-2h until the Molecular Weight Ladder had separated sufficiently and reached the bottom of the gel. For proteins, such as MAP4K4, larger than 70kDa, the gel was run until the smallest two markers of the ladder had eluted from the gel (14 and 17kDa). Equal amounts of protein lysate were loaded between samples for the MAP4K4 knockdown time-course

experiments (25µg crude protein lysate, 25µg crude or 150µg of immunoprecipitated MAP4K4 from FACS-purified EGFP-positive populations).

2.12.2. Electrotransfer, blocking and incubating with antibodies

A wet transfer procedure was used, where the gel and membranes were sandwiched between sponge and paper soaked in 1X Towbin's Electrotransfer Buffer containing 20% (v/v) methanol. The sponge/paper/gel/membrane/paper/sponge sandwich was clamped tightly together after ensuring no air bubbles had formed between the gel and membrane. The sandwich was run at 120V for 1h15min in 1X Towbin's Electrotransfer Buffer containing 20% (v/v) methanol. The membranes were then immersed in Ponceau Red solution (Sigma-Aldrich P7170) for 5min at RT to visualise any bubbles that might have interrupted protein transfer. The membranes were washed in 1X TBS supplemented with 1% (v/v) Tween-20 (1xTBST) and exposed binding sites blocked in 5% non-fat milk in TBST 1X TBST for 1h at RT to minimise background due to non-specific binding of the primary antibody. Membranes were washed once in 1X TBST and incubated with the primary antibody at 4^{o}C overnight with gentle agitation at 40rpm. Primary antibodies used were MAP4K4 (ab56569, ab70424), GAPDH (Cell signalling 2118) and Flag M2 (Sigma-Aldrich F1804) at 1µg/ml, and β-tubulin (Sigma-Aldrich T52201) at 0.5µg/ml. The next day, to remove unbound primary antibody, membranes were washed under rotary agitation at 65rpm for 1h at RT, with 1X TBST replaced at 15min intervals. Primary antibodies were detected by incubation with appropriate horseradish peroxidase (HRP)-conjugated secondary antibodies to mouse or rabbit IgG (Table 2.4), in 0.1% non-fat milk in 1X TBST for 1h at RT, with the exception of HRP-anti-mouse IgG for detection of β-tubulin, which was incubated for 30min. Finally the membranes were immersed in Western blot detection reagent (Promega W1015) for 5min at RT to generate a chemiluminescent signal, where bound HRP-labelled antibodies convert detection reagent to light. Chemiluminescence was detected by exposure to autoradiography film and developed using Compact X4 (Xograph Imaging Systems) an automated film developer in a dark room.

2.13. Protein Immunoprecipitation (IP)

MAP4K4 was immunoprecipitated from FACS-purified EGFP-positive populations to determine knockdown of endogenous protein after transfection with three different shRNAmir constructs. Furthermore, IP was used to investigate the presence and activity of the kinase in hiPSC-CMs. 150µg and 500µg of total protein was immunoprecipitated from HEK293FT expressing MAP4K4-Flag and hiPSC-CMs, respectively. To eliminate non-specific binding by

the antibody of interest, protein extracts were incubated with 1µg of the isotype control (of the corresponding primary antibody) per 500µg of total protein at a final concentration (1µg/µl) with 20µl Protein A/G PLUS-Agarose beads (Santa Cruz sc-2003). Sample volumes were adjusted to 300µl each and mixed by rotation for 1h at 4^{o}C. The agarose beads were collected and discarded by centrifugation at 1000g for 5min at 4^{o}C, and the supernatant (pre-cleared cell lysate) was transferred to a fresh 1.5ml eppendorf tube for IP. The pre-cleared cell lysate were incubated with 5µl of affinity-purified monoclonal MAP4K4 antibody (Abcam ab56569) per 500µg or 2µl of ab70424 per 500µg of protein and mixed by rotation overnight at 4^{o}C. The next day, 20µl of Protein A/G PLUS-Agarose beads were added to each sample and incubated under rotary agitation for 2h at 4^{o}C. Immune-precipitated MAP4K4 bound to agarose beads were collected by centrifugation at 1000g for 2min at 4^{o}C and the beads washed twice with 500µl of Protein Lysis Buffer. After each washing step beads were collected by centrifugation as above. After the final wash the last supernatant was discarded and 4X loading buffer was added to the beads (final volume approx. 40-50µl). IP samples were boiled at 95^{o}C for 5min to denature the protein and elute from the beads. At this stage samples were either centrifuged and proteins separated by SDS-PAGE or stored at -80^{o}C. Protein detected at 50 and 25kDa corresponded to the antibody's heavy and light chains, respectively.

2.14. Kinase assay

The kinase assay was performed using protein lysate from hiPSC-CMs to investigate whether MAP4K4 becomes activated by 250µM of hydrogen peroxide (HP). The kinase assay protocol was carried out as for IP, up to the final wash step. At this point, the agarose beads were washed twice with 1X Kinase Buffer (10X stock, Cell Signalling 9802) and suspended in 50µl of 1X Kinase Buffer supplemented with 200µM ATP (10mM stock, Cell Signalling 9804) and 2mg/ml MBP kinase substrate. The samples were incubated at 30^{o}C for 30min and the reaction was terminated by addition of 20µl of denaturing 4X loading sample buffer. Samples were boiled for 5min and proteins separated by SDS-PAGE. The membrane was probed for phosphorylated MBP substrate with pThr98-MBP (Millipore 05-429,) at 2µg/ml overnight at 4^{o}C overnight. The kinase assay controls performed were two reactions without protein lysate, with or without MBP. Data are not shown.

2.15. Cell-based assays

2.15.1. Lactate Dehydrogenase (LDH) assay

The LDH colorimetric assay was used for the quantification of cell death and cell lysis based on the measurement of lactate dehydrogenase activity in cell culture supernatant, that has been released from the cytosol of cells that lost membrane integrity. The cell culture supernatant (120µl) was collected after cells were treated with cell-death inducing agents (HP or c_2-ceramide), centrifuged at 3000g for 10min to remove cell debris and stored at 4^{o}C until the next day. The assay controls used were: Background, untreated (or Low Control), and a positive (or High Control). The Background control provided information about the LDH activity contained in the assay medium (no cells) and is the value subtracted from all other values. The Low Control provides information about basal background levels of LDH release from the untreated population. The high control provides the maximum releasable LDH activity when all cells are lysed by treatment with 10µl of Lysis Buffer provided with the kit (Roche 04744934001). Prior to assaying the cell-free culture supernatant, the working reagents were reconstituted according to the manual's instructions. From the 120µl of supernatant collected, 50µl was transferred into a 96-well plate, where 50µl of the Reaction Mixture was added into each well. The plates were incubated for 30min at RT and the reaction was stopped with 25µl per well of Stop Solution. The plate was shaken for 10sec to mix the reagents and the absorbance read at 492nm. The reference wavelength was 690nm.

The calculations for measuring Cytotoxicity within hiPSC-CMs populations were:

$$\frac{[(A_{492nm} - A_{690nm})]}{\mu g/well}$$

Where:

$\mu g/well$ = The amount of protein per well determined by the MicroBCA assay

2.15.2. Colorimetric aaspase-3 / aaspase-8 assay

Caspase-3 and Caspase-8 activities were measured by fluorescence and luminescence by multiplexing Apo-ONE® Homogeneous Caspase3/7 Assay (Promega G7790) and Caspase-Glo® 8 Assay (Promega G8201), respectively. HiPSC-CMs were cultured and treated with cell-death inducing agents, and medium was harvested for the LDH assay and replaced with 50µl of serum-free DMEM per well. The Caspase-Glo® 8 Assay

Reagent that uses a luminogenic substrate containing the LETD sequence was prepared by mixing the Caspase-Glo® 8 Buffer with the Substrate followed by addition of the proteasome inhibitor (MG-132) to the mixture for background reduction in cell-based assays. The stock concentration of MG-132 Inhibitor was 20mM in DMSO with a final concentration of 60µM. At the same time, the Apo-ONE® Caspase-3/7 Substrate was thawed and added to the reconstituted Caspase-Glo® 8 reaction mixture at a dilution of 1:200. Equal volume (50µl) of the combined mixture was added to each well. The plates were incubated for 1h at RT and luminescence was recorded using a Paradigm plate reader (Molecular Devices). The caspase-3 activity was recorded at 1h and 3h (Ex485/Em527) and it was empirically found that cell lysis was more efficient at the later time-point in the Caspase-Glo® 8 Reagent. The reconstituted Caspase-Glo® 8 Reagent was stored at 4°C for a maximum of 3 days, otherwise was freshly prepared on the day of the assay. When caspase-3 activity was measured alone, the Apo-ONE® Caspase-3/7 Substrate was mixed with the Apo-ONE® Buffer to make a 1X mixture and used similarly. In this case, cell lysis and caspase-3 activity was recorded optimally after 1h.

2.16. Cytotoxicity high-content assays

2.16.1. NucView™488 / DRAQ7

For investigating the length of time that hiPSC-CMs can be maintained in DMEM and optimisation of FBS concentration, a series of experiments were carried out by multiplexing two dyes; NucView™488 (Biotum 30029), a caspase-3 substrate that allows the real-time monitoring of caspase-3 activity, and DRAQ7 (Biostatus DR71000), a cell-impermeable dye that is only taken up by cells with compromised membrane integrity (thus considered to be dead). After incubation under conditions of interest (2 and 4 days, while varying FBS concentration), 10µl of master mix was added to each well, containing 1µM NucView™488 caspase substrate and 3µM of DRAQ7™ dye. Cells were incubated with the fluorescent dyes for 30min at 37^{o}C followed by fixation in 4% (w/v) PFA for 10min. Cells were washed 3X in 1X PBS, and stained with 2µg/ml DAPI (Life Technologies D1306) for 5min at RT and finally washed once to remove excess DAPI. Fluorescence was recorded on the Cellomics® High Content Screening platform.

2.16.2. AnnexinV / DRAQ7

After maintenance hiPSC-CMs as above, Annexin-V and DRAQ7™ were used to stain cells and further assess/confirm cell death. Cells were washed twice with 1X Annexin-V Binding Buffer (Life Technologies PNN1001) in 1X PBS (without calcium) and 10µl of master mix was added per well, consisting of 2.5µg/ml Annexin-V AlexaFluor® 488 conjugate (Life Technologies A13201), 3µM DRAQ7™ dye and 8µM (or 4µg/ml) Hoechst 33342 nuclear dye (Molecular Probes H1399) in 1X Binding Buffer. The plates were incubated for 15min at 37^{o}C, the dyes removed and serum-free DMEM was added. Fluorescence was visualised and recorded on the Cellomics® High Content Screening platform.

2.16.3. Mitochondrial potential assay

To measure loss of Mitochondrial Potential we used the potentiometric far-red Mitoview™633 dye (Biotum Inc. 70055). Mitoview™633 dye readily diffuses across the plasma membrane and accumulates in the mitochondria. Mitochondria become brightly fluorescent after accumulation of the dye and the staining is dependent upon the mitochondrial membrane potential; thus, apoptotic cells exhibit lower fluorescence compared to healthy cells. Mitoview™633 was purchased as lyophilized aliquots of 50µg and a 200µM stock solution was prepared in anhydrous DMSO (Sigma-Aldrich 276855). Aliquots were protected against light and stored at -20^{o}C. The potentiometric dye was added onto the cells

at 50nM final concentration by preparing a master stock together with 8μM (or 4μg/ml) Hoechst 33342 nuclear dye (Molecular Probes H1399) in DMEM basal medium. Plates were incubated at 37^{o}C for 15min and fluorescence was recorded on the Cellomics® High Content Screening platform (exposure time 0.6ms). As a positive control for loss of mitochondrial membrane potential, cells were treated with chelerythrine (Sigma-Aldrich C2932) at 10μM for 10min (10mM stock in water) with H_2O-treated cells as a vehicle control.

2.16.4. Fluorescence and high-content microscopy

Representative images for the purity of hiPSC-CMs were captured on Observer.Z1a Zeiss Microscope by the AxioCam monochrome camera X-Cite Series 120. The images for both antibody- and isotype-stained samples were acquired under fixed exposure times where background fluorescence was undetectable for each corresponding isotype control. The images were captured for quantitation with the inverted Zeiss Microscopy as part of the Cellomics® High Content Screening Platform (Thermo Scientific). The exposure time for Hoechst 33342 was 0.1ms, for RFP was 0.6ms, for EGFP was 0.03ms, and for DRAQ7 and Mitoview™633 dyes was 0.3ms.

2.17. Bioinformatics analysis

2.17.1. High-content image analysis

All images (in sections 3.1 and 3.2) were analysed under a set of default Cellomics® BioApplication Algorithms that monitor cell features including size, shape, fluorescence and pattern of fluorescence. Images were analysed with two BioApplications: Compartmental Analysis and Target Activation. The Compartmental Analysis was used as a general analysis tool for the measurement of intracellular intensity changes for the analysis of Mitoview™633 experiments.

2.17.2. Customized high-content image analysis

Images (in sections 3.3 and 3.4) were analysed by a customised algorithm that was developed on Definiens – a biomedical image and data analysis software. In summary, the algorithm can be broken down into two rounds of automatic nuclei identification, nuclei segmentation/separation, creation of a mask used to identify the cardiac nature of the cells based on RFP fluorescence and a second mask for the identification of successfully transduced hiPSC-CMs with the shRNAmirs based on EGFP fluorescence. Nuclei identification was based on background correction and an automatic threshold of nuclear intensity. EGFP fluorescence threshold was optimised in order for the EGFP-negative wells to be considered close to zero. The upper and lower thresholds for loss of mitochondrial potential were determined by the untreated and chelerythrine-treated wells.

2.17.3. Statistical analysis

Data are represented as mean ± Standard Error (SE) for a minimum of N=3 replicates, unless stated otherwise. Statistical significance is represented by * $p < 0.05$; ** $p < 0.01$ and *** $p < 0.001$ compared to the relevant control. Differences between groups were examined for statistical significance using One-way ANOVA followed by Tukey or Bonferroni post-hoc test or Two-way ANOVA where stated. Analysis and figures were carried out using GraphPad Prism software. Figures were created in Microsoft Excel or GraphPad Prism and illustrations in Adobe Illustrator and Microsoft PowerPoint.

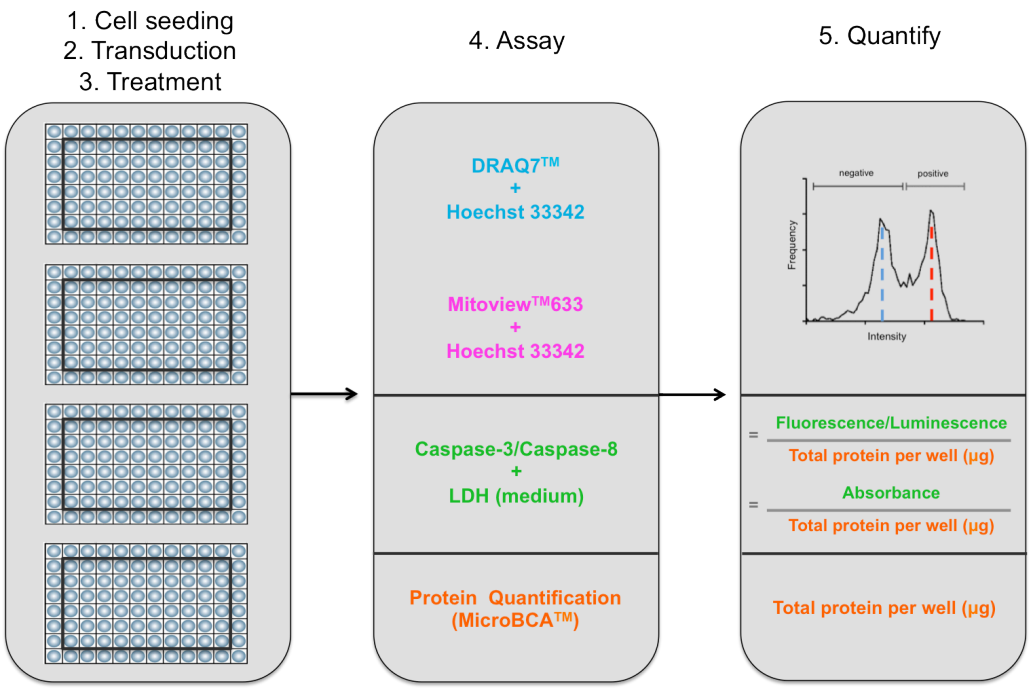


Figure 11: **Schematic of cell death assays.** HiPSC-CMs (CDI) were seeded and maintained as described above. Virus was added on for 8h or 24h, removed and replenished with Maintenance medium for additional 24h. From this point, were switched to a transition medium (plus 2% serum) for 48h, treated with H_2O_2 or c_2-ceramide and assayed at the indicated times (2h and 24h for H_2O_2; 16h and 36h for c_2-ceramide). Images for DRAQ7 and Mitoview assays were quantified using *Definiens* and *Cellomics* and whole well-based assays (caspase-3, caspase-8 and LDH) were quantified and values normalized to the total protein content per well. In the case of optimization of cell culture conditions, transduction was omitted. More details on the reagents see Materials and Methods.

3. Results

3.1. Characterization of hiPSC-CMs

3.1.1. Purity of hiPSC-CMs

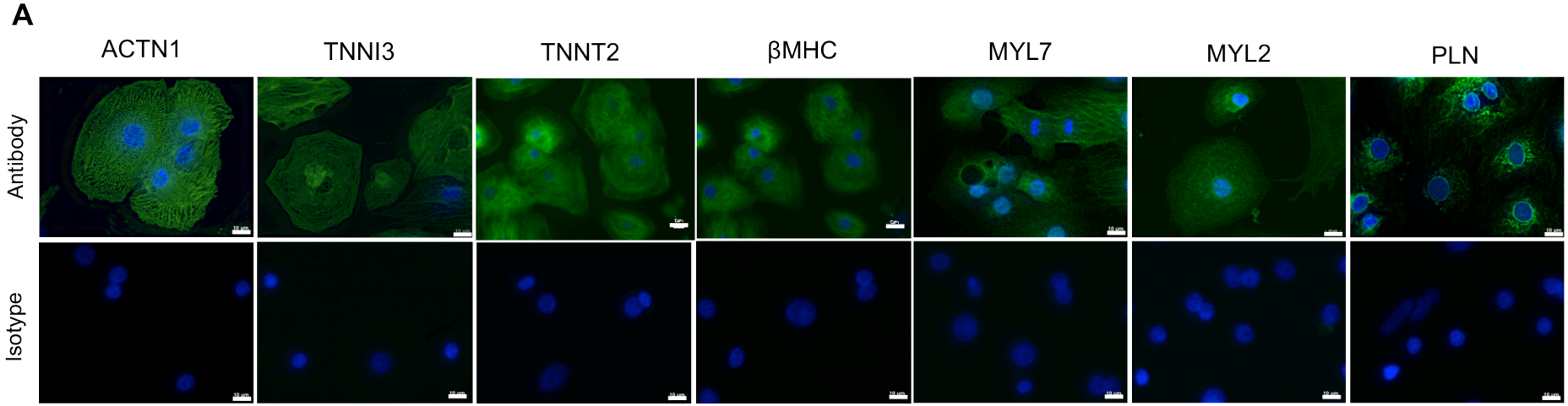
The purity of the proposed human system was crucial to determining the type of phenotypic assays that would be most applicable. An impure, heterogeneous system with large numbers of confounding cells would signify that only cell-based microscopy could be used to interrogate and resolve the level of myocyte death reliably, within a mixed population. By contrast, highly pure, homogeneous human cardiomyocytes would confer versatility for the use of both cell-based and whole-well (lysate) assays. For this reason we characterized the cells in terms of purity and cardiac maturity by immunofluorescence.

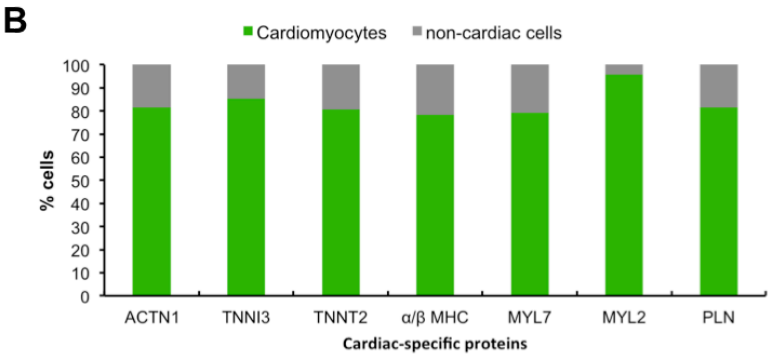
The purity of hiPSC-CMs was characterised using immunofluorescence with seven cardiac-specific antibodies (i.e. ACTC1, TNNI3, TNNT2, MF20 or βMHC, MYL7, MYL2 and PLN) (Fig. 12A and 12B). Quantification of the hiPSC-CMs immunolabeled with the cardiac-specific antibodies confirms the cardiac nature of the cells with purity of 95% for the most prevalent marker tested (Fig. 12). Cells were also co-stained with TNNT2 and PLN, which confirmed the purity of cardiomyocytes between 80-95% (Fig. 13). Representative examples of the de-convoluted images demonstrate a striation pattern (Fig. 12A) that does not resemble the orderly cross-striations found in adult rod-shaped cardiomyocytes (Fig. 12C; kindly provided by Peter O'Gara, Sian E Harding and Anita L. Alvarez), resembling better the patchy myofibrils of fetal cardiomyocytes and of adult cardiomyocytes after their structural disorganization in long-term culture (Eppenberger et al., 1994).

A majority of the hiPSC-CMs co-expressed MLC2a and MLC2v proteins, which exhibit a non-overlapping expression pattern in the adult heart: MLC2a is exclusively expressed in the atria, whereas MLC2v in the ventricles. However, in the embryonic heart MLC2a is initially present in the ventricular compartment, later being downregulated there, but remaining high in the outflow tract, atria, and atrioventricular canal. Whereas MLC2v is co-expressed with MLC2a in the outflow tract and atrioventricular canal, MLC2v is confined to the presumptive ventricles (E9.5-10.5 in the mouse) (Franco et al., 1999; Zammit et al., 2000). Thus the disorganized cross-striation pattern and co-expression of MLC2a and MLC2v validate the embryonic phenotype of the hiPSC-CMs studied. Occasional cells were MLC2a-negative and MLC2v-positive (Fig. 14), whereas others were TNNT2-positive and βMHC-negative (Fig. 14). While further quantitation of these events is required, it is conceivable that the hiPSC-CMs comprise a mixture of cells representing different developmental origins and stages. Specifically, it is possible that MLC2v- and MLC2a-double-positive cells have similarities to the embryonic outflow tract, whereas MLC2v- and MLC2a-singly-positive cells resemble later chamber specification into the ventricular and atrial lineages respectively. Thus, different expression patterns may explain the variability

acquired from different antibody staining in Figure 12A, an interpretation consistent with the reported electrophysiological heterogeneities in these and other preparations of hiPSC-CMs (Ma et al., 2011).

To determine whether the hiPSC-CMs were of ventricular origin, we carried out dual labelling with MF20 antibody that recognizes both α and β sarcomeric myosin heavy chains (MHC) and a βMHC-specific antibody (Fig. 14). The rationale for this analysis is explained briefly below. Adult rodent ventricular cardiomyocytes primarily express αMHC (Myh6), whereas embryonic rodent ventricular cardiomyocytes express βMHC (Myh7) and adult ventricles shift from αMHC to “fetal” βMHC expression in response to haemodynamic overload and other signals. Although human ventricular myocardium, by contrast, contains predominantly βMHC, αMHC also is present, decreasing in heart failure (Miyata et al., 2000; Nakao et al., 1997) as in rodents, αMHC predominates in human atria (Reiser et al., 2001). In the hiPSC-CMs studied here, the majority of cells were positive for βMHC, suggesting these cells were of ventricular lineage. Further quantitation is required with an αMHC-specific antibody (currently not available) to determine the % of cells that are MF20-positive and αMHC-positive to determine the percentage of cells that are of atrial origin.


A
ACTN1
TNNI3
TNNT2
βMHC
MYL7
MYL2
PLN
Antibody
Isotype


B
Cardiomyocytes
non-cardiac cells
% cells
100
90
80
70
60
50
40
30
20
10
0
ACTN1
TNNI3
TNNT2
α/β MHC
MYL7
MYL2
PLN
Cardiac-specific proteins

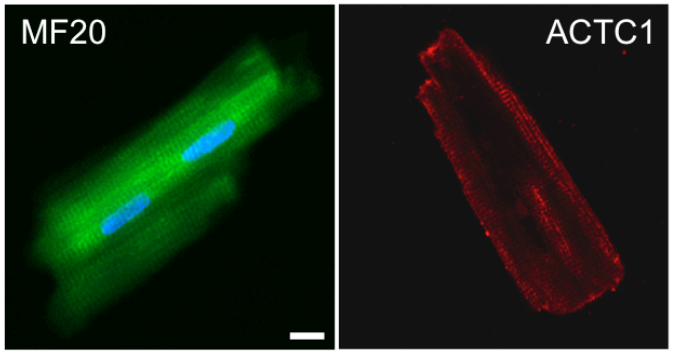

C
MF20
ACTC1

Figure 12: **Characterization and purity of the hiPSC-CMs. (A)** Representative immunocytostaining; seven cardiac structural markers were used to characterize the nature and purity of hiPSC-CMs. Images demonstrate the atypical cross-striation pattern compared to the adult type, particularly visible with antibody staining of ACTN1, TNNI3, TNNT2, and βMHC. The corresponding isotype controls showed no background staining (Table 4). Scale bar, 10μm; Note: Although quatification of MF20 staining is shown at the plot, a βMHC image is presented due to the clearer cross-striation pattern. **(B)** Quantification (*Cellomics*). The percentage of immunopositive cells was 80-95% depending on the antibody tested. Cardiomyocytes were scored based on a fixed intensity threshold for strong antibody staining; negative cells for the corresponding marker were scored as non-cardiac cells. Negative control cells were not used, but antibodies were previously validated against tissue sections of cardiac and non-cardiac origin. **(C)** Representative images of adult cardiomyocytes immunolabeled with MF20 and ACTC1. Scale bar, 10μm. Images kindly provided with permission by Peter O'Gara and Anita L. Alvarez, respectively.

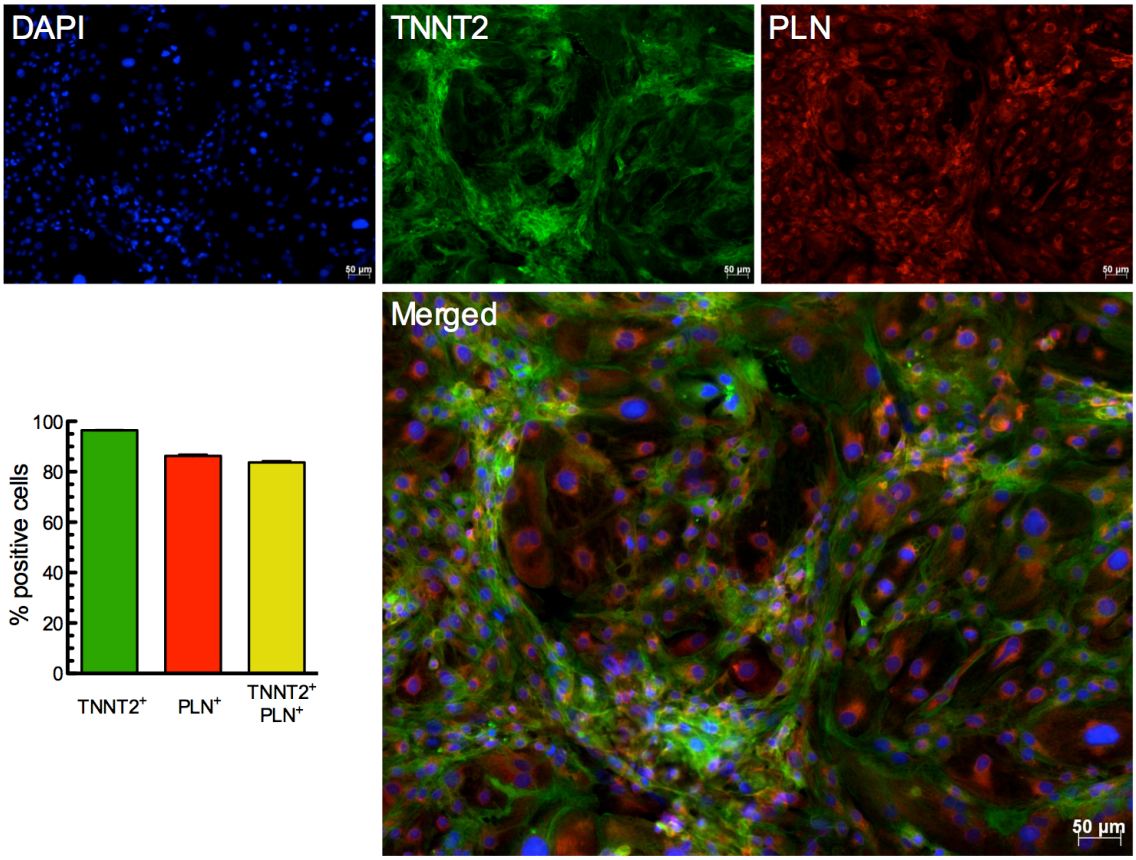


Figure 13: **Highly prevalent expression of TNNT2 and PLN in hiPSC-CMs.** A representative image of cells co-stained for the two indicated cardiac structural proteins. The percentage of PLN^+ and $TNNT2^+$ cells was 85 and 95% respectively, and double-positive cells expressing both TNNT2 and PLN were approximately 80%. Primary antibodies or corresponding isotype controls were incubated together, followed by incubation of species-matched secondary antibodies (Table 5). TNNT2 and PLN were visualized with Alexa488- and Alexa633-conjugated secondary antibodies, respectively. Bar graph showing the % of positive cells as mean ± SE for N = 3 wells.

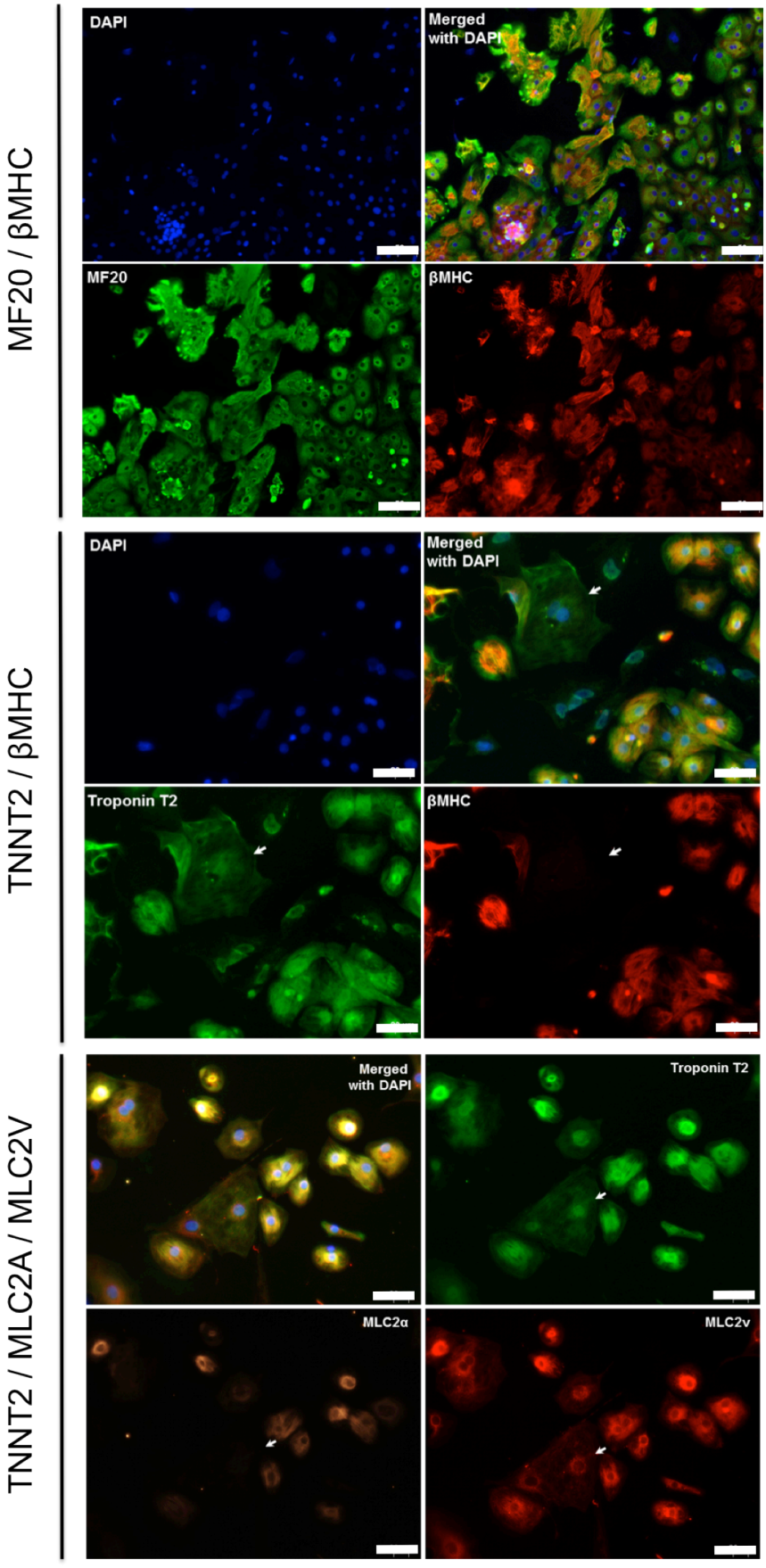


Figure 14: **Heterogeneous hiPSC-CMs comprise a cell mixture of different developmental origins and stages.** HiPSC-CMs were of ventricular lineage as the majority of cells were positive for both MF20 and βMHC (Top); Scale bar: 100μm. Occasional cells were TNNT2-positive and βMHC-negative (Middle) and MLC2a-negative and MLC2v-positive (Bottom). White arrow depicts the single-stained cells. Primary antibodies or corresponding isotype controls were incubated together, followed by incubation of species-matched secondary antibodies (Table 5). Scale bar, 60μm (middle, bottom panel)

3.1.2. HiPSC-CMs are refractory to serum-induced proliferation

Next, we investigated the percentage of proliferating hiPSC-CMs to determine if they faithfully recapitulate the post-mitotic phenotype of adult cardiomyocytes. Furthermore, proliferation of myocytes could compromise the fidelity of cell death response to death agonists. Hence, conditions supporting growth arrest, but permissive for myocyte survival, would allow for the development of both whole-well-based and cell-based assays. HiPSC-CMs were supplied with their own proprietary media for plating and maintenance. Since we were unaware of the possible growth factors, survival factors, and antioxidants in the proprietary medium that might affect survival and inhibit cell death, we first set to optimize short-term culture conditions for 2 or 4 days in a defined medium (from now on called transition medium or TM), prior to death induction by H_2O_2 or c_2-ceramide.

To determine the percentage of hiPSC-CMs undergoing proliferation we used a double-labelling assay with 5'-ethynyl-2'-deoxyuridine (EdU) and phosphorylation of histone H3 at Ser^{10} (PH3). The choice of these complementary markers is explained below. Progression through the cell cycle phases is tightly dependent by the sequential activation and inhibition of regulatory complexes including cyclins and cyclin-dependent kinases (CDKs). Cell division decisions prior to DNA synthesis are normally taken in G_1 phase, which are highly controlled by CDK complexes with cyclins. Such complexes regulate the retinoblastoma protein (pRb) by phosphorylation that consequently release E2F transcription factor and allow activation of transcription of genes required for cell cycle progression. Negative regulators of cyclin-cdk complexes are cdk inhibitors, such as $p21^{Cip1}$, $p27^{Kip1}$, and $p57^{Kip2}$ (Ahuja et al., 2007). To quantify the frequency of cells in **S-phase** where DNA synthesis occurs, EdU labelling was used. EdU is a nucleoside analogue of thymidine, and similar to BrdU, is incorporated into DNA during active DNA synthesis, and allows multiplex antibody staining. The EdU assay is superior to BrdU because it does not require a DNA denaturation step (typically HCl), which can affect antigen recognition sites for antibody counterstaining.

To mark additionally the population of cells in **late G2/M**, i.e., undergoing or preparing to undergo mitosis, we multiplexed EdU with antibody against phosrphorylated Histone H3 (PH3). Histone H3 phosphorylation is found specifically during mitosis and meiosis and is initiated at different phases of the cell cycle in different organisms, but during assembly or condensation metaphase chromosomes are always heavily phosphorylated (Hans and Dimitrov, 2001). In mammalian cells phosphorylation is first detected in late G_2 phase and is maintained through metaphase, with a strong correlation between chromatin condensation and H3 phosphorylation (regulated by Aurora A and B kinases) (Crosio et al., 2002), suggesting an importance in the maintenance of compact chromosome state (Hans and Dimitrov, 2001).

The use of these two proliferation markers in tandem thus allowed for the identification of (i) EdU-positive phospho-H3-negative (EdU^+PH3^-) cells that are undergoing DNA synthesis but have not yet entered metaphase leading to cytokinesis, (ii) EdU-negative phospho-H3-positive (EdU^-PH3^+) cells that entered the M phase or are blocked at the G2/M phase (iii) double-positive (EdU^+PH3^+) cells that are in the transition between S and M phase.

As controls for the cell cycle markers, we tested two mouse cardiac stem cell clones that were clonally derived from the adult cardiac Sca-1^+ side population (SP), whose proliferation profile was previously established in the laboratory (Noseda et al., 2012). In addition, we used HeLa cells as a human reference sample. HeLa cells and adult cardiac stem cells were seeded in their maintenance media in 10% serum for 24h, and serum-starved for 24h and 48h respectively (Fig. 15C). The cell numbers of both SP clones and HeLa cells were significantly reduced in the absence of serum, associated with a significant decrease of EdU^+PH3^- and EdU^+PH3^+ populations. At the same time, a significant increase in the EdU^-PH3^- population of both SP clones and HeLa cells was evident in the serum-deprived cultures, implying that the cells undergoing S phase or are in the transition between S and M phase were arrested in the G_o phase (Fig. 15C). A significant increase of nuclei numbers in these cultures was evident in the presence of serum (Fig. 15D), suggesting that serum promoted cycle progression. EdU^+PH3^- HeLa cells in serum-starved cultures were also significantly decreased compared to the serum-treated cells even though only by approx. 10%, suggesting either for a longer serum starvation window requirement (e.g. 48h) or that the tumour cell line might not require exogenous growth factors to the same extent as untransformed cells.

The hiPSC-CMs were cultured for 48h in various serum concentrations (0, 0.5, 1, 2, 5 and 10% serum). Cells were incubated with EdU for the last 6h of the 48h period, fixed and labelled with an antibody against PH3. Image acquisition and analysis was performed with Cellomics. The percentage of EdU^+PH3^+ cells that have undergone DNA synthesis and are preparing to undergo cytokinesis was in the range of 2-3% across the various sera concentrations and in the absence of serum. The proportion of EdU^-PH3^+ hiPSC-CMs that have undergone DNA synthesis and are most likely blocked at the G2/M phase were in the range of 5-7% irrespective of serum levels (Fig. 14A). The percentage of double-negative hiPSC-CMs population was approx. 85%, suggesting that most cells were refractory to serum-induced proliferation. No significant changes in cell number were observed (Fig. 14A), suggesting that no spontaneous cell death was present that needs to verified with a cell death marker, and that no significant proliferation was observed in the transition medium for 2 days. Thus, these results demonstrate that the majority of hiPSC-CMs are unresponsive to

the various serum concentrations for a period of 2 days in TM after being cultured in MM for 2 weeks.

Interestingly, there was a significant increase of EdU^+PH3^- cells in both 0.5% and 0% serum-supplemented cultures compared to MM, most consistent with traversing S phase and accumulating at the G_2/M checkpoint. While skeletal muscle differentiation and proliferation are mutually exclusive (muscle-specific transcription being promoted by serum withdrawal), it is less obvious how cardiac myocytes, especially hiPSC-CMs, would respond to it. In proliferating mouse cardiomyocytes "immortalised" by conditional expression of SV40 large T antigen, differentiation required not only removal of the transforming gene but also serum withdrawal (Rybkin et al., 2003). However, cardiomyocyte proliferation is permissive for lineage-specific genes (though not necessarily full maturity) in the setting of mouse and human mutations causing sustained proliferation (MacLellan et al., 2005; Shenje et al., 2014) and, notably, in hiPSC-CMs treated with small-molecule inducers of proliferation (Uosaki et al., 2013). Loosely resembling the accumulation of EdU^+PH3^- hiPSC-CMs, neonatal rat cardiomyocytes became less responsive to a serum challenge if cultured first in the absence of serum. Rather than proliferate, they increased DNA synthesis without increasing cell number and gave rise to bi-nucleated cardiomyocytes (thus, karyokinesis uncoupled from cytokinesis) (Ueno et al., 1988). Analogous mechanisms might explain the increase of EdU^+PH3^- cells in serum-starved hiPSC-CMs, provided that the conditions, including any potential endogenous growth factors, were permissive for S phase entry. Indeed, others have previously reported that human ESC-derived cardiomyocytes, unlike mouse ones, remain highly proliferative in serum-free medium (McDevitt et al., 2005).

In conclusion, hiPSC-CMs are refractory to serum-induced proliferation (2-10% FBS) for 2 days in the transition medium, thus providing us with conditions under which the cell death assays can be carried out without a significant confounding effect on cell number via proliferation. Furthermore, the purity of the cardiomyocyte system, at roughly 95%, confirms the applicability of simple, well-based death assays in addition to the more demanding whole-content image-based analyses.

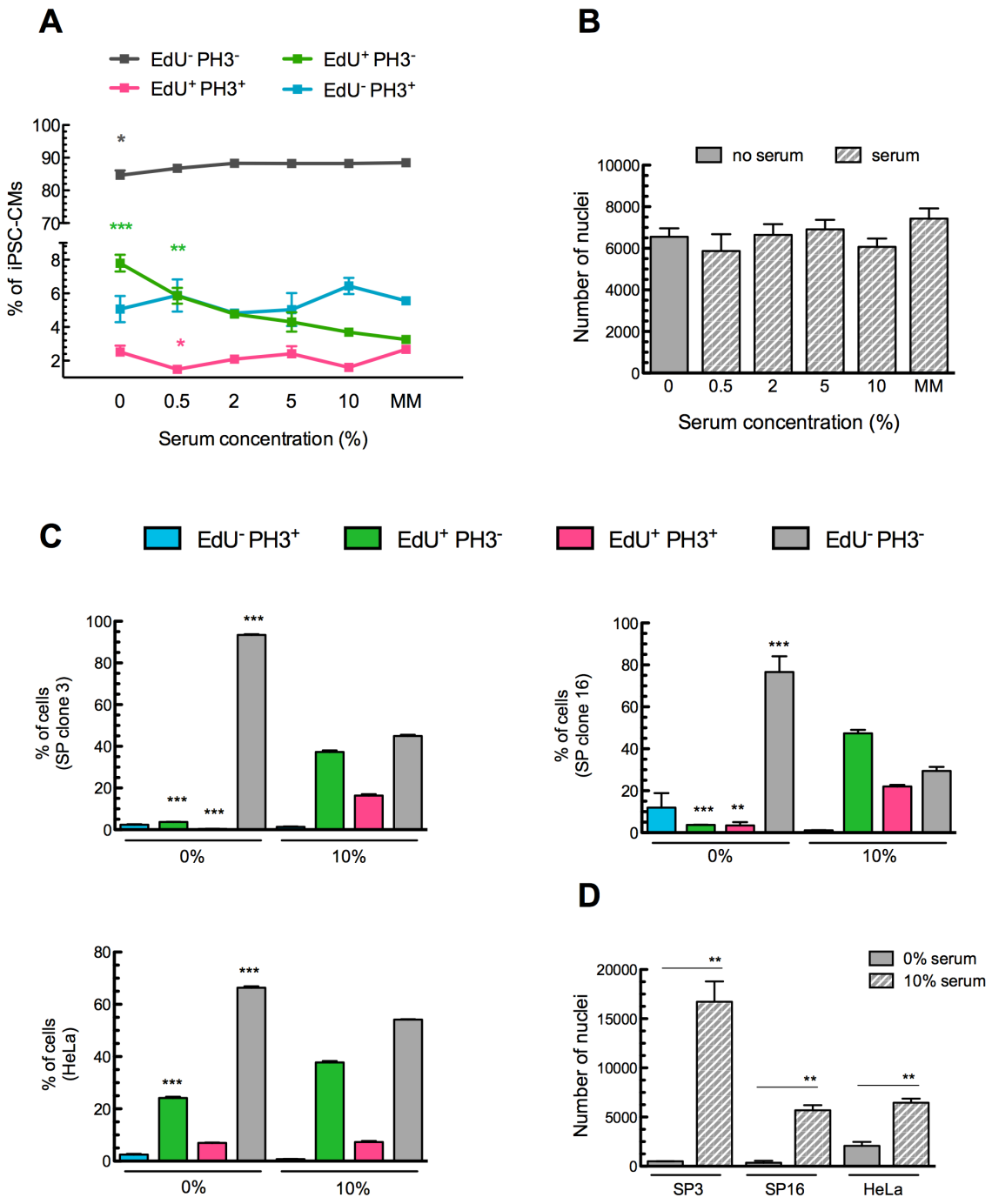


Figure 15: **hiPSC-CMs are refractory to serum-induced proliferation determined by a multiplex assay of EdU and phospho-H3. (A)** Percentage of cells positive for EdU and/or PH3 after culture in various serum concentrations for 2 days. **(B)** No significant change in total cell number (number of nuclei) of hiPSC-CMs was observed under serum-supplemented and –deprived conditions. Asterisks indicate significance of the indicated population compared to the cultures in Maintenance Medium (MM). **(C)** Various double and single-positive populations for the same markers of positive controls (cloned adult cardiac stem cells, HeLa) in the presence or absence of serum. **(D)** Total cell numbers measured by the number of nuclei of the positive control cultures. Statistical analysis of A, B and C was carried out using One-way ANOVA followed by Dunnett's Multiple Comparison's Test, and D with a two-tailed unpaired t-test. (N=3 wells).

3.1.3. HiPSC-CMs express MAP4K4 mRNA and protein

A key aim of the present study was to knockdown endogenous MAP4K4 to investigate its predicted ability to inhibit human cardiac muscle cell death. For this reason, it was important to determine whether the hiPSC-CMs express MAP4K4. We investigated the presence of MAP4K4 RNA in hiPSC-CMs using HEK293T cells as a negative control, based on the Gene Atlas expression profile accessed from the BioGPS gene portal. Conversely, HEK293T cells expressing exogenous epitope-tagged MAP4K4 (MAP4K4-Flag) and HepG2 cells were used as positive controls (Fig. 16). HepG2 cells were previously shown to express MAP4K4, and knockdown of the protein led to cell death inhibition in this background (Liu et al., 2011). MAP4K4 mRNA was expressed 4-fold and 2-fold higher levels in hiPSC-CMs compared to HEK293T and HepG2, respectively.

Firstly, we investigated the expression of MAP4K4 protein in hiPSC-CMs and used two antibodies that discriminate between the two major isoforms, short (SF) and long (LF). Briefly, the SF lacks an Src homology 3 (SH3) domain that may mediate its interaction with cytoskeletal proteins (Yao et al., 1999). Since the two isoforms can equally activate JNK but are differentially expressed in tissues, it is likely that they have tissue-specific regulatory functions (Yao et al., 1999). Initially we tested the specificity of the two antibodies on HEK293T lysates where MAP4K4-Flag-SF or -LF was expressed (Fig. 16). We confirmed that ab56569 had little interaction with the MAP4K4-SF-Flag, whereas ab70424 readily detected both (Fig. 16). This was expected since the peptide sequence used to generate ab56569 is not present in the SF of MAP4K4, whereas both contain the sequence used as immunogen for ab70424 (Fig. 16). Full aligned sequences for MAP4K4-LF and MAP4K4-SF binding regions for the antibodies are depicted in Figure S3.

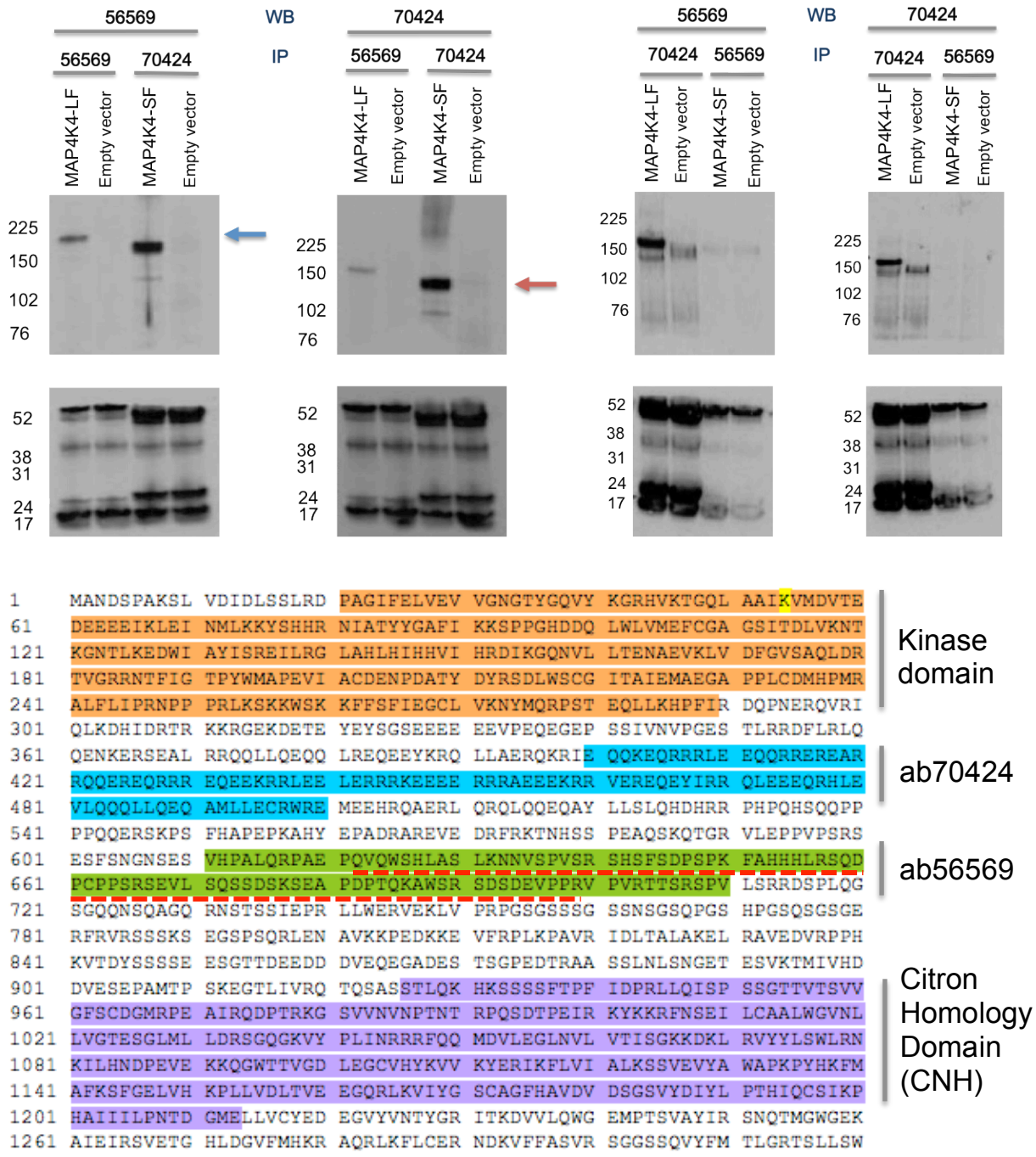


Figure 16: **Testing the specificity of the MAP4K4 antibodies in MAP4K4-LF and -SF protein lysates. (Top)** MAP4K4-LF-Flag and MAP4K4-SF-Flag were immune-precipitated (IP) from HEK293T with ab56569 and ab70424 and detected by Western blotting with the two antibodies as shown. The 17-52kDa bands depict the heavy and light chains of IgG antibodies in the immunoprecipitated samples and indicate equal loading between paired samples with and without exogenous MAP4K4. ab56569 does not detect the short form, whereas ab70424 recognizes both isoforms of MAP4K4. **(Bottom)** The protein sequence of human MAP4K4-LF, highlighting the Kinase and Citron Homology (CNH) domains as well as the binding sites for the two antibodies. The yellow amino acid represents the invariant lysine within the conserved protein kinase ATP-binding pocket. Red-underlined sequence is absent in MAP4K4-SF. Blue and red arrows depict the LF and SF of MAP4K4 respectively.

Having confirmed the specificity of respective antibodies by Western blotting after immunoprecipitation of exogenous MAP4K4, we next investigated the endogenous MAP4K4 protein levels in hiPSC-CMs. As a negative control we used Lysis Buffer without protein lysate, and as positive controls we used lysates from HEK293T cells expressing the long or short MAP4K4-Flag isoform (Fig. 17B). Endogenous MAP4K4 was readily detected in hiPSC-CMs using ab56569 (Fig. 17B), which recognises only the LF. Results with ab70424 were inconclusive, but the it is likely that the ab70424 is more potent in binding MAP4K4 protein when that is expressed at high levels, such as in the case of MAP4K4-Flag. Further protocol optimization is required to maximise the yield of immunoprecipitated MAP4K4 with ab70424. Endogenous MAP4K4 migrated with a lesser Mr than exogenous MAP4K4, which may be attributable to post-translational differences between the cell backgrounds or alternative use of splice variants.

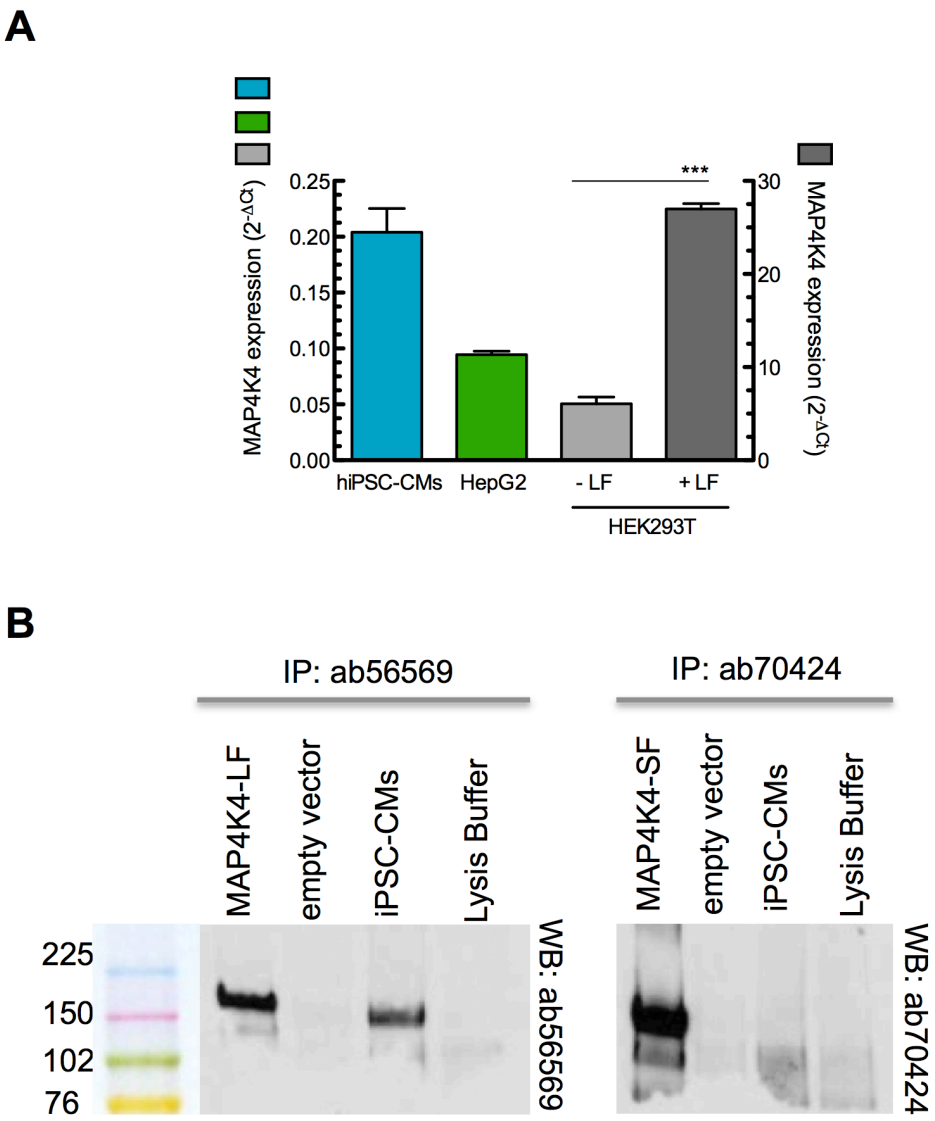


Figure 17: **hiPSC-CMs express MAP4K4 RNA and protein. (A)** *MAP4K4* RNA in hiPSC-CMs was quantitated with qPCR primers that detect most isoforms. HepG2 and MAP4K4-Flag-LF were used as positive controls, and untransfected HEK293T cells as a negative control (N=3). **(B)** Detection of MAP4K4-LF in hiPSC-CMs by immunoprecipitation Empty vector was used as negative control for MAP4K4-Flag-LF and –SF. Lysis Buffer (no protein) was used as a negative control for cross-contamination. Antibody 56569 does not react with MAP4K4-SF whereas ab70424 detects both (Fig. 16). A clear band is observed after immunoprecipitation with ab56569, signifying presence of the long isoform. A specific but less distinct band was visualized with ab70424. The 17-52kDa heavy and light chains of IgG antibodies in the immunoprecipitated samples between paired samples with and without exogenous MAP4K4 were used to verify equal loading (not shown).

3.1.4. Summary

Based on immunolabelling for multiple myofilament proteins and the sarcoplasmic reticulum protein PLN, the hiPSC-CMs were of up to 95% cardiomyocyte purity, based on MLC2v, the most sensitive marker tested. Moreover, the stem cell-derived cardiomyocytes co-expressed at least three cardiac myofilament structural proteins, the largest number we could resolve simultaneously. These included MLC2v and MLC2a, which discriminate between mature atrial and ventricular cells but are co-expressed during early cardiac organogenesis, at the linear heart tube stage (E8.25-8.5) (Fijnvandraat and van Ginneken, 2003). Occasional cells expressing cardiac TNNT2 were negative for MLC2a or β-MHC, likely reflecting differences in chamber specification or maturity. In addition, hiPSC-CMs were found to be refractory to serum-induced proliferation, as assessed with EdU and a phosphorylated Histone-3 antibody, in the transition medium for 2 days. In summary, the high purity of the system will allow for the use of both whole well- and microscopy-based assays and the cells' refractoriness to proliferation even at high serum concentrations will allow the assessment of cell death in response to death-inducing signals without interfering effects on cell number by cell proliferation.

We have also characterized hiPSC-CMs in terms of their MAP4K4 expression at the mRNA and protein levels. MAP4K4 was successfully immunoprecipitated from hiPSC-CMs using the antibody that preferentially recognizes the LF (ab56569), although this experiment bears repetition. No antibodies that preferentially recognize the SF are available, and the present result with the antibody that recognizes both is insufficiently distinct to exclude the possibility that the SF is present. This could be addressed in part using isoform-specific qPCR primers. Whether the different isoforms have different functions in hiPSC-CMs remains to be elucidated, but we note the longer form contains the recognition domain to bind the SH2/SH3 adaptor protein Nck. This validation of endogenous MAP4K4 expression (at the mRNA and protein level) is essential to justify the knockdown of the gene in this cell system and assess its impact on cell death in the presence of relevant death-inducing agents.

3.2. Screening shRNAmir constructs for efficient MAP4K4 knockdown

3.2.1. MAP4K4 knockdown in a heterologous doxycycline-inducible system

Prior to phenotypic assessment of MAP4K4 knockdown in hiPSC-CMs there is a requirement to validate the knockdown efficacy of the shRNAmirs on the protein of interest. For the knockdown of MAP4K4 we have chosen shRNAmirs in lentiviral pGIPZ vectors that co-express EGFP for real-time tracking of EGFP-positive and –negative cells in high-content screening and FACS analysis. In order to select the more effective shRNAmir constructs I have performed a small knockdown screen in a heterologous cell system; that is in HEK293T cells expressing MAP4K4-Flag-LF (from this point onwards written as MAP4K4-Flag). Initially we have set to optimise the FACS purification protocol to circumvent issues of cell clumping and maximise the yield of protein and RNA for downstream application of Western blotting and qPCR. TAK1 is a downstream target from MAP4K4 in cardiomyocytes and is required for the activation of cell death. Initially we were interested in inhibiting both MAP4K4 and TAK1 as proof-of-concept experiments, so I had started screening for the most potent shRNAmirs against TAK1 in HEK293T cells (Fig. 18).

Following 48h after transfection of 5 shRNAmirs against TAK1, HEK293T cells were FACS-sorted or EGFP-purified into $EGFP^{H}$ (high) and $EGFP^{L}$ (low) populations (strategy shown in Fig. S2). Knockdown of RNA of more than 50% of total MAP4K4 levels compared to the NSC (non-silencing control) was observed with 4 shRNAmirs (Fig. 18), from which 3 were selected for testing their potency on protein downregulation by Western blotting (validated by Nasret Harun). GAPDH knockdown by a GAPDH-specific shRNAmir was used as a positive control for the initial screen where approx. 80% reduction of RNA was observed (Fig. 18).

For MAP4K4 knockdown, 5 shRNAmirs against MAP4K4 or NSC were transfected in a doxycycline-inducible HEK293T cell line ($HEK293T^{Dox}$) (generated and provided by Lorna R. Fiedler) (Fig. 19). Briefly, I describe how the $HEK293T^{Dox}$ expresses MAP4K4 in the presence of antibiotics. The tetracycline-inducible system was generated using the Flp-In™ T-REx™ system that allows the generation of stable mammalian cell lines when the gene of interest is expressed after integration in a specific genomic location by site-specific recombination using Flp recombinase. The advantages of the system are, firstly, the generation of isogenic inducible cell lines with a specified integration site circumventing issues of random integration resulting in mutagenesis, and secondly, the lack of cDNA insertion in tandem. Flp recombinase mediates the insertion of MAP4K4-Flag, which is under the control of tetracycline-regulated CMV promoter with a TetO2-binding sites, into the genome at the integrated FRT site (that also expresses Zeocin under the control of SV40

promoter) (O'Gorman et al., 1991; Sauer, 1994). Insertion into the genome at the FRT site leads to inactivation of the Zeocin-fusion gene that is replaced by hygromycin that is now used for the selection of a stable cell line. In the absence of tetracycline (in our case we used doxycycline as a derivative), the Tet repressor forms a homodimer that binds with high affinity on the TetO2 sequence on the promoter for expression of MAP4K4-Flag, thus repressing the transcription of the gene. Upon addition of doxycycline, the antibiotic binds to the Tet repressor homodimer rendering it unable to bind to the TetO2 sequence, thus allowing the induction of MAP4K4-Flag.

HEK293T^{Dox} were seeded and cultured in the absence of antibiotics and doxycycline. The next day doxycycline was added following transfection with the shRNAmirs. EGFP^{H} and EGFP^{L} cells were FACS-sorted after 48h of transfection and collected in RNA*later* solution for preservation of RNA quality until RNA extraction (Fig. 19). However, we had technical difficulties of detecting MAP4K4-Flag RNA, even though the qPCR primers covered most of the splicing isoforms and the protein was readily detected by Western blotting (Fig. 19-20). The experiment was repeated with a fresh batch of HEK293T^{Dox} and with customized primers that recognize the Flag epitope for the exclusive detection of exogenous MAP4K4 (data not shown). Despite the fact we could exclusively detect exogenous MAP4K4 from HEK293T transfected with MAP4K4-Flag, we were unable to detected MAP4K4-Flag in HEK293T^{Dox} due to the qPCR primers not being able to detect the exogenous MAP4K4 (despite a deep coverage by the qPCR primers of most isoforms). Nevertheless, the downregulation of RNA observed only in EGFP^{H} populations was interpreted as an effect on endogenous MAP4K4, where 3 out of 5 shRNAmirs exhibited a more than 50% knockdown compared to the NSC. One shRNAmir (173825) did not downregulate MAP4K4, and, as we found later, withdrawn from the website.

To validate the efficacy of the 3 selected shRNAmirs on a protein level we collected a broader EGFP^{+} population to maximize the yield of protein for downstream application of Western blotting. Initially, cells were FACS-sorted at 24h, 48h, 72h and 96h, from which - due to continuous clumping issues – we managed to collect lysate from only 72h and 96h (Fig. 20). Later, to circumvent cell clumping prior to FACS I decided to use a higher concentration of DN*ase* (at 100ng/ml). As seen from Figure 20A, doxycycline treatment did not increased MAP4K4 RNA at both times (similar to Fig. 19). Furthermore, co-expression of the shRNAmirs led to insufficient RNA downregulation compared to NSC (Fig. 20B). The lack of MAP4K4 reduction can be explained by sorting a broader range of EGFP^{+} population, consisting of both EGFP^{L} and EGFP^{H} populations. Nevertheless, MAP4K4-Flag protein was evident in the presence of doxycycline (Fig. 20C) compared to the absence of the antibiotic, suggesting that the earlier issues in detecting RNA was not because of unresponsiveness to doxycycline. MAP4K4 protein was downregulated with all 3 shRNAmirs compared to the

NSC at 72h, whereas at 96h only 2 shRNAmirs (202781, 68219) exhibited a maintained inhibition effect. MAP4K4 levels with 201856 shRNAmir were increased by 96h, suggesting a decreased knockdown efficacy and experiment repetition is required for validation of the observed result.

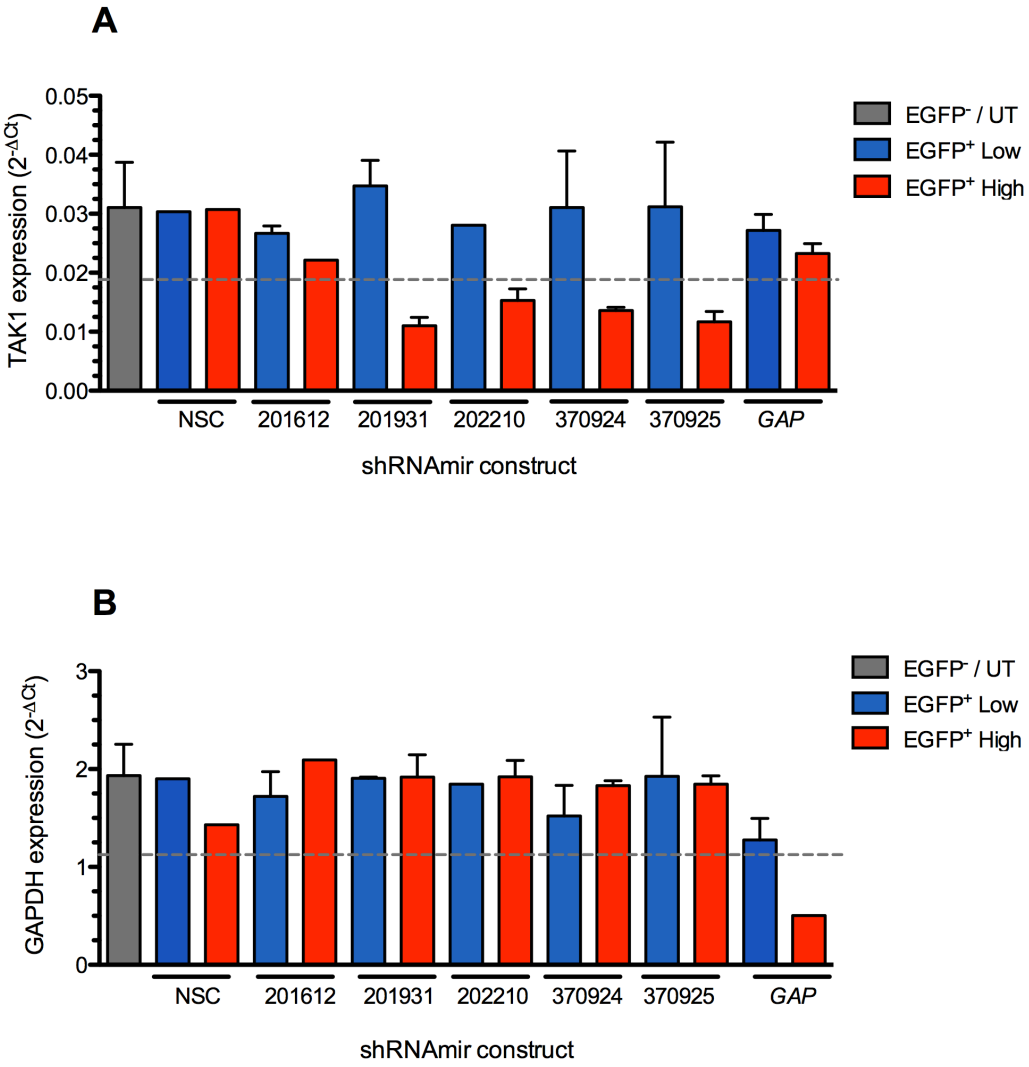


Figure 18: **Screening for potent shRNAmir constructs against TAK1. (A)** RNA was isolated from FACS-sorted low and high EGFP$^+$ HEK293T cells after they were transfected with shRNAmirs against TAK1. TAK1 RNA levels were quantified by qPCR primers that detect most isoforms **(B)** GAPDH RNA levels were measured from the same samples as an internal negative control for GAPDH shRNAmir. The three most potent shRNAmirs were selected that showed more than 50% downregulation of TAK1 (grey line threshold). UT, untransfected; NSC, non-silencing control; *GAP*, *GAPDH* shRNAmir; Bars represent ±SE from N=2

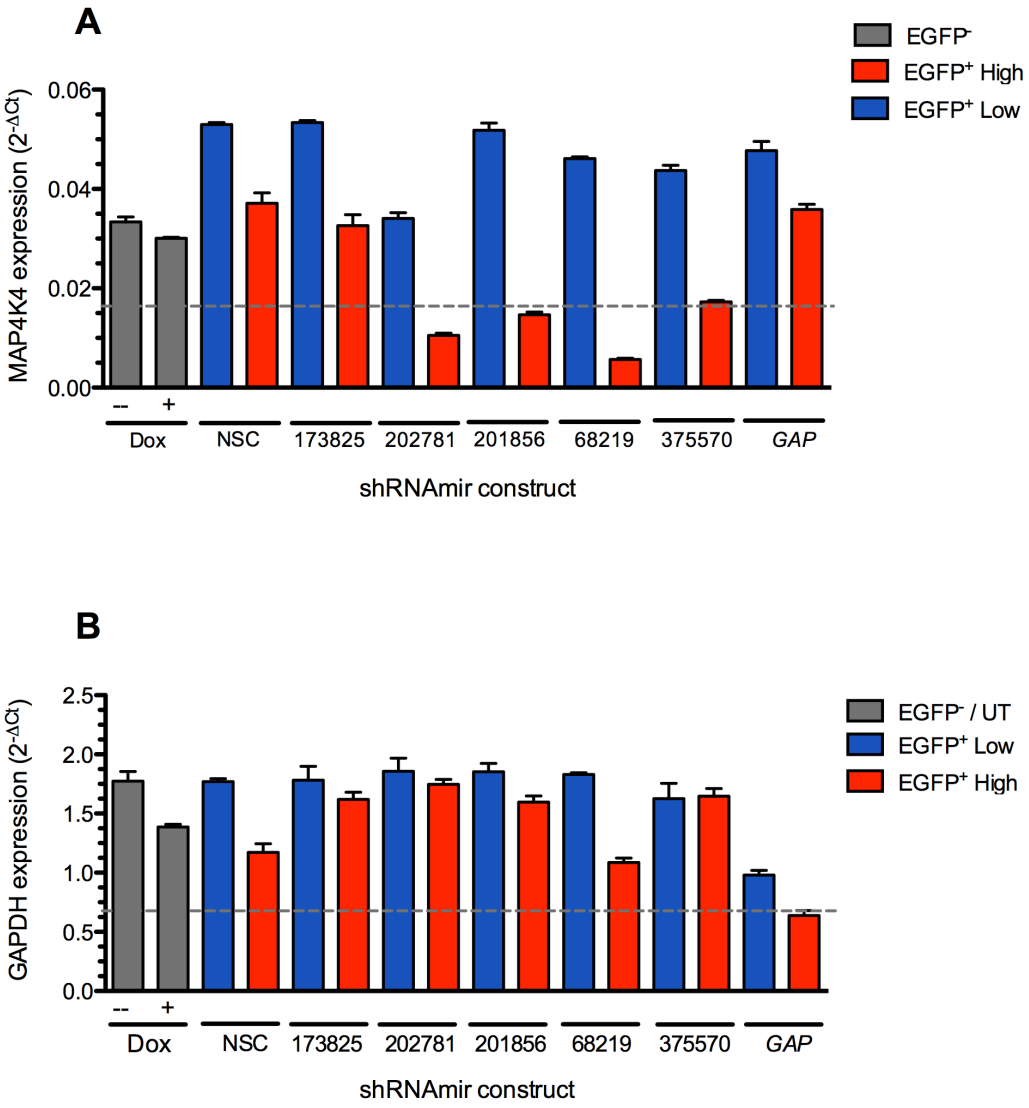


Figure 19: **Screening for potent shRNAmir constructs against MAP4K4. (A)** RNA was isolated from low and high EGFP^{+} cells 48h after transfection of HEK293T^{Dox}. MAP4K4 levels were quantified by qPCR with primers that detect most isoforms **(B)** GAPDH RNA levels were measured from the same samples as a negative control panel for GAPDH shRNAmir. The three most potent shRNAmirs were selected that exhibited the highest RNA downregulation (grey line threshold for 50%). UT, untransfected; NSC, non-silencing control; *GAP*, *GAPDH* shRNAmir; Bars represent ±SE from N=3 technical replicates.

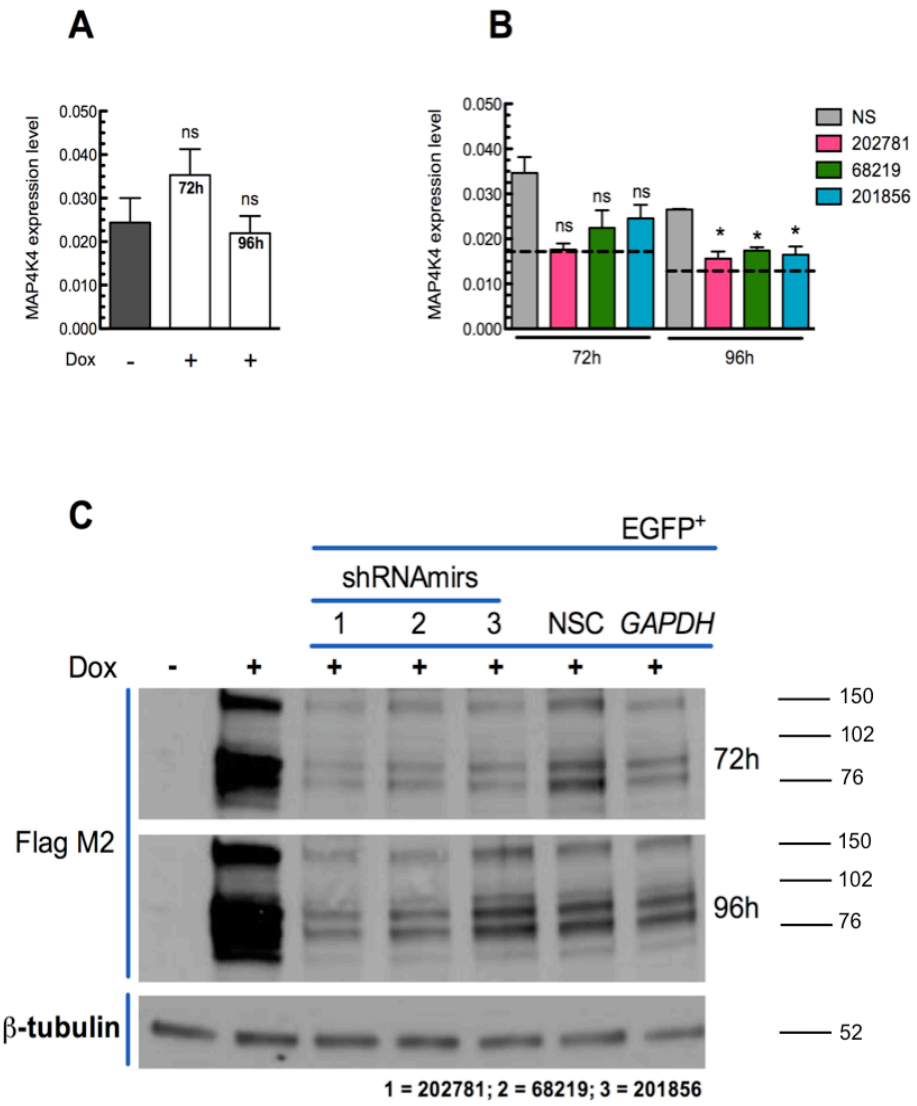


Figure 20: **Investigating potency of shRNAmirs against MAP4K4 in HEK293T^{Dox} cells. (A)** RNA of MAP4K4 in HEK293T^{Dox} in the absence (-) and presence (+) of doxycycline at 72h and 96h. One-way ANOVA with a Bonferrnoni test showed no significance. **(B)** RNA levels of MAP4K4 quantified by qPCR from EGFP^{+} HEK293T^{Dox} cells expressing MAP4K4-Flag collected at 72h and 96h after induction with doxycycline. Bars represent ±SE for technical replicates. Asterisks depict statistical significance calculated with one-way ANOVA followed by Tukey Multiple Comparison Test. **(C)** SDS-PAGE (30µg per lane) blot labeled with an anti-Flag antibody. The top band is around 150kDam whereas the double bands around 102kDa. β-tubulin was used as a loading control at 52kDa. Dox, doxycycline; NSC, non-silencing control; 1-3, shRNAmirs identifier; * p<0.05, **p<0.01, ***p<0.001. Bars represent ±SE from technical replicates (N=1)

3.2.2. MAP4K4 knockdown in a heterologous system with a co-transfection strategy

To circumvent previous technical difficulties, I decided to switch to a co-transfection approach for each shRNAmir with MAP4K4-Flag in HEK293T cells (Fig. 21). As can be seen in Figure 21A, despite the decrease of RNA at 24h at approx. 50%, there was a time-dependent decrease of RNA levels from 48-72h in both NSC- and MAP4K4-depleted samples. This effect was most likely attributed to confluency and dilution of the transfected $EGFP^+$ with the untransfected $EGFP^-$ population (transfection efficiency measured by flow cytometry varied from 30-45%). Decrease of MAP4K4 protein was evidently higher compared to the NSC from 24-96h. Decrease of MAP4K4 protein observed across all shRNAmirs, including the NSC, at 96h was attributed to a dilution effect of $EGFP^+$. Nevertheless, we validated the potency of the 3 shRNAmirs against MAP4K4 protein (Fig. 21B) that resulted in MAP4K4 knockdown.

On the other hand, considering the variability in transfection efficiency, minute differences between the efficacies of shRNAmirs could not be resoluted in the absence of FACS, thus we had set out to use the co-transfection experimental mode with purification of transfected $EGFP^+$ cells by FACS. We purified $EGFP^+$ population for RNA quantification (Fig. 22A) and immunoprecipitated MAP4K4 from $EGFP^+$ protein lysate or crude (non-purified) protein lysate (Fig. 23). The limitations for not solely using $EGFP^+$ protein lysate are time- and quantity-wise requirement for collecting $EGFP^+$ cells via FACS. Immunoprecipitation was an extra measure for maximizing the yield of MAP4K4 for Western blotting, and was used for precipitating MAP4K4 from both $EGFP^+$-sorted and in unsorted cells (crude lysates).

$EGFP^+$ population was sorted 24h, 48h and 72h after co-transfection with the shRNAmirs and MAP4K4-Flag plasmid (Fig 22A). In the absence of shRNAmirs, the level of MAP4K4-Flag was significantly higher than the untransfected control at each corresponding time-point (Fig. 22B), thus solving the earlier issue of not detecting the spiked RNA levels of exogenous MAP4K4. MAP4K4 was significantly decreased to more than 50% in the presence of either shRNAmir compared to the NSC at each time. Significance at 48h was not statistically calculated because of increased ±SE between experiments, but still remained below the 50% threshold. MAP4K4 RNA was decreased at approx. 4.4-fold at 24h, 3.5-fold at 48h and 3.6-fold at 72h compared to the NSC (Fig. 22C). GAPDH knockdown achieved with an shRNAmir against GAPDH was used as a positive control, with significant reduction compared to the NSC (Fig. 22C).

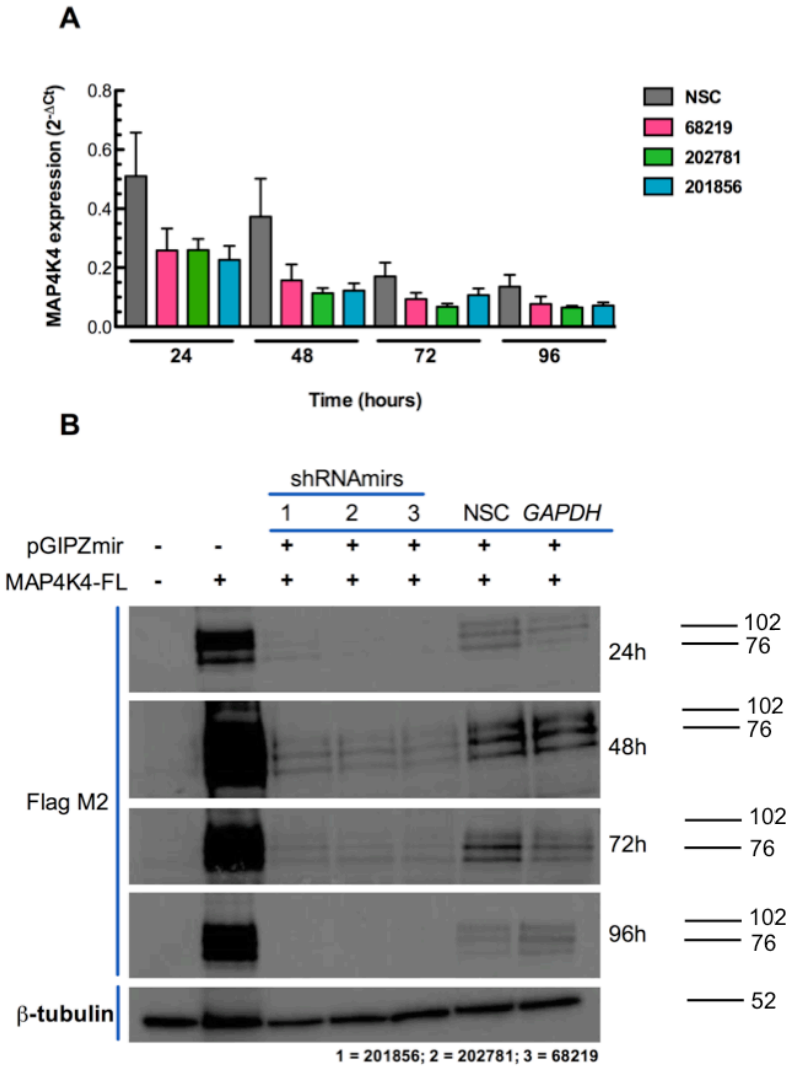


Figure 21: **Investigating potency of shRNAmirs on protein levels with a co-transfection strategy system without FACS.** Protein and RNA were collected from 24h to 96h from HEK293T cells co-transfected with MAP4K4-Flag and one shRNAmir. **(A)** MAP4K4 RNA levels at the corresponding times. ±SE bars were calculated from technical replicates and experiment requires repetition. **(B)** Western blot of crude (non-purified by FACS) protein lysates where MAP4K4 was detected with an anti-Flag antibody between 76-102kDa. β-tubulin was used as a loading control at 52kDa band. pGIPZmir, lentiviral backbone of shRNAmirs; 1-3, shRNAmir identifier. N=1

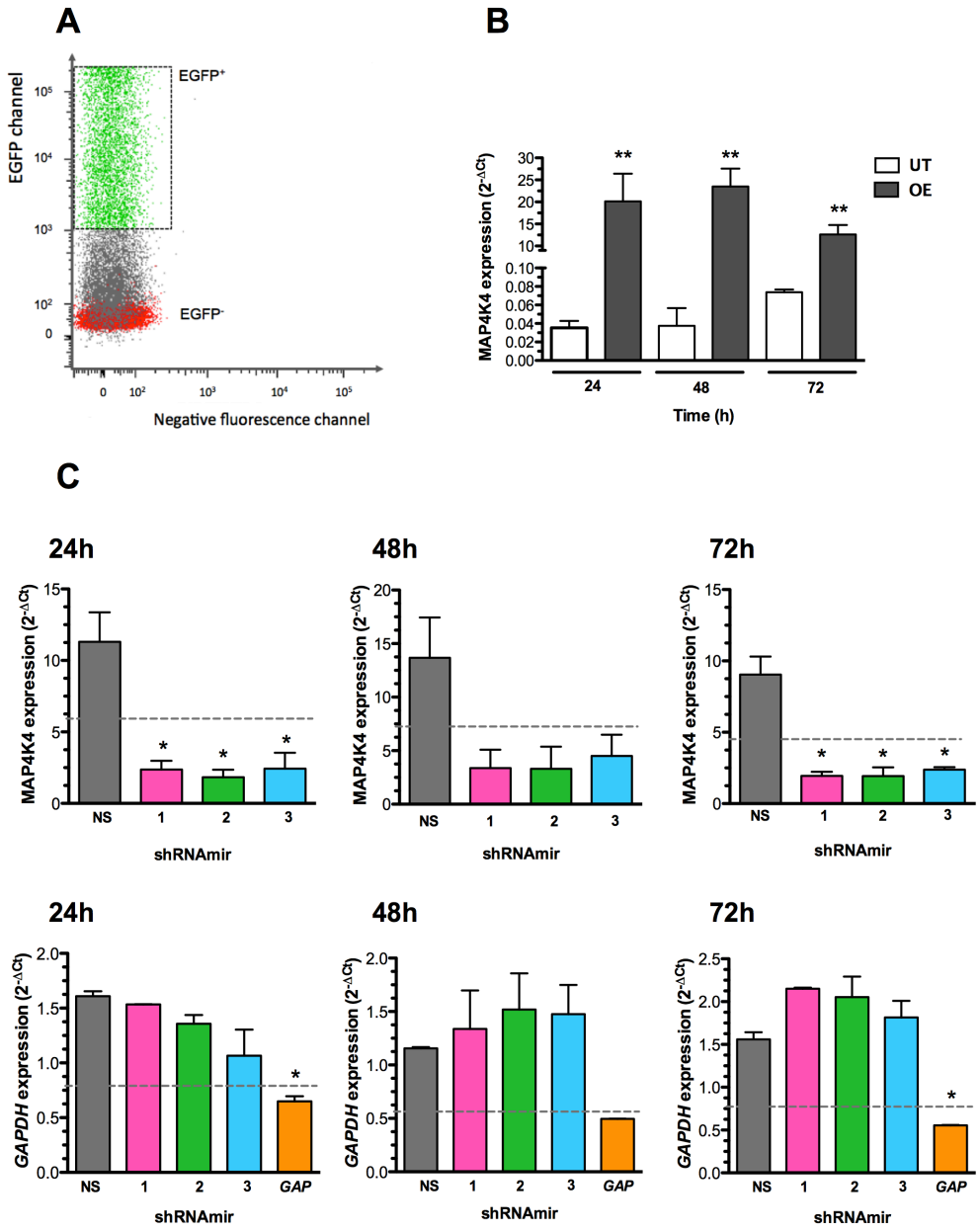


Figure 22: **Investigating the potency of shRNAmir constructs with a co-transfection strategy in HEK293T using FACS.** **(A)** FACS strategy for collecting EGFP^{+} cells for RNA and protein isolation. **(B)** MAP4K4 RNA levels in untransfected (UT) and in cells expressing MAP4K4-Flag (OE) at 24h, 48h and 72h. Asterisks depict significance calculated with unpaired one-tailed t-test. **(C)** MAP4K4 and GAPDH RNA levels in co-transfected samples with MAP4K4-Flag and one shRNAmir. The grey line depicts a 50% MAP4K4 level of the NSC. Asterisks depict statistical significance calculated with one-way ANOVA followed by a Bonferroni test. * p<0.05, **p<0.01, ***p<0.001. Bars represent ±SE from N=2; *GAP*; *GAPDH* shRNAmir, NSC; non-silencing control; 1-3; 68219, 202781, 201856 in this order

To determine the efficacy of knockdown on a protein level by Western blotting using MAP4K4 immunoprecipitation we required a minimum of $1.5x10^6$ $EGFP^+$ cells. We had isolated protein (Fig. 23) to matching RNA samples (Fig. 22). Protein was also isolated from the remaining unsorted cultures (crude $EGFP^+$ lysate) from which MAP4K4 was immunoprecipitated (Fig. 23) and positive control (MAP4K4-Flag) was run at each blot for ease of band identification. Due to the absence of a distinct MAP4K4 band at both 48h and 72h with one of the two biological replicates leading to less conclusive results (data not shown), we are able to show knockdown of MAP4K4 at 24h from one of the two (Fig. 22A). It was clear that even as early as 24h post-transfection, MAP4K4 was absent in the shRNAmir-transfected samples at levels considerably lower to the NSC. Similarly, the level of MAP4K4 immunoprecipitated from crude $EGFP^+$ lysate was significantly lower in the presence of any shRNAmir compared to the NSC (Fig. 23A). Significant reduction of MAP4K4 protein was observed at 24h, 48h and 72h in the second biological replicate (Fig. 23B). Interestingly, 201856 shRNAmir at 24h in both replicates displayed higher MAP4K4 levels compared to 202781 and 68219, suggesting a delay in knocking down MAP4K4.

Finally, a decrease of MAP4K4 protein with the NSC was observed compared to the sample with expressed MAP4K4-Flag alone (in the absence of shRNAmir). We hypothesized that this might be due to a promoter competition effect between the two transfected plasmids (i.e. MAP4K4-Flag and pGIPZmir) that is prevalent between two plasmids that use a strong CMV promoter. For this we co-transfected HEK293T cells with equal amounts of DNA plasmids (μg) at different vector combinations, including an empty vector (Fig. 24). Two-way ANOVA analysis showed that the DNA vector mixture accounts for 58.65% of total variance, while time accounted for 18.48% of total variance and both time and DNA mixture had a significant effect in the downregulation of MAP4K4. Downregulation of MAP4K4 RNA levels with the empty vector that does not contain a scrambled sequence suggests the effect observed with the NSC was not due to off-target effects, but attributed to promoter competition of the co-transfected plasmids.

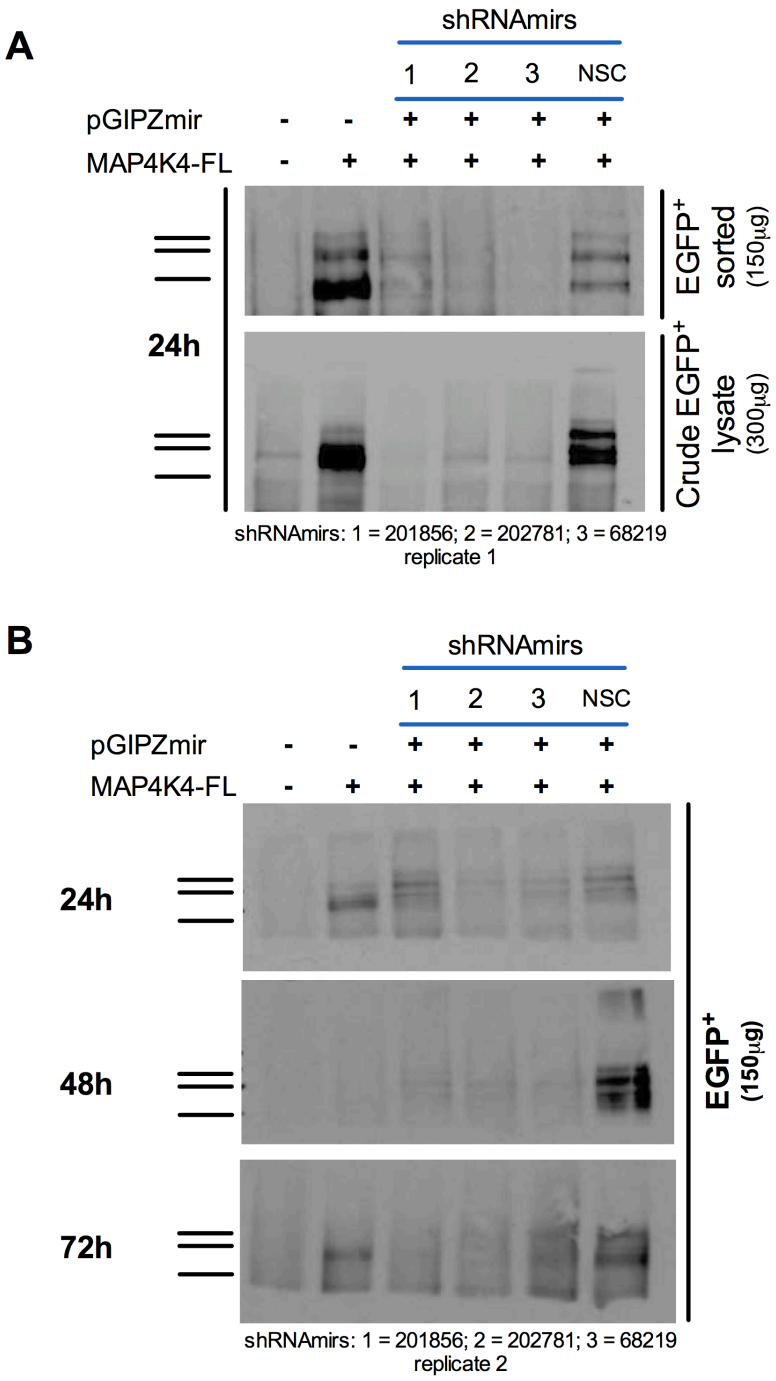
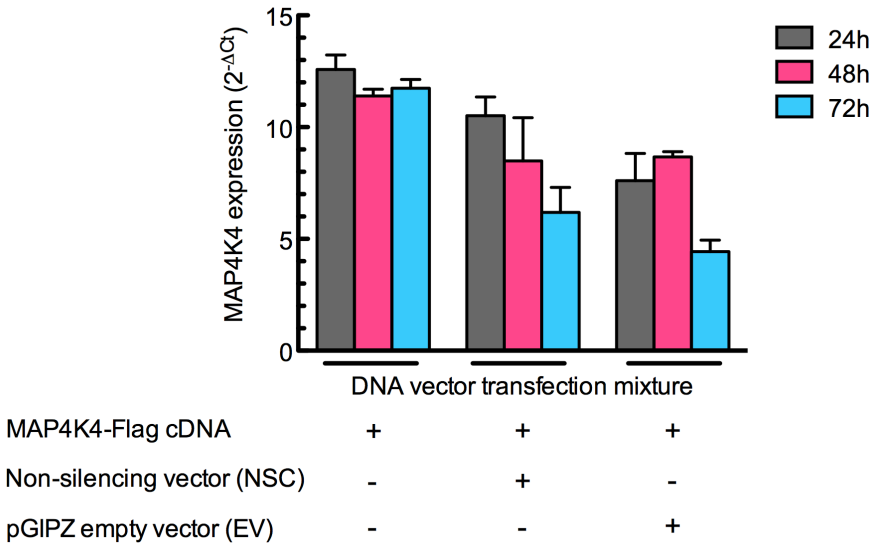


Figure 23: **Immunoprecipitation of MAP4K4 from EGFP$^+$ and crude lysates to validate protein knockdown by the various shRNAmirs. (A)** Biological replicate 1 (N1) where MAP4K4 was immunoprecipitated from sorted (EGFP$^+$) and unsorted (crude) populations at 24h. **(B)** Biological replicate 2 (N2) where MAP4K4 was immunoprecipitated from sorted EGFP$^+$ cells at 24h, 48h and 72h post-transfection with MAP4K4-Flag and one shRNAmir. MAP4K4 (for both N1 and N2) was detected with an anti-Flag M2 antibody. NSC, non-silencing control; pGIPZmir, lentiviral backbone of shRNAmirs; Protein ladder bands are 150, 102 and 76kDa from top to bottom.



Two-way ANOVA			
Source of Variation	**% of total variation**	**P value**	**Significant**
Interaction	10.83	0.1747	ns
Time	18.48	0.0152	*
DNA vector mixture	58.65	0.0003	***

Figure 24: **Promoter competition effect with the co-transfection strategy.** Transfections with equal amounts of either NSC or an empty vector in combination with MAP4K4-Flag plasmid were carried out. $EGFP^+$ cells were sorted and MAP4K4 RNA was quantified by qPCR. Two-way ANOVA with a Bonferroni post-hoc test indicates that the DNA vector mixture and time are significant for the downregulation of MAP4K4. *p<0.05, **p<0.01, ***p<0.001. Bars represent ±SE from N=2

3.2.3. MAP4K4 knockdown in hiPSC-CMs

The lack of hiPSC-CMs proliferation in serum-supplemented media meant that transfection of shRNAmirs was not an option; thus, having determined the potency of the three most effective shRNAmir, I have set out to encapsulate each shRNAmir vector into a viral capsid. After production of the virus, titration was carried out on HeLa cells to determine the concentration of viral particles or else known as transduction units per ml (TU/ml). HeLa cells were transduced with a 10-fold dilution series with a virus, from which $EGFP^+$ cells were analyzed by flow cytometry (Fig. 25A) to determine the concentration of viral particles in TU/ml (Fig. 25B). To determine the Multiplicity of Infection (MOI), that is the number of viral particles per cell (e.g. MOI 10 is analogous to 10 viral particles per cell) required for MAP4K4 knockdown in hiPSC-CMs, we have transduced the cells at MOI 10, 20 and 50 (Fig. 26). As can be seen from Figure 26, MOI50 resulted in approx. more than 70% knockdown with each shRNAmir after 72h post-infection. Thus, MOI 50 was used for investigating our hypothesis.

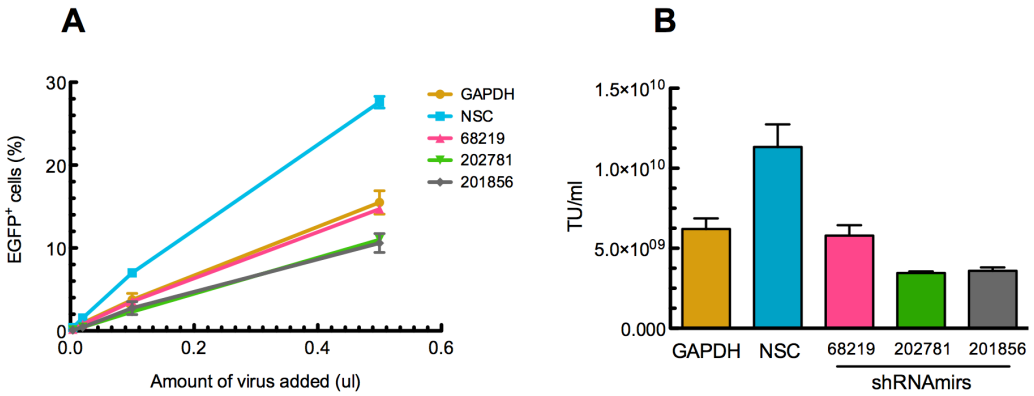


Figure 25: **Titration of viruses on HeLa cells. (A)** HeLa cells were transduced with a 10-fold dilution series of virus collections from NSC and the 3 selected shRNAmirs**.** The percentage of $EGFP^+$ cells was determined by flow cytometry and concentration in TU/ml was calculated as in Materials and Methods. **(B)** The concentration for each virus collection in TU/ml; N=2

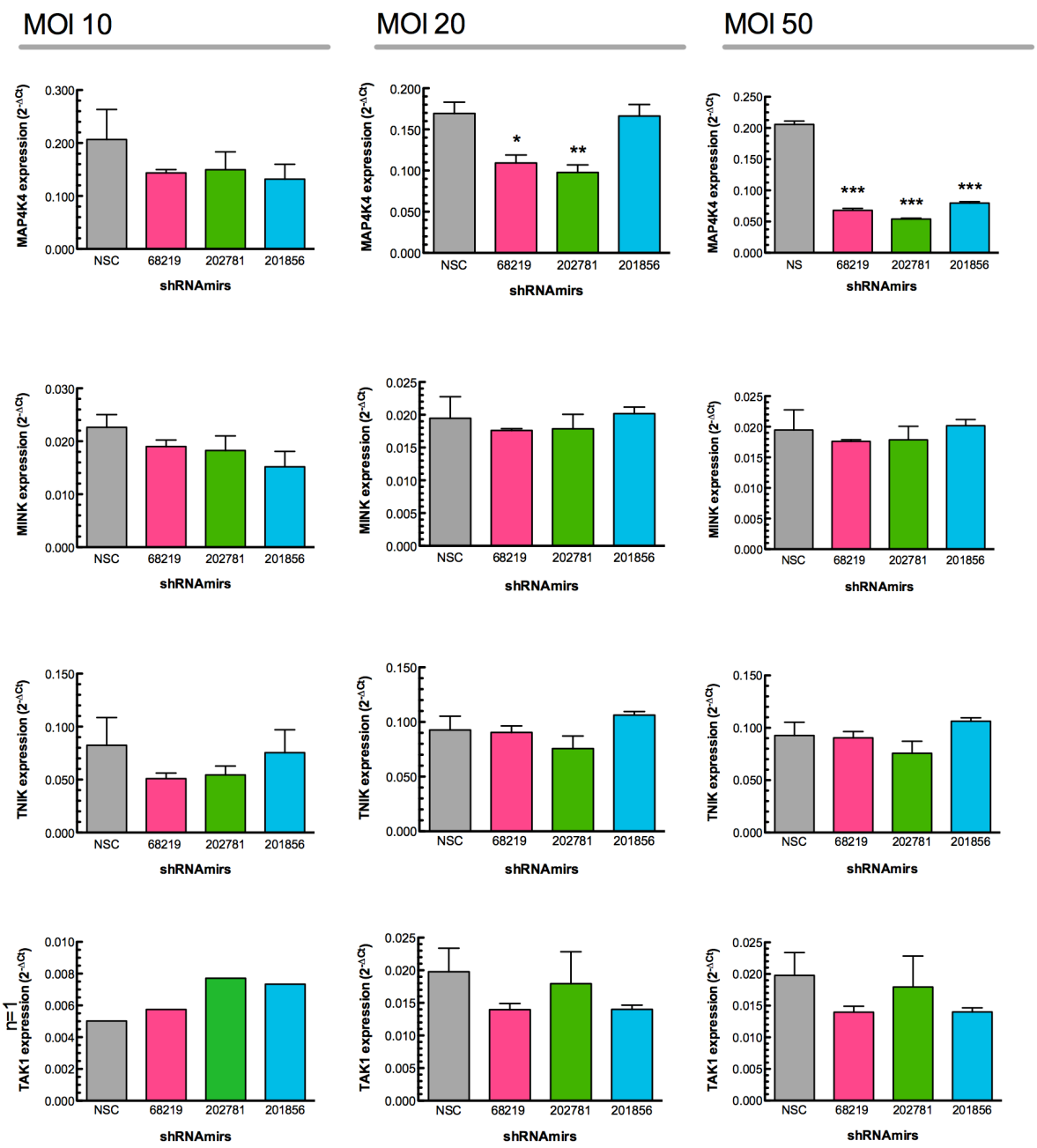


Figure 26: **Investigating various MOIs for significant MAP4K4 knockdown in hiPSC-CMs.** RNA was isolated 72h following transduction with the constructs at MOI10, 20 and 50. The levels of TAK1, MAP4K4, MINK1 and TNIK were quantified by qPCR. Asterisks depict significance by One-way ANOVA and a Bonferroni post-hoc test for *p<0.05, **p<0.01, ***p<0.001. Bars depict ±SE for N=2 (MOI 10), N=2 (MOI 20) and N=3 (MOI 50).

3.2.4. Summary

Prior to phenotypic assessment of MAP4K4 knockdown in hiPSC-CMs, we validated the knockdown efficacy of three shRNAmirs on the protein of interest. Initially I screened a group of shRNAmirs and selected 3 out of 6 that exhibited more than 50% RNA inhibition. To validate the potency of MAP4K4 knockdown on a protein level I used SDS-PAGE with or without immunoprecipitation of MAP4K4. Protein lysates were collected from HEK293T cells from various experimental approaches, such as purified $EGFP^{+}$ or non-purified cells with or without MAP4K4 immunoprecipitation, from a doxycycline-inducible or a co-transfection system. Interestingly, two shRNAmirs (68219, 20782) exhibited a similar downregulation pattern from 24-72h, but 201856 shRNAmir exhibited a delay in MAP4K4 knockdown at 24h compared to the other two (Fig. 23B). Interestingly, MAP4K4 protein levels from $EGFP^{+}$ cells were upregulated at 96h in the presence of 201856 shRNAmir, suggesting a limited knockdown window for this construct (Fig. 20C). RNA downregulation was observed at all times between 24-72h in HEK293T cells in the co-transfection experiments and in $HEK293T^{Dox}$ at 48h. Later, to validate the efficacy of shRNAmirs on endogenous MAP4K4 in hIPSC-CMs, the lentiviral vectors were encapsulated by a viral capsid (virus production) and transduced hiPSC-CMs at various MOIs (10, 20 and 50). Successful knockdown at 72h was achieved from the 3 shRNAmirs at MOI 50, which was used at later experiments under cell death conditions. Interestingly, there was no RNA inhibition of MAP4K4's closest structural relatives, that is TNIK and MINK1, something inconceivable with pharmacological inhibitors, thus signifying the potential of shRNAmir technology as an excellent genetic tool for selective inhibition of a protein of interest in proof-of-concept studies as such.

3.3. MAP4K4 knockdown in hiPSC-CMs followed by H_2O_2

3.3.1. Optimization of cell culture in High-glucose transition medium

HiPSC-CMs were supplied with media of a proprietary formula to support their survival for a minimum of two weeks. The presence of possible antioxidants (i.e. insulin) (Aikawa et al., 2000) or growth factors in the medium would delay or partly prevent cell death induced by the death agonists, thus we set to optimise short-term culture conditions for 2 and 4 days prior to death induction with H_2O_2 or c_2-ceramide in defined media (Transition Medium [TM]; High-glucose [HGTM] or for Low-glucose [LGTM]).

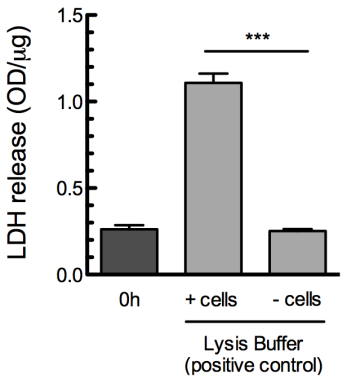
The growth properties and mitochondrial function of hiPSC-CMs from CDI were characterised by Pfizer in media containing different carbon sources as part of a bigger effort to potentially make them a source for *in vitro* cardiotoxicity assessment for drug compounds (Pfizer poster). HiPSC-CMs could be cultured over a period of 7 days in HG and LG media without any significant cytotoxic effects measured by their ATP levels and no differences in their oxygen consumption rate and viability after 21 days. Furthermore, no significant mRNA differences were depicted in genes involved in glycolysis or oxidative stress relative to the heart. So even though there was no obvious counter-indication for using either media we have chosen to culture cells prior to death induction in both HGTM and LGTM.

Here, the conditions of H_2O_2 in HGTM will be described. To determine the dose at which hiPSC-CMs responded to H_2O_2 we carried out a dose-response curve of a 2-fold dilution series (62.5-500μM), from which cell death was quantified by LDH release in the medium (Fig. 27). Lysis Buffer (LB) dissolved at 1:20 in a set of wells was used to determine the maximum LDH release (positive control). Cells were cultured in HGTM for 4 days and then treated with the 2-fold concentration range of H_2O_2. Background cell death (Fig. 27A), recorded at the start of the experiment, shows no difference to the cell death of the VC (i.e. H_2O). As shown on Figure 27B, LDH was significantly increased after 8h with 62.5μM of H_2O_2 and as early as 2h with the rest of the concentrations. Two-way ANOVA analysis indicates that the interaction between time and concentration was highly significant ($p<0.0001$) with 12.31% of total variance to account for the observed effect. Similarly, time and concentration alone were considered highly significant ($p<0.0001$) with 18.79% and 58.76% respectively, to account for cell death (Fig. 27C).

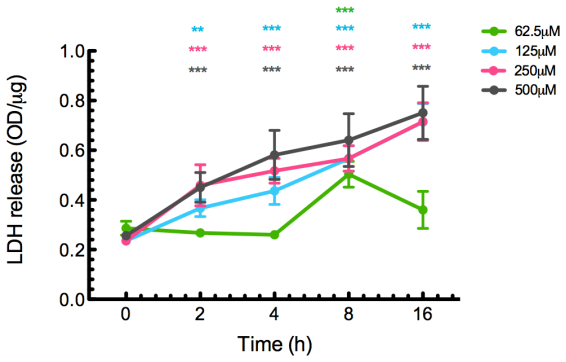
Caspase-3 and caspase-8 activities were measured after treatment with H_2O_2 by fluorescence and luminescence assays respectively at 2h, 4h, 8h and 16h (Fig. 28-29). Activation of either caspase was not evident within the 16h time-window. However, caspase-8 activity was significantly decreased at the same times where a significant increase in LDH release was observed (Fig. 29). No decrease in caspase-8 activity was described with H_2O_2,

until recently, where H_2O_2 was shown to induce expression of miR-874 in cardiomyocytes that targets caspase-8 and subsequently leads to increased necrosis via a RIPK1/RIPK3 mechanism (Wang et al., 2013a). This is the first study implicating an antagonistic effect of cell death by caspase-8 in cardiomyocytes and our preliminary results probably reflect a similar mechanism. However, prior to our knowledge, we interpreted the loss of caspase-8 activity as enzymatic function downregulation due to cell death, thus, unfortunately, we did not record its activity in later experiments with H_2O_2.

A



B



C

Two-Way ANOVA

Source of Variation	% of total variation	P value	Significant
Interaction	13.02	< 0.0001	***
Time	58.51	< 0.0001	***
Concentration	18.33	< 0.0001	***

Figure 27: **Time-dependent dose-response of H_2O_2 in hiPSC-CMs. (A)** Background LDH release (0h) was recorded at the start of the experiment with no difference to the VC (H_2O). Lysis Buffer (LB) dissolved at 1:20 in a set of wells was used to determine the maximum LDH release (positive control). The well with no cells (-cells) served as a control to ensure the medium did not interfere with the assay. Student's t-test for N=3 wells. **(B)** Time-dependent dose-response curve of a 2-fold dilution series (62.5-500µM) of H_2O_2 assayed at 2h, 4h, 8h and 16h. Cells were maintained for 4 days in HGTM (plus 2% serum) prior to the addition of the death agonist. The absorbance values were normalized to the total protein content of each well. **(C)** Two-way ANOVA following by a post-hoc Bonferroni test factoring time and concentration was performed between each concentration to 0h. Statistical significance is depicted with * p<0.05, ** p<0.01, *** p<0.001 and colours represent each concentration. N=6 wells

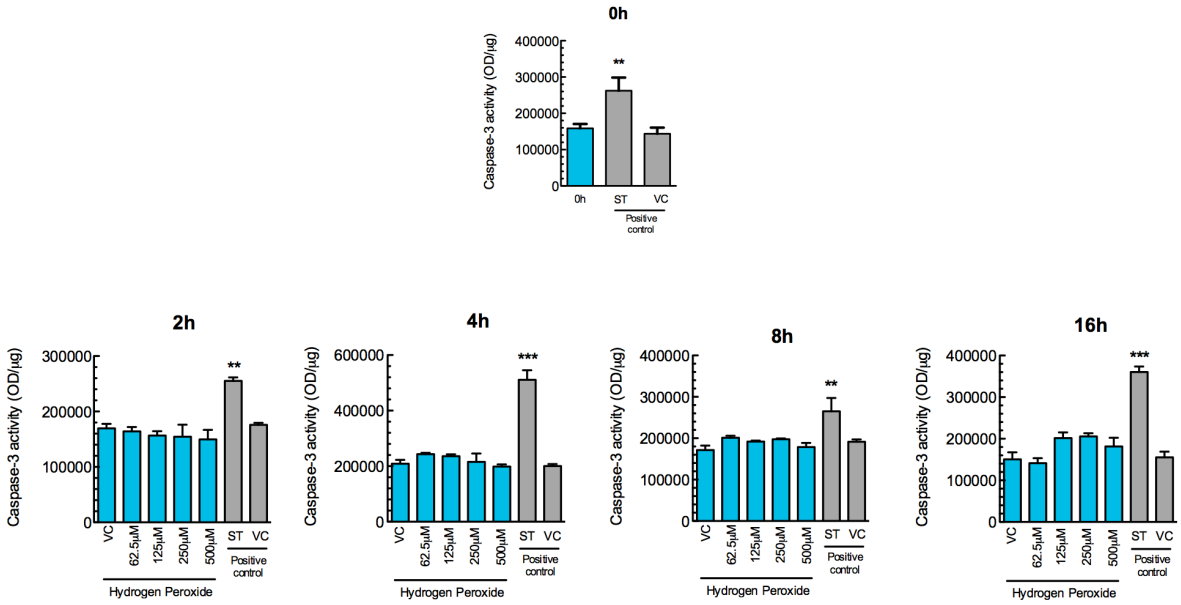


Figure 28: **No Caspase-3 activity was detectable in response to various concentrations of H_2O_2 in hiPSC-CMs.** Cells were treated hiPSC-CMs were cultured 4 days in HGTM (plus 2% serum) followed by treatment with a 2-fold dilution series (62.5-500µM) of H_2O_2. Caspase-3 activity was measured as fluorescence at 0h, 2h, 4h, 8h and 16h. The absorbance values were normalized to the total protein content for each well. Treatment of hiPSC-CMs with 1µM of staurosporine for 5h was carried out as a positive control for caspase-3 induction. Statistical comparisons were carried out between the positive control and its corresponding VC (DMSO), and between the H_2O_2 treatments and its corresponding VC (H_2O). One-way ANOVA with a post-hoc Bonferroni test is depicted with * $p<0.05$, ** $p<0.01$, *** $p<0.001$. Bars represent ±SE for N=3 wells.

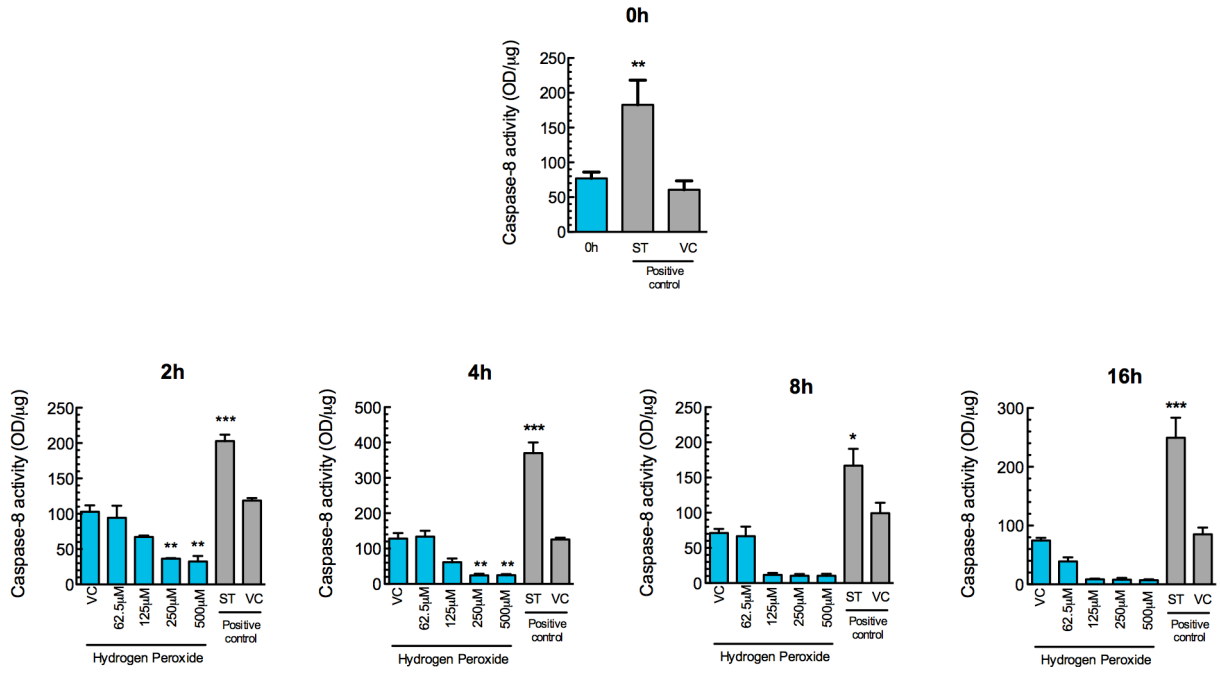


Figure 29: **Caspase-8 activity decreases with increasing H_2O_2 concentration in hiPSC-CMs.** hiPSC-CMs were cultured 4 days in HGTM (plus 2% serum) followed by treatment with a 2-fold dilution series (62.5-500µM) of H_2O_2. Caspase-8 activity was measured as luminescence at 0h, 2h, 4h, 8h and 16h. The absorbance values were normalized to the total protein content for each well. Treatment of hiPSC-CMs with 1µM of staurosporine for 5h was carried out as a positive control for caspase-8 induction. Statistical comparisons were carried out between the positive control and its corresponding VC (DMSO), and between the H_2O_2 treatments and its corresponding VC (H_2O). One-way ANOVA with a post-hoc Bonferroni test is depicted with * $p<0.05$, ** $p<0.01$, *** $p<0.001$. Bars represent ±SE for N=3 wells.

We hypothesized that the prompt cell death observed in hiPSC-CMs was partly due to their prolonged culture (4 days) in 2%LGTM. In an attempt to minimize or delay cell death in hiPSC-CMs we reduced their maintenance in the transition medium from 4 to 2 days while at the same time tested two H_2O_2 concentrations (125 and 250μM).

Cells were cultured for 2 days at HGTM supplemented with either 2% or 0.5% serum and assayed for LDH activity (Fig. 30), caspase-3 activity (Fig. 31) and for loss of mitochondrial potential (Fig. 32) using the Mitoview^{TM} potentiometric dye. Similar to Figure 27, LDH release was detected from as early as 2h with 125μM H_2O_2 when cells were cultured in 2%HGTM and at 4h with 125μM when cells were cultured in 0.5%HGTM. As well, no increase in caspase-3 activity was present under these conditions (Fig. 31). The LDH release was equivalent to the total cell number loss acquired from microscopy-based assay for measuring mitochondrial potential (Fig. 32).

For the measurement of mitochondrial potential, we incubated H_2O_2-treated cultures with the far-red potentiometric dye to allow accumulation in the mitochondria. The dye accumulates in active mitochondria that exhibit a distinct pattern of the mitochondrial networks, but in the case of diminished mitochondrial potential the staining becomes diffuse and is defined by a decrease in intensity. A significant increase in the percentage of cells with diminished mitochondrial potential (Mitoview-negative or MP^- cells) in both 0.5% and 2% HGTM in the presence of either 125μM or 250μM of H_2O_2 were observed, associated with a significant loss of cells. Interestingly, the loss of mitochondrial potential was steeper in the presence of 2%HGTM equivalent to a more prompt decrease in cell number (Fig. 32) and LDH release (Fig. 30). However, since background cell death (0h) measured by LDH release was significantly higher with 0.5%HGTM (Two-tailed t-test, $p<0.05$, not shown) compared to 2%HGTM, we continued using 2%HGTM for 2 days prior to cell death induction with H_2O_2 in the MAP4K4 knockdown experiments.

To conclude, H_2O_2 induces cell death in hiPSC-CMs via loss of mitochondrial potential without caspase-3 activation. Caspase-8 inhibition might be required in H_2O_2-induced cell death, but further investigation, at the very least, with caspase-8-specific inhibitors or shRNAmir against caspase-8 is required.

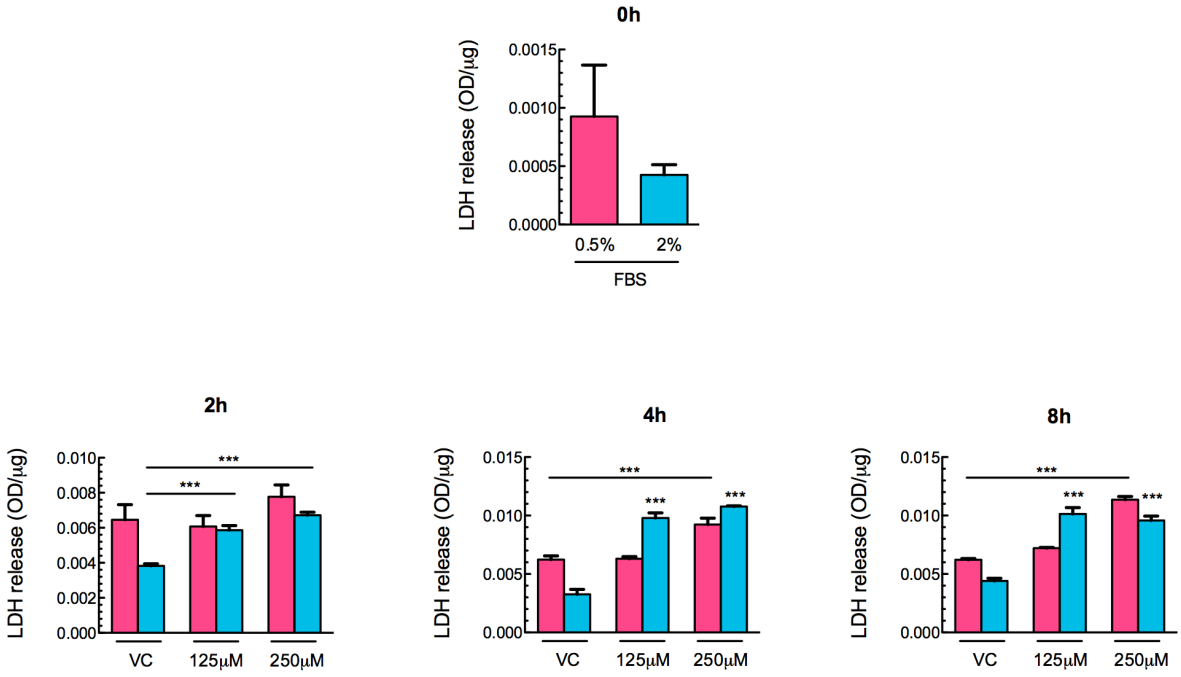


Figure 30: **Cytotoxicity measured by LDH assay under H_2O_2 conditions in 0.5% and 2% HGTM. (Top)** The level of background cell death (at 0h) with 0.5% or 2% serum in HGTM for 2 days; **(Bottom)** LDH was measured at 2h, 4h and 8h following treatment with 125µM and 250µM of H_2O_2. Absorbance values were normalized to the total protein content per well. One-way ANOVA with a post-hoc Bonferroni test is depicted with * p<0.05, ** p<0.01, *** p<0.001. Bars represent ±SE for N=5 wells

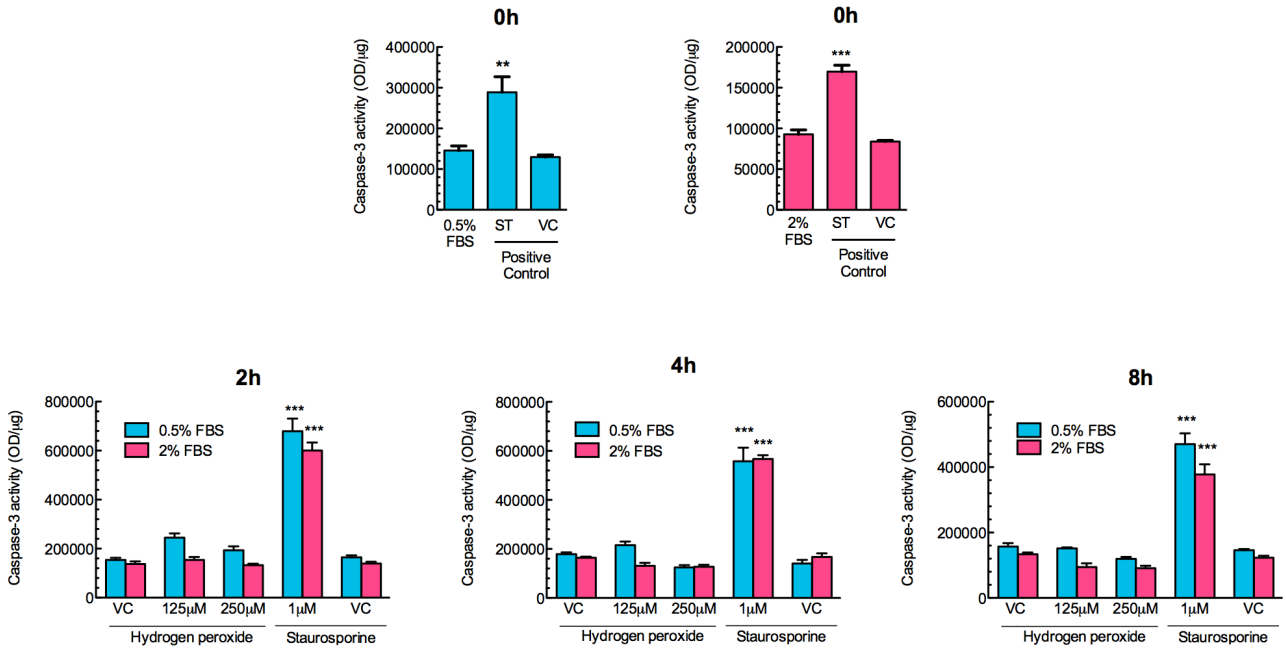


Figure 31: **No caspase-3 activation in response to H_2O_2 in 0.5% or 2%HGTM. (Top)** Background cell death (at 0h) in 0.5% and 2% HGTM for 2 days; **(Bottom)** Fluorescence values for caspase-3 activity were normalised to the total number of protein per well (µg). Staurosporine-treated conditions with 1µM for 5h were used as a positive control for induction of caspase-3 activation. One-way ANOVA with a post-hoc Bonferroni test is depicted with * $p<0.05$, ** $p<0.01$, *** $p<0.001$. Bars represent ±SE for N=5 wells

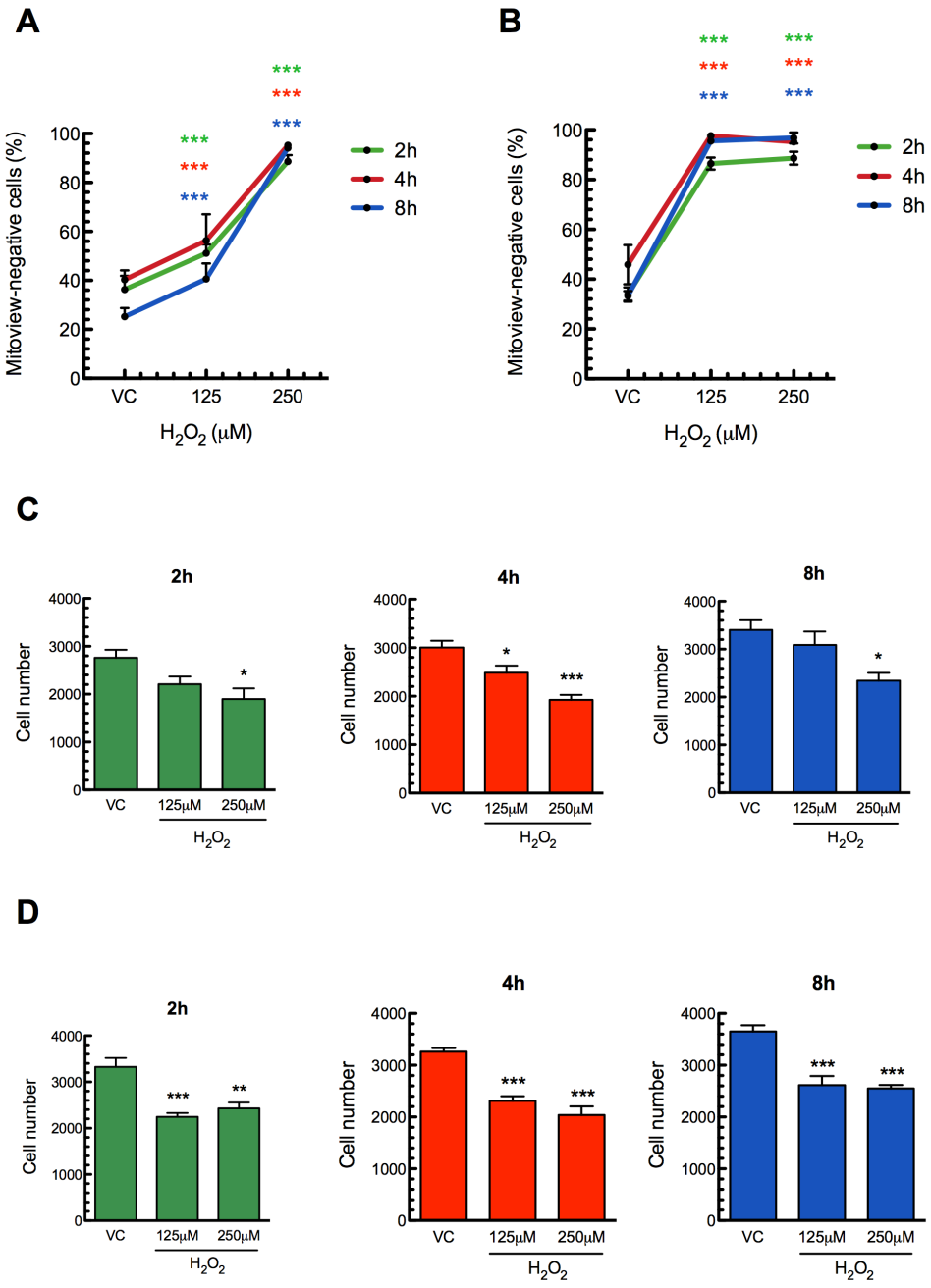


Figure 32: **Diminished mitochondrial potential in hIPSC-CMs with H_2O_2 in 0.5% or 2% HGTM.** H_2O_2-treated (125µM, 250µM) and VC (H_2O) cultures in were incubated with the Mitoview™ potentiometric dye, for at least 20min, to allow accumulation in the mitochondria. Maintenance and treatment with H_2O_2 in HGTM supplemented with **(A)** 0.5% or **(B)** 2% serum. Images were quantified in *Cellomics* and the percentage of Mitoview-negative cells (with diminished mitochondrial potential) is depicted 0.5% and 2%HGTM. **(C)** Total cell numbers at 2h, 4h and 8h in 0.5% serum. **(D)** Total cell numbers at 2h, 4h and 8h in 2% serum. One-way ANOVA (C, D) and two-way ANOVA (A, B) with a post-hoc Bonferroni test depicted with * p<0.05, ** p<0.01, *** p<0.001. Bars represent ±SE for N=5 wells.

3.3.2. MAP4K4 knockdown followed by H_2O_2 treatment in HGTM

Having determined the MOI that results in effective MAP4K4 knockdown (more than 70%) in hiPSC-CMs and having optimized the short-term culture in HGTM for 2 days, we had set out to knockdown MAP4K4 followed by the induction of cell death with H_2O_2 (Fig. 33). In summary, hiPSC-CMs were thawed in plating medium and maintained for additional 5 days in MM; virus was added (day 7) for 8h in 0%HGTM in 50µl followed by addition of MM to a final volume of 120µl per well. Virus-containing medium was removed (day 8) and replenished with fresh MM for 24h. Next day, MM was replaced with 2%HGTM for 2 days and effectively screened at 2h and 24h after the addition of H_2O_2 (Fig. 33).

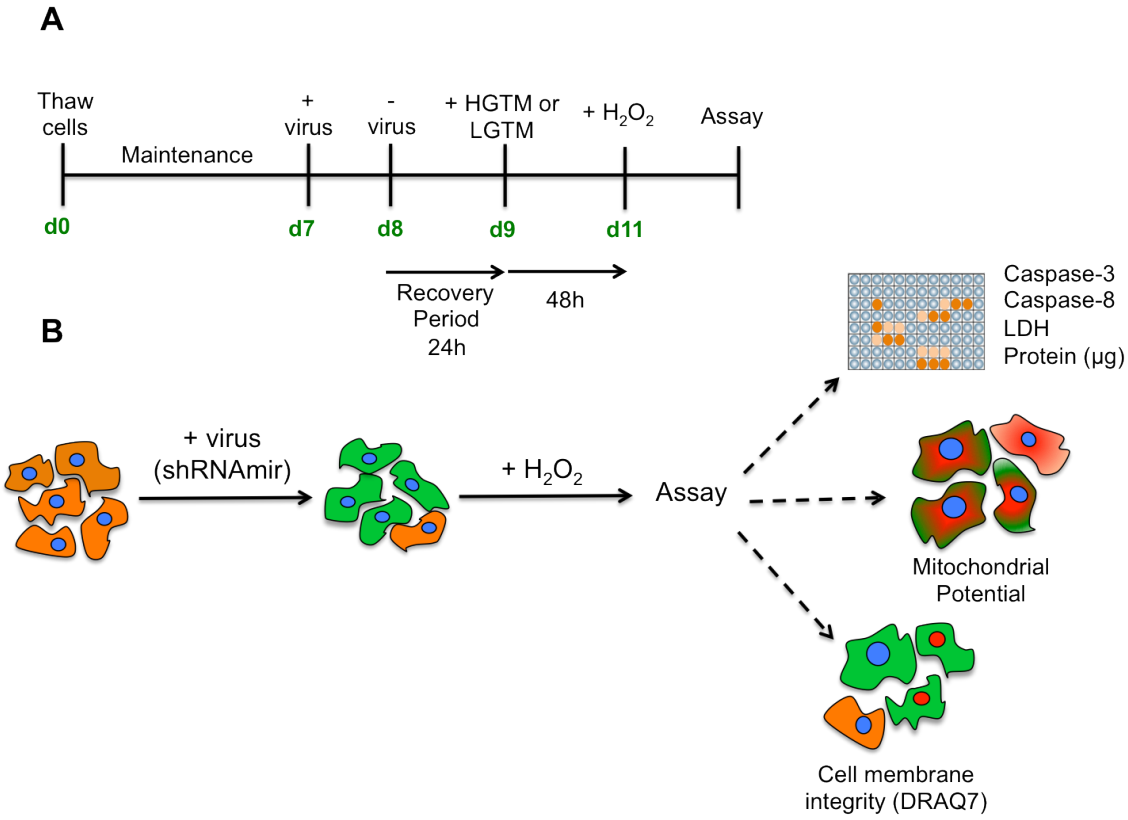


Figure 33: **Schematic timeline of hiPSC-CMs from thawing to screening for cell death (A)** Timeline diagram from the time hiPSC-CMs were thawed until assayed for **(B)** caspase-3 and caspase-8 activities, diminished mitochondrial potential and lost cell membrane integrity using DRAQ7 and LDH assay, in response to H_2O_2. In summary, hiPSC-CMs were thawed and kept for 2d in plating medium and maintained for additional 5 days in MM; virus was added (day 7) for 8h in 0%HGTM in 50µl volume followed by addition of MM to a final volume of 120µl per well. Virus-containing medium was removed (day 8) and replenished with fresh MM for 24h. Next day, MM was replaced with 2%HGTM for 2 days and effectively screened at 2h and 24h after the addition of H_2O_2. A similar timeline was followed with LGTM, but in order to avoid virus cytotoxicity, virus was added for 8h and removed before replenishing with MM.

Microscopy images from the DRAQ7 assay were analysed with a customised algorithm developed on *Definiens* to discriminate distinct hiPSC-CMs populations based on the various fluorophores. DRAQ7 and Mitoview were both detected on the far-red emission spectrum with no overlap with RFP (marker of cardiac nature) and EGFP (marker of transduction). Briefly, the algorithms can be broken down into two rounds of automatic image segmentation after background correction for nuclei/object identification, followed by the creation of three masks (RFP^+, $EGFP^+$, $DRAQ7^+$) – all in that order – defined by the intensities of each fluorophore/image layer. The first mask resulted in the identification of cardiac purity (RFP^+) from which the successfully transduced RFP^+ cells were identified (RFP^+EGFP^+). The dying transduced cardiomyocytes ($RFP^+EGFP^+DRAQ7^+$) were then extracted. Nuclei identification was based on nuclear intensity that was optimal for the identification of both healthy and apoptotic nuclei (Fig. S6). The non-transduced wells were used as a reference for setting EGFP fluorescence threshold close to zero.

The results from the DRAQ7 assay following MAP4K4 depletion and H_2O_2 treatment are described below. Cardiac purity remained above 80% under treated and untreated conditions (Fig. 34) with no overall significant difference between 2h and 24h, suggesting that H_2O_2 had no effect on the RFP. Interestingly, no cell death was observed in the RFP^- population (data not shown), suggesting that the death conditions were specific for the RFP^+ population (also seen in Fig. 41). The levels of cell death in MAP4K4-depleted cardiomyocytes ($RFP^+EGFP^+D7^+$) are seen in Figure 35. Significant decrease in total cell numbers and RFP^+EGFP^+ cells was associated with an increase in $RFP^+EGFP^+D7^+$ with NSC under H_2O_2-treated conditions, an effect not present with MAP4K4 knockdown. This suggests a survival advantage or rescue effect following MAP4K4 depletion. Antithetical to NSC, there was a significant increase in RFP^+EGFP^+ and a decrease in $RFP^+EGFP^+D7^+$ cells with H_2O_2 at 2h, only with the most potent shRNAmir (68219). Exacerbation of cell death was evident at 24h with the least effective shRNAmir (201856) compared to the NSC, as expected, most likely due to ineffective MAP4K4 protein inhibition, that remains to be tested in hiPSC-CMs.

A word of caution however: the significant loss of hiPSC-CMs with the NSC observed even under the VC-treated conditions makes the interpretation problematic. Such increased loss of cell numbers in the NSC can be explained by excessive cytotoxicity of the NSC in HGTM. Taking into account the significant induction of LDH under the H_2O_2 conditions in HGTM (Fig. 27) – with minimal difference to the maximum LDH achieved with the positive control – it is very likely that the addition of NSC exacerbated cytotoxicity in hiPSC-CMs. We excluded the possibility of human error since a similar effect with the NSC occurred in the hands of others (personal communication with Nasret Harun). One explanation behind the prompt response to cell death in response to H_2O_2 that was exacerbated with the addition of

NSC is the high levels of glucose in the medium. Although the metabolism and bioenergetic pathways in hiPSC-CMs are forthcoming, the metabolism of hiPSC-CMs shows more similarities to the fetal cardiomyocytes in that they metabolize lactate for pyruvate production to drive oxidative phosphorylation for generation of ATP (Gaspar et al., 2014; Tohyama et al., 2013). Gene arrays and [^{13}C]-labelling glucose fluxome analysis revealed that cardiomyocytes took up pyruvate into the mitochondria and most intermediate metabolites of the TCA cycle, whereas exhibited low bioenergetics dependence on the glycolytic pathway (Tohyama et al., 2013). Thus, for this reason, we decided to omit the use of HGTM and optimise short-term culture conditions in LGTM supplied with pyruvate.

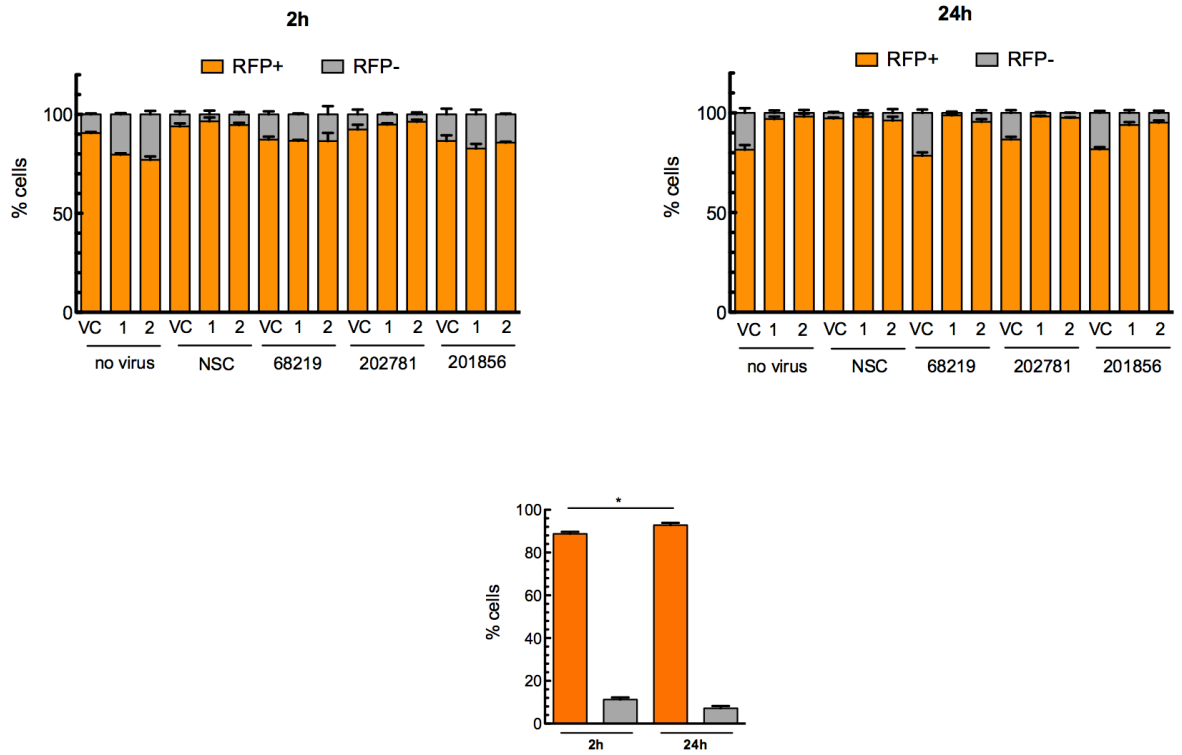


Figure 34: **Cardiac purity of the hiPSC-CMs system under H_2O_2.** The percentage of RFP^+ and RFP^- cells was determined with a customized image analysis algorithm on *Definiens*. **(Top)** Percentage of RFP^+ cells at 2h and 24h under H_2O (VC)- or H_2O_2-treated conditions and; **(Bottom)** Total percentage of RFP^+ between all wells at 2h and 24h. Statistical significance was calculated with one-way ANOVA and a post-hoc Dunnett's test depicted by * $p<0.05$, ** $p<0.01$ and *** $p<0.001$. VC (H_2O), Vehicle control; 1 and 2 stands for 125µM and 250µM of H_2O_2 respectively. Bars represent ±SE for N=3 wells.

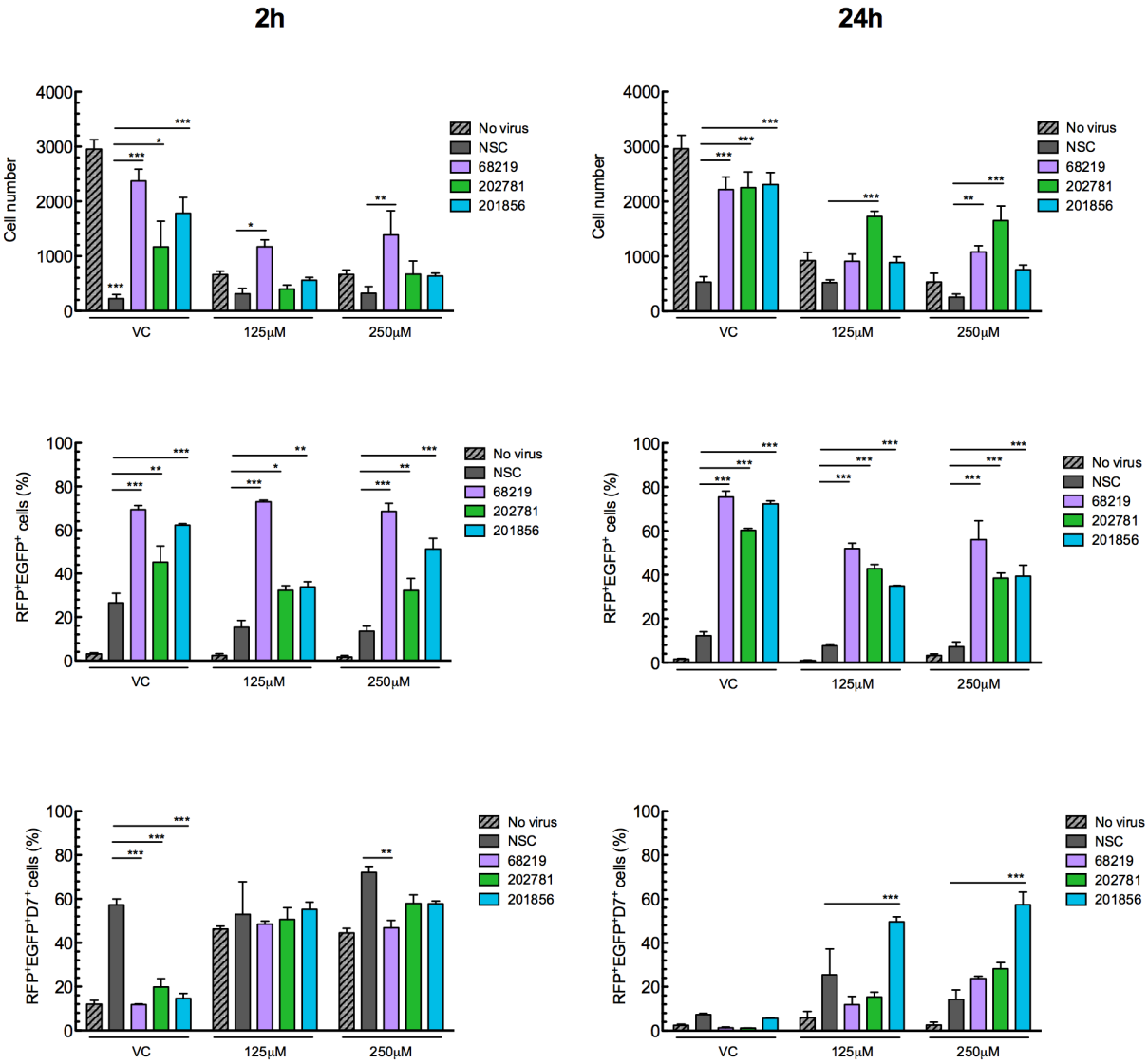


Figure 35: **DRAQ7 assay of MAP4K4-depleted hiPSC-CMs in the presence of H_2O_2. (Top)** Total cell number, **(Middle)** percentage of transduced cardiomyocytes (RFP^+EGFP^+) and **(Bottom)** percentage of dying NSC- or MAP4K4-depleted cardiomyocytes ($RFP^+EGFP^+D7^+$) at 2h and 24h following H_2O_2 treatments (125, 250μM). Statistical significance was calculated with Two-way ANOVA and a post-hoc Bonferroni test depicted by *p<0.05, ** for p<0.01 and ***p<0.001. Comparisons were carried out between NSC- and MAP4K4-deficient cells under H_2O (VC)- or H_2O_2-treated conditions. Bars represent ±SE for N=3 wells.

3.3.3. Optimization of cell culture of hiPSC-CMs in LGTM

Following the difficulties with extensive cytotoxicity in the presence of NSC in HGTM, we set out to re-optimise short-term culture conditions for 2 or 4 days prior to death induction in low glucose (LGTM). The cell death assays used for this purpose were: (i) microscopy-based for AnnexinV/DRAQ7, NucView488/DRAQ7, and loss of mitochondrial potential using a potentiometric dye, and (ii) whole well-based assays for LDH release, caspase-3 and caspase-8 activities.

Annexin V was first discovered as a membrane-associated protein in placental tissue (Inaba et al., 1984) and was first described as an apoptosis marker in mononuclear B cells (Koopman et al., 1994). The flip of phospatidylserine (Annexin V) from the cell membrane into the outer environment is associated with the loss of membrane phospholipid symmetry, also important in the recognition of apoptotic cells by macrophages. In combination with a live cell-impermeable dye, such as DRAQ7, the percentage of early (AnnexinV$^+$D7$^-$ or AV$^+$D7$^-$) and late apoptotic cells (AnnexinV$^+$D7$^+$ or AV$^+$D7$^+$) can be determined. This assay is considered as the golden standard in academia and industry for the interrogation of cytotoxicity. For this we have initially set out to investigate the effect of serum in LGTM using Annexin V in combination with DRAQ7 (Fig. 36). We found no statistical significance in the percentage of AV$^+$D7$^-$ and of AV$^-$D7$^+$ populations, whereas significant increase of the double-positive AV$^+$D7$^+$ population – marking caspase-3 activation that led to DNA fragmentation and/or loss of cell membrane integrity – was observed only after 4 days in 0, 0.1, 0.5 and 1% sera (Fig. 36).

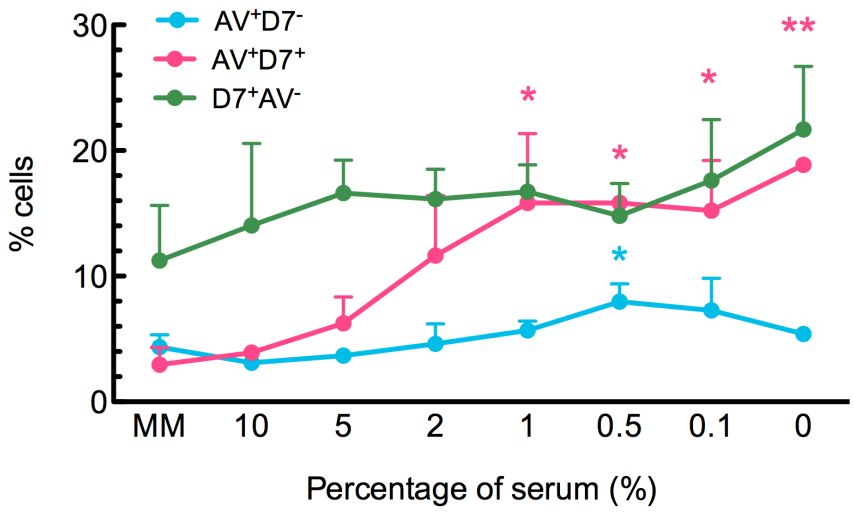


Figure 36: **Annexin V/DRAQ7 assay to assess cytotoxicity of hiPSC-CMs in LGTM for 4 days.** The percentage of AV^+D7^+, AV^+D7^- and AV^-D7^+ cells were determined following culture of hiPSC-CMs in LGTM for 4 days in various sera concentrations. Statistical analysis was carried out with one-way ANOVA and a post-hoc Dunnett's test depicted by * $p<0.05$, ** $p<0.01$ and *** $p<0.001$. Comparisons of each condition were carried out to 10%LGTM. Bars represent ±SE for N=3 wells.

Likewise, cytotoxicity under the same conditions was assessed with different dye combinations (i.e. DRAR7 and NucView™ 488) (Fig. 37). NucView^{TM} 488 is a cell-permeable caspase-3 enzymatic substrate linked to a fluorogenic DNA-binding dye that is attached on a negatively charged DEVD peptide (recognised by active caspase-3 enzyme). The DNA-binding dye is rendered inactive, but upon caspase-3 activity – thus DEVD cleavage – the dye is released, binds to DNA and fluoresces green. Therefore, the fluorogenic substrate can be used for real-time detection of caspase-3 activation in high-content screening. Cells were incubated with NucView^{TM}488 caspase-3-substrate and DRAQ7 dye and various populations were detected: (i) single-positive (NucView488^{+}/DRAQ7^{-}) cells represent caspase-3 activation without lost membrane integrity, (ii) single-positive (NucView488^{-}/DRAQ7^{+}) cells represent lost membrane integrity in the absence of caspase-3 activation (most likely caspase-3-independent cell death) and (iii) double-positive (NucView488^{+}/DRAQ7^{+}) cells represent loss of membrane integrity and/or DNA fragmentation associated with upstream caspase-3 activation (most likely caspase-3-dependent cell death).

Two-way ANOVA depicts a significant increase in double-positive NucView488^{+}/DRAQ7^{+} cells from 2 to 4 days with 0, 0.1, 0.5 and 1% serum compared to 10%LGTM (Fig. 37C). The overall interaction between sera and time does not have a significant cooperative effect, whereas concentration or time alone does. For this, we decided to utilise 2%LGTM for short-term culture of hiPSC-CMs. Interestingly, cells (approx. 25%) were positive for caspase-3 activity alone (NucView488^{+}/DRAQ7^{-}) for 2 days (Fig. 37); and the percentage of these cells increased by 4 days LGTM with low serum (0-2%) (Fig. 37D). Significant decrease in total cell number was only evident at 4 days. Thus, short-term maintenance of hiPSC-CMs in 2%LGTM was carried out for 2 days prior to treatment with the death agonists.

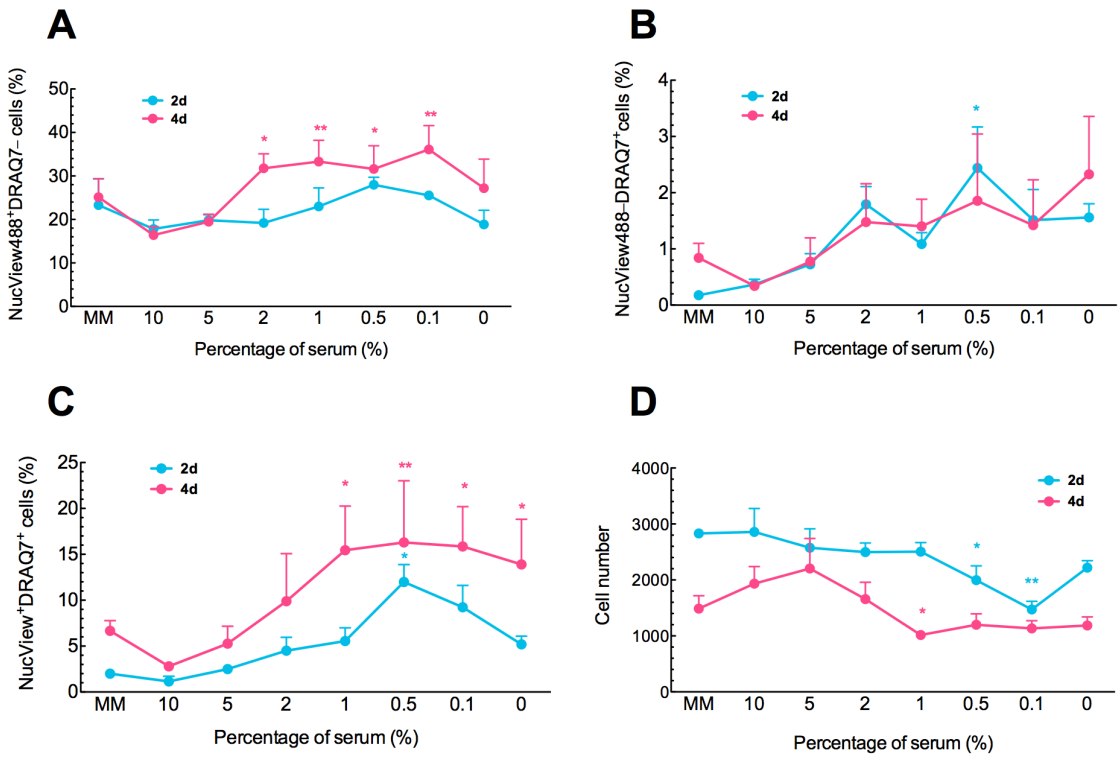
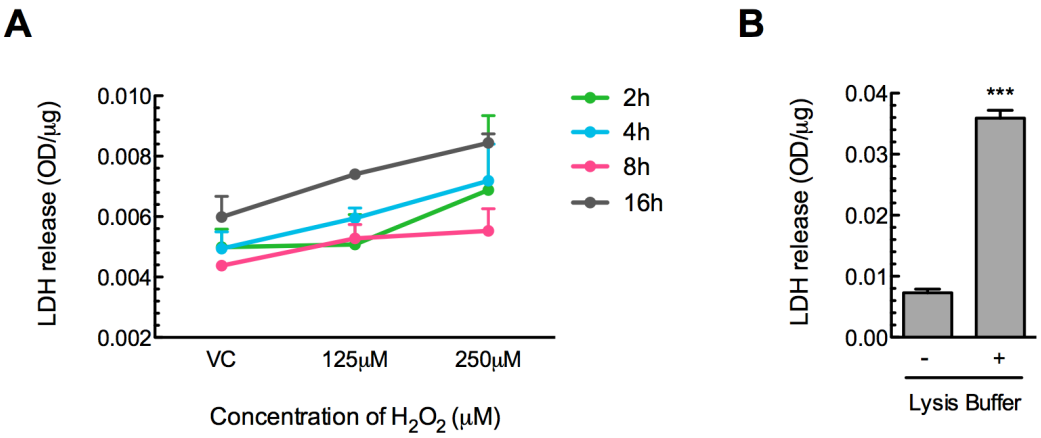


Figure 37: **Cell death assessment of hiPSC-CMs in LGTM with various serum concentrations.** Cells were maintained in LGTM for 2 or 4 days and cytotoxicity was assessed with NucView488 caspase-3-substrate and DRAQ7 dye **(A)** single-positive cells for caspase-3 activation (NucView488^{+}/DRAQ7^{-}), **(B)** single-positive cells with lost membrane integrity in the absence of caspase-3 activation (NucView488^{-}/DRAQ7^{+}), **(C)** Double-positive (NucView488^{+}/DRAQ7^{+}) cells for caspase-3 activation and loss of membrane permeability, and **(D)** total cell number. Statistical analysis was carried out with Two-way ANOVA and a post-hoc Bonferroni test and significance is depicted by * p<0.05, **p<0.01 and ***p<0.001. Comparisons of the various conditions were carried out to 10% LGTM. Bars represent ±SE for N=3 wells.

3.3.4. Optimization of H_2O_2 dose in LGTM

Cell death was sufficiently induced in HGTM with two H_2O_2 concentrations (125μM and 250μM), which were tested in LGTM at 2h, 4h, 8h and 16h. Two-way ANOVA analysis indicates no overall interaction between the two factors (time and concentration), where time alone, although marginally not significant, accounted for 20.9% of total variance (Fig. 38). Concentration alone was considered significant (at $p<0.05$) and accounted for 19.9% of total variance (Fig. 38). Background cell death at the time of experiment was no different to the VC (not shown). Lysis Buffer (LB) was added in a set of wells as a reference for the maximum amount of released LDH. A 10-fold difference was observed between maximal LDH to the H_2O_2-treated cultures, suggesting that the induction of LDH with 125μM and 250μM H_2O_2 is reduced compared to the total cell numbers. Caspase-3 activity remained unchanged at the same times (Fig. 39) and at 24h (Fig. 44) suggesting caspase-3-independent cell death via H_2O_2. Similar to our earlier observations we observed diminished mitochondrial potential at 16h with both H_2O_2 concentrations (Fig. 40) suggesting that H_2O_2 leads to mitochondrial dysfunction (loss of oxidative phosphorylation).



Two-Way ANOVA

Source of Variation	% of total variation	P value	Significant
Interaction	2.79	0.9740	ns
Time	20.96	0.0516	ns
Concentration	19.93	0.0263	*

Figure 38: **Time-dependent dose-response curve of H_2O_2 in hiPSC-CMs in LGTM. (A)** HiPSC-CMs were treated with 125µM and 250µM of H_2O_2 and assayed at 2h, 4h, 8h and 16h for LDH release. Cells were maintained for 2 days in 2%LGTM prior to the addition of H_2O_2. The absorbance values were normalized to the total protein content. Two-way ANOVA was performed (table) with a post-hoc Bonferroni test with comparisons to the 0h (not shown on the plot). **(B)** Lysis Buffer (LB) was added at 1:20 in a set of wells as a reference for maximum LDH. Student's t-test depicted by *p<0.05, **p<0.01 and ***p<0.001. Bars represent ±SE for N=3 wells.

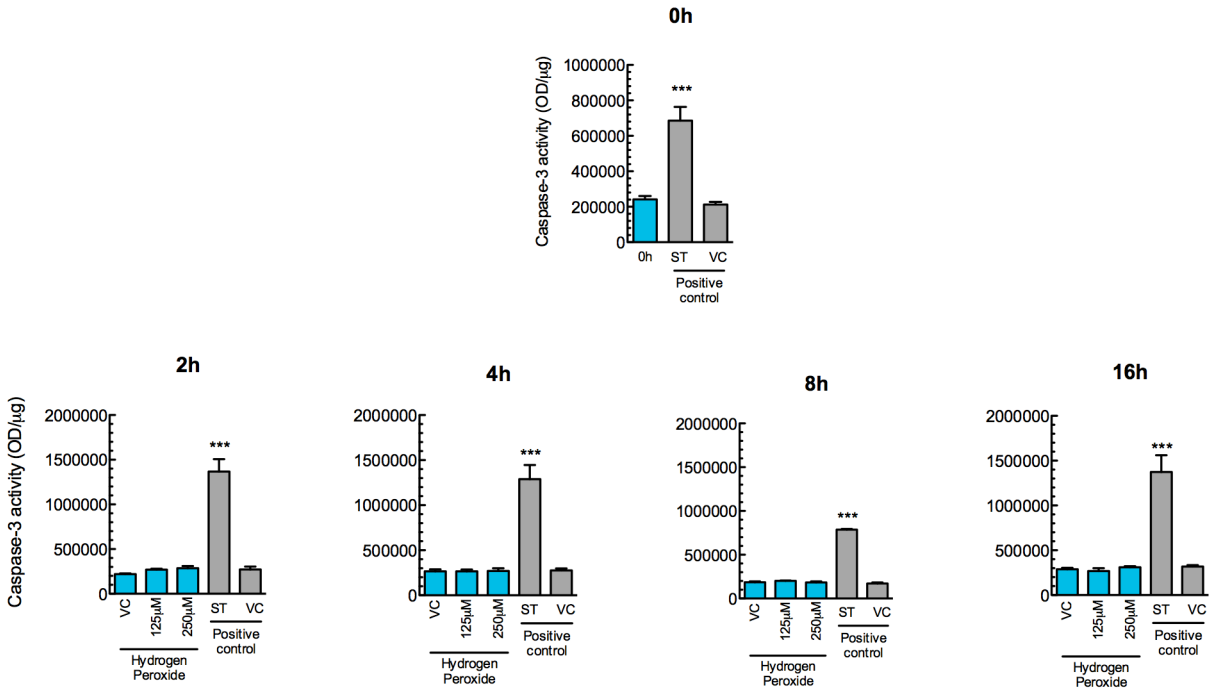


Figure 39: **Caspase-3 was not activated in hiPSC-CMs in response to H_2O_2.** No increase in caspase-3 activity was observed at 2h, 4h, 8h and 16h with 125µM and 250µM of H_2O_2 in 2%LGTM. The absorbance values were normalized to the total protein content per well. Staurosporine-treated wells with 1µM for 5h were used as a positive control for induction of caspase-3. One-way ANOVA with a post-hoc Bonferroni test is depicted by * p<0.05, ** p<0.01, *** p<0.001 *. Bars represent ±SE for N=3 wells.

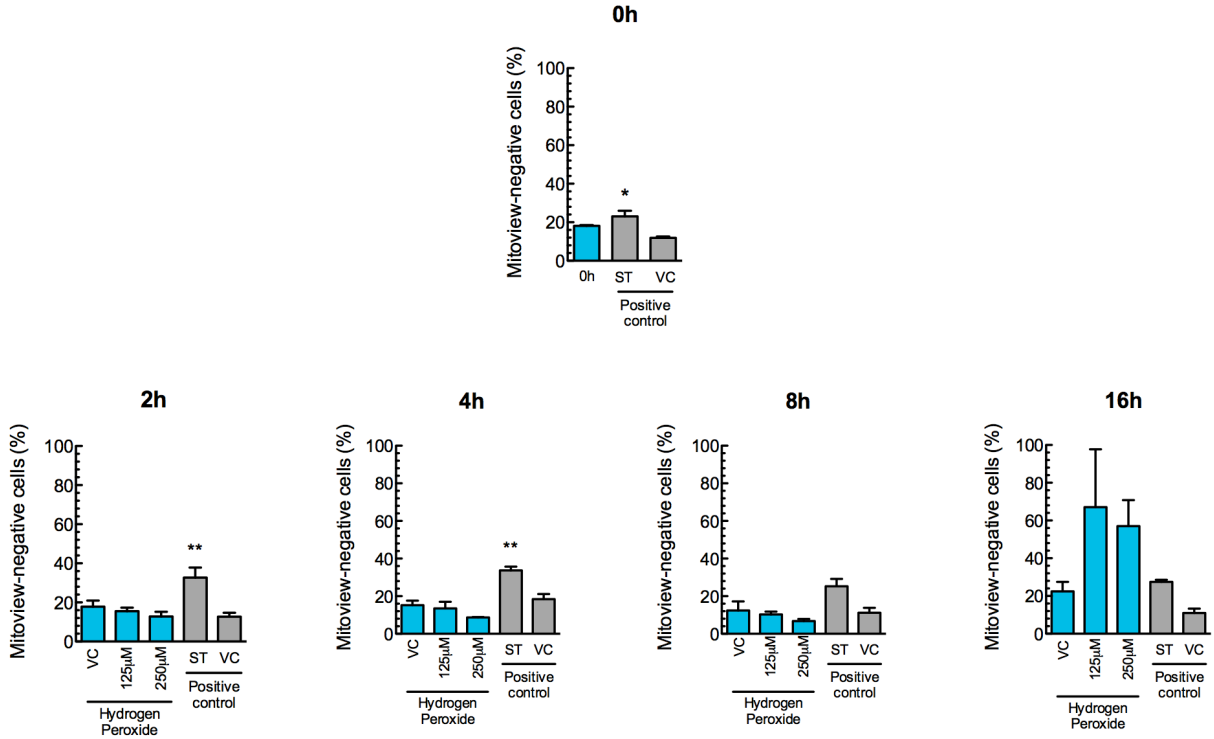


Figure 40: **H_2O_2 mediates cell death hiPSC-CMs via the mitochondria**. Cells were incubated with Mitoview^{TM} and diminished mitochondrial potential was measured as a drop in mitochondrial intensity (Mitoview-negative cells). Diminished mitochondrial potential was observed at 16h with 125µM and 250µM of H_2O_2, but increased variability is due to N=2 wells. Chelerythrine-treated wells were used as a reference to determine the threshold of the intensity. One-way ANOVA with a post-hoc Tukey test was carried depicted by * $p<0.05$, ** $p<0.01$, *** $p<0.001$. Bars represent ±SE for N=3 wells, except for 16h with H_2O_2 with N=2 wells (experiment requires repetition).

3.3.5. MAP4K4 knockdown followed by H_2O_2 treatment in LGTM

Finally, we transduced hiPSC-CMs with shRNAmir-containing viral particles (at MOI 50) that target MAP4K4 and treated the cells with 125, 250 and 500μM of H_2O_2. We decided to use an additional concentration of 500μM, since the level of LDH release at 250μM compared to the maximal induction of LDH was 10-fold lower than what could be achieved (Fig. 37). To avoid virus cytotoxicity that we observed earlier in HGTM with NSC, we minimized the exposure time of the cells to the virus, and instead of overnight incubation we used 8h. We then removed the virus and replenished with MM (Fig. 37).

Microscopy images were analysed with the same customised algorithm described earlier. Additionally, instead of DRAQ7, a similar algorithm was used to identify the cells with diminished mitochondrial potentials using the potentiometric dye. A positive control (chelerythrine-treated wells) was included as a reference to set the upper and lower thresholds for the intensity (Mioulane et al., 2012).

RFP^+ versus RFP^- cells were plotted in Figure 41 as a fold-change between two independent experiments. The inverse relationship between increase of RFP^- cells and an increase of RFP^+ describes the RFP^+-specific death conditions with 125μM and 250μM of H_2O_2. Antithetically, a generic drop in both RFP^+ and RFP^- populations at 500μM suggests an increase level of cytotoxicity causing the loss of both populations. Moreover, cardiac purity (i.e. RFP^+) between untreated and treated wells remains above 80% (0.8 fold-change) at all times (Fig. 41). MAP4K4 knockdown with 68219 shRNAmir under 250μM of H_2O_2 resulted in significant retention of cell number and increase in RFP^+EGFP^+ cells, while at the same time in a significant decrease of $RFP^+EGFP^+D7^+$ cells compared to the NSC. Additionally, MAP4K4 knockdown with 202781 shRNAmir in the presence of 250μM of H_2O_2 resulted in a significant retention of RFP^+EGFP^+ cells and decrease in $RFP^+EGFP^+D7^+$ cells compared to the NSC. This rescue effect was not observed with 201856 shRNAmir; corroborating the inefficacy of this shRNAmir to down-regulate its RNA levels (Fig. 46). Supporting evidence for the salvage of MAP4K4-depleted hiPSC-CMs from cell death is the absence of LDH compared to the NSC (with 68219 shRNAmir) while an increase in LDH was present with 202781 and 201856 shRNAmirs (Fig. 44).

As expected, caspase-3 activity remained unaffected suggesting that H_2O_2 activates cell death mechanisms that are independent of caspase-3-related cell death or that MAP4K4 does not work via a caspase-3-dependent pathway in hiPSC-CMs. This is in contradiction to the inhibition of caspase-3 activation by the expression of a catalytically inactive MAP4K4 form. Interestingly, H_2O_2-treated MAP4K4-depleted hiPSC-CMs resulted in unexpected activation of caspase-8, instead of decrease in activity observed with the overexpression of catalytically inactive MAP4K4 in NRVCs. This implies a distinct role of caspase-8 relative to MAP4K4 that is independent of cell death mechanisms via the extrinsic pathway (discussed

later). Similarly, MAP4K4 knockdown inhibited mitochondrial potential dissipation in hiPSC-CMs. Real-time detection of mitochondrial potential with a potentiometric dye (Mitoview^{TM}), where loss of mitochondrial potential leads to decreased dye retention, thus decreased intensity lead to a decrease in mitoview-negative cells ($RFP^+EGFP^+MP^-$) (Fig. 45). This suggests that MAP4K4 mediates mitochondria-dependent cell death.

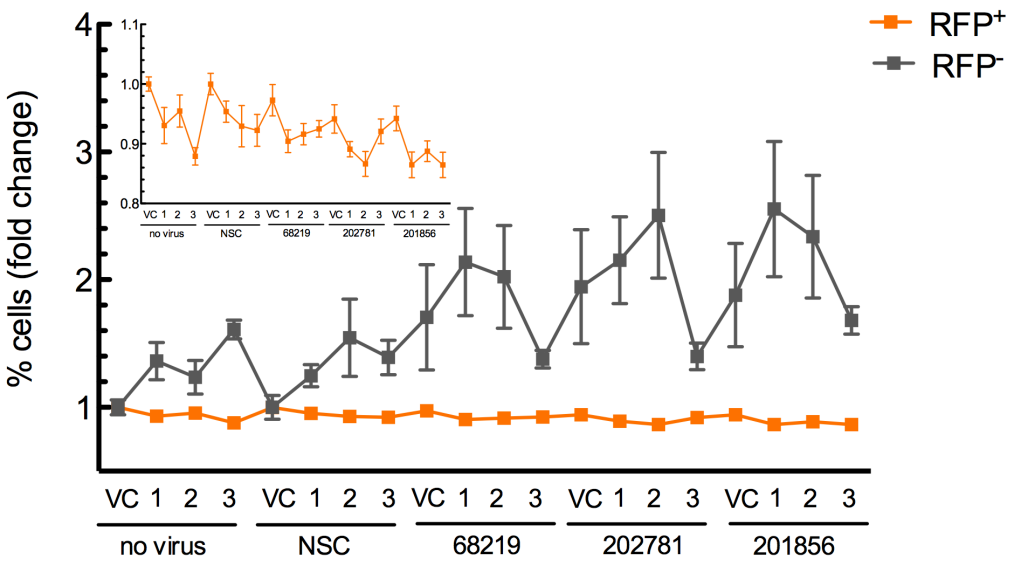


Figure 41: **Cardiac purity of the MAP4K4 knockdown screen in H_2O and H_2O_2 cultures.** The percentage of RFP^+ versus RFP^- cells is presented as fold change (between two independent experiments) under H_2O-treated and H_2O_2-treated conditions. The inlet graph indicates the subtle fluctuation of RFP^+ cells, compared to the obvious changes in the RFP^- population. The percentage of RFP^+ cells of each transduced sample were normalised to the percentage of RFP^+ in the NSC. 1=125µM, 2=250µM, 3=500µM of H_2O_2. VC=Vehicle control

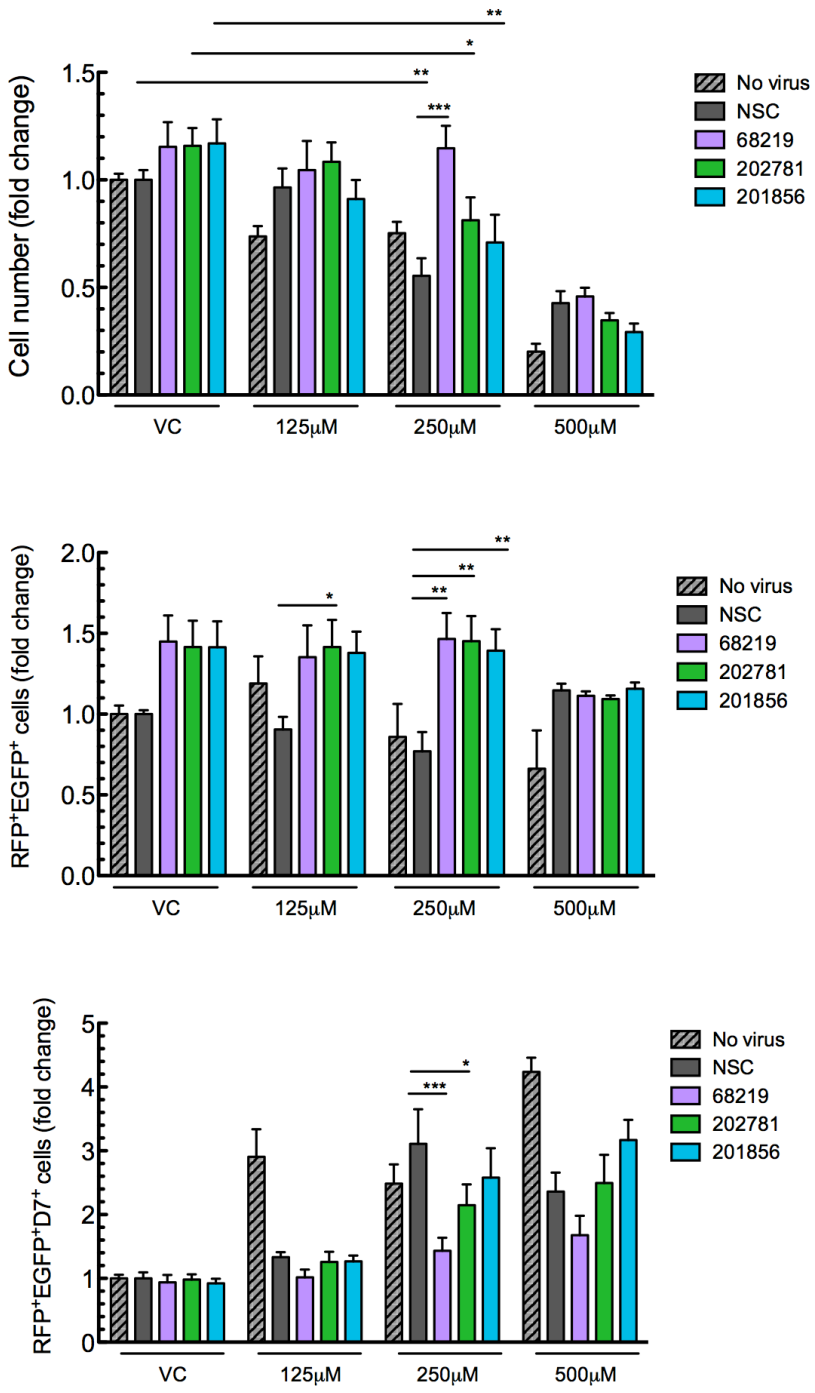


Figure 42: **MAP4K4 knockdown salvages hiPSC-CMs from cell death.** Real-time detection of cell death with DRAQ7 dye that marks cell membrane permeability. Image segmentation resulted in the identification of $RFP^+EGFP^+D7^+$ population – that is the dying MAP4K4-depleted cardiomyocytes. **(Top)** Total cell numbers, **(Middle)** RFP^+EGFP^+ and **(Bottom)** $RFP^+EGFP^+D7^+$ cells represented as fold change between two independent experiments. Statistical significance was calculate with two-way ANOVA followed by a Bonferroni post-hoc test and depicted by * $p<0.05$, ** $p<0.01$, *** $p<0.001$. Bars represent ±SE for N=2

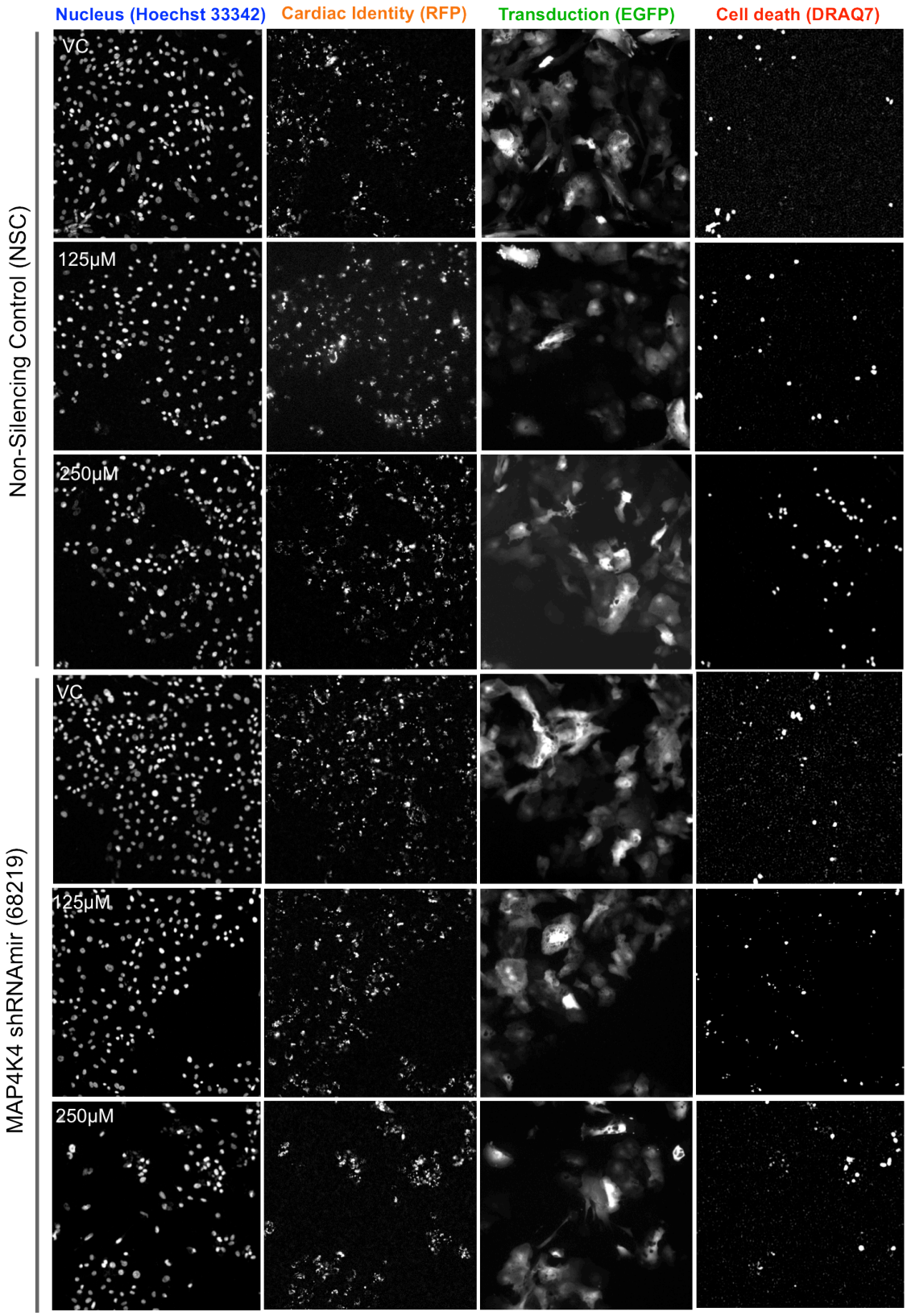


Figure 43: **Images from the DRAQ7 assay.** A representative field, after background correction, from wells of transduced hiPSC-CMs with the NSC and the most potent shRNAmir (68219) treated with the H_2O or H_2O_2 are shown. Each field consists of the four layers (Hoechst, RFP, EGFP and DRAQ7). Images were captured with *Cellomics* and analyzed with a custom-made algorithm in *Definiens*. Nucleus intensity was used for the initial object segmentation, from which the various objects (cells) were grouped based on RFP, EGFP and DRAQ7 intensities.

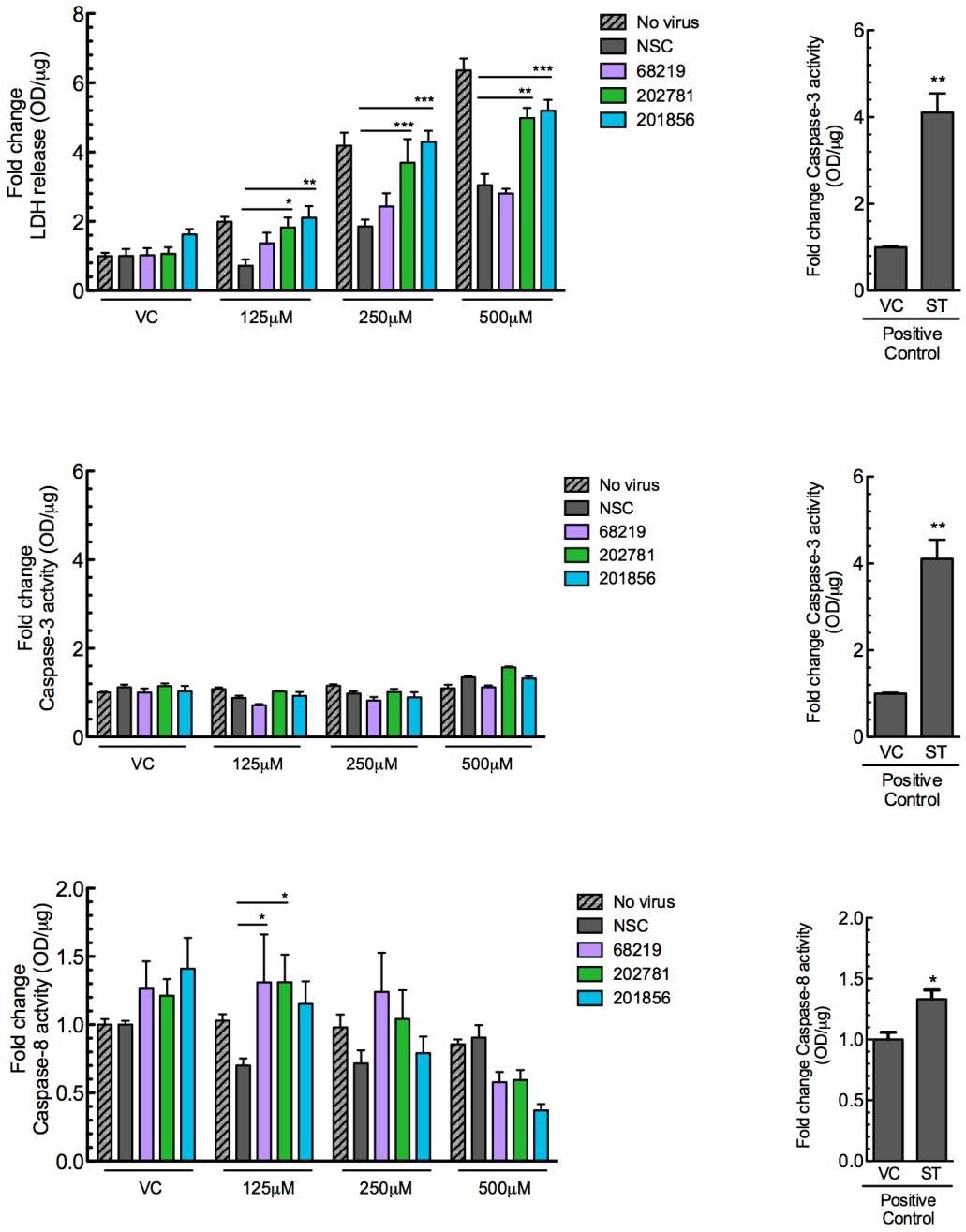


Figure 44: **MAP4K4 knockdown inhibits cell death independent of caspase-3 activation.** Real-time detection of cell death measured as LDH release that marks cell membrane permeability. **(Top)** LDH was detected in the culture medium, and **(Middle)** caspase-3 and **(Bottom)** caspase-8 activities were measured as fluorescence or luminescence intensity, respectively. Right-hand-side grey columns represent the positive controls for induction of LDH and, caspase-3 and -8 activation. Values were normalized to total protein content and presented as fold change between two independed experiments of a total of 9 replicates. Significance is depicted with asterisks calculated with Two-way

ANOVA followed by a Bonferroni post-hoc test. * p<0.05, ** p<0.01, *** p<0.001 Bars represent ±SE for N=2.

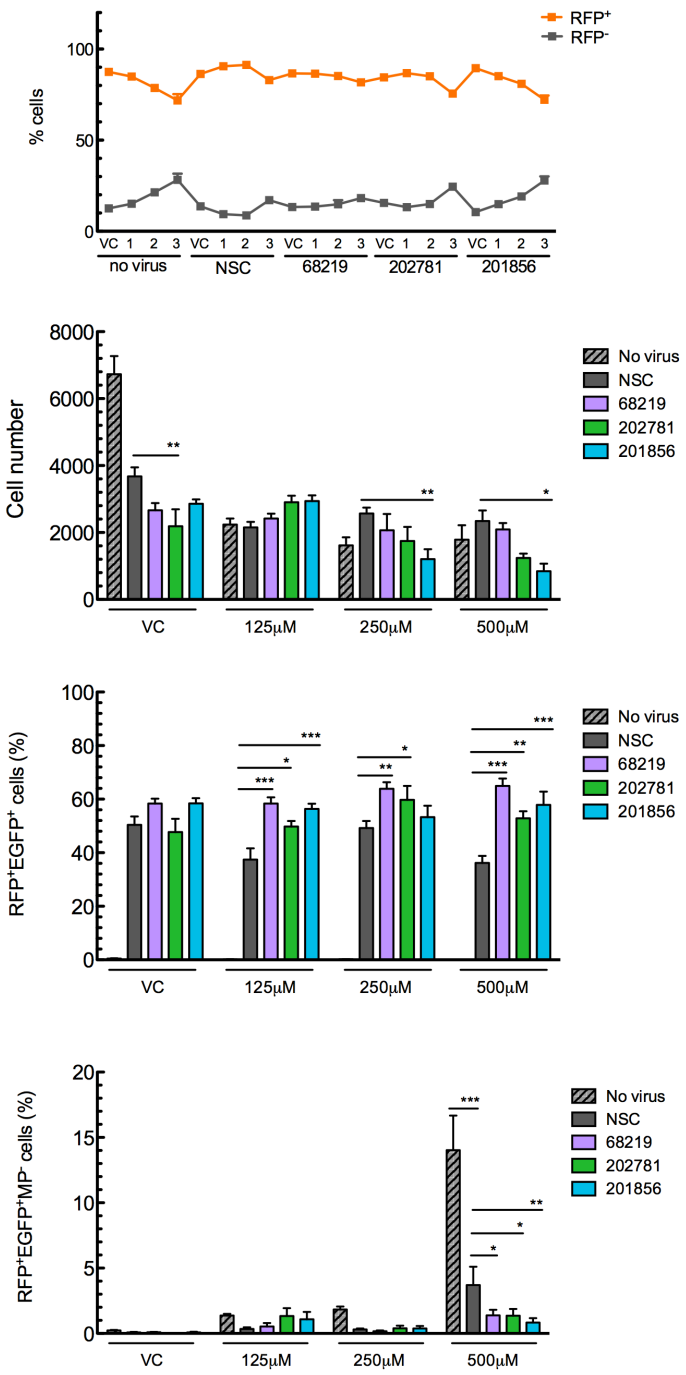


Figure 45: **MAP4K4 knockdown inhibits mitochondrial potential dissipation in hiPSC-CMs.** Real-time detection of mitochondrial potential with a potentiometric dye (Mitoview^{TM}), where loss of

mitochondrial potential resulted in decreased dye retention from the mitochondria, thus decreased intensity. Image analysis resulted in the identification of MAP4K4-depleted cardiomyocytes with diminished mitochondrial potential (RFP+EGFP+MP-). From top to bottom, percentage of RFP^+ and RFP^- cells, total cell number, RFP^+EGFP^+ and $RFP^+EGFP^+MP^-$ cells are indicated. Significance was calculated with Two-way ANOVA followed by a Bonferroni post-hoc test and is depicted by * $p<0.05$, ** $p<0.01$, *** $p<0.001$. Bars represent ±SE of N=6 wells

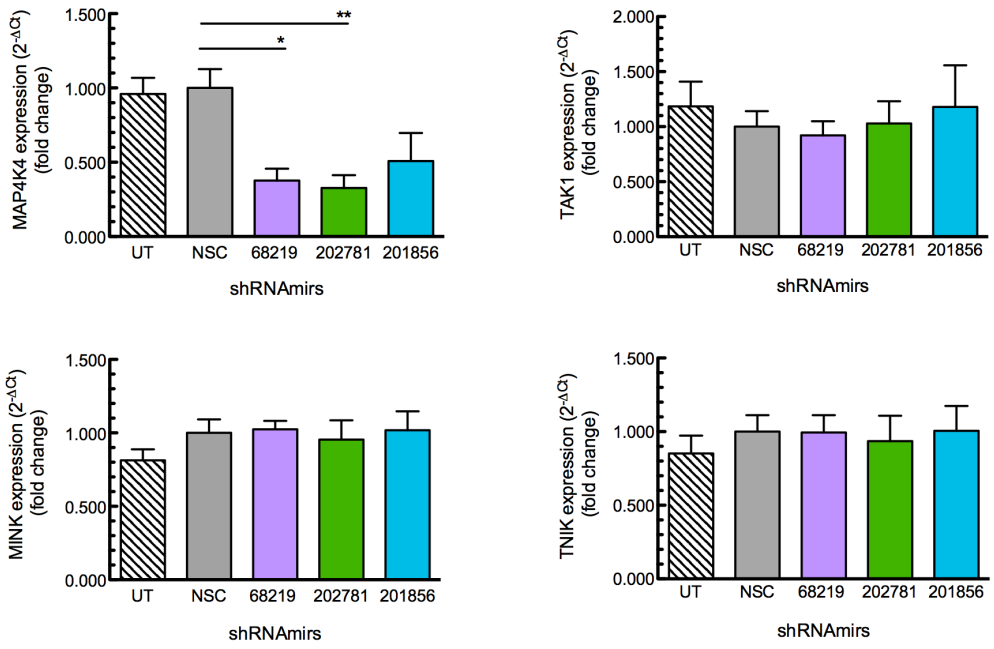


Figure 46: **MAP4K4 knockdown with sRNAmirs constructs validated by qPCR.** RNA knockdown with primers that recognize most MAP4K4 isoforms was validated by qPCR. Significant reduction of MAP4K4 RNA levels with two shRNAmirs (68219, 202781), but not with 201856. MINK1, TNIK and TAK1 RNA levels remained unaffected. Significance was calculated with One-way ANOVA followed by a Bonferroni post-hoc test and is depicted by * $p<0.05$, ** $p<0.01$, *** $p<0.001$. Bars represent ±SE from N=2

3.3.4. Summary

Here, I described the use of various microscopy assays (caspase-3 fluorescence substrate, Annexin V, potentiometric dye in combination with DRAQ7 impermeable dye) and whole well-based assays (caspase-3 and -8, and LDH) that were used to optimize a short-term culture protocol of hiPSC-CMs. Some assays were utilized for optimising cell death conditions with H_2O_2 – under which MAP4K4 knockdown with the most potent shRNAmir resulted in significant reduction of the MAP4K4-depleted dying cardiomyocytes compared to the NSC. The rescue phenotype was not observed with 201856 shRNAmir; corroborating the inefficacy of the latter shRNAmir to down-regulate its RNA levels (Fig. 46). The absence of caspase-3 activation with H_2O_2, suggests that H_2O_2 activates cell death mechanisms that are independent of caspase-3-related cell death and that MAP4K4 mediates cell death via a caspase-3-independent pathway in hiPSC-CMs. Interestingly, treatment with H_2O_2 resulted in decreased levels of caspase-8 activity and knockdown of MAP4K4 under H_2O_2 resulted in activation of caspase-8. This implies a distinct role of caspase-8 in relation to MAP4K4 signalling that is independent of its induction of cell death (discussed later). Similarly, MAP4K4 knockdown inhibited mitochondrial potential dissipation in hiPSC-CMs with H_2O_2, suggesting an involvement of MAP4K4 in mitochondria-dependent cell death.

3.4. MAP4K4 knockdown followed by c_2-ceramide conditions

3.4.1. Optimization of cell death conditions with c_2-ceramide

Similar to the approach with H_2O_2, the optimal conditions for cell death induction were established with c_2-ceramide in hiPSC-CMs. Cell membrane integrity was measured by LDH into the medium and caspase-3 and caspase-8 activities by whole-well-based fluorescence and luminescence assays, respectively. Initially a broad-range time-course was set up using 50μM, 150μM, 200μM and 300μM of c_2-ceramide. The formation of crystals in the medium for dilution ratios higher than 1:1000 (data not shown) was observed leading to presumably crystal-mediated cytotoxicity. This effect was not evident in medium with DMSO (vehicle control) suggesting that the crystal formation was a result of c_2-ceramide, most likely due to poor solubility. At this point, lower concentrations of c_2-ceramide were used, at 0.1μM, 1μM, 5μM and 20μM. Caspase-3 activation was observed at 16h with 5μM and 20μM of c_2-ceramide without caspase-8 activation. Caspase-3 activation with 20μM coincided with statistically significant increase of LDH (Fig. 47), not evident with 5μM. Therefore, 20μM of c_2-ceramide was used in downstream experiments.

The effect of c_2-ceramide on mitochondrial potential in hiPSC-CMs was more puzzling (data not shown). In general, loss of mitochondrial potential is associated with decrease in mitochondrial retention of the potentiometric dye, thus decrease in mitochondrial intensity. Firstly, loss of mitochondrial potential phenotype was more heterogeneous, as approx. 15% of hiPSC-CMs exhibited increase, rather than decrease, in intensity. Cultures of c_2-ceramide-treated hiPSC-CMs at 0.1μM and 1μM exhibited increased intensity in the mitochondria that were predominantly localized in the perinuclear region (data not shown). We hypothesized that the increase in dye retention was likely due to mitochondrial fragmentation, rather than loss of mitochondrial potential. However, since images were acquired with a 10X objective and could only be used to resolve differences in the intensity of the mitochondria and not the typical pattern of mitochondrial network fragmentation (Fig. 47B), we acquired images under a 40X objective with confocal microscopy (Fig. S8). The typical pattern of mitochondria fragmentation with c_2-ceramide treatment was visible, but further quantification of these events is required (currently being analysed).

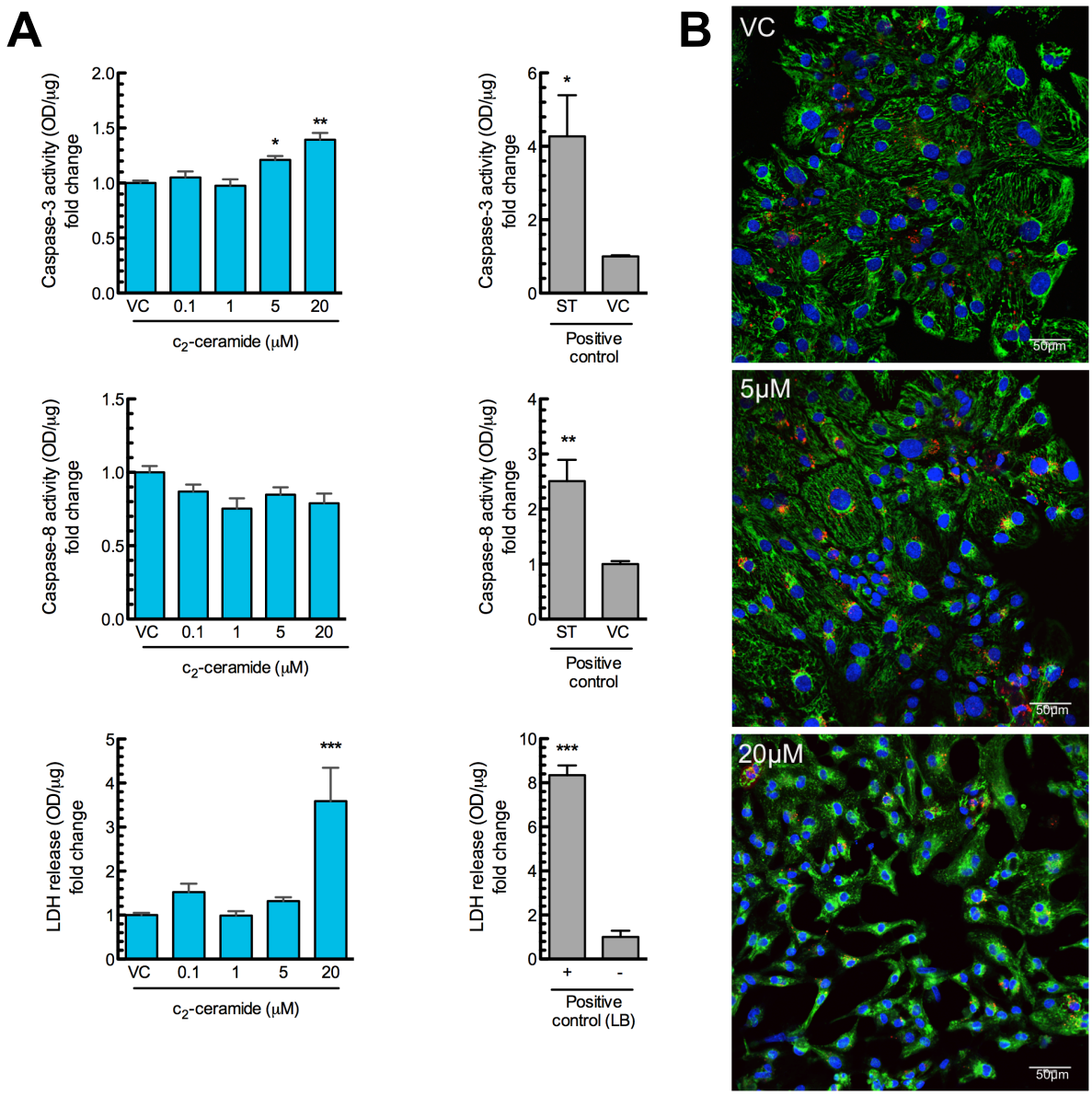


Figure 47: **hiPSC-CMs exhibit caspase-3 activation in response to c_2-ceramide at 16h. (A)** Caspase-3 and caspase-8 activities were measured in a multiplex fluorescence and luminescence assay, respectively, at 16h after treatment with c_2-ceramide. Staurosporine-treated hiPSC-CMs at 1µM for 5h were used as a positive control. LDH release was measured at the corresponding concentrations and was indicative of the total cytotoxicity per well. Lysis solution was added on hiPSC-CMs for 5h as a positive control for maximal LDH release. Statistical significance was calculated with one-way ANOVA and a post-hoc Dunnett's test and, for the positive controls, with a two-tailed t-test. Significance is depicted by * $p<0.05$, ** $p<0.01$ and *** $p<0.001$. **(B)** Representative confocal images of hiPSC-CMs with two concentrations of the agonist, where mitochondrial (green) were stained with the potentiometric dye. Perinuclear red punctuation is RFP. VC, Vehicle control; Bars represent ±SE from N=2

3.4.2. MAP4K4 knockdown in response to c_2-ceramide

Having determined the effective viral MOI for knockdown of MAP4K4 and having optimised the culture conditions in LGTM, the knockdown experiment was set-up (Fig. 46). In summary, hiPSC-CMs were maintained in culture for 7 days at which point virus was added for 8h in LGTM with no serum in 50µl, after which MM was added to a final volume of 120µl overnight for 12h and removed on day 8. Cells were maintained for 24h (48h from the time virus was added), and replaced with LGTM for 2 days. HiPSC-CMs were treated with c_2-ceramide and screened 16h after (Fig. 48).

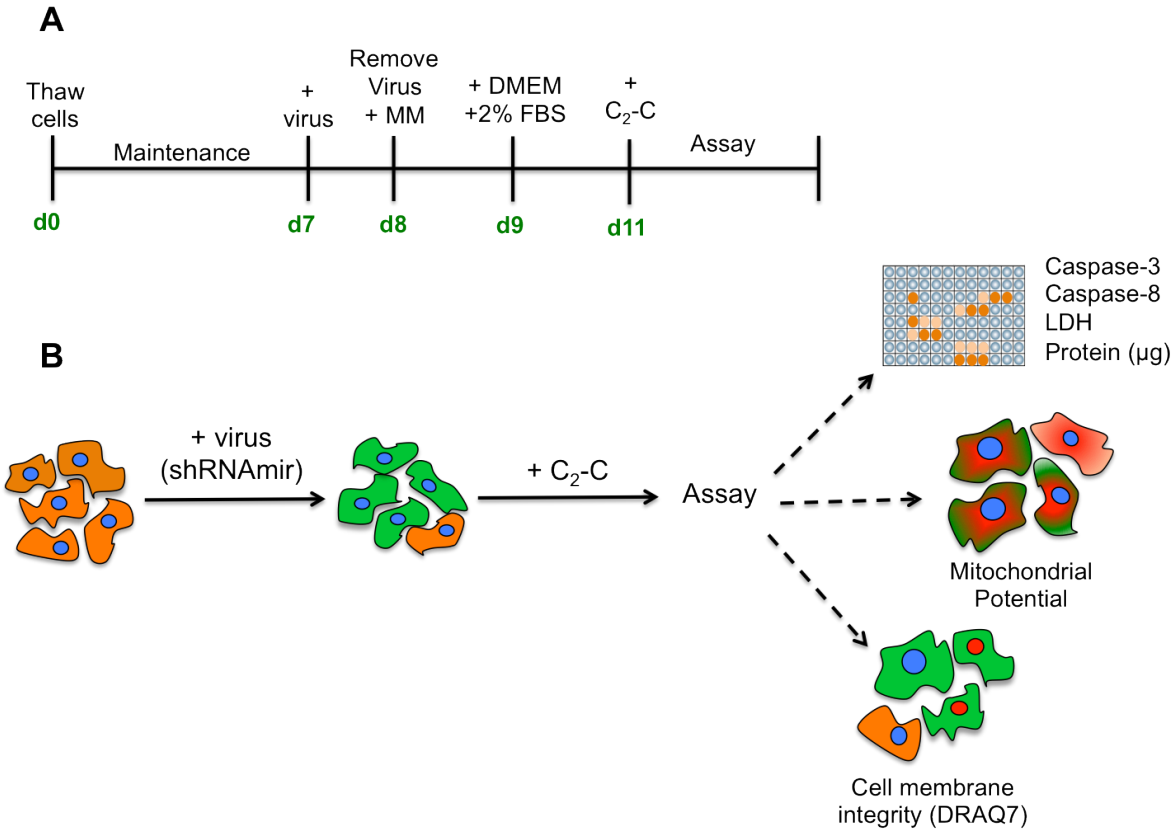


Figure 48: **Schematic timeline of hiPSC-CMs from thawing to screening with c_2-ceramide. (A)** Timeline diagram from the time hiPSC-CMs were thawed until assayed. The timeline is not on scale and days are depicted as d0, d7, d8, d9 and d11. **(B)** hiPSC-CMs were transduced, treated with c_2-ceramide and fluorescence caspase-3 and luminescence caspase-8 activities measured. Medium was collected from the plates to measure LDH activity. Protein quantification was carried out from a parallel plate for normalization purposes of the whole-well-based assays. Mitochondrial potential and cell membrane integrity using DRAQ7 were carried out as microscopy-based assays.

Assessment of cell death and mitochondrial potential was carried out using a customized high-content image analysis algorithm (described earlier) (Fig. 48-50). Firstly, the purity of the hiPSC-CMs cultures was determined based on the RFP fluorescence. Cardiac purity was between 90-100% under treated and untreated conditions at both 16 and 36h (Fig. 49). Subsequently, the percentage of transduced cardiomyocytes (RFP^+EGFP^+) (Fig. 50) and the percentage of dying transduced cardiomyocytes ($RFP^+EGFP^+D7^+$) were determined with no significant loss of cell number (Fig. 49). The RFP^+EGFP^+ proportion was variable between 20-65% depending on the shRNAmir, but with no significant change between baseline and treatment with c_2-ceramide in each case. The percentage of dying hiPSC-CMs was significantly increased in the un-transduced wells at both 16h and 36h with a significant increase between the two times ($p<0.01$, two-way ANOVA with Bonferroni post-hoc test, not shown), suggesting that c_2-ceramide induced cell death under these conditions as described earlier. Cell death in MAP4K4-depleted cardiomyocytes with the most potent shRNAmir did not increase in response to c_2-ceramide treatment compared to the NSC, but did increase by 2-fold when knockdown occurred with the rest shRNAmirs (201781, 201856) (Fig. 50). Thus, MAP4K4 knockdown exhibited a death rescue effect from c_2-ceramide with the most potent shRNAmir assessed by DRAQ7. However, the results are more difficult to interpret since some unintended off-target effects were observed with the innocuous NSC vector.

LDH release was significantly increased at 36h compared to the corresponding VC, but with no significant change between the shRNAmirs and the corresponding NSC (scrambled-equivalent) under c_2-ceramide. Furthermore, the subtle changes in cell death between shRNAmirs at 36h (Fig. 49) are reflected in the unchanged levels of LDH in medium (Fig. 50), suggesting that LDH accumulation at 16h was not sufficient to acquire a good signal.

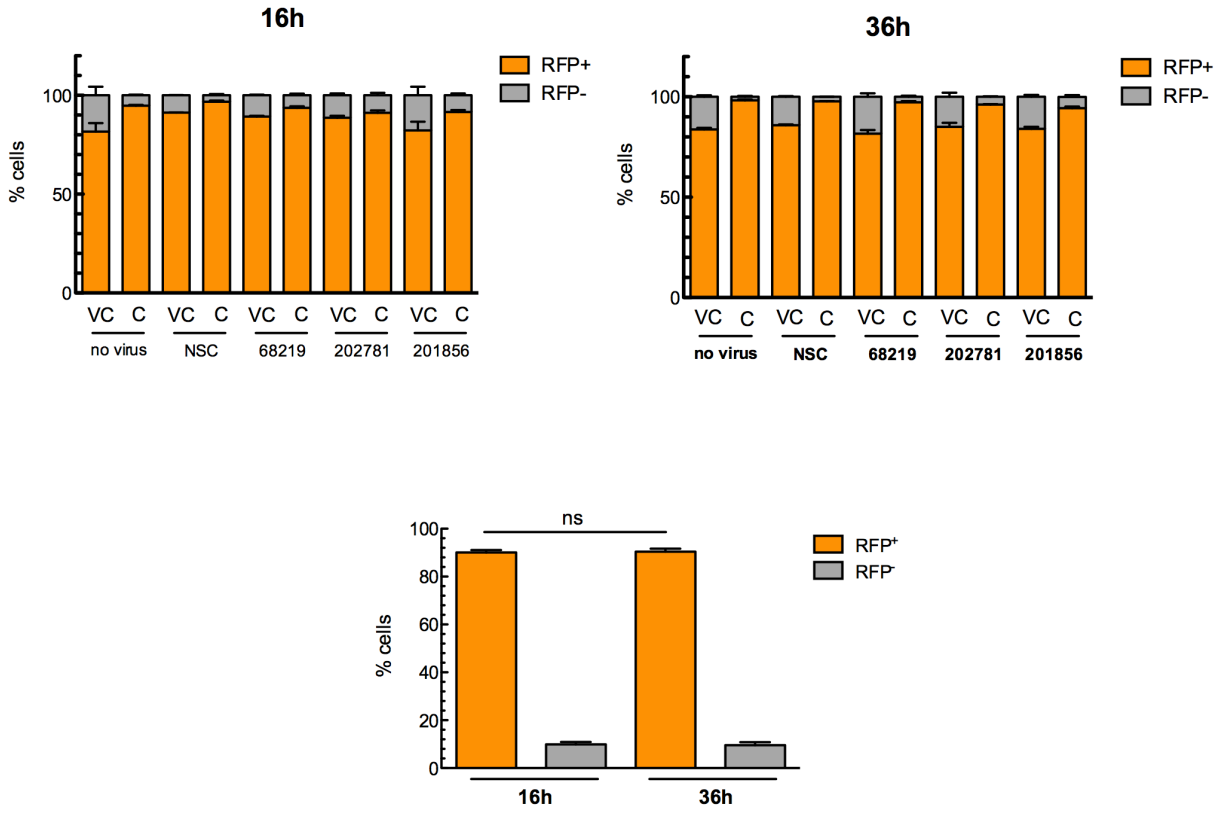


Figure 49: **Cardiac purity of hiPSC-CMs is high under both treated and untreated conditions and times.** HiPSC-CMs contain Myh6-RFP, where RFP is expressed in perinuclear region at a punctuated pattern. RFP intensity was used to discriminate the percentage of RFP^+ and RFP^- cells. The top panel indicates the percentage of RFP^+ cells separately at the two different times, while the bottom panel is indicative of the total percentage of RFP^+ across all wells at both 16h and 36h. Statistical significance is depicted by * for $p<0.05$, ** for $p<0.01$ and *** for $p<0.001$ calculated with One-way ANOVA and Tukey post-hoc test. VC, Vehicle control; C, c_2-ceramide; N=3 wells

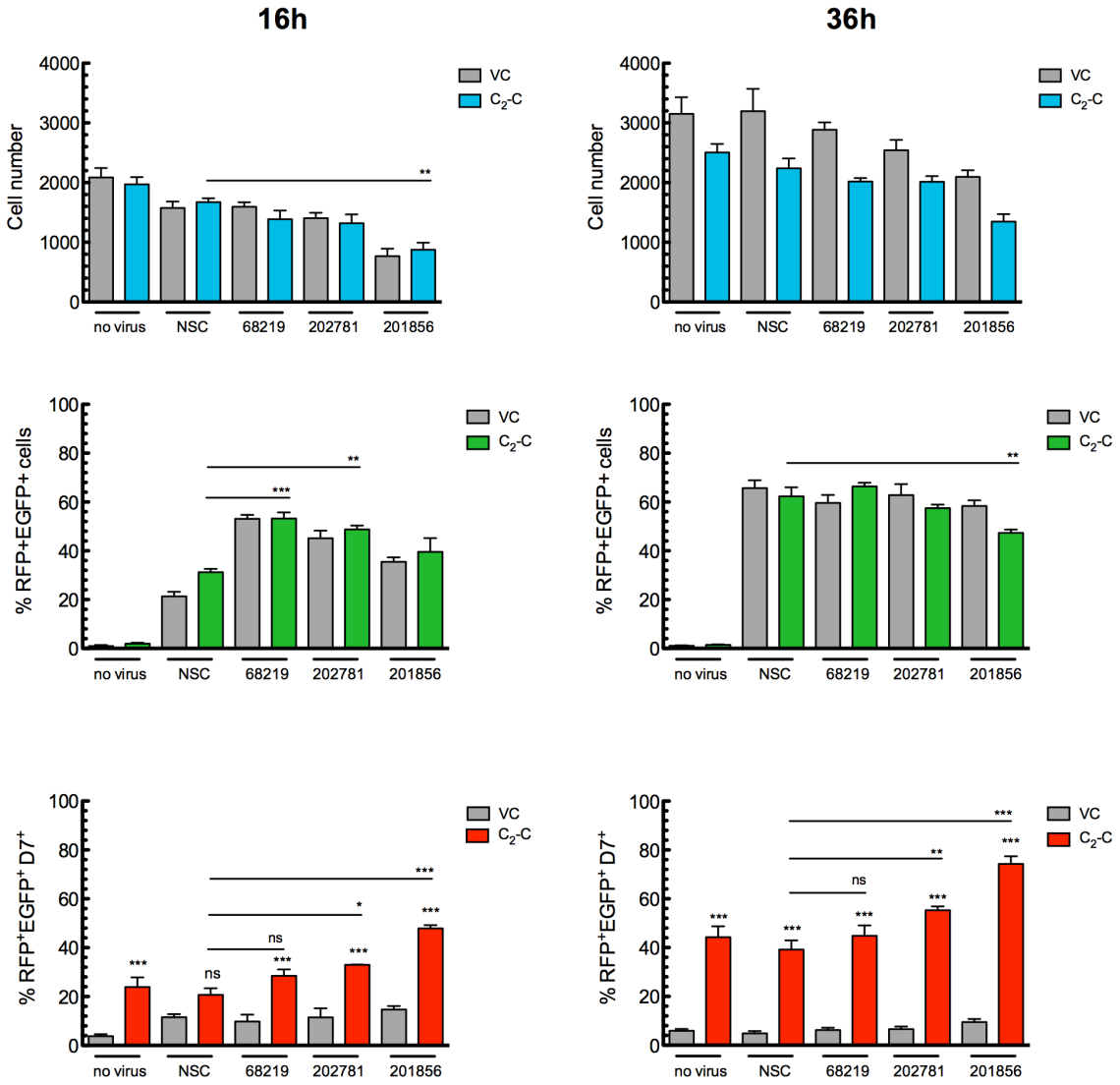


Figure 50: **Cell death assessment by DRAQ7 uptake of MAP4K4-depleted hiPSC-CMs under c_2-ceramide conditions at 16h and 36h. (Top)** Total cell numbers, **(Middle)** Percentage of transduced cells or MAP4K4-depleted cardiomyocytes (RFP^+EGFP^+) and **(Bottom)** percentage of dying MAP4K4-depleted cardiomyocytes ($RFP^+EGFP^+D7^+$). Statistical significance is depicted by * for $p<0.05$, ** for $p<0.01$ and *** for $p<0.001$ with One-way ANOVA and a post-hoc Dunnett's test. Bars represent ±SE for N=3 wells.

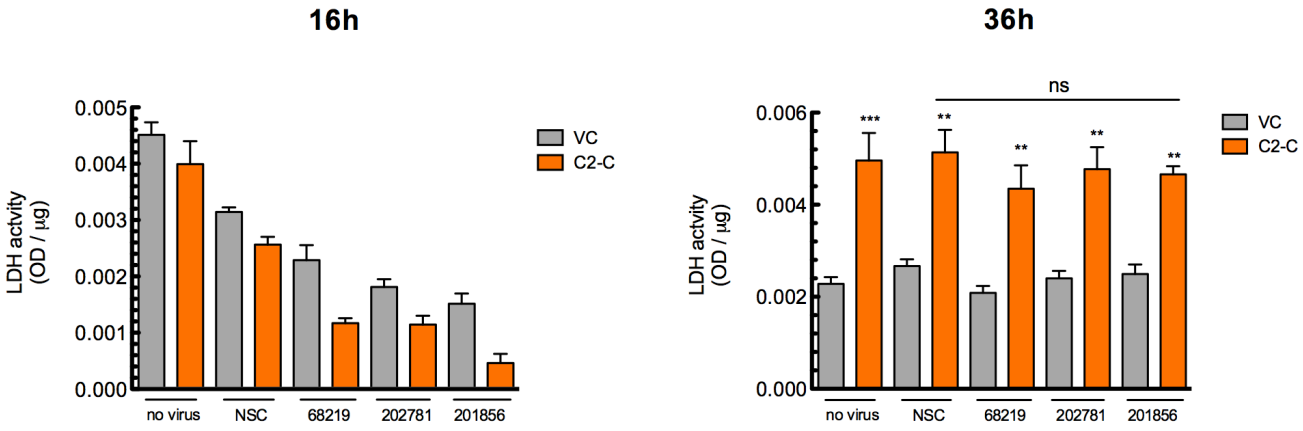


Figure 51: **LDH release in MAP4K4-depleted and c_2-ceramide-treated hiPSC-CMs.** LDH release was significantly increased at 36h with c_2-ceramide, but with no significant change between MAP4K4-depleted cells and NSC. Absorbance values were normalized to the total protein (µg) content. Statistical significance is depicted by * for $p<0.05$, ** for $p<0.01$ and *** for $p<0.001$ with One-way ANOVA and a post-hoc Dunnett's test. VC, Vehicle control; C2-C, c_2-ceramide; N=6 wells

A similar high-content image analysis approach was used to determine the percentage of transduced cardiomyocytes with lost mitochondrial potential ($RFP^+EGFP^+MP^-$). Overall, total cell numbers remained significantly unchanged, with some exceptions (Fig. 50). The percentage of RFP^+EGFP^+ cells was between 40-60% (Fig. 52), similar to the plates used for the DRAQ7 assay (Fig. 50), suggesting relatively low variability between parallel plates. MAP4K4-depleted hiPSC-CMs with two shRNAmirs (202781, 201856) exhibited significant decrease in the fluorescence intensity of the Mitoview at 16h, suggesting a prevention of mitochondrial potential dissipation. However, no such decrease was observed at 36h, suggesting a delaying effect.

Furthermore, at 36h there was a significant increase of caspase-3 activation compared to the baseline conditions, but a significant reduction in caspase-3 activation for two of the shRNAmir constructs (68219, 201856) (Fig. 53). Decreased caspase-3 activity was evident for the most potent shRNAmir at 36h that was associated with no increase in cell death compared to the NSC under c_2-ceramide conditions. Caspase-8 activity remained relatively unchanged at both 16h and 36h (Fig. 53), suggesting that either the extrinsic pathway is not involved in c_2-ceramide-induced cardiomyocyte death or that caspase-8 activation occurred at an earlier point.

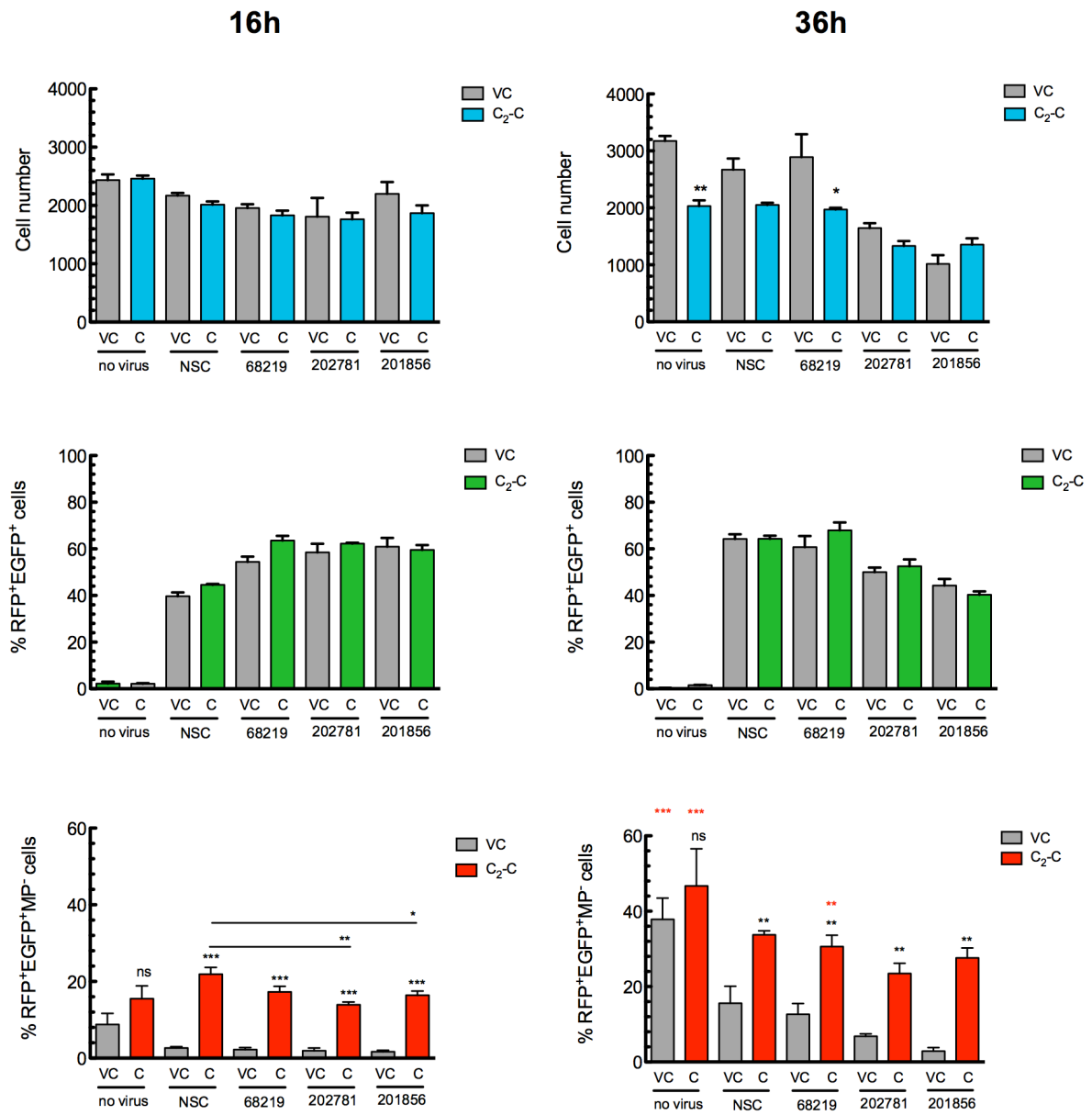


Figure 52: **Mitochondrial membrane potential of MAP4K4-depleted hiPSC-CMs under c_2-ceramide conditions at 16h and 36h. (Top)** Total cell numbers based on the number of nuclei; **(Middle)** Percentage of transduced or MAP4K4-depleted cardiomyocytes (RFP^+EGFP^+); **(Bottom)** Percentage of transduced or MAP4K4-depleted cardiomyocytes with diminished mitochondrial potential ($RFP^+EGFP^+MP^-$). The threshold for loss of mitochondrial potential was determined with the positive control (chelerythrine-treated hiPSC-CMs). Statistical significance was calculated with one-way ANOVA followed by a post-hoc Tukey multiple comparison test and is depicted by * for p<0.05, ** for p<0.01 and *** for p<0.001 Red asterisk depicts significant difference between the two times at the corresponding column using two-way ANOVA with a Bonferroni post-hoc test. C_2-C or C, c_2-ceramide; VC, DMSO; Bars represent ±SE for N=3 wells

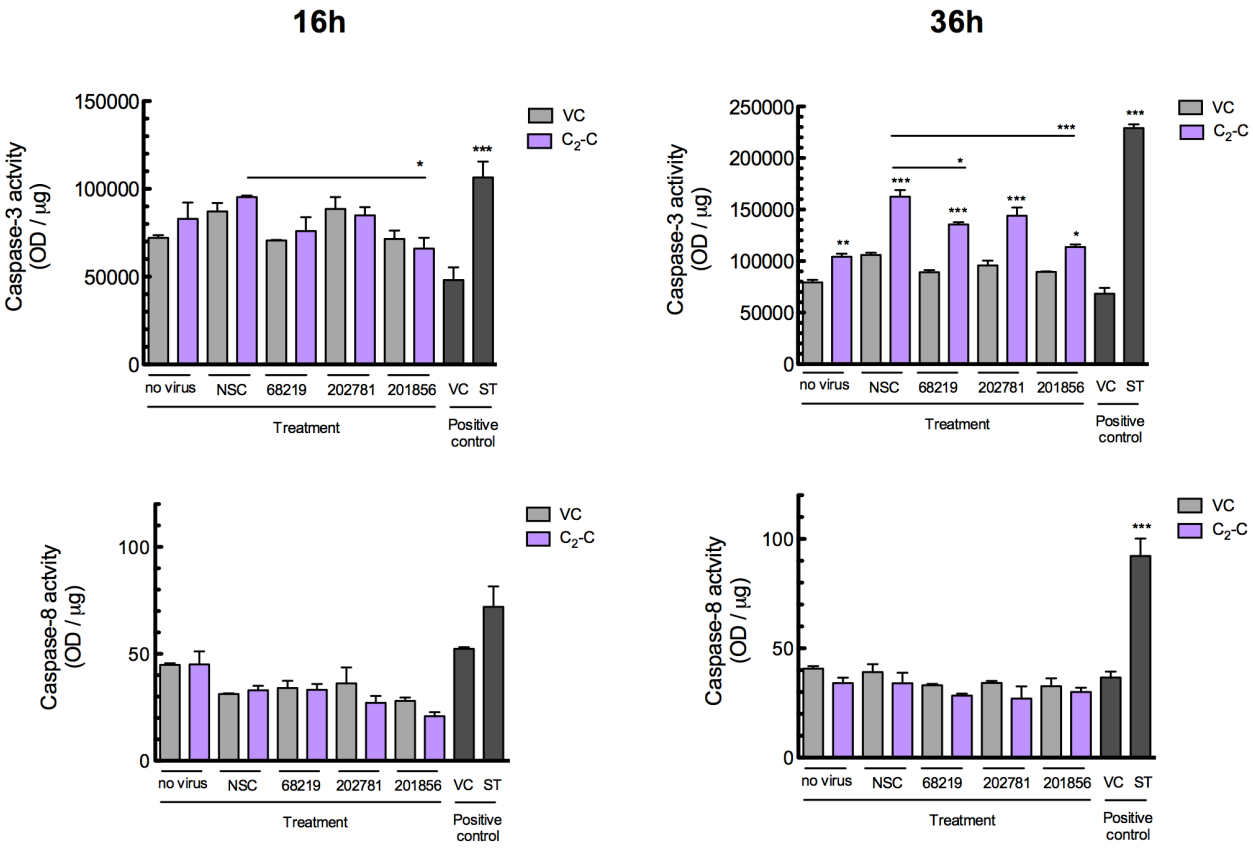


Figure 53: **Caspase-3 activity is reduced in MAP4K4-depleted hiPSC-CMs in c_2-ceramide-treated conditions.** Caspase-3 and Caspase-8 activities were measured in a multiplex fluorescence and luminescence assay, respectively, at 16h and 36h. Values were normalized to the total protein content (µg). Staurosporine-treated hiPSC-CMs at 1µM for 5h were used as positive control for the induction of caspase-3 and -8. Statistical significance is depicted by * for $p<0.05$, ** for $p<0.01$ and *** for $p<0.001$ with One-way ANOVA and Tukey post-hoc test. C_2-C, c_2-ceramide; VC, DMSO; Bars represent ±SE from N=3 wells

3.4.3. Summary

Firstly, we determined cell death induction with c_2-ceramide in hiPSC-CMs, which were subsequently used to induce cell death in MAP4K4-depleted cardiomyocytes. In summary, death of hiPSC-CMs at 16h was associated with increased LDH and caspase-3 activity with 20μM of c_2-ceramide. Furthermore, time-dependent 2-fold increase of cell death was evident with DRAQ7 uptake assay from 16h to 36h. Having determined cell death induction by c_2-ceramide, cells were transduced with three shRNAmirs against MAP4K4 to test whether MAP4K4 knockdown can inhibit cell death in hiPSC-CMs. Cell death in MAP4K4-depleted cardiomyocytes with the most potent shRNAmir remained similar to the NSC in response to c_2-ceramide treatment. A 2-fold increase in cell death with the rest of shRNAmirs (201781, 201856) (Fig. 50) was evident, most likely due to limited efficacy on RNA downregulation. Similarly, caspase-3 activation was inhibited in the presence of the most potent shRNAmir against MAP4K4, suggesting that MAP4K4 mediates cell death in response to c_2-ceramide via the intrinsic pathway. Caspase-8 activity remained unchanged both times, suggesting either that the extrinsic pathway is not involved in c_2-ceramide-induced cardiomyocyte death or that caspase-8 activation occurred at an earlier point.

With regards to mitochondrial potential no significant change was observed between the NSC- and MAP4K4-depleted hiPSC-CMs with the most potent shRNAmir in the presence of c_2-ceramide at both 16h and 36h, but a significant decrease was found with the remaining constructs at 16h. However, since a proportion of hiPSC-CMs exhibited a distinctive pattern of mitochondrial fragmentation assessed by confocal microscopy, further work is required to determine how the mitochondria are affected by c_2-ceramide and the role MAP4K4 signalling plays in these processes.

4. Discussion and Further Work

4.1. Synopsis of key findings

MAP4K4 is a relatively little-studied protein kinase whose involvement in cardiac muscle cell death is evidenced by studies of: (i) failing human hearts, (ii) genetic and pathobiological mouse models of cardiac cell death, (iii) gain-of-function mutations in mouse myocardium, and (iv) gain-of-function mutations, dominant-negative mutations, and RNA interference in cultured NRVCs. However, there is presently no concrete evidence that these or other death-associated kinases have functional importance in a human cardiac muscle cell. Given this unmet need, the aim of this project was to deploy shRNAmir-based technology in hiPSC-CMs as an improved platform for target validation, and specifically to test the hypothesis that knockdown of MAP4K4 will result in inhibition of cardiac muscle cell death provoked by relevant death-agonist agents (i.e. H_2O_2, and c_2-ceramide). Such studies would be the technical and scientific springboard for later, "higher bandwidth" studies of the entire human kinome or other essential mediators.

Based on single and multiple immunolabelling for various cardiac proteins, hiPSC-CMs were up to 95% pure and their expression of endogenous MAP4K4 RNA and protein was confirmed. Co-expression of MLC2v and MLC2a, which discriminate between mature atrial and ventricular cells but are co-expressed during early cardiac organogenesis, at the linear heart tube stage, validate the embryonic nature of these cells. The hiPSC-CMs were refractory to proliferation when cultured for 2 days in high serum concentrations, as assessed by EdU and PH3 staining. This initial homogeneity and the lack of a confounding proliferative subpopulation allowed the multiparametric interrogation of endpoints with simple biochemical well-based assays (caspase-3 and -8 and LDH release), complementing the more highly resolving but complex high content microscopy assays (NucView™ caspase-3 fluorogenic substrate, Annexin V, Mitoview™ potentiometric dye in combination with DRAQ7 impermeable dye).

Next, the knockdown efficacy of three shRNAmirs was validated against exogenous MAP4K4 RNA and protein, in readily transfectable HEK293 cells. Two shRNAmirs (68219, 202781) evoked similar down-regulation from 24-72h, but shRNAmir 201856 exhibited a delay of 24h compared to the others. This limited knockdown window for the latter construct was confirmed in hiPSC-CMs, in which the reduction of endogenous MAP4K4 had limited efficacy on RNA.

Having first developed the necessary phenotypic assays, I determined conditions for short-term (2 day) culture of hiPSC-CMs in defined media (HGTM or LGTM) without a significant background of spontaneous cell death. Using the defined media, we determined the concentration, of both H_2O_2 and c_2-ceramide death agonists, at which iPSC-CMs undergo cell death. Caspase-3 activation was not evident in the presence of H_2O_2, but was present in response to 20μM of c_2-ceramide at 16h. We observed approx. 80% of hiPSC-CMs exhibited

diminished mitochondrial membrane potential as early as 2h in response to H_2O_2 in HGTM. However, only 15% of cells exhibited diminished mitochondrial potential in response to H_2O_2 in LGTM, and that only at 24h. Enhanced toxicity in HGTM was observed with NSC transduction upon H_2O_2 addition that led to significant loss of cell number. Exacerbation of cell death in HGTM was most likely an effect of glucose oxidation by H_2O_2 that led to loss of mitochondrial membrane potential (Shibata et al., 2008). In addition, pluripotent-derived cardiomyocytes exhibited low bioenergetic dependence on the glycolytic pathway and require pyruvate to drive oxidative phosphorylation for generation of ATP (Tohyama et al., 2013). For these reasons we switched to low-glucose-containing medium (LGTM) supplemented with pyruvate.

With the conditions in place to induce and measure cell death in hiPSC-CMs we next moved on to validate our hypothesis, whether MAP4K4 inhibition would rescue hiPSC-CMs from death induced by H_2O_2 and c_2-ceramide. The most potent shRNAmirs reduced endogenous MAP4K4 RNA in hiPSC-CMs, and decreased cell death by 2-fold measured by the preservation of mitochondrial potential and DRAQ7 uptake. The most potent shRNAmir resulted in significant protection of MAP4K4-depleted cardiomyocytes after H_2O_2 treatment, as shown by the number of viable shRNAmir-transduced cells, less DRAQ7 and reduced LDH release. In addition, MAP4K4 knockdown inhibited mitochondrial potential dissipation in hiPSC-CMs by 2-fold, suggesting an involvement of MAP4K4 in mitochondria-dependent H_2O_2-induced cell death. Conversely, the lack of caspase-3 activation at any of times assayed suggests that H_2O_2 caused cell death independently of caspase-3 activity. Thus, cardioprotection by suppressing endogenous MAP4K4 was substantiated in hiPSC-CMs treated with H_2O_2, by four complementary assays: dissipation of mitochondrial membrane potential, DRAQ7 uptake, LDH release, and cell number.

Similarly, MAP4K4 knockdown by the most potent shRNAmir also resulted in protection from c_2-ceramide. Cardioprotection was evident by (i) a significant decrease in caspase-3 activation and by (iii) less cell death as measured by DRAQ7. In general, cell death under all c_2-ceramide-treated conditions was exacerbated as measured by DRAQ7 uptake from 16h to 36h, but remained relatively unchanged between the NSC and the most potent shRNAmir. Cardioprotection with the second potent shRNAmir (202781) was evident by (i) a significant decrease in the % of hiPSC-CMs with diminished of mitochondrial potential. Caspase-8 activity measured at both 16h and 36h remained relatively unchanged, suggesting either that (i) caspase-8 activation was not-important in the activation of caspase-3 and cell death induced by c_2-ceramide (no activation of the extrinsic pathway of apoptosis) or (ii) caspase-8 activation occurred at an earlier time than those measured (a likely explanation, since c_2-ceramide is a surrogate for TNFα).

To conclude, cardioprotection from c_2-ceramide by depleting MAP4K4 was revealed by: preservation of mitochondrial potential, preservation of membrane integrity and caspase-3 inhibition, compared to the NSC. However, c_2-ceramide caused mitochondrial network disintegration (or mitochondrial fission), identified by confocal images, implies that further work is required to delineate the mechanism of mitochondrial fragmentation pathways in hiPSC-CMs intersecting with MAP4K4's pro-apoptotic role. Furthermore, cardioprotection from H_2O_2 by suppressing endogenous MAP4K4 was substantiated in hiPSC-CMs, by dissipation of mitochondrial membrane potential, DRAQ7 uptake, LDH release, and cell number.

4.2. Mechanistic implications

4.2.1. H_2O_2 does not activate caspase-3 in hiPSC-CMs

Treatment of chick embryonic cardiomyocytes with H_2O_2 induced cell death in a time-dependent manner that was prevented by exogenous ARC expression. Cell death was associated with downregulation of caspase-3 RNA levels (Wu et al., 2013) and activation of caspase-3 (Chis et al., 2012). Doxorubicin, as an alternative source of ROS, led to cyt-c release and caspase-3 activation in cardiomyocytes by 3h of exposure (Wang et al., 2001). More importantly, caspase-3 activation is present in I/R and human failing hearts (Narula et al., 1999; Scheubel et al., 2002). However, hiPSC-CMs did not exhibit activation of caspase-3 in response to a various range of H_2O_2 in a time-dependent manner. To determine whether caspase-3 activation was a latter event we also tested for activation of its activity at 36h (Fig. S5) that remained unchanged, suggesting that, in this hiPSC-CMs system, caspase-3-dependent cell death by H_2O_2 is probably not the preferred mechanism of cell death in hiPSC-CMs, which can be resolved by treatment with a caspase-3 inhibitor. However, caspase-3 activation by the intrinsic pathway is the sequence of events of cyt-c release that binds together with proscaspase-9 to Apaf-1. So there is a requirement to eliminate inhibitory mechanisms (such as XIAP, c-IAPs, Smac/DIABLO, Omi/HtrA2, ARC, c-FLIP) for subsequent caspase-3 activation to complete the death circuit (see section 1.5.1). So, an alternative explanation is the mechanistic differences of the cellular inhibitors between hiPSC-CMs and rodent cardiomyocytes; a question that can be easily resolved by Western blotting. Indeed, hESC-CMs exhibited resistance in cell death compared to NRVCs, which was attributed to differences in the levels of caspase-3 activity. Differences in sensitivity to the death agonist was also dependent on the stage of differentiation (early 38d versus late 155d) (Mioulane et al., 2012).

As expected, and based on the absence of caspase-3 activation with H_2O_2 treatment, MAP4K4 knockdown under the same death agonist conditions resulted in increased survival with no changes in caspase-3 activity. The two explanations are that H_2O_2 activates cell death mechanisms that are independent of caspase-3-related cell death (i.e. apoptosis) and/or that MAP4K4 is not required for caspase-3-dependent cell death in hiPSC-CMs. To resolve the latter, kinase assays are required to determine MAP4K4 activation under H_2O_2, similar to the case of MAP4K4 activation in stimulated NRVCs with H_2O_2. Our results with H_2O_2, more likely, represent the conditions of I/R where cell death occurs predominantly by necrosis, where apoptosis or caspase-3 activation is of minor importance (Freude et al., 2000) and MAP4K4 depletion leads to activation of cell survival programs or inhibition of necrosis.

4.2.2. MAP4K4 knockdown in hiPSC-CMs is associated with caspase-8 activation in H_2O_2

Overexpression of a catalytically inactive MAP4K4 in NRVCs and knockdown of MAP4K4 under c_2-ceramide resulted in decreased caspase-3 and caspase-8 activities, suggesting a pro-death mediating role of MAP4K4 in both intrinsic and extrinsic cell death pathways. So, we anticipated that knockdown of MAP4K4 in hiPSC-CMs would lead to inhibition of caspase-8. Paradoxically, a significant increase in caspase-8 activation by H_2O_2 was observed in MAP4K4-depleted cells, compared to cells transduced with the control virus. Likewise, during the early optimization experiments we also observed a concentration- and time-dependent decrease in caspase-8 activity that was associated with an increase in LDH release in hiPSC-CMs treated with H_2O_2. So, is it likely that caspase-8 activation, upon MAP4K4 knockdown, is involved in cell survival?

Caspase-8 activation is most commonly associated with the extrinsic cell death pathway, yet like caspase-3, TAK1, and TNFα may have antithetical effects on cell death or survival depending on context. For example, loss of caspase-8 in skin or gut induced keratinocyte and enterocyte death, respectively, suggesting that caspase-8 is required for cell survival, at least in some settings (Weinlich et al., 2013). Indeed, caspase-8 has an essential role in protective immunity and caspase-8 deficiency in humans and mice abolishes activation of NFκB (Su et al., 2005). Caspase-8 activation induces recruitment of the IKK inhibitor into an adapter complex found in lymphatic tissue that eventually allows the nuclear translocation of NFκB, thus activation of cell survival pathways (Su et al., 2005). But, what is the evidence that caspase-8 activation is pro-survival in the heart? Conditional deletion of caspase-8 in the heart using an αMHC-Cre mouse line did not cause embryonic lethality and no differences in heart weight were observed (Dillon et al., 2012), suggesting a less important role in a cardiac setting. However, conditional caspase-8 activation in the adult myocardium resulted in low levels of cardiomyocyte cell death measured by DNA fragmentation, sufficient to cause dilated lethal cardiomyopathy. From these two studies, it is obvious that the role of extrinsic pathway of cell death is of distinct significance in the embryo and adult heart. This suggests a distinct requirement of caspase-8 in developing versus adult hearts, and since hiPSC-CMs exemplify an embryonic phenotype, this can be the reason for the unexpected phenotype.

Caspase-8, central to both TNFR complexes I and II (signallosomes), interacts with death domain TRADD and FADD proteins, and adaptor TRAF2, and is required to inhibit programmed necrosis by targeting RIP kinase for C-terminal cleavage (Chan et al., 2003). Proteolytic activity of caspase-8, however, is essential for promoting caspase-3 activation and apoptosis via t-Bid cleavage (Gross et al., 1999). Independent of its proteolytic activity, caspase-8 potently activates NFκB as measured by an NFκB luciferase reporter, essential

for cell survival (Hu et al., 2000). Thus, caspase-8 is essential for obstructing necrosis and mediating survival via NFκB. Decrease in caspase-8 activity associated with increased LDH release in the presence of H_2O_2 (Fig. 29) and simultaneous caspase-8 activation in MAP4K4-depleted hiPSC-CMs that exhibited resistance to H_2O_2-induced death advocates an involvement of caspase-8 in activating survival mechanisms – and whether these are via NFκB signalling remains to be determined. This question can be easily addressed by a high-content antibody approach screening for inactivating phosphorylation of IκBs and phosphorylated NFκB (p65), complemented with the application of a Western blot. To clarify the dependence of caspase-8 in this system, MAP4K4-depleted cells would be cultured in the presence or absence of a caspase-8-specific inhibitor (Z-IETD-FMK or CrmA) or by overexpression of miR-874 that was substantially upregulated in response to H_2O_2 leading to caspase-8 suppression (Wang et al., 2013a), or by an shRNAmir against caspase-8.

Caspase-8 activation is also held in check by c-FLIP inhibitor, which interacts with caspase-8 and FADD at the TNF receptors, and with caspase-3 via its caspase-like domain (Shu et al., 1997). Interestingly, it was reported that high levels of c-$FLIP_L$ inhibit caspase-8 and TNFR-mediated cell death, whereas low levels of c-$FLIP_L$ promote activation of caspase-8 (Chang et al., 2002). Cardiac-restricted overexpression of Bcl-2 in transgenic mice with a cardiac-specific secretable TNF partially attenuated apoptosis (Haudek et al., 2007). The rescue phenotype was associated with changes in the intrinsic pathway, such as c-FLIP degradation, cleavage of Bid to t-Bid and caspase-8 activation (Haudek et al., 2007). Bcl-2-dependent suppression of cell death in cardiomyocytes was reported to mediate activation of NFκB via degradation of IKKα (de Moissac et al., 1998). Our rescue phenotype with MAP4K4 depletion partly agrees with caspase-8 activation as in Bcl-2-transgenic mice, maybe representing a similar mechanism of cell death rescue. To test whether caspase-8 activation is linked to low levels of c-$FLIP_L$ or t-Bid cleavage in hiPSC-CMs, cell lysate collected from NSC- and MAP4K4-depleted cardiomyocytes in the presence and absence of H_2O_2 would be analysed by WB. Similar results would be acquired by co-transduction experiments in hiPSC-CMs of various amounts of the two c-FLIP isoforms screened against caspase-8.

Finally, there is no published mechanism that describes the opposing functions of MAP4K4 and NFκB in cardiac muscle, but TAK1 might be the missing link. In the myocardium, TAK1 has a pro-apoptotic function and is required by MAP4K4 to mediate cell death via JNK, independent of its p38-activating function (Zhang et al., 2000). Thus, under agonist-treated conditions, it is likely that MAP4K4 inhibition in hiPSC-CMs by shRNAmirs fails to activate TAK1 and subsequently JNK-mediated cell death. At the same time, increase in caspase-8 activity might lead directly to NFκB activation via direct binding on its promoter (Hu et al., 2000) or via recruitment of TAK1 and IKK complexes to the TNFRI, essential for NFκB activation (Devin et al., 2001; Ea et al., 2006). Thus, it is possible that there are two

TAK1 “functional pools”: one where TAK1 is bound and activated by MAP4K4 to mediate cell death, while a second one recruited onto the TNF receptor mediating cell survival. So one important unaddressed question is whether MAP4K4 directly binds and phosphorylates TAK1. Interestingly, a recent report supports that TAK1 switches from apoptosis to necrosis upon TNF stimulation. Prolonged TAK1 activation induces RIP3 kinase phosphorylation and necrosis, whereas ablation caused caspase-dependent apoptosis (Morioka et al., 2014).

4.2.3. c_2-ceramide activates caspase-3 in hiPSC-CMs

Various agents/stimuli (e.g. chemotherapy, TNFα, radiation) were shown to increase the level of intracellular ceramides, thereby affecting cell growth, differentiation and cell death (Morales et al., 2007) either via downstream kinases (i.e. p38, JNK, MAP4K4 and PKCδ) or affecting the mitochondria directly (Kong et al., 2005; Shirakabe et al., 1997; Sumitomo et al., 2002; Verheij et al., 1996). In the heart, ceramide accumulation has been demonstrated in various I/R models (Argaud et al., 2004; Cordis et al., 1998) and implicated as an apoptosis mediator in cell culture associated with activation of both caspase-3 and caspase-8 (Bielawska et al., 1997; Wang et al., 2000). Other effects of c_2-ceramide on adult rat ventricular cardiomyocytes, when electrically paced, are calcium defects (Relling et al., 2003) and attenuation of high glucose-induced mechanical dysfunctions, (Colligan et al., 2002). MAP4K4 was also activated in response to c_2-ceramide in NRVCs that lead to JNK activation via TAK1 (Xie et al., 2007).

Indeed, treatment of hiPSC-CMs with 20 μ M of c_2-ceramide at 16h exhibited significant increase in caspase-3 activity associated with approx. 4-fold increase in LDH release compared to VC. In addition, MAP4K4 knockdown was associated with significant decrease in caspase-3 activity under c_2-ceramide conditions. These results suggest that c_2-ceramide promotes caspase-3-dependent cell death mediated by MAP4K4, but kinase assays are required to validate MAP4K4 activation under c_2-ceramide, similar to the case of MAP4K4 activation in ceramide-stimulated NRVCs. Our results are partly in agreement with literature where maximal cell loss was reached at approx. 16h after c_2-ceramide treatment (Wang et al., 2000). Furthermore, caspase-3 and caspase-8 inhibition in c_2-ceramide-treated NRVCs using substrate-based caspase inhibitors exhibited increased cell survival, suggesting both intrinsic and extrinsic pathways are involved (Wang et al., 2000). HiPSC-CMs, however, did not exhibit caspase-8 activation with c_2-ceramide treatment, suggesting either that caspase-8 activation occurs at an earlier time (and needs to be tested) or that is not required in c_2-ceramide-induced cell death in these cells. Interestingly, there are effector differences between c_2- and c_6-ceramide species in chronic myelogenous leukaemia cells, in which only c_6-ceramide induces cell death via cleavage of pro-caspase-8 (Nica et al., 2008). Likewise, c_2-ceramide in other cell lines did not cleave caspase-8 (Cuvillier et al., 1998). Thus, two alternative explanations to the lack of caspase-8 are (i) the cell context differences between NRVCs and hiPSC-CMs and (ii) the ceramide species-dependent differences. Thus, treatment of hiPSC-CMs with c_6-ceramide ought to be carried out.

4.2.4. MAP4K4 and the mitochondrial death pathway

The mode of action of H_2O_2 in MEFs and hepatocytes, the most commonly used model to study H_2O_2-mediated cell death, involves the loss of mitochondrial potential and

requires CypD (Baines et al., 2005). Knockdown of CypD led to the lack of mitochondrial potential dissipation and a consequently a decrease in TUNEL-positive cells (Baines et al., 2005). Similarly, H_2O_2 treatment of hiPSC-CMs with 500µM at 24h resulted in a 15% increase of cells exhibiting dissipation of mitochondrial potential. MAP4K4 depletion (with all three shRNAmirs) led to 2-fold decrease in the percentage of MAP4K4-depleted ($EGFP^+$) cardiomyocytes (RFP^+) exhibiting diminished mitochondrial potential (MP^-) ($RFP^+EGFP^+MP^-$) compared to the non-silencing control (NSC). Concurrently, an increase in RFP^+EGFP^+ cells was observed with two most potent shRNAmirs against MAP4K4 compared to the NSC. However, since approx. 60% of hiPSC-CMs exhibited diminished mitochondrial potential (Fig. 40) and only 15% of cells at 24h, it is likely that the 15% represents a subpopulation of cardiomyocytes that were more resistant to cell death. This is not of surprise since the cultures of hiPSC-CMs are mixed populations of atrial, ventricular and nodal cardiomyocytes. Subsequently, a time of 16h is more ideal for screening mitochondrial potential with H_2O_2. Nonetheless, MAP4K4 knockdown led to a reduction of hiPSC-CMs with diminished mitochondrial potential, suggesting an involvement of MAP4K4 via the mitochondrial pathway.

The effect of c_2-ceramide on mitochondrial potential in hiPSC-CMs was more puzzling (data not shown), as approx. 15% of cells exhibited increased intensity of the potentiometric dye and a typical pattern of mitochondria fragmentation in the presence c_2-ceramide. Mitochondrial fragmentation (or fission) has been implicated in cell death of neonatal cardiomyocytes, where exposure to c_2-ceramide at 20-40µM for 6h resulted in an increase in the percentage of cells with mitochondrial fragmentation (Parra et al., 2007). Central to the fusion of outer and inner mitochondrial membranes are mechano-enzymes such as mitofusin-1 and -2 (Mfn-1 and Mfn-2) (Papanicolaou et al., 2011; 2012a; 2012b) and optic atrophy 1 (Opa1). Cytoplasmic protein dynamin-related protein 1 (Drp1) translocates to the mitochondria to interact with fission protein 1 (Fis1) resulting in fission (mitochondrial fragmentation) (Lee et al., 2011). Treatment of neonatal cardiomyocytes with c_2-ceramide resulted in increased mitochondrial protein levels of Drp-1 and Fis1 (Parra et al., 2007) and expression of a dominant-negative Drp-1 mutant - although not in cardiomyocytes - resulted in inhibition of this phenotype (Brooks et al., 2007). Thus, we anticipate that Drp-1 depletion in hiPSC-CMs will likely inhibit mitochondrial fragmentation. Something of particular interest is whether mitochondrial fragmentation is secondary to loss of mitochondrial potential and caspase-3 activation. A simple way to address this two-tier question is to measure mitochondrial potential at earlier times and use a caspase-3 inhibitor peptide to test whether the mitochondrial fragmentation phenotype will be inhibited. A similar question was addressed by Brooks *et al.*, where caspase-3 peptide inhibitors did not prevent mitochondrial

fragmentation and cyt-c release, suggesting that this process is not secondary to caspase-3 activation (Brooks et al., 2007).

MAP4K4 depletion with the most potent shRNAmir led to decrease in caspase-3 activation and preservation of the cell membrane integrity measured by DRAQ7 and LDH, and had no effect on mitochondrial potential (no decrease in MP^- cells) at 16h. However, MAP4K4 depletion with the other two shRNAmirs resulted in increased cell death based on DRAQ7 and LDH, but a significant decrease in MP^- cells at 16h. These results partly reflect the potency differences of the shRNAmir constructs, but also the technical limitations (due to overlapping emission spectra of the dyes) to resolve the proportion of the $DRAQ7^+MP^-$ cardiomyocytes for the identification, or whether different subpopulations of hiPSC-CMs have distinct mechanisms of cell death (i.e. mitochondrial fragmentation or diminished mitochondrial potential). Thus, further work is required to understand the order of ceramide-induced mitochondrial fission and mitochondrial potential depolarization, to further address the involvement of MAP4K4 in these processes.

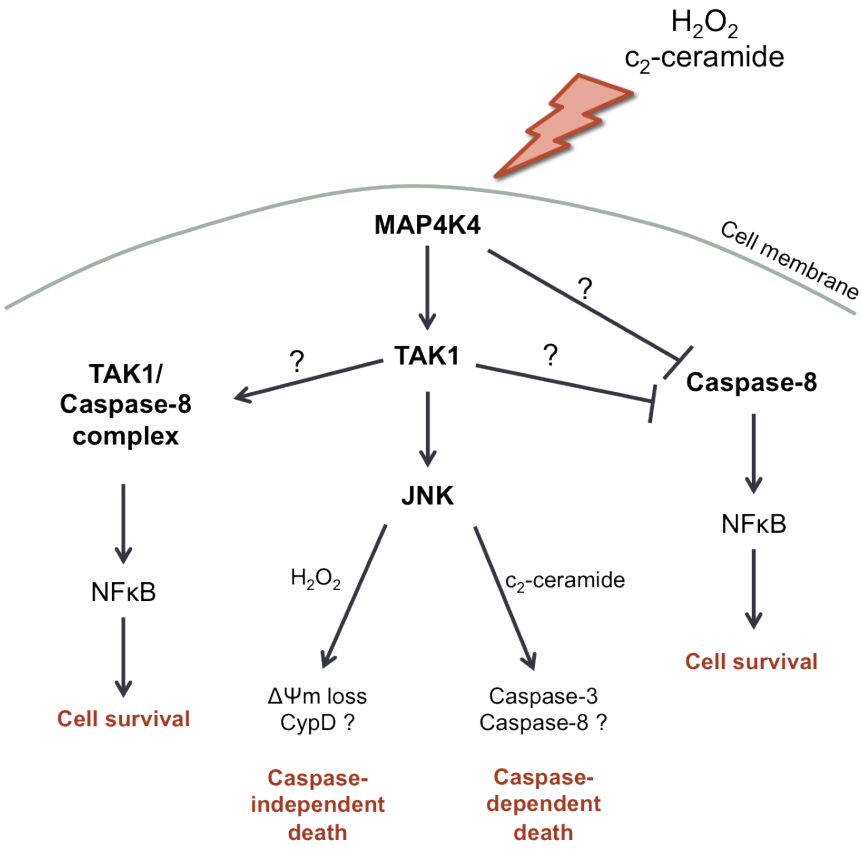


Figure 54: **MAP4K4 signalling axis cartoon with H_2O_2 and c_2-ceramide in hiPSC-CMs.** MAP4K4 depletion in hiPSC-CMs treated with H_2O_2 led to inhibition of cell death via preservation of mitochondrial potential and cell membrane integrity. Activation of caspase-8 might be linked to NFκB survival mechanisms. MAP4K4 might be activated with H_2O_2 to prevent the NFkB pathway or activated with c_2-ceramide to promote caspase-3-dependent cell death.

4.3. Technical considerations

4.3.1. Dissecting cell death in hiPSC-CMs: considerations for platform refinement

The wider aim of the study was to deploy a kinome-wide shRNA-based high-content screen (HCS) in hiPSC-CMs, enabling us to pinpoint regulators of human cardiac cell death and survival. MAP4K4 was knocked-down as a postulated upstream mediator of cardiac apoptosis and was used as a primary platform for cell death assay development. As this was a proof-of-concept study, it was of outmost importance to include a cardiac marker (Myh6 – RFP) and to track the transduced cells (shRNAmir-EGFP). DRAQ7 and Mitoview^{TM} dyes were selected on the basis of their emission spectra, as no overlap with the other fluorophores of the system was present. In addition, DRAQ7 is a cell-impermeable dye of live cells that binds onto DNA in cells with compromised membranes, and similar to the LDH assay, it does not discriminate on the mode of cell death (i.e. apoptosis, necrosis). Similarly, LDH activity was measured in the medium. In addition, intrinsic and extrinsic pathways of cell death were monitored as caspase-3 and caspase-8 activities, respectively, while monitoring mitochondrial membrane depolarization with a potentiometric dye.

However, in the current studies, the single use of either DRAQ7 or Mitoview marker for dissecting cell death can be considered a technical limitation, as we could not extrapolate whether cardiomyocytes with diminished mitochondrial potential were positive for DRAQ7 and *vice versa*. More specifically to the c_2-ceramide study, the LDH assay did not faithfully corroborate the results of the DRAQ7, explaining the differences in sensitivity between whole-well-based and high-content assays. Thus, minute differences in cell death identified by high-content imaging could not be inferred by the activity of LDH released in the medium. This argument can be extrapolated on the caspase-3/8 assays, where an average value was acquired across a mixed population of cells. Alternatively, one might consider the microscopy-based NucView^{TM} caspase-3 substrate if it or an equivalent is made available in far-red, as it currently overlaps with the shRNAmir-EGFP in our present high-throughput *Cellomics* instrumentation. While a caspase-3-YFP sensor (Fujita et al., 2008) can be deconvoluted more readily from EGFP, using spectral unmixing techniques, that would require the transfer of the sensor. A refinement of the caspase-3-YFP sensor is its placement under a cardiac-specific promoter, thus allowing the exclusive examination of caspase-3 activity in cardiomyocytes. For the latter approach, it would be feasible to use hiPSC-CMs without the use of RFP assuming the cultures are as highly pure for cardiomyocytes as the cell studied here, therefore enabling the feasibility for additional dual staining under the red and far-red channel. Further refinement for pathway dissection would be to assay for apoptogen release from the mitochondria, such as cyt-c, apoptosis inducing factor (AIF) and

endonuclease G (EndoG), and other components of the cell death pathways with an antibody-based approach (i.e. t-Bid cleavage).

Unfortunately, DRAQ7 uptake and LDH release was not measured in MAP4K4-depleted NRVCs (Xie et al., 2007), thus hampering direct comparisons between the human and murine models. Nonetheless, our results depict differences in caspase-3 activation with two difference agonists (H_2O_2 and c_2-ceramide) in hiPSC-CMs and provide a platform or disease model for dissecting caspase-3-dependent and –independent cell death, and mitochondrial dynamics.

4.3.2. Potency and specificity of RNA interference against MAP4K4

For knockdown of MAP4K4 we have chosen shRNAmir technology, which is an shRNA sequence embedded in the context of a miRNA loop. In general, shRNAs, opposed to siRNAs, are transcribed in the nucleus where they are processed as pre-shRNAs, transported to the cytoplasm via exportin 5-GTPase and are loaded into the RISC complex. Transcription of shRNAs can be regulated by either RNA polymerase (pol) II or III promoters (Rao et al., 2009). The main advantage of the pGIPZ shRNAmir technology is the transcription of the shRNAmir by an RNA pol II promoter, which unlike the RNA pol III promoter, contains regulatory elements desirable for spatial and temporal control (Giering et al., 2008). Thus, it circumvents the issue of high levels of expression by RNA pol III promoters that, in some cases, can saturate natural endogenous miRNAs (Yi et al., 2005) and can cause tissue damage and cytotoxicity (Giering et al., 2008). Expression of the primary transcript by an RNA pol II promoter contains a hairpin-like stem-loop structure and allows precise processing into shRNAs with a 3'-overhang of 2 nucleotides, which enters the RISC complexed with Argonaute (Ago1-4) proteins. Ago-2 is the only protein with an endonuclease activity that releases the passenger strand after cleavage for mRNA degradation (Rao et al., 2009). Although details for this mechanism are largely unknown, miRNA strands loaded with Ago proteins that lack the endonuclease activity act by pairing to partially complementary sequences to promote translational repression by inhibiting translational initiation (Pillai et al., 2005). Thus, the choice of shRNAmir more closely mimics the bi-functional transcriptional and translational inhibition of genes by microRNAs. In addition, the flexibility of well-characterised pol II promoters permits expression of shRNAmirs in a heterogeneous cell population, or *in vivo*, under lineage-specific or drug-inducible control.

As a first step, we carried out quantitative PCR in readily manipulated HEK293 cells and confirmed more than a 70% decrease in exogenous MAP4K4 RNA. Using the shRNAmirs chosen, at least a 50% reduction of endogenous MAP4K4 resulted in hiPSC-

CMs. No endogenous RNA decrease of MAP4K4's structural relatives, MINK and TNIK was observed in hiPSC-CMs. However, we found differences between the knockdown efficacies of the three shRNAmirs we used against MAP4K4. The least potent shRNAmir (201856) exhibited a delay in exogenous MAP4K4 protein knockdown at 24h compared to the level of protein inhibition of the most potent other shRNAmirs (68219, 202781). Interestingly, cell lysate isolated from FACS-purified MAP4K4-depleted HEK293 cells showed upregulation of MAP4K4 at 96h with the least potent shRNAmir compared to the other two, suggesting a limited knockdown window for this construct, explaining the lack of RNA knockdown and lack of cell death inhibition with H_2O_2 or c_2-ceramide.

Since shRNAmirs recognise and bind either coding regions or 3'UTR sequences, it is likely that 68219 shRNAmir is more potent in affecting the transcript stability or downregulation of RNA and promote translational inhibition, by partial sequence homology (Fig. S4). DNA sequencing of MAP4K4 gene and its upstream sequences can be used to determine the level of homology with the shRNAmirs in hiPSC-CMs. Currently no data are available on the exact MAP4K4 isoforms in hiPSC-CMs, and possible discrepancies in the level of mismatch based on alternative splicing could explain the potency of some shRNAmirs over others. One way to overcome this is by transducing iPSC-CMs with the mixture of shRNAmirs, as this may have a cooperative effect.

4.3.3. Suitability of the innocuous vector control

Some unintended off-target effects with mitochondrial potential and DRAQ7 uptake were observed with the NSC negative control compared to untransduced cells, though its sequence was not homologous to the human genome when searched in *NCBI* and *Ensembl* databases. Specific off-target effects are mediated by partial sequence complementarity to mRNAs that can include toxicity effects related to the shRNAmir sequence itself (Rao et al., 2009). One can argue that a better, more flexible negative control than this proprietary commercial reagent would be the knockdown of a known gene that is non-essential or not present in the cardiac system, such as an shRNAmir against a endoderm-specific gene like PDX1, or a heterologous gene with no counterpart in the human genome like firefly luciferase. To circumvent the false-positives attributable to irreducible off-target effects, it is therefore important to always compare the knockdown of a test gene to equivalently treated cells with a non-silencing construct, not to the untreated ones.

4.3.4. Fidelity of hiPSC-CMs: evidence for heterogeneity and immaturity

The expression gene profile of hiPSC-CMs from CDI was investigated throughout a fine differentiation timescale. The highest purity of cardiomyocytes (monomeric RFP^+ expressed from *Myh6* promoter) was achieved at d28 after antibiotic selection started on d14 (RFP^+ fused with Basticidin resistance gene). The gene expression profile after antibiotic selection from d20 to d120 revealed early mesodermal and cardiomyocyte-specific genes, some of which were NKX2.5, the myosin light and heavy chains (*MYH6, MYH7, MYL2*, and *MYL7*) and cardiac troponins (*TNNI3, TNNT2* and *TNNC1*) (Babiarz et al., 2012).

However, we found that hiPSC-CMs co-expressed myofilament MLC2v and MLC2a proteins, which discriminate between mature atrial and ventricular cells, but are co-expressed during early cardiac organogenesis, at the linear heart tube stage (E8.25-8.5) (Fijnvandraat and van Ginneken, 2003). In addition, by deconvolution microscopy, the cells demonstrate a striation pattern that is less highly ordered than the cross-striations found in adult rod-shaped cardiomyocytes. These observations likely reflect differences in chamber specification or maturity. Indeed, there are multiple literature reports on the pluripotent-derived cardiomyocytes (from both ESCs and iPSCs) resembling immature human embryonic cardiomyocytes (Willems et al., 2009) by multiple criteria. Cardiomyocytes from these sources exhibit poor organized contractile machinery and myofibrillar structure (Babiarz et al., 2012; Lundy et al., 2013) associated with decreased contraction magnitude (Kita-Matsuo et al., 2009; Lundy et al., 2013) compared to adult cardiomyocytes. Their functional properties in contractility kinetics, which are similar to the cardiomyocytes in the developing heart, are reflected as smaller cytosolic Ca^{2+} transient amplitudes and reduced Ca^{2+} content of their sarcoplasmic reticulum (SR) (Liu et al., 2009a; Lundy et al., 2013), most likely attributed to the differential expression profiles of Ca^{2+}-handling and regulatory proteins, such as calsequestrin (CASQ) (Liu et al., 2009a) and the lack of transverse tubules (T-tubules) membrane invaginations along the longitudinal axis of Z-line regions required for rapid electrical excitation (Lieu et al., 2009).

Currently huge interest is drawn towards modulation of maturation of pluripotent cell-derived cardiomyocytes (Yang et al., 2014). Two studies have shown that prolonged cell culture of both human ESC- and iPSC-CMs (80-120 days) elicits a more adult-like phenotype, based on (i) RNA upregulation of CASQ2, an abundant Ca^{2+}-handling protein in the SR (Babiarz et al., 2012) absent in pluripotent cell-derived cardiomyocytes (Dolnikov et al., 2006; Liu et al., 2009a), and (ii) increased density of aligned myofibrils and Z-disk registration depicted by immunocytostaining (Lundy et al., 2013). Indeed, overexpression of CASQ facilitated increased Ca^{2+} SR load, amplitude and kinetics (Liu et al., 2009a). Furthermore, various coating substrates and scaffolds attempt to recapitulate the enhanced stiffness of the adult myocardium compared to the embryonic or neonatal stages. Substrates

with extracellular stiffness of 10kPa significantly enhances the maturation of NRVCs reflected by larger calcium transients, increased SERCA2a expression, greater mechanical force and aligned sarcomeres (Hazeltine et al., 2012; Jacot et al., 2008; Rao et al., 2013). Other maturation efforts involve treatment with biochemical cues, such as of thyroid hormone that increases SERCA2a, MLC2v and αMHC associated with adult-like Ca^{2+} properties (Lee et al., 2010), and 3D culture in micro-fabricated collagen-coated wells subjected to electrical stimulation that led to increased myofibril organization and enhanced electrophysiological and calcium handling properties (Nunes et al., 2013). Even if not essential to resolve the functional requirement for MAP4K4, augmenting the maturity of the human cardiomyocytes tested should, in the long run, enhance the predictive power of the model, especially as applied to high-throughput screening for target validation or to assessing the in-cell activity of potential pharmacological inhibitors.

Another important aspect highlighting the fidelity of the system, is the technology used in deriving iPSC. The use of DNA-integrating viruses for the expression of the pluripotency markers cocktail (including the current system) is considered as the gold standard method for deriving iPSCs. However, one caveat of induced pluripotency by such premature method is the related processes it shares with oncogenic transformation (Riggs et al., 2013), justified by differences of epigenetic and transcriptional profiles between iPSC and ESCs that can lead to incomplete epigenetic reprogramming (Bilic and Izpisua Belmonte, 2012). This can also be seen by the fact that iPSCs retain an expression pattern of the somatic cells from which they are derived (i.e. skin fibroblasts in our system) (somatic cell-of-origin footprint), and fail to show similar levels of pluripotency genes to ESCs, akin to epigenetic memory (Bilic and Izpisua Belmonte, 2012). So the parallel focus should not only be the derivation of human-relevant cardiomyocytes (i.e. in terms of maturity and source), but also on the use of non-DNA-integrating technologies that can minimise genomic aberrations associated in the initial processes of iPSC development (Cheng et al., 2012; Li et al., 2009a; Lian et al., 2012), to avoid affecting genes whose expression would be relevant in the differentiation process and the development of downstream somatic derivatives (i.e. iPSC-derived cardiomyocytes). Recent work also proposes that either (i) pre-existing background mutations of rare parental cells (i.e. skin fibroblasts) can mark their reprogramming fitness or (ii) parental cells with a unique pre-existing genomic background in addition to background mutations captured by DNA-integrating vectors, can lead to iPSC genetic variants (Young et al., 2012). Thus two likely reasons for the resulting embryonic phenotype of iPSC-CMs can be (i) the DNA-integrating viral approach with possible effect on their immature cardiomyocyte phenotype and (ii) the background mutations in parental cells or the ones acquired during the reprogramming process. Thus, it is of outmost priority to understand the

mechanism of reprogramming somatic cells to iPSC and enhance the mutation-free iPSCs in an effortless and efficient way (Zhou et al., 2009).

In the short run, despite biological differences between NRVCs, adult ventricular cardiomyocytes and hiPSC-CMs and the heterogeneity of hiPSC-CMs as a mixed cardiomyocyte population, highly useful work can be carried out to determine more comprehensively the requirement for MAP4K4 signalling in hiPSC-CMs (e.g., in caspase-dependent necrosis and apoptosis), involvement of the TAK1-JNK axis versus other downstream signalling proteins, and other details of the "wiring diagram" for human cardiac muscle cell death. So, it will be extremely relevant in the future to carry out a similar set of experiments on pure hiPSC-derived ventricular-like cardiomyocytes (Karakikes et al., 2014) that might represent more closely the NRVCs, and even more interesting in matured adult-like pluripotent stem cell-derived cardiomyocytes. Differences between human ESC- and iPSC-derived cardiomyocytes in their beat rate and spontaneous activity (Mandel et al., 2012) and in hypertrophic signalling (Foldes et al., 2013), also allows the safe assumption of possible differences in cell death mechanisms (Mioulane et al., 2012), thus questioning whether MAP4K4 is a high-priority death mediator in one cell type over the other.

4.4. Further work

4.4.1. Unaddressed questions about the MAP4K4/TAK1 signalling axis

MAP4K4 knockdown in hiPSC-CMs is in agreement with previous results of inhibition of cell death, via microscopy-based D7 assay, LDH release and dissipation of mitochondrial potential in H_2O_2, thus we proved that MAP4K4 is pro-apoptotic in this system. However, from this study it is clear from the pattern of caspase-3/8 activation in response of H_2O_2 that different signalling pathways operate between hiPSC-CMs and NRVCs, and unaddressed questions remain about the MAP4K4 signalling axis in both cell types.

In NRVCs, co-infection of MAP4K4 with a dominant-negative TAK1 (K63W) mutant blocked the activation of JNK and subsequently suppressed MAP4K4-induced apoptosis, suggesting that TAK1 is essential for the death pathway (Xie et al., 2007). Gain-of-function experiments with catalytically active versus inactive MAP4K4 and TAK1 vectors, shRNA against TAK1 and JNK, and endogenous kinase assays in response to both H_2O_2 and c_2-ceramide would add confidence in the role of MAP4K4 and TAK1 in cell death in hiPSC-CMs, and in JNK as the responsible terminal MAPK. An experiment of even higher priority to prove stringent specificity of the shRNAmirs against MAP4K4 would be rescuing the knockdown of the protein with an RNAi-resistant expression vector.

However, one important piece of the puzzle is whether MAP4K4 directly binds and phosphorylates TAK1. To determine binding, we would use immunoprecipitation of MAP4K4 and detection by an anti-TAK1 antibody on a Western blot and *vice versa* to prove that proteins are found in a complex. The same would be carried out in the presence of the death agonist to check whether the association of the protein is enhanced. For the second part of the question, that is to test phosphorylation of TAK1 by MAP4K4, one needs to prove that MAP4K4 is activated by the agonist cues (i.e. H_2O_2, c_2-ceramide) or by other signals that activate this kinase in rodent cardiomyocytes (TNFα, doxorubicin, Gq, biomechanical stress, ischemia/reperfusion). MAP4K4 can be immunoprecipitated and activity measured by immune complex assay using myelin basic protein (MBP) as the kinase substrate. Then, Myc-tagged catalytically inactive TAK1 would be transduced into hiPSC-CMs, purified and used as a kinase substrate alternative to MBP, for immunoprecipitated MAP4K4 under untreated and agonist-treated conditions.

Currently these studies are limited by the large amounts of total protein required - necessitating high numbers of the costly human stem cell derivative. However, this technical difficulty might be overcome by expressing exogenous MAP4K4-Flag in hiPSC-CMs by virus-mediated gene transfer, therefore reducing the number of cells required to yield sufficient MAP4K4 protein. Surrogate methods that require reduced cell numbers are cell-based ELISA assays that utilize phospho-specific antibodies directly on the cells of interest for screening

the effects of various activators (i.e. death agonists) and inhibitors (i.e. shRNAmirs) on the activity of the protein of interest. Notably, activation-specific phospho-epitope antibodies have been reported for TAK1, e.g., for phosphorylation of the invariant activation loop residue Thr^{187} (Singhirunnusorn et al., 2005). In parallel with studies of human cardiomyocytes, results from a cardiac-specific MAP4K4 loss-of-function in adult mice (using Cre/lox technology or adeno-associated viral delivery of shRNAmirs) would provide conclusive functional evidence on the role of MAP4K4 in I/R and post-ischaemic heart failure.

Importantly, the effect of MAP4K4 in NRVCs was suppressed, even though incompletely, by over-expressing Bcl-2: an experiment that would add confidence in the pro-apoptotic role of MAP4K4 in hiPSC-CMs. If indeed mitochondrial-dependent cell death is important in the response to H_2O_2 (as this dissertation suggests), overexpression of Bcl-2 will exhibit a protective (rescue) phenotype. Similarly, caspase-3 activation in response to c_2-ceramide would be inhibited by overexpression of Bcl-2. A necrotic mechanism for the collapse of mitochondrial potential ($\Delta\Psi_m$), independent of caspase signalling, is mPTP opening, whose inhibition by several mPTP inhibitors (e.g. cyclosporine A [CsA]) or genetic deletion of CypD salvages the myocardium from cell death (Gustafsson and Gottlieb, 2008) and results in resistance to mPTP opening in response oxidative stress (Baines, 2007; Baines et al., 2005; Nakagawa et al., 2005) respectively. Thus, CsA treatment of hiPSC-CMs can be used to determine the proportion of cells undergoing caspase-3-independent/mitochondria-dependent pathway.

With regards to pathway dissection, and as mentioned earlier it will be interesting to carry out a fine-grained time course for caspase-8 activation with c_2-ceramide, as this is likely to be an earlier event. Moreover, shRNAmirs or peptide inhibitors against caspase-8- and caspase-3 can be used to investigate the requirement for caspase-dependent and –independent cell death. Furthermore, we are unaware of the requirement of cell death machinery in hiPSC-CMs, such as the role of RIP1/RIP3, c-IAP1/2, XIAP and ARC in relation to MAP4K4 signalling. To deconvolute their role in the MAP4K4 cascade, one might think to carry out a small-scale high-throughput screen with shRNAmirs against major cell death regulators in the presence of H_2O_2 and c_2-ceramide conditions described here. To conclude, the conditions of cell death following lentiviral delivery of shRNAmirs against MAP4K4, and the phenotypic assays developed for this system can be used in the future for the identification of other pro-apoptotic or pro-survival kinases in hiPSC-CMs via a high-content high-throughput screen.

4.4.2. Pharmacological inhibitors of MAP4K4 or RNAi as a therapeutic strategy

Eventually, the pharmaceutical industry could be interested in inhibiting a clinically relevant and tractable kinase's biological activity. In our lab, to address the therapeutic potential of MAP4K4 as a potential druggable target, we screened for inhibition of the recombinant human MAP4K4 kinase domain against an in-house library of 2000 small molecules. Four out of eight hits with a pIC50>5 were further analyzed by pharmacophore modelling. Kinases with similar charge distribution were tested for inhibition of recombinant MAP4K4 and, by mass spectroscopy, for inhibition of ATP binding to the kinome in human cell lysates (Fiedler et al., 2014). At the time our screen was in progress, two independent studies reported small molecules that target MAP4K4, which inhibit migration, adhesion, invasion and transformation of tumour cells (Gallud et al., 2014; Hampson et al., 2009). Relative to other MAP4K4 inhibitors (Guimarães et al., 2011), our in-house hits exhibited greater specificity and reduced cardiomyocyte toxicity (Fiedler et al., 2014). Currently, we are investigating the cardioprotective effect of these drugs in hiPSC-CMs under c_2-ceramide or H_2O_2 conditions. As the role of TNIK and MINK in the heart remains unknown and it will be interesting to see whether inhibition of all 3 kinases with the drugs (that cannot distinguish between MAP4K4 and these relatives as the shRNAmirs do) can have an additive effect on rescuing cell death.

While pharmacological inhibition of cardiac muscle cell death to salvage jeopardized myocardium is a rational strategy for the 21st century, whose lack of success until now may be due to poorly defined and justified targets, RNAi may offer a future therapeutic promise. Recent findings highlight the possible therapeutic value of siRNAs or miRNAs in various diseases, such as cancer, ocular diseases, Marfan's syndrome and cardiovascular diseases (Grinberg, 2008). Although various complex barriers (such as specificity, delivery to the correct tissue, durability and stability of RNAi, and safety due to immunomodulatory interferon responses) tempered the early excitement for clinical applications, it has opened windows for improvement (reviewed in (Davidson and McCray, 2011)). In fact, miRNAs regulate cardiac development and excitability (Yang et al., 2008a), cardiomyocyte proliferation (Eulalio et al., 2012), and apoptosis (Cheng et al., 2009; Wang et al., 2013a). Recently, RNAi was used in a randomized phase I clinical trial to exhibit safety and efficacy against proprotein convertase subtilisin/kexin type 9 (PCSK9) that bind and target LDL receptor for degradation. Loss-of-function mutations of PCSK9 resulted in reduced cholesterol in the plasma. Treatment with the highest concentration resulted in 70% reduction in plasma LDL with similar proportion of treatment-adverse events between treated and placebo groups (Fitzgerald et al., 2014). In other cases, siRNA is not used as a stand-alone strategy, but adjuvant to chemotherapy, for the latter to enhance its effects (Xu et al.,

2013). Consequently, the use of RNAi and small molecules does not necessarily exclude each other, but can serve as a combinatorial strategy.

4.4.3. Downstream effectors of MAP4K4-dependent signaling

Downstream effectors of MAP4K4 have been described in various disease models. MAP4K4 is characterized as a suppressor of skeletal muscle differentiation independent of the canonical MAPKs (p38, JNK and ERK1/2) (Wang et al., 2013b). Silencing of MAP4K4 in C2C12 myoblasts led to increased levels of myogenic factor 5 (Myf-5) protein at early stage of myogenic differentiation and double knockdowns of MAP4K4 and Myf-5 lead to impaired myogenic differentiation (Wang et al., 2013b). In addition, TNFα treatment of differentiated human skeletal myotubes completely blocked glucose uptake after insulin stimulation, an effect that was prevented by MAP4K4 silencing, suggesting that MAP4K4 is a mediator of insulin resistance that can be prevented by MAP4K4 inhibition (Bouzakri and Zierath, 2007). Downstream targets of MAP4K4 in this system were Akt, Akt substrate 160 (AS160) and insulin receptor substrate-1 (IRS-1) (Bouzakri and Zierath, 2007; Bouzakri et al., 2009). A similar attenuation effect on glucose uptake by MAP4K4 was evident in adipocytes, via inhibition of PPARγ expression (Puri et al., 2008). MAP4K4 also suppressed expression of other adipogenic transcription factors such as C/EBPα, C/EBPβ, and GLUT4. (Puri et al., 2008). MAP4K4 as a negative regulator of glucose uptake can explain the reduced glucose-induced cell death (or cytotoxicity) in MAP4K4-depleted hiPSC-CMs compared to the NSC in high glucose-containing medium in the presence of H_2O_2.

The most well known downstream target of MAP4K4 in the heart is TAK1/JNK from evidence of a dominant negative TAK1 mutant – although direct binding and phosphorylation by MAP4K4 awaits confirmation. Since MAP4K4 is a pro-apoptotic kinase in rodent and human cardiomyocytes, possible other downstream targets can be pro-apoptotic proteins that mediate apoptosis and necrosis. Gene expression analysis of MAP4K4-depleted cells can be one way to investigate transcriptional changes. However, the importance of a kinase, such as MAP4K4, lies in its enzymatic catalytic activity, thus it would be more relevant to establish interactions and phosphorylation partners to elucidate biological pathways. High-throughput technology for this purpose, as an equivalent to microarrays for transcriptomics, is still at a prime stage, but some interesting technologies started to emerge. Past and low-throughput methods include 2D gel electrophoresis. Isolation of proteins from a 2D gel, digestion into peptides and incubation with radioactive ^{32}P, where phospho-peptides are analyzed by mass spectrometry (MS), is a higher throughput variation and directly relevant in determining phosphorylation sites (Campbell and Morrice, 2002). A highly sensitive technology for investigating kinase phosphorylation is MS followed by an *in vitro* phosphorylation reaction between a synthetic peptide library and a recombinant protein

kinase mixture (Ahsan et al., 2013). However, the latter technology requires *a priori* knowledge about the phosphorylated kinases. For studying protein-protein interactions, peptide arrays is attractive technology, where peptides are printed by photolithography on solid support, incubated with recombinant MAP4K4 and detected by various probe methods (reviewed in (Cagney and Emili, 2000; Katz et al., 2011). However, the protein arrays, as with any technology, come with disadvantages; firstly, the peptides are not in their native conformation and the interaction occurs in a controlled extracellular environment, which can lead to false-positive hits. One additional disadvantage is that phosphorylation (i.e. activity) is not represented (Katz et al., 2011).

4.4.4. Upstream mediators of MAP4K4-dependent signaling

Various activators and inhibitors of MAP4K4 were described. The most conspicuous activator of MAP4K4 is TNFα. Recently, miR-30d was shown to inhibit MAP4K4 expression by binding on its 3'UTR region in pancreatic β-cells, reversing the inhibition of insulin secretion mediated by TNFα (Zhao et al., 2012). Similarly, miR-141 and MAP4K4 RNA levels were reverse correlated in pancreatic cancer tissue. Inhibition of proliferation, invasion, clonogenicity and apoptosis in cell lines and decreased tumour volume *in vivo* were associated with inhibition of MAP4K4 by miR-141 (Zhao et al., 2013). Chromatin Immunoprecipitation (ChIP) assays and bioinformatics analysis of the promoter of MAP4K4 gene resulted in the identification of four p53 binding sites (Miled et al., 2005). In macrophages, MAP4K4 silencing by siRNA inhibited TNFα secretion in LPS-treated cells (Aouadi et al., 2009). Activation of MAP4K4 is hypothesised to occur via the TLR4 receptors in inflammatory cells, that alternatively mediates survival via the NFκB pathway. Indeed, NFκB regulates TNFα production, and considering the dichotomous functions of both TNFα and of NFκB, it is plausible that a positive feedback loop might exist between NFκB and TNFα, that could mediate either cell death via MAP4K4 or survival via the NFκB pathway. In adipocytes, TNFα activates MAP4K4 via TNFRI, but not TNFR2, causing phosphorylation of JNK and p38, leading to c-Jun and ATF2 phosphorylation (Tesz et al., 2007). Furthermore, JNK activation was shown to negatively regulate TNFα production via repressing its promoter, an opposing function to p38 that promotes TNFα production in ESC-derived cardiomyocytes (Minamino et al., 1999). By analogy, through p38 or JNK, respectively, MAP4K4 might induce or repress TNFα production in hiPSC-CMs. In the heart, TNFR2-mediated signalling is pro-survival (Burchfield et al., 2010), and it is a possibility that MAP4K4, as a pro-apoptotic kinase, is activated by TNFRI. However, its activation might be dependent on the TNFR complex I or complex II signallosomes: both interesting questions to address.

MAP4K4 was also shown to interact with Rap2, but not Rap1 – similar to TNIK (Taira et al., 2004) – via its citron homology domain (CNH) and localise in the perinuclear region. Rap2 interaction with the kinase also enhanced activation of MAP4K4 (Machida et al., 2004; Taira et al., 2004) that was measured by JNK and c-Jun phosphorylation (Machida et al., 2004). The subcellular localization of MAP4K4 in NRVCs and hiPSC-CMs in relation to Rap2 and other adaptor proteins in the cell membrane is unknown. This is of particular interest, since *Msn* (a MAP4K4 orthologue) was mostly localised in the cytoplasm, but upon treatment with okadaic acid, the bulk of the kinase translocated to the cell membrane (Kaneko et al., 2011). Moreover, a constitutively active form of *Msn* located in the cell membrane also exhibited increased catalytic activity compared to the wild-type form, suggesting that localization determines its catalytic function. Similar studies would be of interest in cardiomyocytes, and could be readily implemented.

In a cardiac setting, activation of endogenous MAP4K4 was evident in response to various pathobiological signals. Myocardium-specific TNFα overexpression resulted in apoptosis with subsequent activation of caspase-8 and t-Bid cleavage (Haudek et al., 2007) associated with activation of MAP4K4 (Xie et al., 2007). Unfortunately, TNFα induction (by LPS stimulation) failed to cause cell death in neonatal cardiomyocytes, opposed to the apoptotic effect on adult cardiomyocytes (Comstock, 1998). In addition, TNFα as a death signal does not cause acute apoptosis in neonatal cardiomyocytes unless co-treated with cycloheximide (a protein synthesis inhibitor) (de Moissac et al., 1998). These observations suggest that a distinct requirement for TNFα might exist between adult and neonatal cardiomyocytes (Behfar et al., 2007). Thus, even if MAP4K4 is pro-apoptotic in hiPSC-CMs, we cannot speculate the consequence of TNFα on these cells. In addition, it is likely that TNFα, similar to JNK, exerts its biphasic effects on a dose-and time-dependent fashion. One extremely interesting experiment to be carried out on hiPSC-CMs would be a fine dose-response curve in the presence and absence of cycloheximide, in the presence of TNFRI or II blocking peptides. If indeed cycloheximide is required, it strengthens the argument for maturation of hiPSC-CMs towards an adult phenotype that better reflects the TNFα / MAP4K4 axis in the heart.

4.4.5. Cardiac cell death: critical gaps and further work

The roadblocks and critical gaps in the field of cardiac muscle cell death are many. More elaborate time-dependent experiments are needed to understand the involvement of each kinase in MI and pathological cardiac hypertrophy. Since finely detailed temporal data are more difficult to acquire with animal experimentation, as this would significantly increase their number, logistical complexity, and cost, such information can be acquired more readily with in vitro cell-based high-content and high-throughput technologies to provide in-depth signalling understanding. Even better, 3D culture is expected to be more predictive of human tissue biology and should be taken advantage of, in planning this kind of experiment.

Furthermore, the incidence, prevalence and timing of apoptosis and necrosis in the heart are problematic to compare because of the diversity of cell culture models (e.g. H9c2, HL-1, neonatal / adult cardiomyocytes). While NRVC cultures are widely used as a model system for investigating cardiomyocyte growth and death, they can be criticized as departing in some details from the phenotype of the adult heart. Despite the utilization of HL-1 and H9c2 cells in studying normal cardiomyocyte function (electric, metabolic and transcription signalling) and pathological conditions (hypertrophy, apoptosis) (Smith et al., 2007; Chen et al., 2013b), their value as cardiomyocyte models has been open to question. HL-1 cells, aside from that they are derived from mouse atrial tumours, contain the SV40 large T-antigen, which permits proliferation and inactivates p53, and thus should only be used to study apoptosis with extreme caution. H9c2 cells, though derived from the rat ventricle, can differentiate alternatively into skeletal muscle, and thus have plasticity for the two striated muscle lineages with no exact equivalent in nature. Therefore, while H9c2 and HL-1 cells can be used for supporting studies, these models should not stand alone to support a hypothesis, without the use of authentic neonatal and adult cardiomyocytes. Even better, in the era of human pluripotent stem cell-derived models, we can slowly move beyond rodent primary cultures.

Having said this, it would be essential for the commercially available hiPSC-CM models to be more financially viable than they currently are for academic researchers. Availability to a wider research audience, other than industry, would allow the faster uptake and robust characterization of these cells. Furthermore, effort should be spent on understanding the mechanisms of reprogramming towards the development of faster, more efficient, innocuous protocols for creating iPSCs and their relevant derivatives during differentiation. In addition, the field urgently requires protocols for improved maturation of hiPSC-CMs into adult-like cardiomyocytes that will potentially exhibit greater relevance to clinical cardiac pathology, pathways, and experimental therapeutics. Finally, cell death machinery proteins should be unanimously included in cell death studies and a compulsory factor considered in future

research grant applications by independent investigators for better understanding of the various branches of cell death.

5. References

Abe, N., Matsunaga, T., Kameda, K., Tomita, H., Fujiwara, T., Ishizaka, H., Hanada, H., Fukui, K., Fukuda, I., Osanai, T., et al. (2006). Increased level of pericardial insulin-like growth factor-1 in patients with left ventricular dysfunction and advanced heart failure. J. Am. Coll. Cardiol. *48*, 1387–1395.

Acehan, D., Jiang, X.J., Morgan, D.G., Heuser, J.E., Wang, X.D., and Akey, C.W. (2002). Three-dimensional structure of the apoptosome: Implications for assembly, procaspase-9 binding, and activation. Mol. Cell *9*, 423–432.

Adhikari, A., Xu, M., and Chen, Z.J. (2007). Ubiquitin-mediated activation of TAK1 and IKK. Oncogene *26*, 3214–3226.

Agrawal, A., Dillon, S., Denning, T.L., and Pulendran, B. (2006). ERK1-/- mice exhibit Th1 cell polarization and increased susceptibility to experimental autoimmune encephalomyelitis. J. Immunol. *176*, 5788–5796.

Ahsan, N., Huang, Y., Tovar-Mendez, A., Swatek, K.N., Zhang, J., Miernyk, J.A., Xu, D., and Thelen, J.J. (2013). A versatile mass spectrometry-based method to both identify kinase client-relationships and characterize signaling network topology. J. Proteome Res. *12*, 937–948.

Ahuja, P., Sdek, P., and MacLellan, W.R. (2007). Cardiac myocyte cell cycle control in development, disease, and regeneration. Phys. Rev. *87*, 521–544.

Aikawa, R., Olson, E.N., Aikawa, R., Nawano, M., Nawano, M., Gu, Y., Gu, Y., Katagiri, H., Katagiri, H., Asano, T., et al. (2000). Insulin prevents cardiomyocytes from oxidative stress-induced apoptosis through activation of PI3 kinase/Akt. Circ. *102*, 2873–2879.

Akhter, S.A., Milano, C.A., Shotwell, K.F., Cho, M.C., Rockman, H.A., Lefkowitz, R.J., and Koch, W.J. (1997). Transgenic mice with cardiac overexpression of alpha1B-adrenergic receptors. In vivo alpha1-adrenergic receptor-mediated regulation of beta-adrenergic signaling. J. Biol. Chem. *272*, 21253–21259.

Allender, S., Scarborough VP., and Rayner, M. (2008). European Cardiovascular Disease statistics ed. British Heart Fountation: London

Anderson, M.E., Zeng, H., Higgins, L.S., Park, J.W., Schulman, H., Guo, M., Lin, G., Crandall, L., Compton, T., Wang, X., et al. (2006). Disease mechanisms and emerging therapies: protein kinases and their inhibitors in myocardial disease. Nat Clin Pract Cardiovasc Med *3*, 437–445.

Andrews, C., Ho, P.D., Dillmann, W.H., Glembotski, C.C., and McDonough, P.M. (2003). The MKK6-p38 MAPK pathway prolongs the cardiac contractile calcium transient, downregulates SERCA2, and activates NF-AT. Cardiovasc. Res. *59*, 46–56.

Anokye-Danso, F., Trivedi, C.M., Juhr, D., Gupta, M., Cui, Z., Tian, Y., Zhang, Y., Yang, W., Gruber, P.J., Epstein, J.A., et al. (2011). Highly Efficient miRNA-Mediated Reprogramming of Mouse and Human Somatic Cells to Pluripotency. Cell Stem Cell *8*, 376–388.

Anson, B.D., Kolaja, K.L., and Kamp, T.J. (2011). Opportunities for use of human iPS cells in predictive toxicology. Clin. Pharmacol. Ther. *89*, 754–758.

Aoki, H. (2002). Direct Activation of Mitochondrial Apoptosis Machinery by c-Jun N-terminal Kinase in Adult Cardiac Myocytes. J. Biol. Chem. *277*, 10244–10250.

Aouadi, M., Takeuchi, J.K., Tesz, G.J., Bruneau, B.G., Nicoloro, S.M., Wang, M., Chouinard,

M., Soto, E., Ostroff, G.R., and Czech, M.P. (2009). Orally delivered siRNA targeting macrophage Map4k4 suppresses systemic inflammation. Nature *458*, 1180–1184.

Arad, M., Benson, D.W., Perez-Atayde, A.R., McKenna, W.J., Sparks, E.A., Kanter, R.J., McGarry, K., Seidman, J.G., and Seidman, C.E. (2002). Constitutively active AMP kinase mutations cause glycogen storage disease mimicking hypertrophic cardiomyopathy. J. Clin. Invest. *109*, 357–362.

Argaud, L., Prigent, A.F., Chalabreysse, L., Loufouat, J., Lagarde, M., and Ovize, M. (2004). Ceramide in the antiapoptotic effect of ischemic preconditioning. Am. J. Physiol. Heart. Circ. Physiol. *286*, 246–251.

Aries, A., Paradis, P., Lefebvre, C., Schwartz, R.J., and Nemer, M. (2004). Essential role of GATA-4 in cell survival and drug-induced cardiotoxicity. Proc. Natl. Acad. Sci. USA *101*, 6975–6980.

Avkiran, M., Rowland, A.J., Cuello, F., and Haworth, R.S. (2008). Protein kinase d in the cardiovascular system: emerging roles in health and disease. Circ. Res. *102*, 157–163.

Babiarz, J.E., Grueneberg, D.A., Ravon, M., Degot, S., Sridhar, S., Pearlberg, J., Ravindran, P., Li, W., Swanson, B., Davies, J.E., et al. (2012). Determination of the human cardiomyocyte mRNA and miRNA differentiation network by fine-scale profiling. Stem Cells Dev. *21*, 1956–1965.

Babiker, F.A., Lips, D., Meyer, R., Delvaux, E., Zandberg, P., Ben Janssen, van Eys, G., Grohé, C., and Doevendans, P.A. (2006). Estrogen Receptor β Protects the Murine Heart Against Left Ventricular Hypertrophy. Arterioscler. Thromb. Vasc. Biol. *26*, 1524–1530.

Baines, C.P. (2007). The mitochondrial permeability transition pore as a target of cardioprotective signaling. Am. J. Physiol. Heart Circ. Physiol. *293*, H903–H904.

Baines, C.P., Kaiser, R.A., Purcell, N.H., Blair, N.S., Osinska, H., Hambleton, M.A., Brunskill, E.W., Sayen, M.R., Gottlieb, R.A., Dorn, G.W., et al. (2005). Loss of cyclophilin D reveals a critical role for mitochondrial permeability transition in cell death. Nature *434*, 658–662.

Baines, C.P., Kaiser, R.A., Sheiko, T., Craigen, W.J., and Molkentin, J.D. (2007). Voltage-dependent anion channels are dispensable for mitochondrial-dependent cell death. Nat. Cell Biol. *9*, 550–555.

Baines, C.P., Zhang, J., Wang, G.-W., Zheng, Y.-T., Xiu, J.X., Cardwell, E.M., Bolli, R., and Ping, P. (2002). Mitochondrial PKCepsilon and MAPK form signaling modules in the murine heart: enhanced mitochondrial PKCepsilon-MAPK interactions and differential MAPK activation in PKCepsilon-induced cardioprotection. Circ. Res. *90*, 390–397.

Balakirev, E.S., and Ayala, F.J. (2003). Pseudogenes: Are they “Junk” or functional DNA? Annu. Rev. Gen. *37*, 123–151.

Bates, E., Bode, C., Costa, M., Gibson, C.M., Granger, C., Green, C., Grimes, K., Harrington, R., Huber, K., et al. (2008). Intracoronary KAI-9803 as an adjunct to primary percutaneous coronary intervention for acute ST-segment elevation myocardial infarction. Circ. *117*, 886–896.

Behfar, A., Perez-Terzic, C., Faustino, R.S., Arrell, D.K., Hodgson, D.M., Yamada, S., Pucéat, M., Niederländer, N., Alekseev, A.E., Zingman, L.V., et al. (2007). Cardiopoietic programming of embryonic stem cells for tumor-free heart repair. J. Exp. Med. *204*, 405–420.

Belzacq, A.S., Vieira, H., Verrier, F., Vandecasteele, G., Cohen, I., Prévost, M.C., Larquet, E., Pariselli, F., Petit, P.X., Kahn, A., et al. (2003). Bcl-2 and bax modulate adenine nucleotide translocase activity. Cancer Res. *63*, 541–546.

Bergmann, O., Bhardwaj, R.D., Bernard, S., Zdunek, S., Barnabé-Heider, F., Walsh, S., Zupicich, J., Alkass, K., Buchholz, B.A., Druid, H., et al. (2009). Evidence for cardiomyocyte renewal in humans. Science *324*, 98–102.

Bernardo, B.C., Weeks, K.L., Pretorius, L., and McMullen, J.R. (2010). Molecular distinction between physiological and pathological cardiac hypertrophy: Experimental findings and therapeutic strategies. Pharmacol. Ther. *128*, 191–227.

Berry, D.L., and Baehrecke, E.H. (2007). Growth arrest and autophagy are required for salivary gland cell degradation in Drosophila. Cell *131*, 1137–1148.

Bhuiyan, M.S., and Fukunaga, K. (2007). Inhibition of HtrA2/Omi ameliorates heart dysfunction following ischemia/reperfusion injury in rat heart in vivo. Eur. J. Pharmacol. *557*, 168–177.

Bielawska, A.E., Shapiro, J.P., Jiang, L., Melkonyan, H.S., Piot, C., Wolfe, C.L., Tomei, L.D., Hannun, Y.A., and Umansky, S.R. (1997). Ceramide is involved in triggering of cardiomyocyte apoptosis induced by ischemia and reperfusion. Am. J. Pathol. *151*, 1257–1263.

Bilic, J., and Izpisua Belmonte, J.C. (2012). Concise Review: Induced Pluripotent Stem Cells Versus Embryonic Stem Cells: Close Enough or Yet Too Far Apart? Stem Cells *30*, 33–41.

Binah, O., Dolnikov, K., Sadan, O., Shilkrut, M., Zeevi-Levin, N., Amit, M., Danon, A., and Itskovitz-Eldor, J. (2007). Functional and developmental properties of human embryonic stem cells-derived cardiomyocytes. J. Electrocardiol. *40*, S192–S196.

Bing, O.H. (1994). Hypothesis: apoptosis may be a mechanism for the transition to heart failure with chronic pressure overload. J. Mol. Cell Cardiol. *26*, 943–948.

Bogoyevitch, M.A., GillespieBrown, J., Ketterman, A.J., Fuller, S.J., BenLevy, R., Ashworth, A., Marshall, C.J., and Sugden, P.H. (1996). Stimulation of the stress-activated mitogen-activated protein kinase subfamilies in perfused heart - p38/RK mitogen-activated protein kinases and c-Jun N-terminal kinases are activated by ischemia/reperfusion. Circ. Res. *79*, 162–173.

Bonacci, T.M., Mathews, J.L., Yuan, C., Lehmann, D.M., Malik, S., Wu, D., Font, J.L., Bidlack, J.M., and Smrcka, A.V. (2006). Differential targeting of Gβγ-subunit signaling with small molecules. Science *312*, 443–446.

Bonow O. R., Mann L. D., Zipes P. D. and Libby P. (2011). Braunwald's Heart Disease: A Textbook of Cardiovascular Medicine, ed. 9th, Philadelphia

Boudoulas, K.D., and Hatzopoulos, A.K. (2009). Cardiac repair and regeneration: the Rubik's cube of cell therapy for heart disease. Dis. Model Mech. *2*, 344–358.

Bouzakri, K., and Zierath, J.R. (2007). MAP4K4 gene silencing in human skeletal muscle prevents tumor necrosis factor-α-induced insulin resistance. J. Biol. Chem. *282*, 7783–7789.

Bouzakri, K., Hotta, A., Zierath, J.R., Cheung, A.Y.L., Farra, N., Vijayaragavan, K., Séguin, C.A., Draper, J.S., Pasceri, P., Maksakova, I.A., et al. (2009). Isolation of human iPS cells using EOS lentiviral vectors to select for pluripotency. Nat. Methods *6*, 370–376.

Bowling, N., Walsh, R.A., Song, G., Estridge, T., Sandusky, G.E., Fouts, R.L., Mintze, K., Pickard, T., Roden, R., Bristow, M.R., et al. (1999). Increased protein kinase C activity and expression of Ca^{2+}-sensitive isoforms in the failing human heart. Circ. *99*, 384–391.

Bowman, J.C., Steinberg, S.F., Jiang, T., Geenen, D.L., Fishman, G.I., and Buttrick, P.M. (1997). Expression of protein kinase C beta in the heart causes hypertrophy in adult mice and sudden death in neonates. J. Clin. Invest. *100*, 2189–2195.

Braz, J.C., Bueno, O.F., Liang, Q., Wilkins, B.J., Dai, Y.-S., Parsons, S., Braunwart, J., Glascock, B.J., Klevitsky, R., Kimball, T.F., et al. (2003). Targeted inhibition of p38 MAPK promotes hypertrophic cardiomyopathy through upregulation of calcineurin-NFAT signaling. J. Clin. Invest. *111*, 1475–1486.

Braz, J.C., Gregory, K., Pathak, A., Zhao, W., Sahin, B., Klevitsky, R., Kimball, T.F., Lorenz, J.N., Nairn, A.C., Liggett, S.B., et al. (2004). PKC-α regulates cardiac contractility and propensity toward heart failure. Nat. Med. *10*, 248–254.

Brocheriou, V., Hagège, A.A., Oubenaïssa, A., Lambert, M., Mallet, V.O., Duriez, M., Wassef, M., Kahn, A., Menasché, P., and Gilgenkrantz, H. (2000). Cardiac functional improvement by a human Bcl-2 transgene in a mouse model of ischemia/reperfusion injury. J. Gene Med. *2*, 326–333.

Brons, I.G.M., Smithers, L.E., Trotter, M.W.B., Rugg-Gunn, P., Sun, B., Chuva de Sousa Lopes, S.M., Howlett, S.K., Clarkson, A., Ahrlund-Richter, L., Pedersen, R.A., et al. (2007). Derivation of pluripotent epiblast stem cells from mammalian embryos. Nature *448*, 191–195.

Brooks, C., Wei, Q., Feng, L., Dong, G., Tao, Y., Mei, L., Xie, Z.-J., and Dong, Z. (2007). Bak regulates mitochondrial morphology and pathology during apoptosis by interacting with mitofusins. Proc. Natl. Acad. Sci. USA *104*, 11649–11654.

Bueno, O.F., and Molkentin, J.D. (2002). Involvement of extracellular signal-regulated kinases 1/2 in cardiac hypertrophy and cell death. Circ. Res. *91*, 776–781.

Bueno, O.F., De Windt, L.J., Tymitz, K.M., Witt, S.A., Kimball, T.R., Klevitsky, R., Hewett, T.E., Jones, S.P., Lefer, D.J., Peng, C.F., et al. (2000). The MEK1-ERK1/2 signaling pathway promotes compensated cardiac hypertrophy in transgenic mice. EMBO J. *19*, 41–50.

Burchfield, J.S., Dong, J.-W., Sakata, Y., Gao, F., Tzeng, H.-P., Topkara, V.K., Entman, M.L., Sivasubramanian, N., and Mann, D.L. (2010). The cytoprotective effects of tumor necrosis factor are conveyed through tumor necrosis factor receptor-associated factor 2 in the heart. Circ. Heart. Fail. *3*, 157–164.

Cagney, G., and Emili, A.Q. (2000). Large-scale functional analysis using peptide or protein arrays : Abstract : Nature Biotechnology. Nat. Biotechnol. *18*, 393–397.

Campbell, D.G., and Morrice, N.A. (2002). Identification of protein phosphorylation sites by a combination of mass spectrometry and solid phase Edman sequencing. J Biomol Tech *13*, 119–130.

Cao, D.J., Wang, Z.V., Battiprolu, P.K., Jiang, N., Morales, C.R., Kong, Y., Rothermel, B.A., Gillette, T.G., and Hill, J.A. (2011). Histone deacetylase (HDAC) inhibitors attenuate cardiac hypertrophy by suppressing autophagy. Proc. Natl. Acad. Sci. USA *108*, 4123–4128.

Casey, L.M., Pistner, A.R., Belmonte, S.L., Migdalovich, D., Stolpnik, O., Nwakanma, F.E., Vorobiof, G., Dunaevsky, O., Matavel, A., Lopes, C.M.B., et al. (2010). Small molecule disruption of G beta gamma signaling inhibits the progression of heart failure. Circ. Res. *107*,

532–539.

Cervantes, D., Crosby, C., and Xiang, Y. (2010). Arrestin orchestrates crosstalk between G protein-coupled receptors to modulate the spatiotemporal activation of ERK MAPK. Circ. Res. *106*, 79–88.

Chakraborti, S., Das, S., Kar, P., Ghosh, B., Samanta, K., Kolley, S., Ghosh, S., Roy, S., and Chakraborti, T. (2007). Calcium signaling phenomena in heart diseases: a perspective. Mol Cell Biochem *298*, 1–40.

Chan, A.Y.M., Soltys, C.-L.M., Young, M.E., Proud, C.G., and Dyck, J.R.B. (2004). Activation of AMP-activated protein kinase inhibits protein synthesis associated with hypertrophy in the cardiac myocyte. J Biol Chem *279*, 32771–32779.

Chan, F., Shisler, J., Bixby, J.G., Felices, M., Zheng, L.X., Appel, M., Orenstein, J., Moss, B., and Lenardo, M.J. (2003). A role for tumor necrosis factor receptor-2 and receptor-interacting protein in programmed necrosis and antiviral responses. J Biol Chem *278*, 51613–51621.

Chang, C.-J., and Bouhassira, E.E. (2012). Zinc-finger nuclease-mediated correction of alpha-thalassemia in iPS cells. Blood *120*, 3906–3914.

Chang, D.W., Xing, Z., Pan, Y., Algeciras-Schimnich, A., Barnhart, B.C., Yaish-Ohad, S., Peter, M.E., and Yang, X. (2002). c-FLIPL is a dual function regulator for caspase-8 activation and CD95-mediated apoptosis. The EMBO Journal *21*, 3704–3714.

Chang, J., Xie, M., Shah, V.R., Schneider, M.D., Entman, M.L., Wei, L., and Schwartz, R.J. (2006). Activation of Rho-associated coiled-coil protein kinase 1 (ROCK-1) by caspase-3 cleavage plays an essential role in cardiac myocyte apoptosis. Proc. Natl. Acad. Sci. USA *103*, 14495–14500.

Chen, C., and Sytkowski, A.J. (2005). Apoptosis-linked gene-2 connects the Raf-1 and ASK1 signalings. Biochem Biophys Res Commun *333*, 51–57.

Chen, J., and Rockman, A. H. (2008). Receptor Signaling Pathways in Heart Failure: Transgenic Mouse Models In: Mebazaa, A., Gheorghiade, M., Zannad, F., Parrillo, J.E. ed, Acute Heart Failure, Springer, p89-111

Chen, J., Fujii, K., Zhang, L., Roberts, T., and Fu, H. (2001a). Raf-1 promotes cell survival by antagonizing apoptosis signal-regulating kinase 1 through a MEK-ERK independent mechanism. Proc. Natl. Acad. Sci. USA *98*, 7783–7788.

Chen, J., Hsieh, A.F.-C., Dharmarajan, K., Masoudi, F.A., and Krumholz, H.M. (2013a). National trends in heart failure hospitalization after acute myocardial infarction for medicare beneficiaries: 1998-2010. Circulation *128*, 2577–2584.

Chen, M., He, H., Zhan, S., Krajewski, S., Reed, J.C., and Gottlieb, R.A. (2001b). Bid is cleaved by calpain to an active fragment in vitro and during myocardial ischemia/reperfusion. J Biol Chem *276*, 30724–30728.

Chen, Q.M., Tu, V.C., Wu, Y., and Bahl, J.J. (2000). Hydrogen Peroxide Dose Dependent Induction of Cell Death or Hypertrophy in Cardiomyocytes. Archives of Biochemistry and Biophysics *373*, 242–248.

Chen, V.C., Stull, R., Joo, D., Cheng, X., and Keller, G. (2008). Notch signaling respecifies the hemangioblast to a cardiac fate. Nat Biotechnol *26*, 1169–1178.

Chen, Y., Decker, K.F., Zheng, D., Matkovich, S.J., Jia, L., and Dorn, G.W. (2013). A

nuclear-targeted alternately spliced Nix/Bnip3L isoform modifies NF-kB mediated cardiac transcription. J Biol Chem *288*, 455–465.

Chen, Y., Lewis, W., Diwan, A., Cheng, E.H.-Y., Matkovich, S.J., and Dorn, G.W. (2010). Dual autonomous mitochondrial cell death pathways are activated by Nix/BNip3L and induce cardiomyopathy. Proc. Natl. Acad. Sci. USA *107*, 9035–9042.

Chen, Z., Chua, C.C., Ho, Y.-S., Hamdy, R.C., and Chua, B.H.L. (2001c). Overexpression of Bcl-2 Attenuates Apoptosis and Protects Against Myocardial I/R Injury in Transgenic Mice. Am. J. Physiol. Heart Circ. Physiol. 2313–2320.

Cheng, E., Sheiko, T.V., Fisher, J.K., Craigen, W.J., and Korsmeyer, S.J. (2003). VDAC2 inhibits BAK activation and mitochondrial apoptosis. Science *301*, 513–517.

Cheng, H., and Force, T. (2010). Molecular mechanisms of cardiovascular toxicity of targeted cancer therapeutics. Circ. Res. *106*, 21–34.

Cheng, L., Hansen, N.F., Zhao, L., Du, Y., Zou, C., Donovan, F.X., Chou, B.-K., Zhou, G., Li, S., Dowey, S.N., et al. (2012). Low incidence of DNA sequence variation in human induced pluripotent stem cells generated by nonintegrating plasmid expression. Cell Stem Cell *10*, 337–344.

Cheng, M., Olivier, P., Diehl, J.A., Fero, M., Roussel, M.F., Roberts, J.M., and Sherr, C.J. (1999). The p21(Cip1) and p27(Kip1) CDK “inhibitors” are essential activators of cyclin D-dependent kinases in murine fibroblasts. EMBO J. *18*, 1571–1583.

Cheng, Y., Liu, X., Zhang, S., Lin, Y., Yang, J., and Zhang, C. (2009). MicroRNA-21 protects against the H_2O_2-induced injury on cardiac myocytes via its target gene PDCD4. J. Mol. Cell Cardiol. *47*, 5–14.

Chien, K.R. (2000). Genomic circuits and the integrative biology of cardiac diseases. Nature *407*, 227–232.

Chiong, M., Wang, Z.V., Pedrozo, Z., Cao, D.J., Troncoso, R., Ibacache, M., Criollo, A., Nemchenko, A., Hill, J.A., and Lavandero, S. (2011). Cardiomyocyte death: mechanisms and translational implications. Cell Death Dis. *2*, 244-254

Chis, R., Sharma, P., Bousette, N., Miyake, T., Wilson, A., Backx, P.H., and Gramolini, A.O. (2012). α-Crystallin B prevents apoptosis after H2O2 exposure in mouse neonatal cardiomyocytes. Am. J. Physiol-Heart Circ. *303*, 967–978.

Choukroun, G., HAJJAR, R., Kyriakis, J.M., Bonventre, J.V., Rosenzweig, A., and Force, T. (1998). Role of the stress-activated protein kinases in endothelin-induced cardiomyocyte hypertrophy. J. Clin. Invest. *102*, 1311–1320.

Choukroun, G., Hajjar, R., Fry, S., del Monte, F., Haq, S., Guerrero, J.L., Picard, M., Rosenzweig, A., and Force, T. (1999). Regulation of cardiac hypertrophy in vivo by the stress-activated protein kinases/c-Jun NH2-terminal kinases. J. Clin. Invest. *104*, 391–398.

Chua, C.C., Gao, J., Ho, Y.-S., Xiong, Y., Xu, X., Chen, Z., Hamdy, R.C., and Chua, B.H.L. (2007). Overexpression of IAP-2 attenuates apoptosis and protects against myocardial ischemia/reperfusion injury in transgenic mice. Biochim. Biophys. Acta *1773*, 577–583.

Churchill, E.N., Murriel, C.L., Chen, C.-H., Mochly-Rosen, D., and Szweda, L.I. (2005). Reperfusion-induced translocation of deltaPKC to cardiac mitochondria prevents pyruvate dehydrogenase reactivation. Circ. Res. *97*, 78–85.

Clarke, S.J., McStay, G.P., and Halestrap, A.P. (2002). Sanglifehrin A acts as a potent inhibitor of the mitochondrial permeability transition and reperfusion injury of the heart by binding to cyclophilin-D at a different site from cyclosporin A. J. Biol. Chem. *277*, 34793–34799.

Clarke, S.J., McStay, G.P., and Halestrap, A.P. (2002). Sanglifehrin A acts as a potent inhibitor of the mitochondrial permeability transition and reperfusion injury of the heart by binding to cyclophilin-D at a different site from cyclosporin Am. J. Biol. Chem. *277*, 793–799.

Colligan, P.B., Relling, D.P., and Ren, J. (2002). Ceramide attenuates high glucose-induced cardiac contractile abnormalities in cultured adult rat ventricular myocytes. Cell. Mol. Biol. *48*, 251–257.

Comstock, K. (1998). LPS-Induced TNFα Release from and Apoptosis in Rat Cardiomyocytes: Obligatory Role for CD14 in Mediating the LPS Response. J. Mol. Cell Cardiol. *30*, 2761–2775.

Condorelli, G., Roncarati, R., Ross, J., Pisani, A., Stassi, G., Todaro, M., Trocha, S., Drusco, A., Gu, Y., Russo, M.A., et al. (2001). Heart-targeted overexpression of caspase3 in mice increases infarct size and depresses cardiac function. Proc. Natl. Acad. Sci. USA *98*, 77–82.

Converso, A., Hartingh, T., Garbaccio, R.M., Tasber, E., Rickert, K., Fraley, M.E., Yan, Y., Kreatsoulas, C., Stirdivant, S., Drakas, B., et al. (2009). Development of thioquinazolinones, allosteric Chk1 kinase inhibitors. Bioorg. Med. Chem. Lett. *19*, 1240–1244.

Cordis, G.A., Yoshida, T., and Das, D.K. (1998). HPTLC analysis of sphingomylein, ceramide and sphingosine in ischemic/reperfused rat heart. J. Pharm. Biomed. Anal. *16*, 1189–1193.

Coulthard, L.R., White, D.E., Jones, D.L., McDermott, M.F., and Burchill, S.A. (2009a). p38(MAPK): stress responses from molecular mechanisms to therapeutics. Trends Mol. Med.*15*, 369–379.

Coulthard, L.R., White, D.E., Jones, D.L., McDermott, M.F., and Burchill, S.A. (2009b). p38(MAPK): stress responses from molecular mechanisms to therapeutics. Trends Mol. Med. *15*, 369–379.

Crosio, C., Fimia, G.M., Loury, R., Kimura, M., Okano, Y., Zhou, H., Sen, S., Allis, C.D., and Sassone-Corsi, P. (2002). Mitotic phosphorylation of histone H3: spatio-temporal regulation by mammalian Aurora kinases. Mol. Cell Biol. *22*, 874–885.

Crow, M.T., Mani, K., Nam, Y.J., and Kitsis, R.N. (2004). The mitochondrial death pathway and cardiac myocyte apoptosis. Circ. Res. *95*, 957–970.

Cuvillier, O., Rosenthal, D.S., Smulson, M.E., and Spiegel, S. (1998). Sphingosine 1-phosphate inhibits activation of caspases that cleave poly(ADP-ribose) polymerase and lamins during Fas- and ceramide-mediated apoptosis in Jurkat T lymphocytes. J. Biol. Chem. *273*, 2910–2916.

Çöl Arslan, S., Yuasa, S., Scheidereit, C., Itabashi, Y., Koshimizu, U., Tanaka, T., Sugimura, K., Kinoshita, M., Hattori, F., Fukami, S.-I., et al. (2011). The Prevalence of TNFα-Induced Necrosis over Apoptosis Is Determined by TAK1-RIP1 Interplay. PLoS ONE *6*, e26069.

D'Angelo, D.D., Sakata, Y., Lorenz, J.N., Boivin, G.P., Walsh, R.A., Liggett, S.B., and Dorn, G.W. (1997). Transgenic Galphaq overexpression induces cardiac contractile failure in mice. Proc. Natl. Acad. Sci. USA *94*, 8121–8126.

Dalloz, F., Osinska, H., and Robbins, J. (2001). Manipulating the contractile apparatus: genetically defined animal models of cardiovascular disease. J. Mol. Cell Cardiol. *33*, 9–25.

Das, A., Xi, L., and Kukreja, R.C. (2008). Protein kinase G-dependent cardioprotective mechanism of phosphodiesterase-5 inhibition involves phosphorylation of ERK and GSK3β. J. Biol. Chem. *283*, 29572–29585.

Davidson, B.L., and McCray, P.B. (2011). Current prospects for RNA interference-based therapies. Nat. Rev. Genet. *12*, 329–340.

Moissac, D., Mustapha, S., Greenberg, A.H., and Kirshenbaum, L.A. (1998). Bcl-2 activates the transcription factor NFκB through the degradation of the cytoplasmic inhibitor IkappaBalpha. J. Biol. Chem. *273*, 946–951.

De Nicola, G.F., Martin, E.D., Chaikuad, A., Bassi, R., Clark, J., Martino, L., Verma, S., Sicard, P., Tata, R., Atkinson, R.A., et al. (2013). Mechanism and consequence of the autoactivation of p38α mitogen-activated protein kinase promoted by TAB1. Nat. Struct. Mol. Biol. *20*, 1182–1190.

Denise Martin, E., De Nicola, G.F., and Marber, M.S. (2012). New therapeutic targets in cardiology: p38α mitogen-activated protein kinase for ischemic heart disease. Circ. *126*, 357–368.

Devin, A., Lin, Y., Yamaoka, S., Li, Z., Karin, M., and Liu, Z.G. (2001). The α and β subunits of IκB Kinase (IKK) mediate TRAF2-dependent IKK recruitment to Tumor Necrosis Factor (TNF) Receptor 1 in response to TNF. Mol. Cell Biol. *21*, 3986–3994.

Dhingra, S., Sharma, A.K., Arora, R.C., Slezak, J., and Singal, P.K. (2009). IL-10 attenuates TNFα-induced NFκB pathway activation and cardiomyocyte apoptosis. Cardiovasc. Res. *82*, 59–66.

Dick, E., Brandt, S., Matsa, E., Young, L.E., Darling, D., and Denning, C. (2011). Faster generation of hiPSCs by coupling high-titer lentivirus and column-based positive selection. Nat. Protoc. *6*, 701–714.

Dillon, C.P., Oberst, A., Weinlich, R., Janke, L.J., Kang, T.-B., Ben-Moshe, T., Mak, T.W., Wallach, D., and Green, D.R. (2012). Survival function of the FADD-Caspase-8-cFLIP$_L$ complex. Cell Rep. *1*, 401–407.

Dimmeler, S., Zeiher, A.M., and Schneider, M.D. (2005). Unchain my heart: the scientific foundations of cardiac repair. J. Clin. Invest. *115*, 572–583.

Diwan, A., Krenz, M., Syed, F.M., Wansapura, J., Ren, X., Koesters, A.G., Li, H., Kirshenbaum, L.A., Hahn, H.S., Robbins, J., et al. (2007). Inhibition of ischemic cardiomyocyte apoptosis through targeted ablation of Bnip3 restrains post-infarction remodeling in mice. J. Clin. Invest. *117*, 2825–2833.

Doggrell, S.A. (2005). Rho-kinase inhibitors show promise in pulmonary hypertension. Expert Opin. Investig. Drugs *14*, 1157–1159.

Dolnikov, K., Shilkrut, M., Zeevi-Levin, N., Gerecht-Nir, S., Amit, M., Danon, A., Itskovitz-Eldor, J., and Binah, O. (2006). Functional properties of human embryonic stem cell-derived cardiomyocytes: intracellular Ca^{2+} handling and the role of sarcoplasmic reticulum in the contraction. Stem Cells *24*, 236–245.

Dorn, G.W., and Force, T. (2005). Protein kinase cascades in the regulation of cardiac

hypertrophy. J. Clin. Invest. *115*, 527–537.

Dorn, G.W., and Mochly-Rosen, D. (2002). Intracellular transport mechanisms of signal transducers. Annu. Rev. Physiol. *64*, 407–429.

Du, C., Fang, M., Li, Y., Li, L., and Wang, X. (2000). Smac, a mitochondrial protein that promotes cytochrome c-dependent caspase activation by eliminating IAP inhibition. Cell *102*, 33–42.

Duerr, R.L., Huang, S., Miraliakbar, H.R., Clark, R., Chien, K.R., and Ross, J. (1995). Insulin-like growth factor-1 enhances ventricular hypertrophy and function during the onset of experimental cardiac failure. J. Clin. Invest. *95*, 619–627.

Ea, C.K., Deng, L., Xia, Z.P., Pineda, G., and Chen, Z.J. (2006). Activation of IKK by TNFalpha requires site-specific ubiquitination of RIP1 and polyubiquitin binding by NEMO. Mol. Cell *22*, 245–257.

Echeverri, C.J., and Perrimon, N. (2006). High-throughput RNAi screening in cultured cells: a user's guide. Nat. Rev. Genet. *7*, 373–384.

El-Armouche, A., Wittköpper, K., Degenhardt, F., Weinberger, F., Didié, M., Melnychenko, I., Grimm, M., Peeck, M., Zimmermann, W.H., Unsöld, B., et al. (2008). Phosphatase inhibitor-1-deficient mice are protected from catecholamine-induced arrhythmias and myocardial hypertrophy. Cardiovasc. Res. *80*, 396–406.

Ellwanger, K., Pfizenmaier, K., Lutz, S., and Hausser, A. (2008). Expression patterns of protein kinase D3 during mouse development. BMC Dev. Biol. *8*, 47.

Engel, F.B., Hsieh, P.C.H., Lee, R.T., and Keating, M.T. (2006). FGF1/p38 MAP kinase inhibitor therapy induces cardiomyocyte mitosis, reduces scarring, and rescues function after myocardial infarction. Proc. Natl. Acad. Sci. USA *103*, 546–551.

Engelhardt, S., Hein, L., Wiesmann, F., and Lohse, M.J. (1999). Progressive hypertrophy and heart failure in β1-adrenergic receptor transgenic mice. Proc. Natl. Acad. Sci. USA *96*, 59–64.

Engh, R.A., and Bossemeyer, D. (2002). Structural aspects of protein kinase control-role of conformational flexibility. Pharmacol. Ther. *93*, 99–111.

Eppenberger, H.M., Hertig, C., and Eppenberger-Eberhardt, M. (1994). Adult rat cardiomyocytes in culture: A model system to study the plasticity of the differentiated cardiac phenotype at the molecular and cellular levels. Trends Cardiovasc. Med. *4*, 187–193.

Eulalio, A., Mano, M., Dal Ferro, M., Zentilin, L., Sinagra, G., Zacchigna, S., and Giacca, M. (2012). Functional screening identifies miRNAs inducing cardiac regeneration. Nature *492*, 376–381.

Feldman, A.M., Combes, A., Wagner, D., Kadakomi, T., Kubota, T., Li, Y.Y., and McTiernan, C. (2000). The role of tumor necrosis factor in the pathophysiology of heart failure. J. Am. Coll. Cardiol. *35*, 537–544.

Feoktistova, M., Fujita, J., Luo, X., Stewart, S.A., Geserick, P., Crane, A.M., Budihardjo, I., Weinberg, R.A., Kellert, B., Souza, M.K., et al. (2011). cIAPs block Ripoptosome formation, a RIP1/Caspase-8 containing intracellular cell death complex differentially regulated by cFLIP isoforms. Mol. Cell *43*, 449–463.

Ferrandi, C., Ballerio, R., Gaillard, P., Giachetti, C., Carboni, S., Vitte, P.-A., Gotteland, J.-P.,

and Cirillo, R. (2004). Inhibition of c-Jun N-terminal kinase decreases cardiomyocyte apoptosis and infarct size after myocardial ischemia and reperfusion in anaesthetized rats. Br. J. Pharmacol. *142*, 953–960.

Ferreira, J.C.B., Brum, P.C., and Mochly-Rosen, D. (2011). βIIPKC and εPKC isozymes as potential pharmacological targets in cardiac hypertrophy and heart failure. J. Mol. Cell Cardiol. *51*, 479–484.

Ferrero, P., Said, M., Sánchez, G., Vittone, L., Valverde, C., Donoso, P., Mattiazzi, A., and Mundina-Weilenmann, C. (2007). Ca^{2+}/calmodulin kinase II increases ryanodine binding and Ca^{2+}-induced sarcoplasmic reticulum Ca^{2+} release kinetics during beta-adrenergic stimulation. J. Mol. Cell Cardiol. *43*, 281–291.

Fiedler, L.R., Chapman, K., Guo, W., Kanaganayagam, S., Low, C., Traulau-Stewart, C., and Schneider, M.D. (2014). MAP4K4 as a Therapeutic Target in Cardiomyocyte Death: Novel inhibitors Identified through Pharmacophore Modelling and Virtual Screening. Heart *100 Suppl 1*, A5.

Fiedler, L.R., Maifoshie E., Schneider M.D. (2014). Mouse models of heart failure: cell signaling and cell survival. In: Stewart L.C. *Mouse Models of The Nuclear Envelopathies and Related Diseases*, Academic Press: Elsevier *109*, p2-232

Fielitz, J., Kim, M.S., Shelton, J.M., Qi, X., Hill, J.A., Richardson, J.A., Bassel-Duby, R., and Olson, E.N. (2008). Requirement of protein kinase D1 for pathological cardiac remodeling. Proc. Natl. Acad. Sci. USA *105*, 59–63.

Fijnvandraat, A.C., van Ginneken, A.C.G., Schumacher, C.A., Boheler, K.R., Lekanne Deprez, R.H., Christoffels, V.M., and Moorman, A.F.M. (2003). Cardiomyocytes purified from differentiated embryonic stem cells exhibit characteristics of early chamber myocardium. J. Mol. Cell Cardiol. *35*, 1461–1472.

Fire, A., Xu, S., Montgomery, M.K., Kostas, S.A., Driver, S.E., and Mello, C.C. (1998). Potent and specific genetic interference by double-stranded RNA in Caenorhabditis elegans. Nature *391*, 806–811.

Fitzgerald, K., Frank-Kamenetsky, M., Shulga-Morskaya, S., Liebow, A., Bettencourt, B.R., Sutherland, J.E., Hutabarat, R.M., Clausen, V.A., Karsten, V., Cehelsky, J., et al. (2014). Effect of an RNA interference drug on the synthesis of proprotein convertase subtilisin/kexin type 9 (PCSK9) and the concentration of serum LDL cholesterol in healthy volunteers: a randomised, single-blind, placebo-controlled, phase 1 trial. Lancet *383*, 60–68.

Flesch, M., Margulies, K.B., Mochmann, H.C., Engel, D., Sivasubramanian, N., and Mann, D.L. (2001). Differential regulation of mitogen-activated protein kinases in the failing human heart in response to mechanical unloading. Circ.*104*, 2273–2276.

Foldes, G., Matsa, E., Kriston-Vizi, J., Leja, T., Mioulane, M., Vauchez, K., Ketteler, R., Schneider, M.D., Denning, C., and Harding, S.E. (2013). Abstract P1458: Key differences in hypertrophic signalling between hESC- and hIPSC-derived cardiomyocytes. Eur. Heart J. 279.

Foo, R.S.Y., Chan, L.K., Kitsis, R.N., and Bennett, M.R. (2007). Ubiquitination and degradation of the anti-apoptotic protein ARC by MDM2. J. Biol. Chem. *282*, 29–35.

Foo, R.S.Y., Mani, K., and Kitsis, R.N. (2005). Death begets failure in the heart. J. Clin. Invest. *115*, 565–571.

Franco, D., Markman, M.M., Wagenaar, G.T., Ya, J., Lamers, W.H., and Moorman, A.F. (1999). Myosin light chain 2a and 2v identifies the embryonic outflow tract myocardium in the developing rodent heart. Anat. Rec. *254*, 135–146.

Frantz, S., Behr, T., Hu, K., Fraccarollo, D., Strotmann, J., Goldberg, E., Ertl, G., Angermann, C.E., and Bauersachs, J. (2007). Role of p38 mitogen-activated protein kinase in cardiac remodelling. Br. J. Pharmacol. *150*, 130–135.

Freude, B., Chudakov, D.M., Zhu, W., Masters, T.N., Lukyanov, S., Shiojima, I., Robicsek, F., Lukyanov, K.A., Ito, Y., Fokin, A., et al. (2000). Apoptosis is initiated by myocardial ischemia and executed during reperfusion. J. Mol. Cell Cardiol. *32*, 197–208.

Fryer, R.M., Patel, H.H., Hsu, A.K., and Gross, G.J. (2001). Stress-activated protein kinase phosphorylation during cardioprotection in the ischemic myocardium. Am. J. Physiol. Heart Circ. Physiol. *281*, 1184–1192.

Fu, Y., and Rubin, C.S. (2011). Protein kinase D: coupling extracellular stimuli to the regulation of cell physiology. EMBO Rep.*12*, 785–796.

Fujita, J., Crane, A.M., Souza, M.K., Dejosez, M., Kyba, M., Flavell, R.A., Thomson, J.A., and Zwaka, T.P. (2008). Caspase activity mediates the differentiation of embryonic stem cells. Cell Stem Cell *2*, 595–601.

Gallud, A., Vaillant, O., Maillard, L.T., Arama, D.P., Dubois, J., Maynadier, M., Lisowski, V., Garcia, M., Martinez, J., and Masurier, N. (2014). Imidazopyridine-fused [1,3]-diazepinones: Synthesis and antiproliferative activity. Eur. J. Med. Chem. *75*, 382–390.

Gang, H., Hai, Y., Dhingra, R., Gordon, J.W., Yurkova, N., Aviv, Y., Li, H., Aguilar, F., Marshall, A., Leygue, E., et al. (2011). A novel hypoxia-inducible spliced variant of mitochondrial death gene Bnip3 promotes survival of ventricular myocytes. Circ. Res. *108*, 1084–1092.

Gaspar, J.A., Doss, M.X., Hengstler, J.G., Cadenas, C., Hescheler, J., and Sachinidis, A. (2014). Unique metabolic features of stem cells, cardiomyocytes, and their progenitors. Circ. Res. *114*, 1346–1360.

Gazin, C., Wajapeyee, N., Gobeil, S., Virbasius, C.-M., and Green, M.R. (2007). An elaborate pathway required for Ras-mediated epigenetic silencing. Nature *449*, 1073–1077.

Gelb, B.D. (2006). Noonan syndrome and related disorders: dysregulated RAS-mitogen activated protein kinase signal transduction. Hum. Mol. Gen. *15*, 220–226.

Giering, J.C., Grimm, D., Storm, T.A., and Kay, M.A. (2008). Expression of shRNA from a tissue-specific pol II promoter is an effective and safe RNAi therapeutic. Mol. Ther. *16*, 1630–1636.

Gottlieb, R.A., Burleson, K.O., Kloner, R.A., Babior, B.M., and Engler, R.L. (1994). Reperfusion injury induces apoptosis in rabbit cardiomyocytes. J. Clin. Invest. *94*, 1621–1628.

Gottlieb, R.A., Echeverri, C.J., Liu, J., Mentzer, R.M., Perrimon, N., Lieu, D.K., Siu, C.W., Fu, J.D., Tan, T.H., and Li, R.A. (2010). Autophagy during cardiac stress: joys and frustrations of autophagy. Annu. Rev. Physiol. *72*, 45–59.

Grimm, M., Zhang, Y.M., and Brown, J.H. (2010). β-Adrenergic receptor signaling in the heart: Role of CaMKII. J. Mol. Cell. Cardiol. *48*, 322–330.

Grinberg, D. (2008). Recent patents relating to siRNAs and therapeutic strategies for genetic diseases. Recent Pat. DNA Gene Seq. *2*, 40–43.

Gross, A., Yin, X.M., Wang, K., Wei, M.C., Jockel, J., Milliman, C., Erdjument-Bromage, H., Tempst, P., and Korsmeyer, S.J. (1999). Caspase cleaved BID targets mitochondria and is required for cytochrome c release, while Bcl-X_L prevents this release but not tumor necrosis factor-R1/Fas death. J. Biol. Chem. *274*, 1156–1163.

Grueneberg, D.A., Degot, S., Pearlberg, J., Li, W., Davies, J.E., Baldwin, A., Endege, W., Doench, J., Sawyer, J., Hu, Y., et al. (2008). Kinase requirements in human cells: I. Comparing kinase requirements across various cell types. Proc. Natl. Acad. Sci. USA *105*, 472–477.

Guerra, S., Leri, A., Wang, X., Finato, N., Di Loreto, C., Beltrami, C.A., Kajstura, J., and Anversa, P. (1999). Myocyte death in the failing human heart is gender dependent. Circ. Res. *85*, 856–866.

Guimarães, C.R.W., Dickins, R.A., Ren, Y., Kakazu, N., Chi, X., Rai, B.K., Hemann, M.T., Sun, C., Abe, T., Chatterjee, P.K., et al. (2011). Understanding the Impact of the P-loop Conformation on Kinase Selectivity. J. Chem. Inf. Model. *51*, 1199–1204.

Gustafsson, A.B., and Gottlieb, R.A. (2008). Heart mitochondria: gates of life and death. Cardiovasc. Res. *77*, 334–343.

Halestrap, A.P., Vallier, L., Xu, R.H., Touboul, T., Peck, R.M., Chng, Z., Li, D.S., Brimpari, M., Feng, X., Hannan, N., et al. (2009). What is the mitochondrial permeability transition pore? J. Mol. Cell Cardiol. *46*, 821–831.

Hamid, T., Gu, Y., Ortines, R.V., Bhattacharya, C., Wang, G., Xuan, Y.T., and Prabhu, S.D. (2009). Divergent tumor necrosis factor receptor-related remodeling responses in heart failure: role of nuclear factor-κB and inflammatory activation. Circ. *119*, 1386–1397.

Hampson, L., He, X.T., Oliver, A.W., Hadfield, J.A., Kemp, T., Butler, J., McGown, A., Kitchener, H.C., and Hampson, I.N. (2009). Analogues of Y27632 increase gap junction communication and suppress the formation of transformed NIH3T3 colonies. Br. J. Cancer *101*, 829–839.

Han, J., Lee, J.D., Bibbs, L., and Ulevitch, R.J. (1994). A Map Kinase Targeted by Endotoxin and Hyperosmolarity in Mammalian-Cells. Science *265*, 808–811.

Hanna, J., Wernig, M., Markoulaki, S., Sun, C.W., Meissner, A., Cassady, J.P., Beard, C., Brambrink, T., Wu, L.C., Townes, T.M., et al. (2007). Treatment of sickle cell anemia mouse model with iPS cells generated from autologous skin. Science *318*, 1920–1923.

Hans, F., and Dimitrov, S. (2001). Histone H3 phosphorylation and cell division. Oncogene *20*, 3021–3027.

Harris, I.S., Zhang, S., Treskov, I., Kovacs, A., Weinheimer, C., and Muslin, A.J. (2004). Raf-1 kinase is required for cardiac hypertrophy and cardiomyocyte survival in response to pressure overload. Circ. *110*, 718–723.

Harrison, B.C., Kim, M.S., van Rooij, E., Plato, C.F., Papst, P.J., Vega, R.B., McAnally, J.A., Richardson, J.A., Bassel-Duby, R., Olson, E.N., et al. (2006). Regulation of cardiac stress signaling by protein kinase D1. Mol. Cell Biol. *26*, 3875–3888.

Hattori, F., Chen, H., Yamashita, H., Tohyama, S., Satoh, Y., Yuasa, S., Li, W., Yamakawa,

H., Tanaka, T., Onitsuka, T., et al. (2009). Nongenetic method for purifying stem cell-derived cardiomyocytes. Nat. Methods *7*, 61–66.

Haudek, S.B., Taffet, G.E., Schneider, M.D., and Mann, D.L. (2007). TNF provokes cardiomyocyte apoptosis and cardiac remodeling through activation of multiple cell death pathways. J. Clin. Invest. *117*, 2692–2701.

Haworth, R. (2000). Expression and Activity of Protein Kinase D/Protein Kinase C μ in Myocardium: Evidence for α_1 -adrenergic receptor- and Protein Kinase C-mediated regulation. J. Mol. Cell Cardiol. *32*, 1013–1023.

Haworth, R.S., Cuello, F., Herron, T.J., Franzen, G., Kentish, J.C., Gautel, M., and Avkiran, M. (2004). Protein kinase D is a novel mediator of cardiac troponin I phosphorylation and regulates myofilament function. Circ. Res. *95*, 1091–1099.

Hayashi, M., Kim, S.W., Imanaka-Yoshida, K., Yoshida, T., Abel, E.D., Eliceiri, B., Yang, Y., Ulevitch, R.J., and Lee, J.D. (2004). Targeted deletion of BMK1/ERK5 in adult mice perturbs vascular integrity and leads to endothelial failure. J. Clin. Invest. *113*, 1138–1148.

Hazeltine, L.B., Simmons, C.S., Salick, M.R., Lian, X., Badur, M.G., Han, W., Delgado, S.M., Wakatsuki, T., Crone, W.C., Pruitt, B.L., et al. (2013). Effects of substrate mechanics on contractility of cardiomyocytes generated from human pluripotent stem cells. Int. J. Biochem. Cell Biol. *2012*, 1–13.

He, S., Wang, L., Miao, L., Wang, T., Du, F., Zhao, L., and Wang, X. (2009). Receptor Interacting Protein Kinase-3 Determines Cellular Necrotic Response to TNFα. Cell *137*, 1100–1111.

Heidenreich, P.A., Albert, N.M., Allen, L.A., Bluemke, D.A., Butler, J., Fonarow, G.C., Ikonomidis, J.S., Khavjou, O., Konstam, M.A., Maddox, T.M., et al. (2013). Forecasting the impact of heart failure in the United States: a policy statement from the American Heart Association. Circ. Heart Fail. *6*, 606–619.

Hein, S., Arnon, E., Kostin, S., Schönburg, M., Elsässer, A., Polyakova, V., Bauer, E.P., Klövekorn, W.-P., and Schaper, J. (2003). Progression from compensated hypertrophy to failure in the pressure-overloaded human heart: structural deterioration and compensatory mechanisms. Circ.*107*, 984–991.

Hibi, M., Lin, A., Smeal, T., Minden, A., and Karin, M. (1993). Identification of an oncoprotein- and UV-responsive protein kinase that binds and potentiates the c-Jun activation domain. Genes Dev. *7*, 2135–2148.

Hilfiker-Kleiner, D., Hilfiker, A., Castellazzi, M., Wollert, K.C., Trautwein, C., Schunkert, H., and Drexler, H. (2006). JunD attenuates phenylephrine-mediated cardiomyocyte hypertrophy by negatively regulating AP-1 transcriptional activity. Cardiovasc. Res. *71*, 108–117.

Hilfiker-Kleiner, D., Hilfiker, A., Kaminski, K., Schaefer, A., Park, J.-K., Michel, K., Quint, A., Yaniv, M., Weitzman, J.B., and Drexler, H. (2005). Lack of JunD promotes Pressure Overload–induced apoptosis, hypertrophic growth, and angiogenesis in the Heart. Circ. *112*, 1470-1477

Hirota, H., Chen, J., Betz, U.A., Rajewsky, K., Gu, Y., Ross, J., Müller, W., and Chien, K.R. (1999). Loss of a gp130 cardiac muscle cell survival pathway is a critical event in the onset of heart failure during biomechanical stress. Cell *97*, 189–198.

Hirota, H., Yoshida, K., Kishimoto, T., and Taga, T. (1995). Continuous activation of gp130, a

signal-transducing receptor component for interleukin 6-related cytokines, causes myocardial hypertrophy in mice. Proc. Natl. Acad. Sci. USA *92*, 4862–4866.

Hochhauser, E., Kivity, S., Offen, D., Maulik, N., Otani, H., Pannet, H., Shneyvays, V., Shainberg, A., Goldshtaub, V., Tobar, A., et al. (2003). Bax ablation protects against myocardial ischemia- reperfusion injury in transgenic mice. Am. J. Physiol. Heart Circ. Physiol. *284*, H2351–H2359.

Holler, N., Zaru, R., Micheau, O., Thome, M., Attinger, A., Valitutti, S., Bodmer, J.L., Schneider, P., Seed, B., and Tschopp, J. (2000). Fas triggers an alternative, caspase-8-independent cell death pathway using the kinase RIP as effector molecule. Nat. Immunol. *1*, 489–495.

Hu, W.H., Johnson, H., and Shu, H.B. (2000). Activation of NFκB by FADD, Casper, and caspase-8. J. Biol. Chem. *275*, 10838–10844.

Huang, Y., Wright, C.D., Kobayashi, S., Healy, C.L., Elgethun, M., Cypher, A., Liang, Q., and O'Connell, T.D. (2008). GATA4 is a survival factor in adult cardiac myocytes but is not required for α_1-adrenergic receptor survival signaling. Am. J. Physiol. Heart Circ. Physiol. *295*, 699–707.

Ieda, M., Umezawa, Y., Tsuchihashi, T., Ivey, K.N., Ross, R.S., Hong, T.-T., Shaw, R.M., and Srivastava, D. (2009). Cardiac fibroblasts regulate myocardial proliferation through β1-integrin signaling. Dev. Cell *16*, 233–244.

Imahashi, K., Schneider, M.D., Steenbergen, C., and Murphy, E. (2004). Transgenic expression of Bcl-2 modulates energy metabolism, prevents cytosolic acidification during ischemia, and reduces ischemia/reperfusion injury. Circ. Res. *95*, 734–741.

Inaba, N., Sato, N., Ijichi, M., Fukazawa, I., Nito, A., Takamizawa, H., Lüben, G., and Bohn, H. (1984). The immunocytochemical location of two membrane-associated placental tissue proteins in human and cynomolgus monkey placentae. Tumour Biol. *5*, 75–85.

Inagaki, K., Begley, R., Ikeno, F., and Mochly-Rosen, D. (2005). Cardioprotection by ε-protein kinase C activation from ischemia: continuous delivery and antiarrhythmic effect of an epsilon-protein kinase C-activating peptide. Circ. *111*, 44–50.

Inagaki, K., Hahn, H.S., Dorn, G.W., and Mochly-Rosen, D. (2003). Additive protection of the ischemic heart *ex vivo* by combined treatment with δ-protein kinase C inhibitor and epsilon-protein kinase C activator. Circ. *108*, 869–875.

Inagaki, K., Koyanagi, T., Berry, N.C., Sun, L., and Mochly-Rosen, D. (2008). Pharmacological inhibition of ε-protein kinase C attenuates cardiac fibrosis and dysfunction in hypertension-induced heart failure. Hypertension *51*, 1565–1569.

Inoue, H., and Yamanaka, S. (2011). The use of induced pluripotent stem cells in drug development. Clin. Pharmacol. Ther. *89*, 655–661.

Itzhaki, I., Maizels, L., Huber, I., Zwi-Dantsis, L., Caspi, O., Winterstern, A., Feldman, O., Gepstein, A., Arbel, G., Hammerman, H., et al. (2011). Modelling the long QT syndrome with induced pluripotent stem cells. Nature *471*, 225–229.

Izumiya, Y., Kim, S., Izumi, Y., Yoshida, K., Yoshiyama, M., Matsuzawa, A., Ichijo, H., and Iwao, H. (2003). Apoptosis signal-regulating kinase 1 plays a pivotal role in angiotensin II-induced cardiac hypertrophy and remodeling. Circ. Res. *93*, 874–883.

Jacot, J.G., McCulloch, A.D., and Omens, J.H. (2008). Substrate stiffness affects the functional maturation of neonatal rat ventricular myocytes. Biophys. J. *95*, 3479–3487.

Jeremias, I., Kupatt, C., Martin-Villalba, A., Habazettl, H., Schenkel, J., Boekstegers, P., and Debatin, K.M. (2000). Involvement of CD95/Apo1/Fas in cell death after myocardial ischemia. Circ. *102*, 915–920.

Kai, H., Muraishi, A., Sugiu, Y., Nishi, H., Seki, Y., Kuwahara, F., Kimura, A., Kato, H., and Imaizumi, T. (1998). Expression of Proto-oncogenes and Gene Mutation of Sarcomeric Proteins in Patients With Hypertrophic Cardiomyopathy. Circ. *83*, 595–601.

Kaiser, R.A., Kaiser, R.A., Liang, Q., Bueno, O., Huang, Y., Lackey, T., Klevitsky, R., Hewett, T.E., and Molkentin, J.D. (2005). Genetic Inhibition or Activation of JNK1/2 Protects the Myocardium from Ischemia-Reperfusion-induced Cell Death in Vivo. J. Biol. Chem. *280*, 602–608.

Kaiser, R.A., Bueno, O.F., Lips, D.J., Doevendans, P.A., Jones, F., Kimball, T.F., and Molkentin, J.D. (2004). Targeted inhibition of p38 mitogen-activated protein kinase antagonizes cardiac injury and cell death following ischemia-reperfusion *in vivo*. J. Biol. Chem. *279*, 15524–15530.

Kaneko, S., Chen, X., Lu, P., Yao, X., Wright, T.G., Rajurkar, M., Kariya, K.-I., Mao, J., Ip, Y.T., and Xu, L. (2011). Smad inhibition by the Ste20 kinase Misshapen. Proc. Natl. Acad. Sci. USA *108*, 11127–11132.

Kang, P.M., and Izumo, S. (2000). Apoptosis and Heart Failure: A critical review of the literature. Circ. Res. *86*, 1107–1113.

Kao, Y.H., Liou, J.P., Chung, C.C., Lien, G.S., Kuo, C.C., Chen, S.A., and Chen, Y.J. (2013). Histone deacetylase inhibition improved cardiac functions with direct antifibrotic activity in heart failure. Int. J. Cardiol. *168*, 4178–4183.

Karakikes, I., Senyei, G.D., Hansen, J., Kong, C.-W., Azeloglu, E.U., Stillitano, F., Lieu, D.K., Wang, J., Ren, L., Hulot, J.-S., et al. (2014). Small molecule-mediated directed differentiation of human embryonic stem cells toward ventricular cardiomyocytes. Stem Cells Transl. Med. *3*, 18–31.

Karch, J., Kwong, J.Q., Burr, A.R., Sargent, M.A., Elrod, J.W., Peixoto, P.M., Martinez-Caballero, S., Osinska, H., Cheng, E.H.Y., Robbins, J., et al. (2013). Bax and Bak function as the outer membrane component of the mitochondrial permeability pore in regulating necrotic cell death in mice. Elife *2*, 1-21

Katz, C., Levy-Beladev, L., Rotem-Bamberger, S., Rito, T., Rüdiger, S.G.D., and Friedler, A. (2011). Studying protein-protein interactions using peptide arrays. Chem. Soc. Rev. *40*, 2131–2145.

Kerkela, R., Grazette, L., Yacobi, R., Iliescu, C., Patten, R., Beahm, C., Walters, B., Shevtsov, S., Pesant, S., Clubb, F.J., et al. (2006). Cardiotoxicity of the cancer therapeutic agent imatinib mesylate. Nat. Med. *12*, 908–916.

Khan, J.M., Lyon, A.R., and Harding, S.E. (2013). The case for induced pluripotent stem cell-derived cardiomyocytes in pharmacological screening. Br. J. Pharmacol. *169*, 304–317.

Kim, A.S., Miller, E.J., Wright, T.M., Li, J., Qi, D., Atsina, K., Zaha, V., Sakamoto, K., and Young, L.H. (2011). A small molecule AMPK activator protects the heart against ischemia–reperfusion injury. J. Mol. Cell Cardiol. *51*, 24–32.

Kim, J.K., Pedram, A., Razandi, M., and Levin, E.R. (2006). Estrogen prevents cardiomyocyte apoptosis through inhibition of reactive oxygen species and differential regulation of p38 kinase isoforms. J. Biol. Chem. *281*, 6760–6767.

Kimura, T.E., Jin, J., Zi, M., Prehar, S., Liu, W., Oceandy, D., Abe, J.I., Neyses, L., Weston, A.H., Cartwright, E.J., et al. (2010). Targeted deletion of the extracellular signal-regulated protein kinase 5 attenuates hypertrophic response and promotes pressure overload-induced apoptosis in the heart. Circ. Res. *106*, 961–U282.

Kita-Matsuo, H., Barcova, M., Prigozhina, N., Salomonis, N., Wei, K., Jacot, J.G., Nelson, B., Spiering, S., Haverslag, R., Kim, C., et al. (2009). Lentiviral vectors and protocols for creation of stable hESC lines for fluorescent tracking and drug resistance selection of cardiomyocytes. PLoS ONE *4*, e5046.

Klein, G., Schaefer, A., Hilfiker-Kleiner, D., Oppermann, D., Shukla, P., Quint, A., Podewski, E., Hilfiker, A., Schröder, F., Leitges, M., et al. (2014). Increased Collagen Deposition and Diastolic Dysfunction but Preserved Myocardial Hypertrophy After Pressure Overload in Mice Lacking PKCε. Circ. Res. *96*, 748–755.

Knaapen, M.W., Davies, M.J., De Bie, M., Haven, A.J., Martinet, W., and Kockx, M.M. (2001). Apoptotic versus autophagic cell death in heart failure. Cardiovasc. Res. *51*, 304–312.

Knight, R.J., and Buxton, D.B. (1996). Stimulation of c-Jun Kinase and Mitogen-Activated Protein Kinase by Ischemia and Reperfusion in the Perfused Rat Heart. Biochem. Biophys. Res. Commun. *218*, 83–88.

Kokoszka, J.E., Waymire, K.G., Levy, S.E., Sligh, J.E., Cai, J., Jones, D.P., MacGregor, G.R., and Wallace, D.C. (2004). The ADP/ATP translocator is not essential for the mitochondrial permeability transition pore. Nature *427*, 461–465.

Kola, I., and Landis, J. (2004). Can the pharmaceutical industry reduce attrition rates? Nat. Rev. Drug Disc. *3*, 711–715.

Kolfschoten, I.G.M., van Leeuwen, B., Berns, K., Mullenders, J., Beijersbergen, R.L., Bernards, R., Voorhoeve, P.M., and Agami, R. (2005). A genetic screen identifies PITX1 as a suppressor of RAS activity and tumorigenicity. Cell *121*, 849–858.

Kompa, A.R., See, F., Lewis, D.A., Adrahtas, A., Cantwell, D.M., Wang, B.H., and Krum, H. (2008). Long-term but not short-term p38 mitogen-activated protein kinase inhibition improves cardiac function and reduces cardiac remodeling post-myocardial infarction. J. Pharmacol. Exp. Ther. *325*, 741–750.

Kong, J.Y., Klassen, S.S., and Rabkin, S.W. (2005). Ceramide activates a mitochondrial p38 mitogen-activated protein kinase: a potential mechanism for loss of mitochondrial transmembrane potential and apoptosis. Mol. Cell Biochem. *278*, 39–51.

Kong, L., Andrassy, M., Chang, J.S., Huang, C., Asai, T., Szabolcs, M.J., Homma, S., Liu, R., Zou, Y.S., Leitges, M., et al. (2008). PKCβ modulates ischemia-reperfusion injury in the heart. Am. J. Physiol. Heart Circ. Physiol. *294*, H1862–H1870.

Kontaridis, M.I., Yang, W., Bence, K.K., Cullen, D., Wang, B., Bodyak, N., Ke, Q., Hinek, A., Kang, P.M., Liao, R., et al. (2008). Deletion of *Ptpn11* (Shp2) in cardiomyocytes causes dilated cardiomyopathy via effects on the extracellular signal−regulated kinase/mitogen-activated protein kinase and RhoA signaling pathways. Circ. *117*, 1423–1435.

Koopman, G., Reutelingsperger, C.P., Kuijten, G.A., Keehnen, R.M., Pals, S.T., and van Oers, M.H. (1994). Annexin V for flow cytometric detection of phosphatidylserine expression on B cells undergoing apoptosis. Blood *84*, 1415–1420.

Kostin, S., Pool, L., Elsässer, A., Hein, S., Drexler, H.C.A., Arnon, E., Hayakawa, Y., Zimmermann, R., Bauer, E., Klövekorn, W.-P., et al. (2003). Myocytes die by multiple mechanisms in failing human hearts. Circ. Res. *92*, 715–724.

Kostyak, J.C., Hunter, J.C., and Korzick, D.H. (2006). Acute PKCδ inhibition limits ischaemia-reperfusion injury in the aged rat heart: role of GSK-3β. Cardiovasc. Res. *70*, 325–334.

Koyanagi, T., Noguchi, K., Ootani, A., Inagaki, K., Robbins, R.C., and Mochly-Rosen, D. (2007). Pharmacological inhibition of PKCε suppresses chronic inflammation in murine cardiac transplantation model. J. Mol. Cell Cardiol. *43*, 517–522.

Koziris, L.P., Hickson, R.C., Chatterton, R.T., Groseth, R.T., Christie, J.M., Goldflies, D.G., and Unterman, T.G. (1999). Serum levels of total and free IGF-I and IGFBP-3 are increased and maintained in long-term training. J. Appl. Physiol. *86*, 1436–1442.

Krystof, V., Chamrád, I., Jorda, R., and Kohoutek, J. (2010). Pharmacological targeting of CDK9 in cardiac hypertrophy. Med. Res. Rev. *30*, 646–666.

Kubota, T., McTiernan, C.F., Frye, C.S., Slawson, S.E., Lemster, B.H., Koretsky, A.P., Demetris, A.J., and Feldman, A.M. (1997a). Dilated cardiomyopathy in transgenic mice with cardiac-specific overexpression of tumor necrosis factor-alpha. Circ. Res. *81*, 627–635.

Kubota, T., McTiernan, C.F., Frye, C.S., Demetris, A.J., and Feldman, A.M. (1997b). Cardiac-specific overexpression of tumor necrosis factor-alpha causes lethal myocarditis in transgenic mice. J. Card. Fail. *3*, 117–124.

Kuida, K., Haydar, T.F., Kuan, C.Y., Gu, Y., Taya, C., Karasuyama, H., Su, M.S., Rakic, P., and Flavell, R.A. (1998). Reduced apoptosis and cytochrome c-mediated caspase activation in mice lacking caspase 9. Cell *94*, 325–337.

Kumphune, S., Bassi, R., Jacquet, S., Sicard, P., Clark, J.E., Verma, S., Avkiran, M., O'Keefe, S.J., and Marber, M.S. (2010). A chemical genetic approach reveals that p38alpha MAPK activation by diphosphorylation aggravates myocardial infarction and is prevented by the direct binding of SB203580. J. Biol. Chem. *285*, 2968–2975.

Kurrelmeyer, K.M., Michael, L.H., Baumgarten, G., Taffet, G.E., Peschon, J.J., Sivasubramanian, N., Entman, M.L., and Mann, D.L. (2000). Endogenous tumor necrosis factor protects the adult cardiac myocyte against ischemic-induced apoptosis in a murine model of acute myocardial infarction. Proc. Natl. Acad. Sci. USA *97*, 5456–5461.

Kuschel, M., Karczewski, P., Hempel, P., Schlegel, W.P., Krause, E.G., and Bartel, S. (1999). Ser16 prevails over Thr17 phospholamban phosphorylation in the beta-adrenergic regulation of cardiac relaxation. Am. J. Physiol. *276*, 1625–1633.

Kyoi, S., Otani, H., Matsuhisa, S., Akita, Y., Tatsumi, K., Enoki, C., Fujiwara, H., Imamura, H., Kamihata, H., and Iwasaka, T. (2006). Opposing effect of p38 MAP kinase and JNK inhibitors on the development of heart failure in the cardiomyopathic hamster. Cardiovasc Res *69*, 888–898.

Kyriakis, J.M., Carpenter, M.K., Avruch, J., Rosler, E.S., Fisk, G.J., Brandenberger, R., Ares, X., Miura, T., Lucero, M., and Rao, M.S. (2012). Mammalian MAPK Signal Transduction Pathways Activated by Stress and Inflammation: A 10-Year Update. Physiol. Rev. *92*, 689–

737.

Kytö, V., Saraste, A., Saukko, P., Henn, V., Pulkki, K., Vuorinen, T., and Voipio-Pulkki, L.-M. (2004). Apoptotic cardiomyocyte death in fatal myocarditis. Am. J. Cardiol. *94*, 746–750.

LaBaer, J., Garrett, M.D., Stevenson, L.F., Slingerland, J.M., Sandhu, C., Chou, H.S., Fattaey, A., and Harlow, E. (1997). New functional activities for the p21 family of CDK inhibitors. Genes Dev. *11*, 847–862.

Laflamme, M.A., Chen, K.Y., Naumova, A.V., Muskheli, V., Fugate, J.A., Dupras, S.K., Reinecke, H., Xu, C., Hassanipour, M., Police, S., et al. (2007). Cardiomyocytes derived from human embryonic stem cells in pro-survival factors enhance function of infarcted rat hearts. Nat. Biotechnol. *25*, 1015–1024.

Lamothe, B., Lai, Y., Xie, M., Schneider, M.D., and Darnay, B.G. (2013). TAK1 Is essential for osteoclast differentiation and is an important modulator of cell death by apoptosis and necroptosis. Mol. Cell Biol. *33*, 582–595.

Lee, J.D., Ulevitch, R.J., and Han, J.H. (1995). Primary structure of BMK1: A new mammalian MAP kinase. Biochem. Biophys. Res. Commun. *213*, 715–724.

Lee, P., Sata, M., Lefer, D.J., Factor, S.M., Walsh, K., and Kitsis, R.N. (2003). Fas pathway is a critical mediator of cardiac myocyte death and MI during ischemia-reperfusion in vivo. Am. J. Physiol. Heart Circ. Physiol. *284*, H456–H463.

Lee, Y.K., Ng, K.M., Chan, Y.C., Lai, W.H., Au, K.W., Ho, C.Y.J., Wong, L.Y., Lau, C.P., Tse, H.F., and Siu, C.W. (2010). Triiodothyronine promotes cardiac differentiation and maturation of embryonic stem cells via the classical genomic pathway. Mol. Endocrinol. *24*, 1728–1736.

Lee, Y., Lee, H.Y., Hanna, R.A., and Gustafsson, A.B. (2011). Mitochondrial autophagy by Bnip3 involves Drp1-mediated mitochondrial fission and recruitment of Parkin in cardiac myocytes. Am. J. Physiol-Heart Circ. *301*, H1924–H1931.

Leschik, J., Stefanovic, S., Brinon, B., and Pucéat, M. (2008). Cardiac commitment of primate embryonic stem cells. Nat. Protoc. *3*, 1381–1387.

Li, D., Tapscoft, T., Gonzalez, O., Burch, P.E., Quiñones, M.A., Zoghbi, W.A., Hill, R., Bachinski, L.L., Mann, D.L., and Roberts, R. (1999). Desmin mutation responsible for idiopathic dilated cardiomyopathy. Circ. *100*, 461–464.

Li, H.-L., Yin, R., Chen, D., Liu, D., Wang, D., Yang, Q., and Dong, Y.-G. (2007). Long-term activation of adenosine monophosphate-activated protein kinase attenuates pressure-overload-induced cardiac hypertrophy. J. Cell. Biochem. *100*, 1086–1099.

Li, M., Georgakopoulos, D., Lu, G., Hester, L., Kass, D.A., Hasday, J., and Wang, Y. (2005). p38 MAP kinase mediates inflammatory cytokine induction in cardiomyocytes and extracellular matrix remodeling in heart. Circ. *111*, 2494–2502.

Li, R.K., Li, G., Mickle, D.A., Weisel, R.D., Merante, F., Luss, H., Rao, V., Christakis, G.T., and Williams, W.G. (1997). Overexpression of transforming growth factor-β1 and insulin-like growth factor-I in patients with idiopathic hypertrophic cardiomyopathy. Circ. *96*, 874–881.

Li, W., Wei, W., Zhu, S., Zhu, J., Shi, Y., Lin, T., Hao, E., Hayek, A., Deng, H., and Ding, S. (2009a). Generation of rat and human induced pluripotent stem cells by combining genetic reprogramming and chemical inhibitors. Cell Stem Cell *4*, 16–19.

Li, Y., Liang, J., Siu, T., Hu, E., Rossi, M.A., Barnett, S.F., Defeo-Jones, D., Jones, R.E.,

Robinson, R.G., Leander, K., et al. (2009b). Allosteric inhibitors of Akt1 and Akt2: discovery of [1,2,4]triazolo[3,4-f][1,6]naphthyridines with potent and balanced activity. Bioorg. Med. Chem. Lett. *19*, 834–836.

Lian, X., Zhang, J., Azarin, S.M., Zhu, K., Hazeltine, L.B., Bao, X., Hsiao, C., Kamp, T.J., and Palecek, S.P. (2012). Directed cardiomyocyte differentiation from human pluripotent stem cells by modulating Wnt/β-catenin signaling under fully defined conditions. Nat. Protoc. *8*, 162–175.

Liang, Q., Wiese, R.J., Bueno, O.F., Dai, Y.S., Entman, M.L., and Molkentin, J.D. (2001). The transcription factor GATA4 is activated by extracellular signal-regulated kinase 1- and 2-mediated phosphorylation of serine 105 in cardiomyocytes. Mol. Cell Biol. *21*, 7460–7469.

Liang, Q., Bueno, O.F., Wilkins, B.J., Kuan, C.-Y., Xia, Y., and Molkentin, J.D. (2003). c-Jun N-terminal kinases (JNK) antagonize cardiac growth through cross-talk with calcineurin-NFAT signaling. EMBO J. *22*, 5079–5089.

Liao, P., Georgakopoulos, D., Kovacs, A., Zheng, M., Lerner, D., Pu, H., Saffitz, J., Chien, K., Xiao, R.P., Kass, D.A., et al. (2001). The in vivo role of p38 MAP kinases in cardiac remodeling and restrictive cardiomyopathy. Proc. Natl. Acad. Sci. USA *98*, 12283–12288.

Liao, P., Wang, S.Q., Wang, S., Zheng, M., Zheng, M., Zhang, S.J., Cheng, H., Wang, Y., and Xiao, R.P. (2002). p38 mitogen-activated protein kinase mediates a negative inotropic effect in cardiac myocytes. Circ. Res. *90*, 190–196.

Leist, M., Single, B., Castoldi, A.F., Kühnle, S., and Nicotera, P. (1997). Intracellular Adenosine Triphosphate (ATP) concentration: A switch in the decision between apoptosis and necrosis. J. Exp. Med. *185*, 1481–1486.

Lieu, D.K., Liu, J., Siu, C.W., McNerney, G.P., Tan, T.-H., Abu-Khalil, A., Huser, T., and Li, R.A. (2009). Absence of transverse tubules contributes to non-uniform Ca^{2+} wavefronts in mouse and human embryonic stem cell–derived cardiomyocytes. Stem Cells Dev. *18*, 1493–1500.

Liggett, S.B., Tepe, N.M., Lorenz, J.N., Canning, A.M., Jantz, T.D., Mitarai, S., Yatani, A., and Dorn, G.W. (2000). Early and delayed consequences of β_2-adrenergic receptor overexpression in mouse hearts: critical role for expression level. Circ. *101*, 1707–1714.

Lim, S.Y., Cao, F., Davidson, S.M., Wagner, R.A., Mocanu, M.M., Wilson, K.D., Yellon, D.M., Xie, X., Smith, C.C.T., Fu, J.D., et al. (2007). The cardioprotective effect of necrostatin requires the cyclophilin-D component of the mitochondrial permeability transition pore. Cardiovasc. Drugs Ther. *21*, 467–469.

Lin, Y., Devin, A., Rodriguez, Y., and Liu, Z.G. (1999). Cleavage of the death domain kinase RIP by Caspase-8 prompts TNF-induced apoptosis. Genes Dev. *13*, 2514–2526.

Ling, H., Zhang, T., Pereira, L., Means, C.K., Cheng, H., Gu, Y., Dalton, N.D., Peterson, K.L., Chen, J., Bers, D., et al. (2009). Requirement for Ca^{2+}/calmodulin–dependent kinase II in the transition from pressure overload–induced cardiac hypertrophy to heart failure in mice. J. Clin. Invest. *119*, 1230.

Lips, D.J., Bueno, O.F., Wilkins, B.J., Purcell, N.H., Kaiser, R.A., Lorenz, J.N., Voisin, L., Saba-El-Leil, M.K., Meloche, S., Pouysségur, J., et al. (2004). MEK1-ERK2 signaling pathway protects myocardium from ischemic injury in vivo. Circ. *109*, 1938–1941.

Liu, A.W., Wang, Z., Cai, J., Xu, G., Zhao, X.L., Wu, Y., Jiang, T.H., Guan, Y., He, T.F., Cui,

L., et al. (2011). ShRNA-targeted MAP4K4 inhibits hepatocellular carcinoma growth. Clin. Cancer Res. *17*, 710–720

Liu, H., Pedram, A., and Kim, J.K. (2010). Oestrogen prevents cardiomyocyte apoptosis by suppressing p38 -mediated activation of p53 and by down-regulating p53 inhibition on p38. Cardiovasc. Res. *89*, 119–128.

Liu, H.H., Xie, M., Schneider, M.D., and Chen, Z.J. (2006). Essential role of TAK1 in thymocyte development and activation. Proc. Natl. Acad. Sci. USA *103*, 11677–11682.

Liu, H.-R., Gao, E., Hu, A., Tao, L., Qu, Y., Most, P., Koch, W.J., Christopher, T.A., Lopez, B.L., Alnemri, E.S., et al. (2004). Role of Omi/HtrA2 in apoptotic cell death after myocardial ischemia and reperfusion. Circ. *111*, 90–96.

Liu, J., Lieu, D.K., Siu, C.W., Fu, J.D., Tan, T.-H., and Li, R.A. (2009a). Facilitated maturation of Ca^{2+} handling properties of human embryonic stem cell-derived cardiomyocytes by calsequestrin expression. Am. J. Physiol. Cell Physiol. *297*, 152–159.

Liu, Q., Chen, X., MacDonnell, S.M., Kranias, E.G., Lorenz, J.N., Leitges, M., Houser, S.R., and Molkentin, J.D. (2009b). Protein Kinase Cα, but not PKCβ or PKCγ, regulates contractility and heart failure susceptibility: Implications for ruboxistaurin as a novel therapeutic approach. Circ. Res. *105*, 194–200.

Liu, Q., and Molkentin, J.D. (2011). Protein kinase Cα as a heart failure therapeutic target. J. Mol. Cell Cardiol. *51*, 474–478.

Liu, W., Zi, M., Jin, J., Prehar, S., Oceandy, D., Kimura, T.E., Lei, M., Neyses, L., Weston, A.H., Cartwright, E.J., et al. (2009c). Cardiac-specific deletion of Mkk4 reveals its role in pathological hypertrophic remodeling but not in physiological cardiac growth. Circ. Res. *104*, 905–914.

Liu, Y.H., Wang, D.H., Rhaleb, N.E., Yang, X.P., Xu, J., Sankey, S.S., Rudolph, A.E., and Carretero, O.A. (2005b). Inhibition of p38 mitogen-activated protein kinase protects the heart against cardiac remodeling in mice with heart failure resulting from myocardial infarction. J. Card. Fail. *11*, 74–81.

Liu, Z.-G. (2005). Molecular mechanism of TNF signaling and beyond. Cell Res. *15*, 24–27.

Lloyd-Jones, D., Adams, R., Carnethon, M., de Simone, G., Ferguson, T.B., Flegal, K., Ford, E., Furie, K., Go, A., Greenlund, K., et al. (2009). Heart disease and stroke statistics-2009 update: a report from the American Heart Association Statistics Committee and Stroke Statistics Subcommittee. Circ. *119*, 21–181.

Logue, S.E., Gustafsson, A.B., Samali, A., Saman, A., and Gottlieb, R.A. (2005). Ischemia/reperfusion injury at the intersection with cell death. J. Mol. Cell Cardiol. *38*, 21–33.

Lombardo, L.J., Lee, F.Y., Chen, P., Norris, D., Barrish, J.C., Behnia, K., Castaneda, S., Cornelius, L.A.M., Das, J., Doweyko, A.M., et al. (2004). Discovery of N-(2-chloro-6-methyl-phenyl)-2-(6-(4-(2-hydroxyethyl)-piperazin-1-yl)-2-methylpyrimidin-4-ylamino)thiazole-5-carboxamide (BMS-354825), a dual Src/Abl kinase inhibitor with potent antitumor activity in preclinical assays. J. Med. Chem. *47*, 6658–6661.

Lorenz, K., Schmitt, J.P., Schmitteckert, E.M., and Lohse, M.J. (2009). A new type of ERK1/2 autophosphorylation causes cardiac hypertrophy. Nat. Med. *15*, 75–83.

Lu, B., and Palacino, J. (2013). A novel human embryonic stem cell-derived Huntington's

disease neuronal model exhibits mutant huntingtin (mHTT) aggregates and soluble mHTT-dependent neurodegeneration. Faseb J. *27*, 1820–1829.

Ludwig, T.E., Bergendahl, V., Levenstein, M.E., Yu, J., Probasco, M.D., and Thomson, J.A. (2006). Feeder-independent culture of human embryonic stem cells. Nat. Methods *3*, 637–646.

Lundy, S.D., Zhu, W.-Z., Regnier, M., and Laflamme, M. (2013). Structural and functional maturation of cardiomyocytes derived From human pluripotent stem cells. Stem Cells Dev. *22*, 1991–2002.

Nichols A. (2007). High Content Screening as Screening Tool in Drug Discovery. In: Taylor Lancing D., Haskins R. J., and Giuliano A. K. eds. *High Content Screening: A powerful approach to Systems Cell Biology and Drug Discovery*, New Jersey: Humana Press, p379-414

Nichols M, Townsend N, Luengo-Fernandez R, Leal J, Gray A, Scarborough P, and Rayner M (2012). European cardiovascular disease statistics 2012. European Heart Network, Brussels, Eur. Soc. Cardiol. Sophia Antipolis.

Ma, D., Wei, H., Lu, J., Ho, S., Zhang, G., Sun, X., Oh, Y., Tan, S.H., Ng, M.L., Shim, W., et al. (2013). Generation of patient-specific induced pluripotent stem cell-derived cardiomyocytes as a cellular model of arrhythmogenic right ventricular cardiomyopathy. Eur. Heart J. *34*, 1122–1133.

Ma, J., Guo, L., Fiene, S.J., Anson, B.D., Thomson, J.A., Kamp, T.J., Kolaja, K.L., Swanson, B.J., and January, C.T. (2011). High purity human-induced pluripotent stem cell-derived cardiomyocytes: electrophysiological properties of action potentials and ionic currents. Am. J. Physiol. Heart Circ. Physiol. *301*, 2006–2017.

Ma, X.L., Kumar, S., Gao, F., Louden, C.S., Lopez, B.L., Christopher, T.A., Wang, C., Lee, J.C., Feuerstein, G.Z., and Yue, T.L. (1999). Inhibition of p38 Mitogen-Activated Protein Kinase Decreases Cardiomyocyte Apoptosis and Improves Cardiac Function After Myocardial Ischemia and Reperfusion. Circ. *99*, 1685–1691.

Ma, X., Liu, H., Foyil, S.R., Godar, R.J., Weinheimer, C.J., Hill, J.A., and Diwan, A. (2012). Impaired autophagosome clearance contributes to cardiomyocyte death in ischemia/reperfusion injury. Circ. *125*, 3170–3181.

MacDonnell, S.M., Weisser-Thomas, J., Kubo, H., Hanscome, M., Liu, Q., Jaleel, N., Berretta, R., Chen, X., Brown, J.H., Sabri, A.K., et al. (2009). CaMKII negatively regulates calcineurin-NFAT signaling in cardiac myocytes. Circ. Res. *105*, 316–325.

Machida, N., Machida, N., Umikawa, M., Umikawa, M., Takei, K., Takei, K., Sakima, N., Sakima, N., Myagmar, B.-E., Myagmar, B.-E., et al. (2004). Mitogen-activated protein kinase kinase kinase kinase 4 as a putative effector of Rap2 to activate the c-Jun N-terminal kinase. J. Biol. Chem. *279*, 15711–15714.

Mackay, K. (1999). An Inhibitor of p38 Mitogen-activated Protein Kinase Protects Neonatal Cardiac Myocytes from Ischemia. J. Biol. Chem. *274*, 6272–6279.

MacLellan, W.R., Garcia, A., Oh, H., Frenkel, P., Jordan, M.C., Roos, K.P., and Schneider, M.D. (2005). Overlapping roles of pocket proteins in the myocardium are unmasked by germ line deletion of p130 plus heart-specific deletion of Rb. Mol. Cell Biol. *25*, 2486–2497.

Magnus, D. (2010). Translating Stem Cell Research: Challenges at the Research Frontier. J.

Law Med. Ethics *38*, 267–276.

Maiuri, M.C., Le Toumelin, G., Criollo, A., Rain, J.-C., Gautier, F., Juin, P., Tasdemir, E., Pierron, G., Troulinaki, K., Tavernarakis, N., et al. (2007). Functional and physical interaction between Bcl-x_L and a BH3-like domain in Beclin-1. EMBO J. *26*, 2527–2539.

Mandel, Y., Weissman, A., Schick, R., Barad, L., Novak, A., Meiry, G., Goldberg, S., Lorber, A., Rosen, M.R., Itskovitz-Eldor, J., et al. (2012). Human embryonic and induced pluripotent stem cell-derived cardiomyocytes exhibit beat rate variability and power-law behavior. Circ. *125*, 883–893.

Mann, D.L. (2005). Targeted anticytokine therapy and the failing heart. Am. J. Cardiol. *95*, 9C–16C.

Mann, D.L., McMurray, J.J.V., Packer, M., Swedberg, K., Borer, J.S., Colucci, W.S., Djian, J., Drexler, H., Feldman, A., Kober, L., et al. (2004). Targeted anticytokine therapy in patients with chronic heart failure: results of the Randomized Etanercept Worldwide Evaluation (RENEWAL). Circ. *109*, 1594–1602.

Manning, G., Carreon, J.R., Shaner, N.C., Mahon, K.P., Steinbach, P.A., Kelley, S.O., and Tsien, R.Y. (2002). The Protein kinase complement of the human genome. Science *298*, 1912–1934.

Martindale, J.J., Fernandez, R., Thuerauf, D., Whittaker, R., Gude, N., Sussman, M.A., and Glembotski, C.C. (2006). Endoplasmic reticulum stress gene induction and protection from ischemia/reperfusion injury in the hearts of transgenic mice with a tamoxifen-regulated form of ATF6. Circ. Res. *98*, 1186–1193.

Marzo, I., Brenner, C., Zamzami, N., Jürgensmeier, J.M., Brozena, S., Vieira, H.L., Prévost, M.C., Xie, Z., Matsuyama, S., Reed, J.C., et al. (1998). Bax and adenine nucleotide translocator cooperate in the mitochondrial control of apoptosis. Science *281*, 2027–2031.

Matsui, Y., Takagi, H., Qu, X., Abdellatif, M., Sakoda, H., Asano, T., Levine, B., and Sadoshima, J. (2007). Distinct roles of autophagy in the heart during ischemia and reperfusion. Circ. *100*, 914–922.

Matsumoto-Ida, M., Takimoto, Y., Aoyama, T., Akao, M., Takeda, T., and Kita, T. (2006). Activation of TGF-β1-TAK1-p38 MAPK pathway in spared cardiomyocytes is involved in left ventricular remodeling after myocardial infarction in rats. Am. J. Physiol. Heart Circ. Physiol. *290*, H709–H715.

Matsunaga, K., Morita, E., Saitoh, T., Akira, S., Ktistakis, N.T., Izumi, T., Noda, T., and Yoshimori, T. (2010). Autophagy requires endoplasmic reticulum targeting of the PI3-kinase complex via Atg14L. J. Cell Biol. *190*, 511–521.

Matsunaga, K., Saitoh, T., Tabata, K., Omori, H., Satoh, T., Kurotori, N., Maejima, I., Shirahama-Noda, K., Ichimura, T., Isobe, T., et al. (2009). Two Beclin 1-binding proteins, Atg14L and Rubicon, reciprocally regulate autophagy at different stages. Nat. Cell Biol. *11*, 385–396.

Mayr, M., Chung, Y.L., Mayr, U., McGregor, E., Troy, H., Baier, G., Leitges, M., Dunn, M.J., Griffiths, J.R., and Xu, Q. (2004). Loss of PKC-δ alters cardiac metabolism. Am. J. Physiol. Heart Circ. Physiol. *287*, H937–H945.

McCaw, B.J., Chow, S.Y., Wong, E.S.M., Tan, K.L., Guo, H., and Guy, G.R. (2005). Identification and characterization of mErk5-T, a novel Erk5/Bmk1 splice variant. Gene *345*,

183–190.

McDevitt, T.C., Laflamme, M.A., and Murry, C.E. (2005). Proliferation of cardiomyocytes derived from human embryonic stem cells is mediated via the IGF/PI 3-kinase/Akt signaling pathway. J. Mol. Cell Cardiol. *39*, 865–873.

McMullen, J.R., Shioi, T., Huang, W.-Y., Zhang, L., Tarnavski, O., Bisping, E., Schinke, M., Kong, S., Sherwood, M.C., Brown, J., et al. (2004). The insulin-like growth factor 1 receptor induces physiological heart growth via the phosphoinositide 3-kinase(p110alpha) pathway. J. Biol. Chem. *279*, 4782–4793.

Menick, D.R., Renaud, L., Buchholz, A., Müller, J.G., Zhou, H., Kappler, C.S., Kubalak, S.W., Conway, S.J., and Xu, L. (2007). Regulation of Ncx1 gene expression in the normal and hypertrophic heart. Ann. N Y Acad. Sci. *1099*, 195–203.

Mercola, M., Ruiz-Lozano, P., and Schneider, M.D. (2011). Cardiac muscle regeneration: lessons from development. Genes Dev. *25*, 299–309.

Merkle, S., Frantz, S., Schön, M.P., Bauersachs, J., Buitrago, M., Frost, R.J.A., Schmitteckert, E.M., Lohse, M.J., and Engelhardt, S. (2007). A role for caspase-1 in heart failure. Circ. Res. *100*, 645–653.

Métrich, M., Lucas, A., Gastineau, M., Samuel, J.-L., Heymes, C., Morel, E., and Lezoualc'h, F. (2008). Epac mediates beta-adrenergic receptor-induced cardiomyocyte hypertrophy. Circ. Res. *102*, 959–965.

Mihaylova, M.M., and Shaw, R.J. (2011). The AMPK signalling pathway coordinates cell growth, autophagy and metabolism. Nat. Cell Biol. *13*, 1016–1023.

Milano, C.A., Dolber, P.C., Rockman, H.A., Bond, R.A., Venable, M.E., Allen, L.F., and Lefkowitz, R.J. (1994). Myocardial expression of a constitutively active alpha 1B-adrenergic receptor in transgenic mice induces cardiac hypertrophy. Proc. Natl. Acad. Sci. USA *91*, 10109–10113.

Milano, G., Morel, S., Bonny, C., Samaja, M., Segesser, von, L.K., Nicod, P., and Vassalli, G. (2006). A peptide inhibitor of c-Jun NH2-terminal kinase reduces myocardial ischemia-reperfusion injury and infarct size *in vivo*. Am. J. Physiol. Heart Circ. *292*, 1828–1835.

Miled, C., Miled, C., Pontoglio, M., Pontoglio, M., Garbay, S., Garbay, S., Yaniv, M., Yaniv, M., Weitzman, J.B., and Weitzman, J.B. (2005). A genomic map of p53 binding sites identifies novel p53 targets involved in an apoptotic network. Cancer Res. *65*, 5096–5104.

Minamino, T., Yujiri, T., Papst, P.J., Chan, E.D., Johnson, G.L., and Terada, N. (1999). MEKK1 suppresses oxidative stress-induced apoptosis of embryonic stem cell-derived cardiac myocytes. Proc. Natl. Acad. Sci. USA *96*, 15127–15132.

Minamino, T., Komuro, I., and Kitakaze, M. (2010). Endoplasmic reticulum stress as a therapeutic target in cardiovascular disease. Circ. Res. *107*, 1071–1082.

Minamino, T., Yujiri, T., Terada, N., Taffet, G.E., Michael, L.H., Johnson, G.L., and Schneider, M.D. (2002). MEKK1 is essential for cardiac hypertrophy and dysfunction induced by Gq. Proc. Natl. Acad. Sci. USA *99*, 3866–3871.

Mioulane, M., Kidder, B.L., Bailey, S.N., Földes, G., Palmer, S., Ali, S.M., Ali, N.N., Knott, J.G., Carpenter, A.E., Schneider, M.D., et al. (2012). Development of high content imaging methods for cell death detection in human pluripotent stem cell-derived cardiomyocytes. J.

Cardiovasc. Transl. Res. *5*, 593–604.

Miyata, S., Minobe, W., Bristow, M.R., and Leinwand, L.A. (2000). Myosin heavy chain isoform expression in the failing and nonfailing human heart. Circ. Res. *86*, 386–390.

Mochly-Rosen, D., Wu, G., Hahn, H., Osinska, H., Liron, T., Lorenz, J.N., Yatani, A., Robbins, J., and Dorn, G.W. (2000). Cardiotrophic effects of protein kinase C epsilon: analysis by in vivo modulation of PKCepsilon translocation. Circ. Res. *86*, 1173–1179.

Moffat, J., and Sabatini, D.M. (2006). Building mammalian signalling pathways with RNAi screens. Nat. Rev. Mol. Cell Biol. *7*, 177–187.

Molkentin, J.D. (2004). Calcineurin-NFAT signaling regulates the cardiac hypertrophic response in coordination with the MAPKs. Cardiovasc. Res. *63*, 467–475.

Mollova, M., Bersell, K., Walsh, S., Savla, J., Das, L.T., Park, S.-Y., Silberstein, L.E., Remedios, Dos, C.G., Graham, D., Colan, S., et al. (2013). Cardiomyocyte proliferation contributes to heart growth in young humans. Proc. Natl. Acad. Sci. USA *110*, 1446–1451.

Morales, A., Lee, H., Goñi, F.M., Kolesnick, R., and Fernandez-Checa, J.C. (2007). Sphingolipids and cell death. Apoptosis *12*, 923–939.

Morioka, S., Broglie, P., Omori, E., Ikeda, Y., Takaesu, G., Matsumoto, K., and Ninomiya-Tsuji, J. (2014). TAK1 kinase switches cell fate from apoptosis to necrosis following TNF stimulation. J. Cell Biol. *204*, 607–623.

Müller, M., Fleischmann, B.K., Selbert, S., Ji, G.J., Endl, E., Middeler, G., Müller, O.J., Schlenke, P., Frese, S., Wobus, A.M., et al. (2000). Selection of ventricular-like cardiomyocytes from ES cells in vitro. Faseb J. *14*, 2540–2548.

Mummery, C.L., Zhang, J., Ng, E.S., Elliott, D.A., Elefanty, A.G., and Kamp, T.J. (2012). Differentiation of human embryonic stem cells and induced pluripotent stem cells to cardiomyocytes: A methods overview. Circ. Res. *111*, 344–358.

Mummery, C.L., Davis, R.P., and Krieger, J.E. (2010). Challenges in using stem cells for cardiac repair. Science Transl. Med. *2*, 1–5.

Nakagawa, T., Shimizu, S., Watanabe, T., Yamaguchi, O., Otsu, K., Yamagata, H., Inohara, H., Kubo, T., and Tsujimoto, Y. (2005). Cyclophilin D-dependent mitochondrial permeability transition regulates some necrotic but not apoptotic cell death. Nature *434*, 652–658.

Nakai, A., Yamaguchi, O., Takeda, T., Higuchi, Y., Hikoso, S., Taniike, M., Omiya, S., Mizote, I., Matsumura, Y., Asahi, M., et al. (2007). The role of autophagy in cardiomyocytes in the basal state and in response to hemodynamic stress. Nat. Med. *13*, 619–624.

Nakao, K., Minobe, W., Roden, R., Bristow, M.R., and Leinwand, L.A. (1997). Myosin heavy chain gene expression in human heart failure. J. Clin. Invest. *100*, 2362–2370.

Nakayama, H., Chen, X., Baines, C.P., Klevitsky, R., Zhang, X., Zhang, H., Jaleel, N., Chua, B.H.L., Hewett, T.E., Robbins, J., et al. (2007). Ca^{2+}- and mitochondrial-dependent cardiomyocyte necrosis as a primary mediator of heart failure. J. Clin. Invest. *117*, 2431–2444.

Nam, Y.J., Mani, K., Ashton, A.W., Peng, C.F., Krishnamurthy, B., Hayakawa, Y., Lee, P., Korsmeyer, S.J., and Kitsis, R.N. (2004). Inhibition of both the extrinsic and intrinsic death pathways through nonhomotypic death-fold interactions. Mol. Cell *15*, 901–912.

Nam, Y.J., Mani, K., Wu, L., Peng, C.F., Calvert, J.W., Foo, R.S.Y., Krishnamurthy, B., Miao, W., Ashton, A.W., and Lefer, D.J. (2007). The apoptosis inhibitor ARC undergoes Ubiquitin-Proteasomal-mediated degradation in response to death stimuli identification of a degradation-resistant mutant. J. Biol. Chem. *282*, 5522–5528.

Narula, J., Haider, N., Virmani, R., DiSalvo, T.G., Kolodgie, F.D., Hajjar, R.J., Schmidt, U., Semigran, M.J., Dec, G.W., and Khaw, B.A. (1996). Apoptosis in myocytes in end-stage heart failure. N. Engl. J. Med. *335*, 1182–1189.

Narula, J., Pandey, P., Arbustini, E., Haider, N., Narula, N., Kolodgie, F.D., Bello, B.D., Semigran, M.J., Bielsa-Masdeu, A., and Dec, G.W. (1999). Apoptosis in heart failure: release of cytochrome c from mitochondria and activation of caspase-3 in human cardiomyopathy. Proc. Natl. Acad. Sci. USA *96*, 8144–8149.

Nemoto, S., Sheng, Z., and Lin, A. (1998). Opposing effects of Jun kinase and p38 mitogen-activated protein kinases on cardiomyocyte hypertrophy. Mol. Cell Biol. *18*, 3518–3526.

Nhan, T.Q., Liles, W.C., and Schwartz, S.M. (2006). Physiological functions of caspases beyond cell death. Am. J. Pathol. *169*, 729–737.

Nica, A.F., Tsao, C.C., Watt, J.C., Jiffar, T., Kurinna, S., Jurasz, P., Konopleva, M., Andreeff, M., Radomski, M.W., and Ruvolo, P.P. (2008). Ceramide promotes apoptosis in chronic myelogenous leukemia-derived K562 cells by a mechanism involving caspase-8 and JNK. Cell Cycle *7*, 3362–3370.

Nickson, P., Toth, A., and Erhardt, P. (2007). PUMA is critical for neonatal cardiomyocyte apoptosis induced by endoplasmic reticulum stress. Cardiovasc. Res. *73*, 48–56.

Nikolaou, K., Nikolaou, K., Tsagaratou, A., Tsagaratou, A., Eftychi, C., Eftychi, C., Kollias, G., Kollias, G., Mosialos, G., Mosialos, G., et al. (2012). Inactivation of the deubiquitinase CYLD in hepatocytes causes apoptosis, inflammation, fibrosis, and cancer. Cancer Cell *21*, 738–750.

Nishida, K., Yamaguchi, O., Hirotani, S., Hikoso, S., Higuchi, Y., Watanabe, T., Takeda, T., Osuka, S., Morita, T., Kondoh, G., et al. (2004). p38 mitogen-activated protein kinase plays a critical role in cardiomyocyte survival but not in cardiac hypertrophic growth in response to pressure overload. Mol. Cell Biol. *24*, 10611–10620.

Noma, T., Lemaire, A., Prasad, S.V.N., Barki-Harrington, L., Tilley, D.G., Chen, J., Le Corvoisier, P., Violin, J.D., Wei, H., Lefkowitz, R.J., et al. (2007). β-Arrestin–mediated β1-adrenergic receptor transactivation of the EGFR confers cardioprotection. J. Clin. Invest. *117*, 2445–2458.

Noseda, M., De Smith, A.J., Leja, T., Rao, P.H., Al-Beidh, F., Pavia, M.S.A., Blakemore, A.I., and Schneider, M.D. (2012). The Cdkn2a/2b tumour suppressor locus is a hot spot for genome instability in mouse cardiac progenitor cells. Cardiovasc. Res. *93*, 59–59.

Nunes, S.S., Miklas, J.W., Liu, J., Aschar-Sobbi, R., Xiao, Y., Zhang, B., Jiang, J., Massé, S., Gagliardi, M., Hsieh, A., et al. (2013). Biowire: a platform for maturation of human pluripotent stem cell-derived cardiomyocytes. Nat. Methods *10*, 781–787.

Okada, K.-I., Minamino, T., Tsukamoto, Y., Liao, Y., Tsukamoto, O., Takashima, S., Hirata, A., Fujita, M., Nagamachi, Y., Nakatani, T., et al. (2004). Prolonged endoplasmic reticulum stress in hypertrophic and failing heart after aortic constriction: possible contribution of endoplasmic reticulum stress to cardiac myocyte apoptosis. Circ. *110*, 705–712.

Olivetti, G., Abbi, R., Quaini, F., Kajstura, J., Cheng, W., Nitahara, J.A., Quaini, E., Di Loreto, C., Beltrami, C.A., Krajewski, S., et al. (1997). Apoptosis in the failing human heart. N. Engl. J. Med. *336*, 1131–1141.

Olson, E.N., Rual, J.F., Chakraborti, S., Chinnadurai, G., Das, S., Vijayalingam, S., Kar, P., Gibson, S.B., Ghosh, B., Samanta, K., et al. (2004). A decade of discoveries in cardiac biology. Nat. Med. *10*, 467–474.

Olson, T.M., Michels, V.V., Thibodeau, S.N., Tai, Y.S., and Keating, M.T. (1998). Actin mutations in dilated cardiomyopathy, a heritable form of heart failure. Science *280*, 750–752.

Omori, E., Omori, E., Matsumoto, K., Matsumoto, K., Zhu, S., Zhu, S., Smart, R.C., Smart, R.C., Ninomiya-Tsuji, J., and Ninomiya-Tsuji, J. (2010). Ablation of TAK1 upregulates reactive oxygen species and selectively kills tumor cells. Cancer. Res. *70*, 8417–8425.

ONeill, E., Rushworth, L., Baccarini, M., and Kolch, W. (2004). Role of the kinase MST2 in suppression of apoptosis by the proto-oncogene product Raf-1. Science *306*, 2267–2270.

Ono, K., and Han, J. (2000). The p38 signal transduction pathway: activation and function. Cell. Signal. *12*, 1–13.

Oster, H., Abraham, D., and Leitges, M. (2006). Expression of the protein kinase D (PKD) family during mouse embryogenesis. Gene Expres. Patt. *6*, 400–408.

Owens, D.M., and Keyse, S.M. (2007). Differential regulation of MAP kinase signalling by dual-specificity protein phosphatases. Oncogene *26*, 3203–3213.

Pandit, B., Sarkozy, A., Pennacchio, L.A., Carta, C., Oishi, K., Martinelli, S., Pogna, E.A., Schackwitz, W., Ustaszewska, A., Landstrom, A., et al. (2007). Gain-of-function RAF1 mutations cause Noonan and LEOPARD syndromes with hypertrophic cardiomyopathy. Nat. Genet. *39*, 1007–1012.

Paoletti, R., Maffei, A., Madaro, L., Notte, A., Stanganello, E., Cifelli, G., Carullo, P., Molinaro, M., Lembo, G., and Bouché, M. (2010). Protein kinase Cθ is required for cardiomyocyte survival and cardiac remodeling. Cell Death Dis *1*, 4–9.

Papanicolaou, K.N., Khairallah, R.J., Ngoh, G.A., Chikando, A., Luptak, I., O'Shea, K.M., Riley, D.D., Lugus, J.J., Colucci, W.S., Lederer, W.J., et al. (2011). Mitofusin-2 Maintains Mitochondrial Structure and Contributes to Stress-Induced Permeability Transition in Cardiac Myocytes. Mol. Cell Biol. *31*, 1309–1328.

Papanicolaou, K.N., Kikuchi, R., Ngoh, G.A., Coughlan, K.A., Dominguez, I., Stanley, W.C., and Walsh, K. (2012a). Mitofusins 1 and 2 Are Essential for Postnatal Metabolic Remodeling in Heart. Circ. Res. *111*, 1012–1025.

Papanicolaou, K.N., Ngoh, G.A., Dabkowski, E.R., O'Connell, K.A., Ribeiro, R.F.J., Stanley, W.C., and Walsh, K. (2012b). Cardiomyocyte deletion of mitofusin-1 leads to mitochondrial fragmentation and improves tolerance to ROS-induced mitochondrial dysfunction and cell death. Am. J. Physiol. Heart Circ. Physiol. *302*, 167–179.

Paricio, N., Feiguin, F., Boutros, M., Eaton, S., and Mlodzik, M. (1999). The Drosophila STE20-like kinase Misshapen is required downstream of the Frizzled receptor in planar polarity signaling. EMBO J. *18*, 4669–4678.

Parra, V., Parra, V., Eisner, V., Eisner, V., Chiong, M., Chiong, M., Criollo, A., Criollo, A., Moraga, F., Moraga, F., et al. (2007). Changes in mitochondrial dynamics during ceramide-

induced cardiomyocyte early apoptosis. Cardiovasc. Res. *77*, 387–397.

Parrizas, M., Saltiel, A.R., and LeRoith, D. (1997). Insulin-like growth factor 1 inhibits apoptosis using the phosphatidylinositol 3'-kinase and mitogen-activated protein kinase pathways. J. Biol. Chem. *272*, 154–161.

Patterson, C., Portbury, A.L., Schisler, J.C., and Willis, M.S. (2011). Tear me down: role of calpain in the development of cardiac ventricular hypertrophy. Circ. Res. *109*, 453–462.

Pattingre, S., Tassa, A., Qu, X., Garuti, R., Liang, X.H., Mizushima, N., Packer, M., Schneider, M.D., and Levine, B. (2005). Bcl-2 antiapoptotic proteins inhibit Beclin 1-dependent autophagy. Cell *122*, 927–939.

Petrich, B.G., Eloff, B.C., Lerner, D.L., Kovacs, A., Saffitz, J.E., Rosenbaum, D.S., and Wang, Y. (2004). Targeted activation of c-Jun N-terminal kinase *in vivo* induces restrictive cardiomyopathy and conduction defects. J. Biol. Chem. *279*, 15330–15338.

Petrich, B.G., Molkentin, J.D., and Wang, Y. (2003). Temporal activation of c-Jun N-terminal kinase in adult transgenic heart via cre-loxP-mediated DNA recombination. Faseb J. *17*, 749–751.

Pillai, R.S., Bhattacharyya, S.N., Artus, C.G., Zoller, T., Cougot, N., Basyuk, E., Bertrand, E., and Filipowicz, W. (2005). Inhibition of translational initiation by Let-7 MicroRNA in human cells. Science *309*, 1573–1576.

Pomerantz, B.J., Reznikov, L.L., Harken, A.H., and Dinarello, C.A. (2001). Inhibition of caspase 1 reduces human myocardial ischemic dysfunction via inhibition of IL-18 and IL-1beta. Proc. Natl. Acad. Sci. USA *98*, 2871–2876.

Pontén, A., Li, X., Thorén, P., Aase, K., Sjöblom, T., Östman, A., and Eriksson, U. (2003). Transgenic overexpression of platelet-derived growth factor-C in the mouse heart induces cardiac fibrosis, hypertrophy, and dilated cardiomyopathy. Am. J. Pathol. *163*, 673–682.

Potts, M.B., Vaughn, A.E., McDonough, H., Patterson, C., and Deshmukh, M. (2005). Reduced Apaf-1 levels in cardiomyocytes engage strict regulation of apoptosis by endogenous XIAP. J. Cell Biol. *171*, 925–930.

Potts, P.R., Singh, S., Knezek, M., Thompson, C.B., and Deshmukh, M. (2003). Critical function of endogenous XIAP in regulating caspase activation during sympathetic neuronal apoptosis. J. Cell Biol. *163*, 789–799.

Pufall, M.A., and Graves, B.J. (2002). Autoinhibitory domains: modular effectors of cellular regulation. Annu. Rev. Cell Dev. Biol. *18*, 421–462.

Purcell, N.H., Wilkins, B.J., York, A., Saba-El-Leil, M.K., Meloche, S., Robbins, J., and Molkentin, J.D. (2007). Genetic inhibition of cardiac ERK1/2 promotes stress-induced apoptosis and heart failure but has no effect on hypertrophy *in vivo*. Proc. Natl. Acad. Sci. USA *104*, 14074–14079.

Puri, V., Virbasius, J.V., Guilherme, A., and Czech, M.P. (2008). RNAi screens reveal novel metabolic regulators: RIP140, MAP4k4 and the lipid droplet associated fat specific protein (FSP) 27. Acta Physiol. *192*, 103–115.

Qi, M., and Elion, E.A. (2005). MAP kinase pathways. J. Cell Sci. *118*, 3569–3572.

Rais, Y., Zviran, A., Geula, S., Gafni, O., Chomsky, E., Viukov, S., Mansour, A.A., Caspi, I., Krupalnik, V., Zerbib, M., et al. (2013). Deterministic direct reprogramming of somatic cells to

pluripotency. Nature *502*, 65–70.

Ramirez, M.T., Sah, V.P., Zhao, X.L., Hunter, J.J., Chien, K.R., and Brown, J.H. (1997). The MEKK-JNK Pathway Is Stimulated by α1-Adrenergic Receptor and Ras Activation and Is Associated with in Vitroand in Vivo Cardiac Hypertrophy. J. Biol. Chem. *272*, 14057–14061.

Ramos, J.W. (2008). The regulation of extracellular signal-regulated kinase (ERK) in mammalian cells. Int. J. Biochem. Cell Biol. *40*, 2707–2719.

Rana, P., Anson, B., Engle, S., and Will, Y. (2012). Characterization of human-induced pluripotent stem cell-derived cardiomyocytes: bioenergetics and utilization in safety screening. Toxicol. Sci. *130*, 117–131.

Rao, C., Prodromakis, T., Kolker, L., Chaudhry, U.A.R., Trantidou, T., Sridhar, A., Weekes, C., Camelliti, P., Harding, S.E., Darzi, A., et al. (2013). The effect of microgrooved culture substrates on calcium cycling of cardiac myocytes derived from human induced pluripotent stem cells. Biomaterials *34*, 2399–2411.

Rao, D.D., Vorhies, J.S., Senzer, N., and Nemunaitis, J. (2009). siRNA vs. shRNA: Similarities and differences. Adv. Drug Deliv. Rev. *61*, 746–759.

Ravikumar, B., Futter, M., Jahreiss, L., Korolchuk, V.I., Lichtenberg, M., Luo, S., Massey, D.C.O., Menzies, F.M., Narayanan, U., Renna, M., et al. (2009). Mammalian macroautophagy at a glance. J. Cell Sci. *122*, 1707–1711.

Regan, C.P., Li, W., Boucher, D.M., Spatz, S., Su, M.S., and Kuida, K. (2002). Erk5-null mice display multiple extraembryonic vascular and embryonic cardiovascular defects. Proc. Natl. Acad. Sci. USA *99*, 9248–9253.

Reiser, P.J., Portman, M.A., Ning, X.H., and Schomisch Moravec, C. (2001). Human cardiac myosin heavy chain isoforms in fetal and failing adult atria and ventricles. Am. J. Physiol. Heart Circ. Physiol. *280*, 1814–1820.

Relling, D.P., Hintz, K.K., and Ren, J. (2003). Acute exposure of ceramide enhances cardiac contractile function in isolated ventricular myocytes. Br. J. Pharmacol. *140*, 1163–1168.

Remondino, A., Kwon, S.H., Communal, C., Pimentel, D.R., Sawyer, D.B., Singh, K., and Colucci, W.S. (2003). β-adrenergic receptor-stimulated apoptosis in cardiac myocytes is mediated by reactive oxygen species/c-Jun NH_2-terminal kinase-dependent activation of the mitochondrial pathway. Circ. Res. *92*, 136–138.

Riedl J. S. and Scott L. F. (2009). Caspases: Activation, Regulation, and Function In: X.-M. Yin, Z. Dong. eds. *Essentials of Apoptosis: A guide for Basic and Clinical Research*, ed. 2nd, New York: Humana Press, p3-24

Riggs, J.W., Barrilleaux, B.L., Varlakhanova, N., Bush, K.M., Chan, V., and Knoepfler, P.S. (2013). Induced Pluripotency and Oncogenic Transformation Are Related Processes. Stem Cells Dev. *22*, 37–50.

Risco, A., del Fresno, C., Mambol, A., Alsina-Beauchamp, D., MacKenzie, K.F., Yang, H.-T., Barber, D.F., Morcelle, C., Arthur, J.S.C., Ley, S.C., et al. (2012). p38γ and p38δ kinases regulate the Toll-like receptor 4 (TLR4)-induced cytokine production by controlling ERK1/2 protein kinase pathway activation. Proc. Natl. Acad. Sci. USA *109*, 11200–11205.

Robinton, D.A., and Daley, G.Q. (2012). The promise of induced pluripotent stem cells in research and therapy. Nature *481*, 295–305.

Rohrer, D.K., Desai, K.H., Jasper, J.R., Stevens, M.E., Regula, D.P., Barsh, G.S., Bernstein, D., and Kobilka, B.K. (1996). Targeted disruption of the mouse beta1-adrenergic receptor gene: developmental and cardiovascular effects. Proc. Natl. Acad. Sci. USA *93*, 7375–7380.

Rose, B.A., Force, T., and Wang, Y. (2010). Mitogen-activated protein kinase signaling in the heart: angels versus demons in a heart-breaking tale. Physiol. Rev. *90*, 1507–1546.

Roskoski, R. (2012). ERK1/2 MAP kinases: structure, function, and regulation. Pharmacol. Res. *66*, 105–143.

Rothermel, B.A., and Hill, J.A. (2008). Autophagy in load-induced heart disease. Circ. Res. *103*, 1363–1369.

Ruehr, M.L., Russell, M.A., and Bond, M. (2004). A-kinase anchoring protein targeting of protein kinase A in the heart. J. Mol. Cell Cardiol. *37*, 653–665.

Rybkin, I.I., Markham, D.W., Yan, Z., Bassel-Duby, R., Williams, R.S., and Olson, E.N. (2003). Conditional Expression of SV40 T-antigen in Mouse Cardiomyocytes Facilitates an Inducible Switch from Proliferation to Differentiation. J. Biol. Chem. *278*, 15927–15934.

Sachse et al., (2008). Exploring the Full Power of Combining High Throughput RNAi with High Content ReadOuts: From Target Discovery Screens to Drug Modifier Studies In: Haney A. S. ed. *High Content Screening: Science, Techniques and Applications*, New Jersey: Wiley, p145-185

Sadoshima, J., Montagne, O., Wang, Q., Yang, G., Warden, J., Liu, J., Takagi, G., Karoor, V., Hong, C., Johnson, G.L., et al. (2002). The MEKK1-JNK pathway plays a protective role in pressure overload but does not mediate cardiac hypertrophy. J. Clin. Invest. *110*, 271–279.

Sag, C.M., Wadsack, D.P., Khabbazzadeh, S., Abesser, M., Grefe, C., Neumann, K., Opiela, M.K., Backs, J., Olson, E.N., Brown, J.H., et al. (2009). Calcium/calmodulin-dependent protein kinase II contributes to cardiac arrhythmogenesis in heart failure. Circ. Heart Fail. *2*, 664–675.

Said, M., Mundina-Weilenmann, C., Vittone, L., and Mattiazzi, A. (2002). The relative relevance of phosphorylation of the Thr(17) residue of phospholamban is different at different levels of beta-adrenergic stimulation. Eur. J. Physiol. *444*, 801–809.

Satoh, M., Matter, C.M., Ogita, H., Takeshita, K., Wang, C.Y., Dorn, G.W., and Liao, J.K. (2007). Inhibition of apoptosis-regulated signaling kinase-1 and prevention of congestive heart failure by estrogen. Circ. *115*, 3197–3204.

Scarabelli, T.M., and Gottlieb, R.A. (2004). Functional and clinical repercussions of myocyte apoptosis in the multifaceted damage by ischemia/reperfusion injury: old and new concepts after 10 years of contributions. Cell Death Differ. *11*, S144–S152.

Scherz-Shouval, R., Shvets, E., Fass, E., Shorer, H., Gil, L., and Elazar, Z. (2007). Reactive oxygen species are essential for autophagy and specifically regulate the activity of Atg4. EMBO J. *26*, 1749–1760.

Scheubel, R.J., Bartling, B., Simm, A., Silber, R.E., Drogaris, K., Darmer, D., and Holtz, J. (2002). Apoptotic pathway activation from mitochondria and death receptors without caspase-3 cleavage in failing human myocardium: fragile balance of myocyte survival? J. Am. Coll. Cardiol. *39*, 481–488.

Schlabach, M.R., Luo, J., Solimini, N.L., Hu, G., Xu, Q., Li, M.Z., Zhao, Z., Smogorzewska, A., Sowa, M.E., Ang, X.L., et al. (2008). Cancer proliferation gene discovery through functional genomics. Science *319*, 620–624.

Schneider, M.D. (2005). Cyclophilin D: knocking on death's door. Science *2005*, pe26–pe26.

Schwertz, H., Carter, J.M., Abdudureheman, M., Russ, M., Buerke, U., Schlitt, A., Müller-Werdan, U., Prondzinsky, R., Werdan, K., and Buerke, M. (2007). Myocardial ischemia/reperfusion causes VDAC phosphorylation which is reduced by cardioprotection with a p38 MAP kinase inhibitor. Proteom. *7*, 4579–4588.

See, F., Thomas, W., Way, K., Tzanidis, A., Kompa, A., Lewis, D., Itescu, S., and Krum, H. (2004). p38 mitogen-activated protein kinase inhibition improves cardiac function and attenuates left ventricular remodeling following myocardial infarction in the rat. J. Am. Coll. Cardiol. *44*, 1679–1689.

Segers, V.F.M., and Lee, R.T. (2008). Stem-cell therapy for cardiac disease. Nature *451*, 937–942.

Seidman, J.G., and Seidman, C. (2001). The genetic basis for cardiomyopathy: from mutation identification to mechanistic paradigms. Cell *104*, 557–567.

Serneri, G.G., Modesti, P.A., Boddi, M., Cecioni, I., Paniccia, R., Coppo, M., Galanti, G., Simonetti, I., Vanni, S., Papa, L., et al. (1999). Cardiac growth factors in human hypertrophy. Relations with myocardial contractility and wall stress. Circ. Res. *85*, 57–67.

Shao, Z., Bhattacharya, K., Hsich, E., Park, L., Walters, B., Germann, U., Wang, Y.-M., Kyriakis, J., Mohanlal, R., Kuida, K., et al. (2005). c-Jun N-Terminal Kinases Mediate Reactivation of Akt and Cardiomyocyte Survival After Hypoxic Injury In Vitro and In Vivo. Circ. Res. *98*, 111–118.

Sharrocks, A.D., Yang, S.-H., and Galanis, A. (2000). Docking domains and substrate-specificity determination for MAP kinases. Trends Biochem. Sci. *25*, 448–453.

Shchemelinin, I., Sefc, L., and Necas, E. (2006). Protein kinases, their function and implication in cancer and other diseases. Folia Biol. (Praha) *52*, 81–100.

Sheng, Z., Knowlton, K., Chen, J., Hoshijima, M., Brown, J.H., and Chien, K.R. (1997). Cardiotrophin 1 (CT-1) inhibition of cardiac myocyte apoptosis via a mitogen-activated protein kinase-dependent pathway. Divergence from downstream CT-1 signals for myocardial cell hypertrophy. J. Biol. Chem. *272*, 5783–5791.

Shenje, L.T., Andersen, P., Halushka, M.K., Lui, C., Fernandez, L., Collin, G.B., Amat-Alarcon, N., Meschino, W., Cutz, E., Chang, K., et al. (2014). Mutations in Alström protein impair terminal differentiation of cardiomyocytes. Nat. Comm. *5*, 3416.

Sheridan, D.J., Autelitano, D.J., Wang, B., Percy, E., Woodcock, E.A., and Du, X.J. (2000). Beta(2)-adrenergic receptor overexpression driven by alpha-MHC promoter is downregulated in hypertrophied and failing myocardium. Cardiovasc. Res. *47*, 133–141.

Shibata, H., Ichikawa, T., Nakao, K., Miyaaki, H., Takeshita, S., Akiyama, M., Fujimoto, M., Miuma, S., Kanda, S., Yamasaki, H., et al. (2008). A high glucose condition sensitizes human hepatocytes to hydrogen peroxide-induced cell death. Mol. Med. Rep. *1*, 379–385.

Shih, C., and Weinberg, R.A. (1982). Isolation of a transforming sequence from a human bladder carcinoma cell line. Cell *29*, 161–169.

Shimizu, S., Narita, M., and Tsujimoto, Y. (1999). Bcl-2 family proteins regulate the release of apoptogenic cytochrome c by the mitochondrial channel VDAC. Nature *399*, 483–487.

Shirakabe, K., Yamaguchi, K., Shibuya, H., Irie, K., Matsuda, S., Moriguchi, T., Gotoh, Y., Matsumoto, K., and Nishida, E. (1997). TAK1 mediates the ceramide signaling to stress-activated protein kinase/c-Jun N-terminal kinase. J. Biol. Chem. *272*, 8141–8144.

Shirwany, N.A., and Zou, M.H. (2010). AMPK in cardiovascular health and disease. Acta Pharmacol. Sinica. *31*, 1075–1084.

Shizukuda, Y., and Buttrick, P.M. (2001). Protein kinase C(epsilon) modulates apoptosis induced by beta-adrenergic stimulation in adult rat ventricular myocytes via extracellular signal-regulated kinase (ERK) activity. J. Mol. Cell Cardiol. *33*, 1791–1803.

Shu, H.B., Halpin, D.R., and Goeddel, D.V. (1997). Casper is a FADD- and caspase-related inducer of apoptosis. Immunity *6*, 751–763.

Silva, J.M., Li, M.Z., Chang, K., Ge, W., Golding, M.C., Rickles, R.J., Siolas, D., Hu, G., Paddison, P.J., Schlabach, M.R., et al. (2005). Second-generation shRNA libraries covering the mouse and human genomes. Nat. Genet. *37*, 1281–1288.

Silva, J.M., Marran, K., Parker, J.S., Silva, J., Golding, M., Schlabach, M.R., Elledge, S.J., Hannon, G.J., and Chang, K. (2008). Profiling essential genes in human mammary cells by multiplex RNAi screening. Science *319*, 617–620.

Singhirunnusorn, P., Suzuki, S., Kawasaki, N., Saiki, I., and Sakurai, H. (2005). Critical roles of threonine 187 phosphorylation in cellular stress-induced rapid and transient activation of transforming growth factor-beta-activated kinase 1 (TAK1) in a signaling complex containing TAK1-binding protein TAB1 and TAB2. J. Biol. Chem. *280*, 7359–7368.

Sinha, S., and Levine, B. (2008). The autophagy effector Beclin 1: a novel BH3-only protein. Oncogene *27*, S137–S148.

Smith, C.C.T., Ding, G., Davidson, S.M., Fu, M., Lim, S.Y., Qin, Q., Simpkin, J.C., LEWIS, W., Hothersall, J.S., KIM, H., et al. (2007). Necrostatin: a potentially novel cardioprotective agent? Cardiovasc. Drugs Ther. *21*, 227–233.

Somers, A., Jean, J.-C., Sommer, C.A., Omari, A., Ford, C.C., Mills, J.A., Ying, L., Sommer, A.G., Jean, J.M., Smith, B.W., et al. (2010). Generation of transgene-free lung disease-specific human induced pluripotent stem cells using a single excisable lentiviral stem cell cassette. Stem Cells *28*, 1728–1740.

Song, Z.F., Ji, X.P., Li, X.X., Wang, S.J., and Wang, S.H. (2008). Inhibition of the activity of poly (ADP-ribose) polymerase reduces heart ischaemia/reperfusion injury via suppressing JNK-mediated AIF translocation. J. Cell. Mol. Med. *12*, 1220–1228.

Sossalla, S., Fluschnik, N., Schotola, H., Ort, K.R., Neef, S., Schulte, T., Wittköpper, K., Renner, A., Schmitto, J.D., Gummert, J., et al. (2010). Inhibition of elevated Ca^{2+}/calmodulin-dependent protein kinase II improves contractility in human failing myocardium. Circ. Res. *107*, 1150–1161.

Su, H., Bidère, N., Zheng, L., Cubre, A., Sakai, K., Dale, J., Salmena, L., Hakem, R., Straus, S., and Lenardo, M. (2005). Requirement for caspase-8 in NF-kappaB activation by antigen receptor. Science *307*, 1465–1468.

Su, H.F., Samsamshariat, A., Fu, J., Shan, Y.X., Chen, Y.H., Piomelli, D., and Wang, P.H.

(2006). Oleylethanolamide activates Ras-Erk pathway and improves myocardial function in doxorubicin-induced heart failure. Endocrinology *147*, 827–834.

Su, Y.C., Treisman, J.E., and Skolnik, E.Y. (1998). The Drosophila Ste20-related kinase misshapen is required for embryonic dorsal closure and acts through a JNK MAPK module on an evolutionarily conserved signaling pathway. Genes Dev. *12*, 2371–2380.

Sumitomo, M., Ohba, M., Asakuma, J., Asano, T., Kuroki, T., Asano, T., and Hayakawa, M. (2002). Protein kinase Cdelta amplifies ceramide formation via mitochondrial signaling in prostate cancer cells. J. Clin. Invest. *109*, 827–836.

Suzuki, M., Youle, R.J., and Tjandra, N. (2000). Structure of Bax: coregulation of dimer formation and intracellular localization. Cell *103*, 645–654.

Sy, J.C., Seshadri, G., Yang, S.C., Brown, M., Oh, T., Dikalov, S., Murthy, N., and Davis, M.E. (2008). Sustained release of a p38 inhibitor from non-inflammatory microspheres inhibits cardiac dysfunction. Nat. Mater. *7*, 863–868.

Tachibana, H., Perrino, C., Takaoka, H., Davis, R.J., Naga Prasad, S.V., and Rockman, H.A. (2006). JNK1 is required to preserve cardiac function in the early response to pressure overload. Biochem. Biophys. Res. Commun. *343*, 1060–1066.

Taira, K., Umikawa, M., Takei, K., Myagmar, B.E., Shinzato, M., Machida, N., Uezato, H., Nonaka, S., and Kariya, K. (2004). The Traf2- and Nck-interacting kinase as a putative effector of Rap2 to regulate actin cytoskeleton. J. Biol. Chem. *279*, 49488–49496.

Takahashi, K., and Yamanaka, S. (2006). Induction of pluripotent stem cells from mouse embryonic and adult fibroblast cultures by defined factors. Cell *126*, 663–676.

Takahashi, N., Calderone, A., Izzo, N.J., Mäki, T.M., Marsh, J.D., and Colucci, W.S. (1994). Hypertrophic stimuli induce transforming growth factor-β1 expression in rat ventricular myocytes. J. Clin. Invest. *94*, 1470–1476.

Takeishi, Y., Ping, P., Bolli, R., Kirkpatrick, D.L., Hoit, B.D., and Walsh, R.A. (2000). Transgenic overexpression of constitutively active protein kinase C epsilon causes concentric cardiac hypertrophy. Circ. Res. *86*, 1218–1223.

Tanaka, M., Fuentes, M.E., Yamaguchi, K., Durnin, M.H., Dalrymple, S.A., Hardy, K.L., and Goeddel, D.V. (1999). Embryonic lethality, liver degeneration, and impaired NF-kappa B activation in IKK-beta-deficient mice. Immunity *10*, 421–429.

Tanaka, N. (1995). Ventricular Expression of a MLC-2v-ras Fusion Gene Induces Cardiac Hypertrophy and Selective Diastolic Dysfunction in Transgenic Mice. J. Biol. Chem. *270*, 23173–23178.

Tanaka, N., Ryoke, T., Hongo, M., Mao, L., Rockman, H.A., Clark, R.G., and Ross, J. (1998). Effects of growth hormone and IGF-I on cardiac hypertrophy and gene expression in mice. Am. J. Physiol. *275*, 393–399.

Taniike, M., Yamaguchi, O., Tsujimoto, I., Hikoso, S., Takeda, T., Nakai, A., Omiya, S., Mizote, I., Nakano, Y., Higuchi, Y., et al. (2008). Apoptosis Signal-Regulating Kinase 1/p38 Signaling Pathway Negatively Regulates Physiological Hypertrophy. Circ. *117*, 545–552.

Tannous, P., Zhu, H., Johnstone, J.L., Shelton, J.M., Rajasekaran, N.S., Benjamin, I.J., Nguyen, L., Gerard, R.D., Levine, B., Rothermel, B.A., et al. (2008). Autophagy is an adaptive response in desmin-related cardiomyopathy. Proc. Natl. Acad. Sci. USA *105*, 9745–

9750.

Tatake, R.J., O'Neill, M.M., Kennedy, C.A., Wayne, A.L., Jakes, S., Wu, D., Kugler, S.Z.J., Kashem, M.A., Kaplita, P., and Snow, R.J. (2008). Identification of pharmacological inhibitors of the MEK5/ERK5 pathway. Biochem. Biophys. Res. Commun. *377*, 120–125.

Taylor L.D. (2007). Past, Present and Future of High Content Screening and the Field of Cellomics. In: Taylor L.D., Haskins R.J., and Giuliano A.K. eds. *High Content Screening: A powerful approach to Systems Cell Biology and Drug Discovery*, New Jersey: Humana Press, p3-19

Tecle, H., Shao, J., Li, Y., Kothe, M., Kazmirski, S., Penzotti, J., Ding, Y.H., Ohren, J., Moshinsky, D., Coli, R., et al. (2009). Beyond the MEK-pocket: can current MEK kinase inhibitors be utilized to synthesize novel type III NCKIs? Does the MEK-pocket exist in kinases other than MEK? Bioorg. Med. Chem. Lett. *19*, 226–229.

Tenhunen, O., Rysa, J., Ilves, M., Soini, Y., Ruskoaho, H., and Leskinen, H. (2006). Identification of cell cycle regulatory and inflammatory genes as predominant targets of p38 mitogen-activated protein kinase in the heart. Circ. Res. *99*, 485–493.

Terai, K., Hiramoto, Y., Masaki, M., Sugiyama, S., Kuroda, T., Hori, M., Kawase, I., and Hirota, H. (2005). AMP-activated protein kinase protects cardiomyocytes against hypoxic injury through attenuation of endoplasmic reticulum stress. Mol. Cell Biol. *25*, 9554–9575.

Tesz, G.J., Guilherme, A., Guntur, K.V., Hubbard, A.C., Tang, X., Chawla, A., and Czech, M.P. (2007). Tumor necrosis factor α (TNFα) stimulates Map4k4 expression through TNFα receptor 1 signaling to c-Jun and activating transcription factor 2. J. Biol. Chem. *282*, 19302–19312.

Thuerauf, D.J., Marcinko, M., Gude, N., Rubio, M., Sussman, M.A., and Glembotski, C.C. (2006). Activation of the unfolded protein response in infarcted mouse heart and hypoxic cultured cardiac myocytes. Circ. Res. *99*, 275–282.

Tian, R., Musi, N., D'Agostino, J., Hirshman, M.F., and Goodyear, L.J. (2001). Increased adenosine monophosphate-activated protein kinase activity in rat hearts with pressure-overload hypertrophy. Circ. *104*, 1664–1669.

Tohyama, S., Hattori, F., Sano, M., Hishiki, T., Nagahata, Y., Matsuura, T., Hashimoto, H., Suzuki, T., Yamashita, H., Satoh, Y., et al. (2013). Distinct metabolic flow enables large-scale purification of mouse and human pluripotent stem cell-derived cardiomyocytes. Cell Stem Cell *12*, 127–137.

Toko, H., Takahashi, H., Kayama, Y., Okada, S., Minamino, T., Terasaki, F., Kitaura, Y., and Komuro, I. (2010). ATF6 is important under both pathological and physiological states in the heart. J. Mol. Cell Cardiol. *49*, 113–120.

Tournier, C., Dong, C., Turner, T.K., Jones, S.N., Flavell, R.A., and Davis, R.J. (2001). MKK7 is an essential component of the JNK signal transduction pathway activated by proinflammatory cytokines. Genes Dev. *15*, 1419–1426.

Tournier, C., Hess, P., Yang, D.D., Xu, J., Turner, T.K., Nimnual, A., Bar-Sagi, D., Jones, S.N., Flavell, R.A., and Davis, R.J. (2000). Requirement of JNK for stress-induced activation of the cytochrome c-mediated death pathway. Science *288*, 870–874.

Townsend N, Wickramasinghe K, Bhatnagar P, Smolina K, Nichols M, Leal J, Luengo-Fernandez R, Rayner M (2012). *Coronary heart disease statistics 2012 edition.* British Heart Foundation: London.

Ueno, H., Perryman, M.B., Roberts, R., and Schneider, M.D. (1988). Differentiation of cardiac myocytes after mitogen withdrawal exhibits three sequential states of the ventricular growth response. J. Cell Biol. *107*, 1911–1918.

Ueyama, T., Kawashima, S., Sakoda, T., Rikitake, Y., Ishida, T., Kawai, M., Yamashita, T., Ishido, S., Hotta, H., and Yokoyama, M. (2000). Requirement of activation of the extracellular signal-regulated kinase cascade in myocardial cell hypertrophy. J. Mol. Cell Cardiol. *32*, 947–960.

Uosaki, H., Magadum, A., Seo, K., Fukushima, H., Takeuchi, A., Nakagawa, Y., Moyes, K.W., Narazaki, G., Kuwahara, K., Laflamme, M., et al. (2013). Identification of chemicals inducing cardiomyocyte proliferation in developmental stage-specific manner with pluripotent stem cells. Circ. Cardiovasc. Genet. *6*, 624–633.

Uozumi, H., Hiroi, Y., Zou, Y., Takimoto, E., Toko, H., Niu, P., Shimoyama, M., Yazaki, Y., Nagai, R., and Komuro, I. (2001). gp130 plays a critical role in pressure overload-induced cardiac hypertrophy. J. Biol. Chem. *276*, 23115–23119.

van Hoof, D., Dormeyer, W., Braam, S.R., Passier, R., Monshouwer-Kloots, J., Ward-van Oostwaard, D., Heck, A.J.R., Krijgsveld, J., and Mummery, C.L. (2010). Identification of cell surface proteins for antibody-based selection of human embryonic stem cell-derived cardiomyocytes. J. Proteome Res. *9*, 1610–1618.

van Oort, R.J., van Rooij, E., Bourajjaj, M., Schimmel, J., Jansen, M.A., van der Nagel, R., Doevendans, P.A., Schneider, M.D., van Echteld, C.J.A., and de Windt, L.J. (2006). MEF2 activates a genetic program promoting chamber dilation and contractile dysfunction in calcineurin-induced heart failure. Circ. *114*, 298–308.

Varfolomeev, E.E., Schuchmann, M., Luria, V., Chiannilkulchai, N., Beckmann, J.S., Mett, I.L., Rebrikov, D., Brodianski, V.M., Kemper, O.C., Kollet, O., et al. (1998). Targeted disruption of the mouse Caspase 8 gene ablates cell death induction by the TNF receptors, Fas/Apo1, and DR3 and is lethal prenatally. Immunity *9*, 267–276.

Vecchione, C., Fratta, L., Rizzoni, D., Notte, A., Poulet, R., Porteri, E., Frati, G., Guelfi, D., Trimarco, V., Mulvany, M.J., et al. (2002). Cardiovascular influences of $\alpha_{1\beta}$-adrenergic receptor defect in mice. Circ. *105*, 1700–1707.

Vega, R.B., Harrison, B.C., Meadows, E., Roberts, C.R., Papst, P.J., Olson, E.N., and McKinsey, T.A. (2004). Protein kinases C and D mediate agonist-dependent cardiac hypertrophy through nuclear export of histone deacetylase 5. Mol. Cell Biol. *24*, 8374–8385.

Verhagen, A.M., Ekert, P.G., Pakusch, M., Silke, J., Connolly, L.M., Reid, G.E., Moritz, R.L., Simpson, R.J., and Vaux, D.L. (2000). Identification of DIABLO, a mammalian protein that promotes apoptosis by binding to and antagonizing IAP proteins. Cell *102*, 43–53.

Verhagen, A.M., Silke, J., Ekert, P.G., Pakusch, M., Kaufmann, H., Connolly, L.M., Day, C.L., Tikoo, A., Burke, R., Wrobel, C., et al. (2002). HtrA2 promotes cell death through its serine protease activity and its ability to antagonize inhibitor of apoptosis proteins. J. Biol. Chem. *277*, 445–454.

Verheij, M., Bose, R., Lin, X.H., Yao, B., Jarvis, W.D., Grant, S., Birrer, M.J., Szabo, E., Zon, L.I., Kyriakis, J.M., et al. (1996). Requirement for ceramide-initiated SAPK/JNK signalling in

stress-induced apoptosis. Nature *380*, 75–79.

Vila-Petroff, M., Salas, M.A., Said, M., Valverde, C.A., Sapia, L., Portiansky, E., Hajjar, R.J., Kranias, E.G., Mundina-Weilenmann, C., and Mattiazzi, A. (2007). CaMKII inhibition protects against necrosis and apoptosis in irreversible ischemia–reperfusion injury. Cardiovasc. Res. *73*, 689–698.

Villarreal, F.J., and Dillmann, W.H. (1992). Cardiac hypertrophy-induced changes in mRNA levels for TGF-beta 1, fibronectin, and collagen. Am. J. Physiol. *262*, H1861–H1866.

Wakasaki, H., Koya, D., Schoen, F.J., Jirousek, M.R., Ways, D.K., Hoit, B.D., Walsh, R.A., and King, G.L. (1997). Targeted overexpression of protein kinase C beta2 isoform in myocardium causes cardiomyopathy. Proc. Natl. Acad. Sci. USA *94*, 9320–9325.

Wan, Y.Y., Chi, H., Xie, M., Schneider, M.D., and Flavell, R.A. (2006). The kinase TAK1 integrates antigen and cytokine receptor signaling for T cell development, survival and function. Nat. Immunol. *7*, 851–858.

Wang, G.W., Klein, J.B., and Kang, Y.J. (2001). Metallothionein inhibits doxorubicin-induced mitochondrial cytochrome-c release and caspase-3 activation in cardiomyocytes. J. Pharmacol. Exp. Ther. *298*, 461–468.

Wang, J., and Lenardo, M.J. (2000). Roles of caspases in apoptosis, development, and cytokine maturation revealed by homozygous gene deficiencies. J. Cell Sci. *113*, 753–757.

Wang, J., Zhen, L., Klug, M.G., Wood, D., Wu, X., and Mizrahi, J. (2000). Involvement of caspase 3- and 8-like proteases in ceramide-induced apoptosis of cardiomyocytes. J. Card. Fail. *6*, 243–249.

Wang, K., Liu, F., Zhou, L.Y., Ding, S.L., Long, B., Liu, C.Y., Sun, T., Fan, Y.Y., Sun, L., and Li, P.F. (2013a). miR-874 regulates myocardial necrosis by targeting caspase-8. Cell Death Dis. *4*, e709–e719.

Wang, L., Wang, L., Du, F., Du, F., Wang, X., and Wang, X. (2008). TNF-α Induces Two Distinct Caspase-8 Activation Pathways. Cell *133*, 693–703.

Wang, M., Amano, S.U., Flach, R.J.R., Chawla, A., Aouadi, M., and Czech, M.P. (2013b). Identification of Map4k4 as a novel suppressor of skeletal muscle differentiation. Mol. Cell Biol. *33*, 678–687.

Wang, W., Zhu, W., Wang, S., Yang, D., Crow, M.T., Xiao, R.P., and Cheng, H. (2004). Sustained beta1-adrenergic stimulation modulates cardiac contractility by Ca^{2+}/calmodulin kinase signaling pathway. Circ. Res. *95*, 798–806.

Wang, Y.B., Su, B., Sah, V.P., Brown, J.H., Han, J.H., and Chien, K.R. (1998a). Cardiac hypertrophy induced by mitogen-activated protein kinase kinase 7, a specific activator for c-Jun NH2-terminal kinase in ventricular muscle cells. J. Biol. Chem. *273*, 12684–12684.

Wang, Y., Huang, S., Sah, V.P., Ross, J., Brown, J.H., Han, J., and Chien, K.R. (1998b). Cardiac muscle cell hypertrophy and apoptosis induced by distinct members of the p38 mitogen-activated protein kinase family. J. Biol. Chem. *273*, 2161–2168.

Wang, Y., Whelan, R.S., Kaplinskiy, V., and Kitsis, R.N. (2007). Mitogen-Activated Protein Kinases in Heart Development and Diseases. Circ. *116*, 1413–1423.

Wang, Y., Huang, G., Vogel, P., Neale, G., Reizis, B., and Chi, H. (2012a). Transforming growth factor beta-activated kinase 1 (TAK1)-dependent checkpoint in the survival of

dendritic cells promotes immune homeostasis and function. Proc. Natl. Acad. Sci. USA *109*, E343–E352.

Wang, Y., Zheng, C.G., Jiang, Y., Zhang, J., Chen, J., Yao, C., Zhao, Q., Liu, S., Chen, K., Du, J., et al. (2012b). Genetic correction of β-thalassemia patient-specific iPS cells and its use in improving hemoglobin production in irradiated SCID mice. Cell Res. *22*, 637–648.

Watanabe, K.-I., Ma, M., Hirabayashi, K.-I., Gurusamy, N., Veeraveedu, P.T., Prakash, P., Zhang, S., Muslin, A.J., Kodama, M., and Aizawa, Y. (2007a). Swimming stress in DN 14-3-3 mice triggers maladaptive cardiac remodeling: role of p38 MAPK. Am. J. Physiol. Heart Circ. Physiol. *292*, H1269–H1277.

Watanabe, K., Ueno, M., Kamiya, D., Nishiyama, A., Matsumura, M., Wataya, T., Takahashi, J.B., Nishikawa, S., Nishikawa, S.I., Muguruma, K., et al. (2007b). A ROCK inhibitor permits survival of dissociated human embryonic stem cells. Nat. Biotechnol. *25*, 681–686.

Wei, J., Wang, W., Chopra, I., Li, H.F., Dougherty, C.J., Adi, J., Adi, N., Wang, H., and Webster, K.A. (2011). c-Jun N-terminal Kinase (JNK-1) confers protection against brief but not extended ischemia during acute myocardial infarction. J. Biol. Chem. *286*, 13995–14006.

Wei, M.C., Lindsten, T., Mootha, V.K., Weiler, S., Gross, A., Ashiya, M., Thompson, C.B., and Korsmeyer, S.J. (2000). tBID, a membrane-targeted death ligand, oligomerizes BAK to release cytochrome c. Genes Dev. *14*, 2060–2071.

Weinlich, R., Oberst, A., Dillon, C.P., Janke, L.J., Milasta, S., Lukens, J.R., Rodriguez, D.A., Gurung, P., Savage, C., Kanneganti, T.D., et al. (2013). Protective roles for caspase-8 and cFLIP in adult homeostasis. Cell Rep. *5*, 340–348.

Wencker, D., Chandra, M., Nguyen, K., Miao, W., Garantziotis, S., Factor, S.M., Shirani, J., Armstrong, R.C., and Kitsis, R.N. (2003). A mechanistic role for cardiac myocyte apoptosis in heart failure. J. Clin. Invest. *111*, 1497–1504.

Westbrook, T.F., Martin, E.S., Schlabach, M.R., Leng, Y., Liang, A.C., Feng, B., Zhao, J.J., Roberts, T.M., Mandel, G., Hannon, G.J., et al. (2005). A genetic screen for candidate tumor suppressors identifies REST. Cell *121*, 837–848.

Weston, C.R., and Davis, R.J. (2007). The JNK signal transduction pathway. Curr. Opin. Cell Biol. *19*, 142–149.

Whelan, R.S., Kaplinskiy, V., and Kitsis, R.N. (2010). Cell death in the pathogenesis of heart disease: mechanisms and significance. Annu. Rev. Physiol. *72*, 19–44.

Willems, E., Bushway, P.J., and Mercola, M. (2009). Natural and synthetic regulators of embryonic stem cell cardiogenesis. Pediatr. Cardiol. *30*, 635–642.

Willems, E., Spiering, S., Davidovics, H., Lanier, M., Xia, Z., Dawson, M., Cashman, J., and Mercola, M. (2011). Small-molecule inhibitors of the Wnt pathway potently promote cardiomyocytes from human embryonic stem cell-derived mesoderm. Circ. Res. *109*, 360–364.

Wood, D.E., Thomas, A., Devi, L.A., Berman, Y., Beavis, R.C., Reed, J.C., and Newcomb, E.W. (1998). Bax cleavage is mediated by calpain during drug-induced apoptosis. Oncogene *17*, 1069–1078.

Wu, L., Xi, Z., Guo, R., Liu, S., Yang, S., Liu, D., Dong, S., and Guo, D. (2013). Exogenous ARC down-regulates caspase-3 expression and inhibits apoptosis of broiler chicken

cardiomyocytes exposed to hydrogen peroxide. Avian Pathol. *42*, 32–37.

Wurdak, H., Zhu, S., Romero, A., Lorger, M., Watson, J., Chiang, C.Y., Zhang, J., Natu, V.S., Lairson, L.L., Walker, J.R., et al. (2010). An RNAi screen identifies TRRAP as a regulator of brain tumor-initiating cell differentiation. Cell Stem Cell *6*, 37–47.

Xiao, L., Pimentel, D.R., Wang, J., Singh, K., Colucci, W.S., and Sawyer, D.B. (2001a). Role of reactive oxygen species and NAD(P)H oxidase in alpha 1-adrenoceptor signaling in adult rat cardiac myocytes. Am. J. Physiol. Cell Physiol. *282*, 926–934.

Xiao, L., Pimental, D.R., Amin, J.K., Singh, K., Sawyer, D.B., and Colucci, W.S. (2001b). MEK1/2–ERK1/2 mediates α1-adrenergic receptor-stimulated hypertrophy in adult rat ventricular myocytes. J. Mol. Cell Cardiol. *33*, 779–787.

Xie, M., Zhang, D., Dyck, J.R.B., Li, Y., Zhang, H., Morishima, M., Mann, D.L., Taffet, G.E., Baldini, A., Khoury, D.S., et al. (2006). A pivotal role for endogenous TGF-beta-activated kinase-1 in the LKB1/AMP-activated protein kinase energy-sensor pathway. Proc. Natl. Acad. Sci. USA *103*, 17378–17383.

Xie, M., Zhang, D., Wang, S.C., Sano, M., Wang, X., Pocius, J.S., Taffet, G.E., Michael, L.H., Entman, M.L., Mann, D.L., et al. (2007). Abstract 1949: The Protein Kinase MAP4K4 Is Activated in Failing Human Hearts and Mediates Cardiomyocyte Apoptosis in Experimental Models, in vitro and in vivo. Circ. *116*.

Xu, C., Bailly-Maitre, B., and Reed, J.C. (2005). Endoplasmic reticulum stress: cell life and death decisions. J. Clin. Invest. *115*, 2656–2664.

Xu, X., Xie, K., Zhang, X.-Q., Pridgen, E.M., Park, G.Y., Cui, D.S., Shi, J., Wu, J., Kantoff, P.W., Lippard, S.J., et al. (2013). Enhancing tumor cell response to chemotherapy through nanoparticle-mediated codelivery of siRNA and cisplatin prodrug. Proc. Natl. Acad. Sci. USA *110*, 18638–18643.

Xu, X.Q., Graichen, R., Soo, S.Y., Balakrishnan, T., Rahmat, S.N.B., Sieh, S., Tham, S.C., Freund, C., Moore, J., Mummery, C., et al. (2008). Chemically defined medium supporting cardiomyocyte differentiation of human embryonic stem cells. Differentiation *76*, 958–970.

Yamaguchi, O., Watanabe, T., Nishida, K., Kashiwase, K., Higuchi, Y., Takeda, T., Hikoso, S., Hirotani, S., Asahi, M., Taniike, M., et al. (2004). Cardiac-specific disruption of the c-raf-1 gene induces cardiac dysfunction and apoptosis. J. Clin. Invest. *114*, 937–943.

Yan, C., Luo, H.L., Lee, J.D., Abe, J.I., and Berk, B.C. (2001). Molecular cloning of mouse ERK5/BMK1 splice variants and characterization of ERK5 functional domains. J. Biol. Chem. *276*, 10870–10878.

Yang, B., Lu, Y., and Wang, Z. (2008a). Control of cardiac excitability by microRNAs. Cardiovasc. Res. *79*, 571–580.

Yang, J. (1997). Prevention of apoptosis by Bcl-2: Release of cytochrome c from mitochondria blocked. Science *275*, 1129–1132.

Yang, L., Soonpaa, M.H., Adler, E.D., Roepke, T.K., Kattman, S.J., Kennedy, M., Henckaerts, E., Bonham, K., Abbott, G.W., Linden, R.M., et al. (2008b). Human cardiovascular progenitor cells develop from a KDR^{+} embryonic-stem-cell-derived population. Nature *453*, 524–528.

Yang, X., Pabon, L., and Murry, C.E. (2014). Engineering adolescence: maturation of human

pluripotent stem cell-derived cardiomyocytes. Circ. Res. *114*, 511–523.

Yang, Y., Zhu, W.Z., Joiner, M.L., Zhang, R., Oddis, C.V., Hou, Y., Yang, J., Price, E.E., Gleaves, L., Eren, M., et al. (2006). Calmodulin kinase II inhibition protects against myocardial cell apoptosis *in vivo*. Am. J. Physiol. Heart Circ. Physiol. *291*, 3065–3075.

Yao, S., Chen, S., Clark, J., Hao, E., Beattie, G.M., Hayek, A., and Ding, S. (2006). Long-term self-renewal and directed differentiation of human embryonic stem cells in chemically defined conditions. Proc. Natl. Acad. Sci. USA *103*, 6907–6912.

Yao, Y., Li, W., Wu, J., Germann, U.A., Su, M.S.S., Kuida, K., and Boucher, D.M. (2003). Extracellular signal-regulated kinase 2 is necessary for mesoderm differentiation. Proc. Natl. Acad. Sci. USA *100*, 12759–12764.

Yao, Z., Zhou, G., Wang, X.S., Brown, A., Diener, K., Gan, H., and Tan, T.H. (1999). A novel human STE20-related protein kinase, HGK, that specifically activates the c-Jun N-terminal kinase signaling pathway. J. Biol. Chem. *274*, 2118–2125.

Yeh, J.K., Aloia, J.F., Chen, M., Ling, N., Koo, H.C., and Millard, W.J. (1994). Effect of growth hormone administration and treadmill exercise on serum and skeletal IGF-I in rats. Am. J. Physiol. *266*, E129–E135.

Yeh, W.C., Itie, A., Elia, A.J., Ng, M., Shu, H.B., Wakeham, A., Mirtsos, C., Suzuki, N., Bonnard, M., Goeddel, D.V., et al. (2000). Requirement for casper (c-FLIP) in regulation of death receptor-induced apoptosis and embryonic development. Immunity *12*, 633–642.

Yeh, W.C., la Pompa, de, J.L., McCurrach, M.E., Shu, H.B., Elia, A.J., Shahinian, A., Ng, M., Wakeham, A., Khoo, W., Mitchell, K., et al. (1998). FADD: Essential for embryo development and signaling from some, but not sll, inducers of apoptosis. Science *279*, 1954–1958.

Yi, R., Doehle, B.P., Qin, Y., Macara, I.G., and Cullen, B.R. (2005). Overexpression of exportin 5 enhances RNA interference mediated by short hairpin RNAs and microRNAs. RNA *11*, 220–226.

Yin, T.G., Sandhu, G., Wolfgang, C.D., Burrier, A., Webb, R.L., Rigel, D.F., Hai, T.W., and Whelan, J. (1997). Tissue-specific pattern of stress kinase activation in ischemic/reperfused heart and kidney. J. Biol. Chem. *272*, 19943–19950.

Young, M.A., Larson, D.E., Sun, C.W., George, D.R., Ding, L., Miller, C.A., Lin, L., Pawlik, K.M., Chen, K., Fan, X., et al. (2012). Background mutations in parental cells account for most of the genetic heterogeneity of induced pluripotent stem cells. Cell Stem Cell *10*, 570–582.

Yu, J., Chau, K.F., Vodyanik, M.A., Jiang, J., and Jiang, Y. (2011). Efficient feeder-free episomal reprogramming with small molecules. PLoS ONE *6*, e17557.

Yu, X.C., Acehan, D., Menetret, J.F., Booth, C.R., Ludtke, S.J., Riedl, S.J., Shi, Y.G., Wang, X.D., and Akey, C.W. (2005). A structure of the human apoptosome at 12.8 angstrom resolution provides insights into this cell death platform. Structure *13*, 1725–1735.

Yu, Y., Ge, N., Xie, M., Sun, W., Burlingame, S., Pass, A.K., Nuchtern, J.G., Zhang, D., Fu, S., Schneider, M.D., et al. (2008). Phosphorylation of Thr-178 and Thr-184 in the TAK1 T-loop is required for interleukin (IL)-1-mediated optimal NFkappaB and AP-1 activation as well as IL-6 gene expression. J. Biol. Chem. *283*, 24497–24505.

Yue, T.L., Gu, J.L., Wang, C., Reith, A.D., Lee, J.C., Mirabile, R.C., Kreutz, R., Wang, Y.,

Maleeff, B., Parsons, A.A., et al. (2000). Extracellular signal-regulated kinase plays an essential role in hypertrophic agonists, endothelin-1 and phenylephrine-induced cardiomyocyte hypertrophy. J. Biol. Chem. *275*, 37895–37901.

Yussman, M.G., Toyokawa, T., Odley, A., Lynch, R.A., Wu, G., Colbert, M.C., Aronow, B.J., Lorenz, J.N., and Dorn, G.W. (2002). Mitochondrial death protein Nix is induced in cardiac hypertrophy and triggers apoptotic cardiomyopathy. Nat. Med. *8*, 725–730.

Zammit, P.S., Kelly, R.G., Franco, D., Brown, N., Moorman, A.F., and Buckingham, M.E. (2000). Suppression of atrial myosin gene expression occurs independently in the left and right ventricles of the developing mouse heart. Dev. Dyn. *217*, 75–85.

Zandstra, P., Bauwens, C., Yin, T., and Liu, Q. (2003). Scalable production of embryonic stem cell-derived cardiomyocytes. Tissue Engineering *9*, 767–778.

Zechner, D., Thuerauf, D.J., Hanford, D.S., McDonough, P.M., and Glembotski, C.C. (1997). A role for the p38 mitogen-activated protein kinase pathway in myocardial cell growth, sarcomeric organization, and cardiac-specific gene expression. J. Cell Biol. *139*, 115–127.

Zhang, D., Gaussin, V., Taffet, G.E., Belaguli, N.S., Yamada, M., Schwartz, R.J., Michael, L.H., Overbeek, P.A., and Schneider, M.D. (2000). TAK1 is activated in the myocardium after pressure overload and is sufficient to provoke heart failure in transgenic mice. Nat. Med. *6*, 556–563.

Zhang, J., Wilson, G.F., Soerens, A.G., Koonce, C.H., Yu, J., Palecek, S.P., Thomson, J.A., and Kamp, T.J. (2009a). Functional cardiomyocytes derived from human induced pluripotent stem cells. Circ. Res. *104*, e30–e41.

Zhang, J., Li, X.X., Bian, H.J., Liu, X.B., Ji, X.P., and Zhang, Y. (2009b). Inhibition of the activity of Rho-kinase reduces cardiomyocyte apoptosis in heart ischemia/reperfusion via suppressing JNK-mediated AIF translocation. Clin. Chim. Acta *401*, 76–80.

Zhang, L., Malik, S., Pang, J., Wang, H., Park, K.M., Yule, D.I., Blaxall, B.C., and Smrcka, A.V. (2013). Phospholipase cε hydrolyzes perinuclear phosphatidylinositol 4-phosphate to regulate cardiac hypertrophy. Cell *153*, 216–227.

Zhang, S., Weinheimer, C., Courtois, M., Kovacs, A., Zhang, C.E., Cheng, A.M., Wang, Y., and Muslin, A.J. (2003). The role of the Grb2–p38 MAPK signaling pathway in cardiac hypertrophy and fibrosis. J. Clin. Invest. *111*, 833–841.

Zhang, Y.M., Bo, J., Taffet, G.E., Chang, J., Shi, J., Reddy, A.K., Michael, L.H., Schneider, M.D., Entman, M.L., Schwartz, R.J., et al. (2006). Targeted deletion of ROCK1 protects the heart against pressure overload by inhibiting reactive fibrosis. Faseb J. *20*, 916–925.

Zhao, G., Wang, B., Liu, Y., Zhang, J.G., Deng, S.C., Qin, Q., Tian, K., Li, X., Zhu, S., Niu, Y., et al. (2013). miRNA-141, downregulated in pancreatic cancer, inhibits cell proliferation and invasion by directly targeting MAP4K4. Mol. Cancer Ther. *12*, 2569–2580.

Zhao, X., Mohan, R., Özcan, S., and Tang, X. (2012). MicroRNA-30d induces insulin transcription factor MafA and insulin production by targeting mitogen-activated protein 4 kinase 4 (MAP4K4) in pancreatic β-cells. J. Biol. Chem. *287*, 31155–31164.

Zheng, M., Dilly, K., Santos Cruz, Dos, J., Li, M., Gu, Y., Ursitti, J.A., Chen, J., Ross, J., Chien, K.R., Lederer, J.W., et al. (2004). Sarcoplasmic reticulum calcium defect in Ras-induced hypertrophic cardiomyopathy heart. Am. J. Physiol. Heart Circ. Physiol. *286*, 424–433.

Zhong, Y., Wang, Q.J., Li, X., Yan, Y., Backer, J.M., Chait, B.T., Heintz, N., and Yue, Z. (2009). Distinct regulation of autophagic activity by Atg14L and Rubicon associated with Beclin 1-phosphatidylinositol-3-kinase complex. Nat. Cell Biol. *11*, 468–476.

Zhou, G.C., Bao, Z.Q., and Dixon, J.E. (1995). Components of a new human protein-kinase signal-transduction pathway. J. Biol. Chem. *270*, 12665–12669.

Zhou, H., Wu, S., Joo, J.Y., Zhu, S., Han, D.W., Lin, T., Trauger, S., Bien, G., Yao, S., Zhu, Y., et al. (2009). Generation of induced pluripotent stem cells using recombinant proteins. Cell Stem Cell *4*, 381–384.

Zhu, H., Tannous, P., Johnstone, J.L., Kong, Y., Shelton, J.M., Richardson, J.A., Le, V., Levine, B., Rothermel, B.A., and Hill, J.A. (2007). Cardiac autophagy is a maladaptive response to hemodynamic stress. J. Clin. Invest. *117*, 1782–1793.

Zhu, W.Z., Wang, S.Q., Chakir, K., Yang, D., Zhang, T., Brown, J.H., Devic, E., Kobilka, B.K., Cheng, H., and Xiao, R.P. (2003). Linkage of beta1-adrenergic stimulation to apoptotic heart cell death through protein kinase A-independent activation of Ca^{2+}/calmodulin kinase II. J. Clin. Invest. *111*, 617–625.

6. Appendix

6.1. Supplementary Material and Methods

4% Formaldehyde (PFA)

40g PFA

800ml 1X PBS

Glass bottle placed at approx. 60^{o}C waterbath

Solution cooled, filtered and adjusted to 1L

pH adjusted to pH 6.9

Stored aliquots at -20oC

FACS Buffer

1x PBS (Ca^{2+}/Mg^{2+} free)

1mM EDTA

25mM HEPES (pH 7.0)

2% FBS

0.2µm filter-sterilised

Stored at 4^{o}C

0.2% Triton X

2ml Triton X-100

1L 1X PBS

0.02% Triton X

10ml 0.2% Triton X

1L 1X PBS

Protein Lysis Buffer

20mM TrisHCl pH 8

150mM NaCl

10% glycerol (optional)

1% Triton-X

2mM EDTA

Western Blot Solutions

1.5 M TrisHCl (pH 8.8)

Tris base 27.23g

80 ml water

Adjust to pH 8.8 with 6N HCl

Make up to final volume of 150ml with distilled water

Store at RT

0.5 M TrisHCl (pH 6.8)

Tris base 6.1g

80 ml water

Adjust to pH 6.8 with 6N HCl

Make up to final volume of 100ml with distilled water

Store at RT

10% SDS (Sodium Dodecyl Sulfate)

Add 10g SDS in 90ml water

Stir gently to dissolve

Make up to final volume of 100ml with distilled water

10% APS (Ammonium Persulfate)

Add 10g APS in 90mL water

Stir gently to dissolve

Make up to final volume of 100ml with distilled water

1.5M TrisHCl pH 8.8

18.15g Tris Base

60ml water

Adjust pH to 8.8

Make up to final volume of 100ml with distilled water

0.5M TrisHCl pH 6.8

6g Tris Base in 60ml water

Adjust pH to 6.8

Make up to final volume of 100ml with distilled water

Protein Loading Buffer

4X Laemmli Loading Buffer	
Reagents	Volume (ml)
0.5M TrisHCl (pH 6.8)	4.4
Glycerol	4.4
SDS (20%)	2.2
Bromophenol Blue (1%)	0.5
β-mercaptoethanol	0.5

Upper and Lower SDS-PAGE gels

Lower Gel (10%)		Upper Gel (4%)	
Reagents	**Volume (ml)**	**Reagents**	**Volume (ml)**
Acrylamide (30%)	6.6	Acrylamide (30%)	0.66
Water	8	Water	3
1.5M TrisHCl (pH 8.8)	5	0.5M Tris-HCl (pH 6.8)	1.25
SDS (10%)	0.2	SDS (10%)	0.05
APS (10%)	0.15	APS (10%)	0.025
TEMED	15	TEMED	0.005

SDS-PAGE and Electro-transfer Buffers

10X Running Buffer (1L)		10X Towbin's Buffer (1L)*	
Reagents	**Volume (g)**	**Reagents**	**Volume (ml)**
Tris-Base	30.3	Tris-Base	30.3
Glycine	144	Glycine	144
SDS	10	SDS	0
* 20% Methanol added in 1X Buffer before use			

Membrane Washing Buffer

10X TBS (1L)	
Reagents	**Volume (g)**
Trizma HCl	24.23
NaCl	80.06
pH to 7.6 with pure HCl or NaOH To make 1L of 1X TBST add 1ml Tween20	

6.2. Supplementary Figures

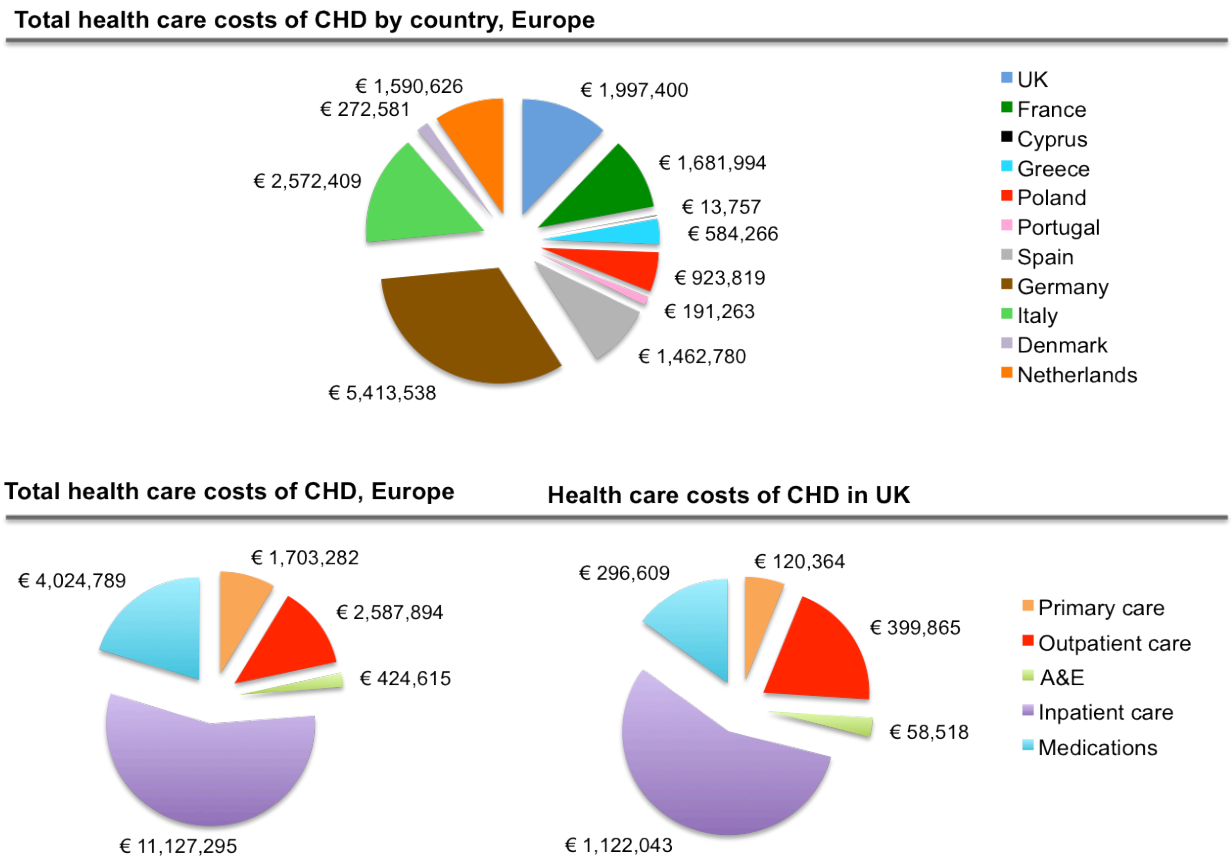


Figure S1: **Health care costs of CHD in Europe and UK.** Data were acquired from the European Cardiovascular Disease Statistics 2012 report (Nichols et al., 2012).

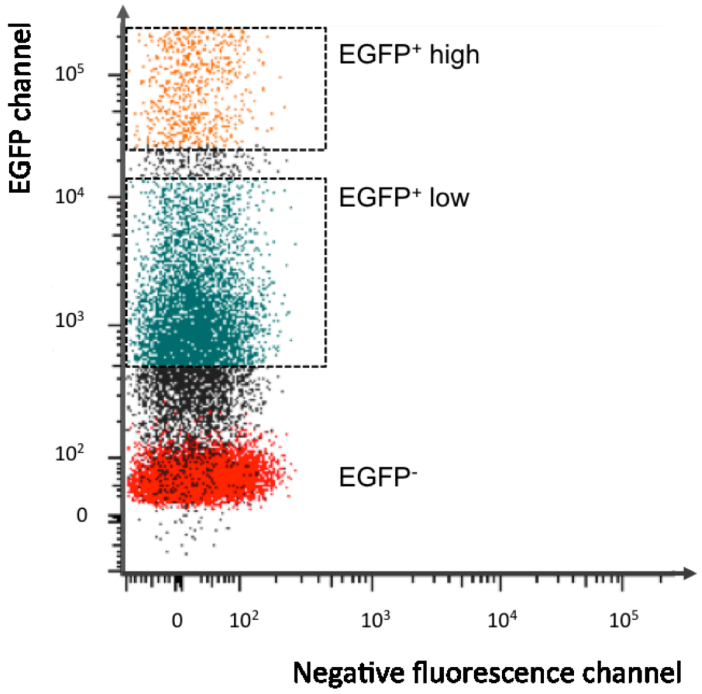


Figure S2: **Strategy for purification of EGFP^{H} and EGFP^{L} populations by FACS.** High- and low-expressing (EGFP^{H}, EGFP^{L}) HEK293T or HEK293T^{Dox} cells were gated as illustrated and purified on the basis of EGFP fluorescence for the initial knockdown screen of MAP4K4 using various shRNAmirs constructs. Three shRNAmirs that exhibited the highest degree of RNA downregulation were selected and encapsulated by a virus for downstream transduction applications.

```
MAP4K4_202_1320      MANDSPAKSLVDIDLSSLRDPAGIFELVEVVGNGTYGQVYKGRHVKTGQLAAIKVMDVTE 60
MAP4K4_001_1239      MANDSPAKSLVDIDLSSLRDPAGIFELVEVVGNGTYGQVYKGRHVKTGQLAAIKVMDVTE 60
MAP4K4_204_1279      ------------MLQALQLRTGFFCFRVLVALSPCALHDSGR-LTTG------SFNVVR 40
                                 *.:*:  :*:* :  :*. .. .   .** :.**       ::*..

MAP4K4_202_1320      DEEEEIKLEINMLKKYSHHRNIATYYGAFIKKSPPGHDDQLWLVMEFCGAGSITDLVKNT 120
MAP4K4_001_1239      DEEEEIKLEINMLKKYSHHRNIATYYGAFIKKSPPGHDDQLWLVMEFCGAGSITDLVKNT 120
MAP4K4_204_1279      DEEEEIKLEINMLKKYSHHRNIATYYGAFIKKSPPGHDDQLWLVMEFCGAGSITDLVKNT 100
                     ************************************************************

MAP4K4_202_1320      KGNTLKEDWIAYISREILRGLAHLHIHHVIHRDIKGQNVLLTENAEVKLVDFGVSAQLDR 180
MAP4K4_001_1239      KGNTLKEDWIAYISREILRGLAHLHIHHVIHRDIKGQNVLLTENAEVKLVDFGVSAQLDR 180
MAP4K4_204_1279      KGNTLKEDWIAYISREILRGLAHLHIHHVIHRDIKGQNVLLTENAEVKLVDFGVSAQLDR 160
                     ************************************************************

MAP4K4_202_1320      TVGRRNTFIGTPYWMAPEVIACDENPDATYDYRSDLWSCGITAIEMAEGAPPLCDMHPMR 240
MAP4K4_001_1239      TVGRRNTFIGTPYWMAPEVIACDENPDATYDYRSDLWSCGITAIEMAEGAPPLCDMHPMR 240
MAP4K4_204_1279      TVGRRNTFIGTPYWMAPEVIACDENPDATYDYRSDLWSCGITAIEMAEGAPPLCDMHPMR 220
                     ************************************************************

MAP4K4_202_1320      ALFLIPRNPPPRLKSKKWSKKFFSFIEGCLVKNYMQRPSTEQLLKHPFIRDQPNERQVRI 300
MAP4K4_001_1239      ALFLIPRNPPPRLKSKKWSKKFFSFIEGCLVKNYMQRPSTEQLLKHPFIRDQPNERQVRI 300
MAP4K4_204_1279      ALFLIPRNPPPRLKSKKWSKKFFSFIEGCLVKNYMQRPSTEQLLKHPFIRDQPNERQVRI 280
                     ************************************************************

MAP4K4_202_1320      QLKDHIDRTRKKRGEKDETEYEYSGSEEEEEEVPEQEGEPSSIVNVPGESTLRRDFLRLQ 360
MAP4K4_001_1239      QLKDHIDRTRKKRGEKDETEYEYSGSEEEEEEVPEQEGEPSSIVNVPGESTLRRDFLRLQ 360
MAP4K4_204_1279      QLKDHIDRTRKKRGEKDETEYEYSGSEEEEEEVPEQEGEPSSIVNVPGESTLRRDFLRLQ 340
                     ************************************************************

MAP4K4_202_1320      QENKERSEALRRQQLLQEQQLREQEEYKRQLLAERQKRIEQQKEQRRRLEEQQRREREAR 420
MAP4K4_001_1239      QENKERSEALRRQQLLQEQQLREQEEYKRQLLAERQKRIEQQKEQRRRLEEQQRREREAR 420
MAP4K4_204_1279      QENKERSEALRRQQLLQEQQLREQEEYKRQLLAERQKRIEQQKEQRRRLEEQQRREREAR 400
                     ************************************************************

MAP4K4_202_1320      RQQEREQRRREQEEKRRLEELERRRKEEEERRRAEEEKRRVEREQEYIRRQLEEEQRHLE 480
MAP4K4_001_1239      RQQEREQRRREQEEKRRLEELERRRKEEEERRRAEEEKRRVEREQEYIRRQLEEEQRHLE 480
MAP4K4_204_1279      RQQEREQRRREQEEKRRLEELERRRKEEEERRRAEEEKRRVEREQEYIRRQLEEEQRHLE 460
                     ************************************************************

MAP4K4_202_1320      VLQQQLLQEQAMLLECRWREMEEHRQAERLQRQLQQEQAYLLSLQHDHRRPHPQHSQQPP 540
MAP4K4_001_1239      VLQQQLLQEQAMLLECRWREMEEHRQAERLQRQLQQEQAYLLSLQHDHRRPHPQHSQQPP 540
MAP4K4_204_1279      VLQQQLLQEQAMLL------------------------------HDHRRPHPQHSQQPP 489
                     **************                               ***************

MAP4K4_202_1320      PPQQERSKPSFHAPEPKAHYEPADRAREVEDRFRK--TNHSSPEAQSKQTG--------- 589
MAP4K4_001_1239      PPQQERSKPSFHAPEPKAHYEPADRAREVEDRFRK--TNHSSPEAQSKQTG--------- 589
MAP4K4_204_1279      PPQQERSKPSFHAPEPKAHYEPADRAREVQWSHLASLKNNVSPVSRSHSFSDPSPKFAHH 549
                     ******************************:  .    .*: ** ::*:. .

MAP4K4_202_1320      --RVLEPPVPSRSESFS-NGNSESVHPALQRPAEPQVQWSHLASLKNNVSPVSRSHSFSD 646
MAP4K4_001_1239      --RVLEPPVPSRSESFS-NGNSESVHPALQRPAEP------------------------- 621
MAP4K4_204_1279      HLRSQDPCPPSRSEVLSQSSDSKSEAPDPTQKAWS------------------------- 584
                       *  :*  ***** :* ..:*:*  *   : * .

MAP4K4_202_1320      PSPKFAHHHLRSQDPCPPSRSEVLSQSSDSKSEAPDPTQKAWSRSDSDEVPPRVPVRTTS 706
MAP4K4_001_1239      ----------------------------------------------------QVPVRTTS 629
MAP4K4_204_1279      -------------------------------------------RSDSDEVPPRVPVRTTS 601
                                                                 :*******

MAP4K4_202_1320      RSPVLSRRDSPLQGSGQQNSQAGQRNSTSSIEPRLLWERVEKLVPRPGSGSSSGSSNSGS 766
MAP4K4_001_1239      RSPVLSRRDSPLQGSGQQNSQAGQRNSTS-IEPRLLWERVEKLVPRPGSGSSSGSSNSGS 688
MAP4K4_204_1279      RSPVLSRRDSPLQGSGQQNSQAGQRNSTSSIEPRLLWERVEKLVPRPGSGSSSGSSNSGS 661
                     ***************************** ******************************

MAP4K4_202_1320      QPGSHPGSQSGSGERFRVRSSSKSEGSPSQRLENAVKKPEDKKEVFRPLKPAVRIDLTAL 826
MAP4K4_001_1239      QPGSHPGSQSGSGERFRVRSSSKSEGSPSQRLENAVKKPEDKKEVFRPLKPA---DLTAL 745
MAP4K4_204_1279      QPGSHPGSQSGSGERFRVRSSSKSEGSPSQRLENAVKKPEDKKEVFRPLKPAVRIDLTAL 721
                     ************************************************   *****

MAP4K4_202_1320      AKELRAVEDVRPPHKVTDYSSSSEESGTTDEEDDDVEQEGADESTSGPEDTRAASSLNLS 886
MAP4K4_001_1239      AKELRAVEDVRPPHKVTDYSSSSEESGTTDEEDDDVEQEGADESTSGPEDTRAASSLNLS 805
MAP4K4_204_1279      AKELRAVEDVRPPHKVTDYSSSSEESGTTDEEDDDVEQEGADESTSGPEDTRAASSLNLS 781
                     ************************************************************

MAP4K4_202_1320      NGETESVKTMIVHDDVESEPAMTPSKEGTLIVRQ--------------------------- 920
MAP4K4_001_1239      NGETESVKTMIVHDDVESEPAMTPSKEGTLIVRQ--------------------------- 839
```

```
MAP4K4_204_1279      NGETESVKTMIVHDDVESEPAMTPSKEGTLIVRQSTVDQKRASHHESNGFAGRIHLLPDL 841
                     *********************************

MAP4K4_202_1320      -------------------------------------TQSASSTLQKHKSSSSFTPFID 942
MAP4K4_001_1239      -------------------------------------TQSASSTLQKHKSSSSFTPFID 861
MAP4K4_204_1279      LQQSHSSSTSSTSSSPSSSQPTPTMSPQTPQDKLTANETQSASSTLQKHKSSSSFTPFID 901
                                                         **********************

MAP4K4_202_1320      PRLLQISPSSGTTVTSVVGFSCDGMRPEAIRQDPTRKGSVVNVNPTNTRPQSDTPEIRKY 1002
MAP4K4_001_1239      PRLLQISPSSGTTVTSVVGFSCDGMRPEAIRQDPTRKGSVVNVNPTNTRPQSDTPEIRKY 921
MAP4K4_204_1279      PRLLQISPSSGTTVTSVVGFSCDGMRPEAIRQDPTRKGSVVNVNPTNTRPQSDTPEIRKY 961
                     ************************************************************

MAP4K4_202_1320      KKRFNSEILCAALWGVNLLVGTESGLMLLDRSGQGKVYPLINRRRFQQMDVLEGLNVLVT 1062
MAP4K4_001_1239      KKRFNSEILCAALWGVNLLVGTESGLMLLDRSGQGKVYPLINRRRFQQMDVLEGLNVLVT 981
MAP4K4_204_1279      KKRFNSEILCAALWGVNLLVGTESGLMLLDRSGQGKVYPLINRRRFQQMDVLEGLNVLVT 1021
                     ************************************************************

MAP4K4_202_1320      ISGKKDKLRVYYLSWLRNKILHNDPEVEKKQGWTTVGDLEGCVHYKVVKYERIKFLVIAL 1122
MAP4K4_001_1239      ISGKKDKLRVYYLSWLRNKILHNDPEVEKKQGWTTVGDLEGCVHYKVVKYERIKFLVIAL 1041
MAP4K4_204_1279      ISGKKDKLRVYYLSWLRNKILHNDPEVEKKQGWTTVGDLEGCVHYKVVKYERIKFLVIAL 1081
                     ************************************************************

MAP4K4_202_1320      KSSVEVYAWAPKPYHKFMAFKSFGELVHKPLLVDLTVEEGQRLKVIYGSCAGFHAVDVDS 1182
MAP4K4_001_1239      KSSVEVYAWAPKPYHKFMAFKSFGELVHKPLLVDLTVEEGQRLKVIYGSCAGFHAVDVDS 1101
MAP4K4_204_1279      KSSVEVYAWAPKPYHKFMAFKSFGELVHKPLLVDLTVEEGQRLKVIYGSCAGFHAVDVDS 1141
                     ************************************************************

MAP4K4_202_1320      GSVYDIYLPTHIQCSIKPHAIIILPNTDGMELLVCYEDEGVYVNTYGRITKDVVLQWGEM 1242
MAP4K4_001_1239      GSVYDIYLPTHIQCSIKPHAIIILPNTDGMELLVCYEDEGVYVNTYGRITKDVVLQWGEM 1161
MAP4K4_204_1279      GSVYDIYLPTHIQCSIKPHAIIILPNTDGMELLVCYEDEGVYVNTYGRITKDVVLQWGEM 1201
                     ************************************************************

MAP4K4_202_1320      PTSVAYIRSNQTMGWGEKAIEIRSVETGHLDGVFMHKRAQRLKFLCERNDKVFFASVRSG 1302
MAP4K4_001_1239      PTSVAYIRSNQTMGWGEKAIEIRSVETGHLDGVFMHKRAQRLKFLCERNDKVFFASVRSG 1221
MAP4K4_204_1279      PTSVAYIRSNQTMGWGEKAIEIRSVETGHLDGVFMHKRAQRLKFLCERNDKVFFASVRSG 1261
                     ************************************************************

MAP4K4_202_1320      GSSQVYFMTLGRTSLLSW 1320
MAP4K4_001_1239      GSSQVYFMTLGRTSLLSW 1239
MAP4K4_204_1279      GSSQVYFMTLGRTSLLSW 1279
                     ******************
```

Figure S3: **MAP4K4 isoforms.** MAP4K4_202 (ENST00000324219), MAP4K4_001 (ENST00000347699), and MAP4K4_204 (ENST00000350878) are 1320, 1239 and 1279aa in length and 4116, 3792 and 3919bp in length, respectively. The last two isoforms are considered short isoforms of the full-length protein (MAP4K4_202). Putative sequences for antibody binding are colour-shaded (blue for ab56569; green for ab70424).


MAP4K4_202_1320 CTGGTCTGCGGCTGAGATACACAGAGCGACAGAGACATTTATTGTTATTTGTTTTTTGGT 60
MAP4K4_001_1239 --
MAP4K4_204_1279 --
MAP4K4_202_1320 GGCAAAAAGGGAAAATGGCGAACGACTCCCCTGCAAAAAGTCTGGTGGACATCGACCTCT 120
MAP4K4_001_1239 --------------ATGGCGAACGACTCCCCTGCAAAAAGTCTGGTGGACATCGACCTCT 46
MAP4K4_204_1279 ------------------------------ATGCTACAGGCCT-------------TACA 17
.***:*.*.* ** :*:
MAP4K4_202_1320 CCTCCCTGCGGGATCCTGCTGGGATTTTTGAGCTGGTGGAAGTGGTTGGAAATGGCACCT 180
MAP4K4_001_1239 CCTCCCTGCGGGATCCTGCTGGGATTTTTGAGCTGGTGGAAGTGGTTGGAAATGGCACCT 106
MAP4K4_204_1279 GCTTCGTACTGGCTTCTTCTG-TTTTAGGGTGTTGGTGGCACTTTCTCCCTGTG----CT 72
** * *.* **.* ** *** :**: *:* ******.* * * .:.** **
MAP4K4_202_1320 ATGGACAAGTCTATAAGGGTCGACATGTTAAAACGGGTCAGTTGGCAGCCATCAAAGTTA 240
MAP4K4_001_1239 ATGGACAAGTCTATAAGGGTCGACATGTTAAAACGGGTCAGTTGGCAGCCATCAAAGTTA 166
MAP4K4_204_1279 TTG--CATGACTCTGGCAGAC------TTACCACAGG---------ATCATTCAACGT-- 113
:** **:*:**.*.. .*:* ***..**.** * *.:****.**
MAP4K4_202_1320 TGGATGTCACTGAGGATGAAGAGGAAGAAATCAAACTGGAGATAAATATGCTAAAGAAAT 300
MAP4K4_001_1239 TGGATGTCACTGAGGATGAAGAGGAAGAAATCAAACTGGAGATAAATATGCTAAAGAAAT 226
MAP4K4_204_1279 ----TGTCAG---GGATGAAGAGGAAGAAATCAAACTGGAGATAAATATGCTAAAGAAAT 166
***** **********
MAP4K4_202_1320 ACTCTCATCACAGAAACATTGCAACATATTATGGTGCTTTCATCAAAAAGAGCCCTCCAG 360
MAP4K4_001_1239 ACTCTCATCACAGAAACATTGCAACATATTATGGTGCTTTCATCAAAAAGAGCCCTCCAG 286
MAP4K4_204_1279 ACTCTCATCACAGAAACATTGCAACATATTATGGTGCTTTCATCAAAAAGAGCCCTCCAG 226
MAP4K4_202_1320 GACATGATGACCAACTCTGGCTTGTTATGGAGTTCTGTGGGGCTGGGTCCATTACAGACC 420
MAP4K4_001_1239 GACATGATGACCAACTCTGGCTTGTTATGGAGTTCTGTGGGGCTGGGTCCATTACAGACC 346
MAP4K4_204_1279 GACATGATGACCAACTCTGGCTTGTTATGGAGTTCTGTGGGGCTGGGTCCATTACAGACC 286
MAP4K4_202_1320 TTGTGAAGAACACCAAAGGGAACACACTCAAAGAAGACTGGATCGCTTACATCTCCAGAG 480
MAP4K4_001_1239 TTGTGAAGAACACCAAAGGGAACACACTCAAAGAAGACTGGATCGCTTACATCTCCAGAG 406
MAP4K4_204_1279 TTGTGAAGAACACCAAAGGGAACACACTCAAAGAAGACTGGATCGCTTACATCTCCAGAG 346
MAP4K4_202_1320 AAATCCTGAGGGGACTGGCACATCTTCACATTCATCATGTGATTCACCGGGATATCAAGG 540
MAP4K4_001_1239 AAATCCTGAGGGGACTGGCACATCTTCACATTCATCATGTGATTCACCGGGATATCAAGG 466
MAP4K4_204_1279 AAATCCTGAGGGGACTGGCACATCTTCACATTCATCATGTGATTCACCGGGATATCAAGG 406
MAP4K4_202_1320 GCCAGAATGTGTTGCTGACTGAGAATGCAGAGGTGAAACTTGTTGACTTTGGTGTGAGTG 600
MAP4K4_001_1239 GCCAGAATGTGTTGCTGACTGAGAATGCAGAGGTGAAACTTGTTGACTTTGGTGTGAGTG 526
MAP4K4_204_1279 GCCAGAATGTGTTGCTGACTGAGAATGCAGAGGTGAAACTTGTTGACTTTGGTGTGAGTG 466
MAP4K4_202_1320 CTCAGCTGGACAGGACTGTGGGGCGGAGAAATACGTTCATAGGCACTCCCTACTGGATGG 660
MAP4K4_001_1239 CTCAGCTGGACAGGACTGTGGGGCGGAGAAATACGTTCATAGGCACTCCCTACTGGATGG 586
MAP4K4_204_1279 CTCAGCTGGACAGGACTGTGGGGCGGAGAAATACGTTCATAGGCACTCCCTACTGGATGG 526
MAP4K4_202_1320 CTCCTGAGGTCATCGCCTGTGATGAGAACCCAGATGCCACCTATGATTACAGAAGTGATC 720
MAP4K4_001_1239 CTCCTGAGGTCATCGCCTGTGATGAGAACCCAGATGCCACCTATGATTACAGAAGTGATC 646
MAP4K4_204_1279 CTCCTGAGGTCATCGCCTGTGATGAGAACCCAGATGCCACCTATGATTACAGAAGTGATC 586
MAP4K4_202_1320 TTTGGTCTTGTGGCATTACAGCCATTGAGATGGCAGAAGGTGCTCCCCCTCTCTGTGACA 780
MAP4K4_001_1239 TTTGGTCTTGTGGCATTACAGCCATTGAGATGGCAGAAGGTGCTCCCCCTCTCTGTGACA 706
MAP4K4_204_1279 TTTGGTCTTGTGGCATTACAGCCATTGAGATGGCAGAAGGTGCTCCCCCTCTCTGTGACA 646
MAP4K4_202_1320 TGCATCCAATGAGAGCACTGTTTCTCATTCCCAGAAACCCTCCTCCCCGGCTGAAGTCAA 840
MAP4K4_001_1239 TGCATCCAATGAGAGCACTGTTTCTCATTCCCAGAAACCCTCCTCCCCGGCTGAAGTCAA 766
MAP4K4_204_1279 TGCATCCAATGAGAGCACTGTTTCTCATTCCCAGAAACCCTCCTCCCCGGCTGAAGTCAA 706
MAP4K4_202_1320 AAAAATGGTCGAAGAAGTTTTTTAGTTTTATAGAAGGGTGCCTGGTGAAGAATTACATGC 900
MAP4K4_001_1239 AAAAATGGTCGAAGAAGTTTTTTAGTTTTATAGAAGGGTGCCTGGTGAAGAATTACATGC 826
MAP4K4_204_1279 AAAAATGGTCGAAGAAGTTTTTTAGTTTTATAGAAGGGTGCCTGGTGAAGAATTACATGC 766
MAP4K4_202_1320 AGCGGCCCTCTACAGAGCAGCTTTTGAAACATCCTTTTATAAGGGATCAGCCAAATGAAA 960
MAP4K4_001_1239 AGCGGCCCTCTACAGAGCAGCTTTTGAAACATCCTTTTATAAGGGATCAGCCAAATGAAA 886
MAP4K4_204_1279 AGCGGCCCTCTACAGAGCAGCTTTTGAAACATCCTTTTATAAGGGATCAGCCAAATGAAA 826

```
                    ************************************************************

MAP4K4_202_1320     GGCAAGTTAGAATCCAGCTTAAGGATCATATAGATCGTACCAGGAAGAAGAGAGGCGAGA 1020
MAP4K4_001_1239     GGCAAGTTAGAATCCAGCTTAAGGATCATATAGATCGTACCAGGAAGAAGAGAGGCGAGA 946
MAP4K4_204_1279     GGCAAGTTAGAATCCAGCTTAAGGATCATATAGATCGTACCAGGAAGAAGAGAGGCGAGA 886
                    ************************************************************

MAP4K4_202_1320     AAGATGAAACTGAGTATGAGTACAGTGGGAGTGAGGAAGAAGAGGAGGAAGTGCCTGAAC 1080
MAP4K4_001_1239     AAGATGAAACTGAGTATGAGTACAGTGGGAGTGAGGAAGAAGAGGAGGAAGTGCCTGAAC 1006
MAP4K4_204_1279     AAGATGAAACTGAGTATGAGTACAGTGGGAGTGAGGAAGAAGAGGAGGAAGTGCCTGAAC 946
                    ************************************************************

MAP4K4_202_1320     AGGAAGGAGAGCCAAGTTCCATTGTGAACGTGCCTGGTGAGTCTACTCTTCGCCGAGATT 1140
MAP4K4_001_1239     AGGAAGGAGAGCCAAGTTCCATTGTGAACGTGCCTGGTGAGTCTACTCTTCGCCGAGATT 1066
MAP4K4_204_1279     AGGAAGGAGAGCCAAGTTCCATTGTGAACGTGCCTGGTGAGTCTACTCTTCGCCGAGATT 1006
                    ************************************************************

MAP4K4_202_1320     TCCTGAGACTGCAGCAGGAGAACAAGGAACGTTCCGAGGCTCTTCGGAGACAACAGTTAC 1200
MAP4K4_001_1239     TCCTGAGACTGCAGCAGGAGAACAAGGAACGTTCCGAGGCTCTTCGGAGACAACAGTTAC 1126
MAP4K4_204_1279     TCCTGAGACTGCAGCAGGAGAACAAGGAACGTTCCGAGGCTCTTCGGAGACAACAGTTAC 1066
                    ************************************************************

MAP4K4_202_1320     TACAGGAGCAACAGCTCCGGGAGCAGGAAGAATATAAAAGGCAACTGCTGGCAGAGAGAC 1260
MAP4K4_001_1239     TACAGGAGCAACAGCTCCGGGAGCAGGAAGAATATAAAAGGCAACTGCTGGCAGAGAGAC 1186
MAP4K4_204_1279     TACAGGAGCAACAGCTCCGGGAGCAGGAAGAATATAAAAGGCAACTGCTGGCAGAGAGAC 1126
                    ************************************************************

MAP4K4_202_1320     AGAAGCGGATTGAGCAGCAGAAAGAACAGAGGCGACGGCTAGAAGAGCAACAAAGGAGAG 1320
MAP4K4_001_1239     AGAAGCGGATTGAGCAGCAGAAAGAACAGAGGCGACGGCTAGAAGAGCAACAAAGGAGAG 1246
MAP4K4_204_1279     AGAAGCGGATTGAGCAGCAGAAAGAACAGAGGCGACGGCTAGAAGAGCAACAAAGGAGAG 1186
                    ************************************************************

MAP4K4_202_1320     AGCGGGAAGCTAGAAGGCAGCAGGAACGTGAACAGCGAAGGAGAGAACAAGAAGAAAAGA 1380
MAP4K4_001_1239     AGCGGGAAGCTAGAAGGCAGCAGGAACGTGAACAGCGAAGGAGAGAACAAGAAGAAAAGA 1306
MAP4K4_204_1279     AGCGGGAAGCTAGAAGGCAGCAGGAACGTGAACAGCGAAGGAGAGAACAAGAAGAAAAGA 1246
                    ************************************************************

MAP4K4_202_1320     GGCGTCTAGAGGAGTTGGAGAGAAGGCGCAAAGAAGAAGAGGAGAGGAGACGGGCAGAAG 1440
MAP4K4_001_1239     GGCGTCTAGAGGAGTTGGAGAGAAGGCGCAAAGAAGAAGAGGAGAGGAGACGGGCAGAAG 1366
MAP4K4_204_1279     GGCGTCTAGAGGAGTTGGAGAGAAGGCGCAAAGAAGAAGAGGAGAGGAGACGGGCAGAAG 1306
                    ************************************************************

MAP4K4_202_1320     AAGAAAAGAGGAGAGTTGAAAGAGAACAGGAGTATATCAGGCGACAGCTAGAAGAGGAGC 1500
MAP4K4_001_1239     AAGAAAAGAGGAGAGTTGAAAGAGAACAGGAGTATATCAGGCGACAGCTAGAAGAGGAGC 1426
MAP4K4_204_1279     AAGAAAAGAGGAGAGTTGAAAGAGAACAGGAGTATATCAGGCGACAGCTAGAAGAGGAGC 1366
                    ************************************************************

MAP4K4_202_1320     AGCGGCACTTGGAAGTCCTTCAGCAGCAGCTGCTCCAGGAGCAGGCCATGTTACTGGAGT 1560
MAP4K4_001_1239     AGCGGCACTTGGAAGTCCTTCAGCAGCAGCTGCTCCAGGAGCAGGCCATGTTACTGGAGT 1486
MAP4K4_204_1279     AGCGGCACTTGGAAGTCCTTCAGCAGCAGCTGCTCCAGGAGCAGGCCATGTTACTG---- 1422
                    ************************************************************

MAP4K4_202_1320     GCCGATGGCGGGAGATGGAGGAGCACCGGCAGGCAGAGAGGCTCCAGAGGCAGTTGCAAC 1620
MAP4K4_001_1239     GCCGATGGCGGGAGATGGAGGAGCACCGGCAGGCAGAGAGGCTCCAGAGGCAGTTGCAAC 1546
MAP4K4_204_1279     ------------------------------------------------------------


MAP4K4_202_1320     AAGAACAAGCATATCTCCTGTCTCTACAGCATGACCATAGGAGGCCGCACCCGCAGCACT 1680
MAP4K4_001_1239     AAGAACAAGCATATCTCCTGTCTCTACAGCATGACCATAGGAGGCCGCACCCGCAGCACT 1606
MAP4K4_204_1279     ------------------------------CATGACCATAGGAGGCCGCACCCGCAGCACT 1453
                                                 ******************************

MAP4K4_202_1320     CGCAGCAGCCGCCACCACCGCAGCAGGAAAGGAGCAAGCCAAGCTTCCATGCTCCCGAGC 1740
MAP4K4_001_1239     CGCAGCAGCCGCCACCACCGCAGCAGGAAAGGAGCAAGCCAAGCTTCCATGCTCCCGAGC 1666
MAP4K4_204_1279     CGCAGCAGCCGCCACCACCGCAGCAGGAAAGGAGCAAGCCAAGCTTCCATGCTCCCGAGC 1513
                    ************************************************************

MAP4K4_202_1320     CCAAAGCCCACTACGAGCCTGCTGACCGAGCGCGAGAGGTGGAAGATAGATTTAGGAAAA 1800
MAP4K4_001_1239     CCAAAGCCCACTACGAGCCTGCTGACCGAGCGCGAGAGGTGGAAGATAGATTTAGGAAAA 1726
MAP4K4_204_1279     CCAAAGCCCACTACGAGCCTGCTGACCGAGCGCGAGAGGTACAG---TGGTCCCACCTGG 1570
                    ***************************************. *.   :*.*  .. .:..

MAP4K4_202_1320     CTAACCACAGCTCCCCTGAAGCCCAGTCTAAGCAGACAGGCAGAGTATTGGAGCCACCAG 1860
MAP4K4_001_1239     CTAACCACAGCTCCCCTGAAGCCCAGTCTAAGCAGACAGGCAGAGTATTGGAGCCACCAG 1786
MAP4K4_204_1279     CATCTCTCAAGAACAATGTTTCCCCTGTCTCGCGATCC--CATTCCTTCAGTGACCCTTC 1628
                    *::. *:**. :.*..**:: ***.    :.**..:*.  ** :  :* .*:*.*.* :

MAP4K4_202_1320     TGCCTTCCCGATCAGAGTCTTTTTCCAATGGCAACTCCGAGTCTGTGCATCCCGCCCTGC 1920
```

```
MAP4K4_001_1239      TGCCTTCCCGATCAGAGTCTTTTTCCAATGGCAACTCCGAGTCTGTGCATCCCGCCCTGC 1846
MAP4K4_204_1279      TCCCAAATTTGCACACCACCATCTTCGTTCTCAGGACCCATGTCCACCTTCCCGCAGTGA 1688
                     * **::.   . .... :* :* * *.:*  **. :** *     : *:******. **.

MAP4K4_202_1320      AGAGACCAGCGGAGCCACAGGTACAGTGGTCCCACCTGGCATCTCTCAAGAACAATGTTT 1980
MAP4K4_001_1239      AGAGACCAGCGGAGCCACAG---------------------------------------- 1866
MAP4K4_204_1279      GGTGCTCAGTCAGAGCTCTG---------------------------------------- 1708
                     .*:*. ***  ... *:*:*

MAP4K4_202_1320      CCCCTGTCTCGCGATCCCATTCCTTCAGTGACCCTTCTCCCAAATTTGCACACCACCATC 2040
MAP4K4_001_1239      ------------------------------------------------------------
MAP4K4_204_1279      ------------------------------------------------------------


MAP4K4_202_1320      TTCGTTCTCAGGACCCATGTCCACCTTCCCGCAGTGAGGTGCTCAGTCAGAGCTCTGACT 2100
MAP4K4_001_1239      ------------------------------------------------------------
MAP4K4_204_1279      ------------------------------------------------------------ACT 1711


MAP4K4_202_1320      CTAAGTCAGAGGCGCCTGACCCTACCCAAAAGGCTTGGTCTAGATCAGACAGTGACGAGG 2160
MAP4K4_001_1239      ------------------------------------------------------------
MAP4K4_204_1279      CTAAGTCAGAGGCGCCTGACCCTACCCAAAAGGCTTGGTCTAGATCAGACAGTGACGAGG 1771


MAP4K4_202_1320      TGCCTCCAAGGGTTCCTGTGAGAACAACATCTCGCTCCCCTGTTCTGTCCCGTCGAGATT 2220
MAP4K4_001_1239      -----------GTTCCTGTGAGAACAACATCTCGCTCCCCTGTTCTGTCCCGTCGAGATT 1915
MAP4K4_204_1279      TGCCTCCAAGGGTTCCTGTGAGAACAACATCTCGCTCCCCTGTTCTGTCCCGTCGAGATT 1831
                                ************************************************


MAP4K4_202_1320      CCCCACTGCAGGGCAGTGGGCAGCAGAATAGCCAGGCAGGACAGAGAAACTCCACCAGCA 2280
MAP4K4_001_1239      CCCCACTGCAGGGCAGTGGGCAGCAGAATAGCCAGGCAGGACAGAGAAACTCCACCAG-- 1973
MAP4K4_204_1279      CCCCACTGCAGGGCAGTGGGCAGCAGAATAGCCAGGCAGGACAGAGAAACTCCACCAGCA 1891
                     ************************************************************


MAP4K4_202_1320      GTATTGAGCCCAGGCTTCTGTGGGAGAGAGTGGAGAAGCTGGTGCCCAGACCTGGCAGTG 2340
MAP4K4_001_1239      -TATTGAGCCCAGGCTTCTGTGGGAGAGAGTGGAGAAGCTGGTGCCCAGACCTGGCAGTG 2032
MAP4K4_204_1279      GTATTGAGCCCAGGCTTCTGTGGGAGAGAGTGGAGAAGCTGGTGCCCAGACCTGGCAGTG 1951
                      ************************************************************


MAP4K4_202_1320      GCAGCTCCTCAGGGTCCAGCAACTCAGGATCCCAGCCCGGGTCTCACCCTGGGTCTCAGA 2400
MAP4K4_001_1239      GCAGCTCCTCAGGGTCCAGCAACTCAGGATCCCAGCCCGGGTCTCACCCTGGGTCTCAGA 2092
MAP4K4_204_1279      GCAGCTCCTCAGGGTCCAGCAACTCAGGATCCCAGCCCGGGTCTCACCCTGGGTCTCAGA 2011
                     ************************************************************


MAP4K4_202_1320      GTGGCTCCGGGGAACGCTTCAGAGTGAGATCATCATCCAAGTCTGAAGGCTCTCCATCTC 2460
MAP4K4_001_1239      GTGGCTCCGGGGAACGCTTCAGAGTGAGATCATCATCCAAGTCTGAAGGCTCTCCATCTC 2152
MAP4K4_204_1279      GTGGCTCCGGGGAACGCTTCAGAGTGAGATCATCATCCAAGTCTGAAGGCTCTCCATCTC 2071
                     ************************************************************


MAP4K4_202_1320      AGCGCCTGGAAAATGCAGTGAAAAAACCTGAAGATAAAAAGGAAGTTTTCAGACCCCTCA 2520
MAP4K4_001_1239      AGCGCCTGGAAAATGCAGTGAAAAAACCTGAAGATAAAAAGGAAGTTTTCAGACCCCTCA 2212
MAP4K4_204_1279      AGCGCCTGGAAAATGCAGTGAAAAAACCTGAAGATAAAAAGGAAGTTTTCAGACCCCTCA 2131
                     ************************************************************


MAP4K4_202_1320      AGCCTGCTGTAAGGATTGATCTGACCGCACTGGCCAAAGAGCTTCGAGCAGTGGAAGATG 2580
MAP4K4_001_1239      AGCCTGCTG---------ATCTGACCGCACTGGCCAAAGAGCTTCGAGCAGTGGAAGATG 2263
MAP4K4_204_1279      AGCCTGCTGTAAGGATTGATCTGACCGCACTGGCCAAAGAGCTTCGAGCAGTGGAAGATG 2191
                     *********         ****************************************


MAP4K4_202_1320      TACGGCCACCTCACAAAGTAACGGACTACTCCTCATCCAGTGAGGAGTCGGGGACGACGG 2640
MAP4K4_001_1239      TACGGCCACCTCACAAAGTAACGGACTACTCCTCATCCAGTGAGGAGTCGGGGACGACGG 2323
MAP4K4_204_1279      TACGGCCACCTCACAAAGTAACGGACTACTCCTCATCCAGTGAGGAGTCGGGGACGACGG 2251
                     ************************************************************


MAP4K4_202_1320      ATGAGGAGGACGACGATGTGGAGCAGGAAGGGGCTGACGAGTCCACCTCAGGACCAGAGG 2700
MAP4K4_001_1239      ATGAGGAGGACGACGATGTGGAGCAGGAAGGGGCTGACGAGTCCACCTCAGGACCAGAGG 2383
MAP4K4_204_1279      ATGAGGAGGACGACGATGTGGAGCAGGAAGGGGCTGACGAGTCCACCTCAGGACCAGAGG 2311
                     ************************************************************


MAP4K4_202_1320      ACACCAGAGCAGCGTCATCTCTGAATTTGAGCAATGGTGAAACGGAATCTGTGAAAACCA 2760
MAP4K4_001_1239      ACACCAGAGCAGCGTCATCTCTGAATTTGAGCAATGGTGAAACGGAATCTGTGAAAACCA 2443
MAP4K4_204_1279      ACACCAGAGCAGCGTCATCTCTGAATTTGAGCAATGGTGAAACGGAATCTGTGAAAACCA 2371
                     ************************************************************


MAP4K4_202_1320      TGATTGTCCATGATGATGTAGAAAGTGAGCCGGCCATGACCCCATCCAAGGAGGGCACTC 2820
MAP4K4_001_1239      TGATTGTCCATGATGATGTAGAAAGTGAGCCGGCCATGACCCCATCCAAGGAGGGCACTC 2503
MAP4K4_204_1279      TGATTGTCCATGATGATGTAGAAAGTGAGCCGGCCATGACCCCATCCAAGGAGGGCACTC 2431
                     ************************************************************
```

```
MAP4K4_202_1320      TAATCGTCCGCCAGA---------------------------------------------- 2835
MAP4K4_001_1239      TAATCGTCCGCCAGA---------------------------------------------- 2518
MAP4K4_204_1279      TAATCGTCCGCCAGAGTACAGTTGACCAAAAGCGTGCCAGCCATCATGAGAGCAATGGCT 2491
                     ***************

MAP4K4_202_1320      ------------------------------------------------------------
MAP4K4_001_1239      ------------------------------------------------------------
MAP4K4_204_1279      TTGCCGGTCGCATTCACCTCTTGCCAGATCTCTTACAGCAAAGCCATTCCTCCTCCACTT 2551


MAP4K4_202_1320      ------------------------------------------------------------
MAP4K4_001_1239      ------------------------------------------------------------
MAP4K4_204_1279      CCTCCACCTCCTCCTCCCCATCCTCCAGCCAGCCGACACCCACCATGTCCCCACAGACAC 2611


MAP4K4_202_1320      ----------------------------CTCAGTCCGCTAGTAGCACACTCCAGAAACACA 2868
MAP4K4_001_1239      ----------------------------CTCAGTCCGCTAGTAGCACACTCCAGAAACACA 2551
MAP4K4_204_1279      CCCAGGACAAGCTCACTGCTAATGAGACTCAGTCCGCTAGTAGCACACTCCAGAAACACA 2671
                                                 **********************************

MAP4K4_202_1320      AATCTTCCTCCTCCTTTACACCTTTTATAGACCCCAGATTACTACAGATTTCTCCATCTA 2928
MAP4K4_001_1239      AATCTTCCTCCTCCTTTACACCTTTTATAGACCCCAGATTACTACAGATTTCTCCATCTA 2611
MAP4K4_204_1279      AATCTTCCTCCTCCTTTACACCTTTTATAGACCCCAGATTACTACAGATTTCTCCATCTA 2731
                     ************************************************************

MAP4K4_202_1320      GCGGAACAACAGTGACATCTGTGGTGGGATTTTCCTGTGATGGGATGAGACCAGAAGCCA 2988
MAP4K4_001_1239      GCGGAACAACAGTGACATCTGTGGTGGGATTTTCCTGTGATGGGATGAGACCAGAAGCCA 2671
MAP4K4_204_1279      GCGGAACAACAGTGACATCTGTGGTGGGATTTTCCTGTGATGGGATGAGACCAGAAGCCA 2791
                     ************************************************************

MAP4K4_202_1320      TAAGGCAAGATCCTACCCGGAAAGGCTCAGTGGTCAATGTGAATCCTACCAACACTAGGC 3048
MAP4K4_001_1239      TAAGGCAAGATCCTACCCGGAAAGGCTCAGTGGTCAATGTGAATCCTACCAACACTAGGC 2731
MAP4K4_204_1279      TAAGGCAAGATCCTACCCGGAAAGGCTCAGTGGTCAATGTGAATCCTACCAACACTAGGC 2851
                     ************************************************************

MAP4K4_202_1320      CACAGAGTGACACCCCGGAGATTCGTAAATACAAGAAGAGGTTTAACTCTGAGATTCTGT 3108
MAP4K4_001_1239      CACAGAGTGACACCCCGGAGATTCGTAAATACAAGAAGAGGTTTAACTCTGAGATTCTGT 2791
MAP4K4_204_1279      CACAGAGTGACACCCCGGAGATTCGTAAATACAAGAAGAGGTTTAACTCTGAGATTCTGT 2911
                     ************************************************************

MAP4K4_202_1320      GTGCTGCCTTATGGGGAGTGAATTTGCTAGTGGGTACAGAGAGTGGCCTGATGCTGCTGG 3168
MAP4K4_001_1239      GTGCTGCCTTATGGGGAGTGAATTTGCTAGTGGGTACAGAGAGTGGCCTGATGCTGCTGG 2851
MAP4K4_204_1279      GTGCTGCCTTATGGGGAGTGAATTTGCTAGTGGGTACAGAGAGTGGCCTGATGCTGCTGG 2971
                     ************************************************************

MAP4K4_202_1320      ACAGAAGTGGCCAAGGGAAGGTCTATCCTCTTATCAACCGAAGACGATTTCAACAAATGG 3228
MAP4K4_001_1239      ACAGAAGTGGCCAAGGGAAGGTCTATCCTCTTATCAACCGAAGACGATTTCAACAAATGG 2911
MAP4K4_204_1279      ACAGAAGTGGCCAAGGGAAGGTCTATCCTCTTATCAACCGAAGACGATTTCAACAAATGG 3031
                     ************************************************************

MAP4K4_202_1320      ACGTACTTGAGGGCTTGAATGTCTTGGTGACAATATCTGGCAAAAAGGATAAGTTACGTG 3288
MAP4K4_001_1239      ACGTACTTGAGGGCTTGAATGTCTTGGTGACAATATCTGGCAAAAAGGATAAGTTACGTG 2971
MAP4K4_204_1279      ACGTACTTGAGGGCTTGAATGTCTTGGTGACAATATCTGGCAAAAAGGATAAGTTACGTG 3091
                     ************************************************************

MAP4K4_202_1320      TCTACTATTTGTCCTGGTTAAGAAATAAAATACTTCACAATGATCCAGAAGTTGAGAAGA 3348
MAP4K4_001_1239      TCTACTATTTGTCCTGGTTAAGAAATAAAATACTTCACAATGATCCAGAAGTTGAGAAGA 3031
MAP4K4_204_1279      TCTACTATTTGTCCTGGTTAAGAAATAAAATACTTCACAATGATCCAGAAGTTGAGAAGA 3151
                     ************************************************************

MAP4K4_202_1320      AGCAGGGATGGACAACCGTAGGGGATTTGGAAGGATGTGTACATTATAAAGTTGTAAAAT 3408
MAP4K4_001_1239      AGCAGGGATGGACAACCGTAGGGGATTTGGAAGGATGTGTACATTATAAAGTTGTAAAAT 3091
MAP4K4_204_1279      AGCAGGGATGGACAACCGTAGGGGATTTGGAAGGATGTGTACATTATAAAGTTGTAAAAT 3211
                     ************************************************************

MAP4K4_202_1320      ATGAAAGAATCAAATTTCTGGTGATTGCTTTGAAGAGTTCTGTGGAAGTCTATGCGTGGG 3468
MAP4K4_001_1239      ATGAAAGAATCAAATTTCTGGTGATTGCTTTGAAGAGTTCTGTGGAAGTCTATGCGTGGG 3151
MAP4K4_204_1279      ATGAAAGAATCAAATTTCTGGTGATTGCTTTGAAGAGTTCTGTGGAAGTCTATGCGTGGG 3271
                     ************************************************************

MAP4K4_202_1320      CACCAAAGCCATATCACAAATTTATGGCCTTTAAGTCATTTGGAGAATTGGTACATAAGC 3528
MAP4K4_001_1239      CACCAAAGCCATATCACAAATTTATGGCCTTTAAGTCATTTGGAGAATTGGTACATAAGC 3211
MAP4K4_204_1279      CACCAAAGCCATATCACAAATTTATGGCCTTTAAGTCATTTGGAGAATTGGTACATAAGC 3331
                     ************************************************************

MAP4K4_202_1320      CATTACTGGTGGATCTCACTGTTGAGGAAGGCCAGAGGTTGAAAGTGATCTATGGATCCT 3588
MAP4K4_001_1239      CATTACTGGTGGATCTCACTGTTGAGGAAGGCCAGAGGTTGAAAGTGATCTATGGATCCT 3271
```

```
MAP4K4_204_1279      CATTACTGGTGGATCTCACTGTTGAGGAAGGCCAGAGGTTGAAAGTGATCTATGGATCCT 3391
                     ************************************************************

MAP4K4_202_1320      GTGCTGGATTCCATGCTGTTGATGTGGATTCAGGATCAGTCTATGACATTTATCTACCAA 3648
MAP4K4_001_1239      GTGCTGGATTCCATGCTGTTGATGTGGATTCAGGATCAGTCTATGACATTTATCTACCAA 3331
MAP4K4_204_1279      GTGCTGGATTCCATGCTGTTGATGTGGATTCAGGATCAGTCTATGACATTTATCTACCAA 3451
                     ************************************************************

MAP4K4_202_1320      CACATATCCAGTGTAGCATCAAACCCCATGCAATCATCATCCTCCCCAATACAGATGGAA 3708
MAP4K4_001_1239      CACATATCCAGTGTAGCATCAAACCCCATGCAATCATCATCCTCCCCAATACAGATGGAA 3391
MAP4K4_204_1279      CACATATCCAGTGTAGCATCAAACCCCATGCAATCATCATCCTCCCCAATACAGATGGAA 3511
                     ************************************************************

MAP4K4_202_1320      TGGAGCTTCTGGTGTGCTATGAAGATGAGGGGGTTTATGTAAACACATATGGAAGGATCA 3768
MAP4K4_001_1239      TGGAGCTTCTGGTGTGCTATGAAGATGAGGGGGTTTATGTAAACACATATGGAAGGATCA 3451
MAP4K4_204_1279      TGGAGCTTCTGGTGTGCTATGAAGATGAGGGGGTTTATGTAAACACATATGGAAGGATCA 3571
                     ************************************************************

MAP4K4_202_1320      CCAAGGATGTAGTTCTACAGTGGGGAGAGATGCCTACATCAGTAGCATATATTCGATCCA 3828
MAP4K4_001_1239      CCAAGGATGTAGTTCTACAGTGGGGAGAGATGCCTACATCAGTAGCATATATTCGATCCA 3511
MAP4K4_204_1279      CCAAGGATGTAGTTCTACAGTGGGGAGAGATGCCTACATCAGTAGCATATATTCGATCCA 3631
                     ************************************************************

MAP4K4_202_1320      ATCAGACAATGGGCTGGGGAGAGAAGGCCATAGAGATCCGATCTGTGGAAACTGGTCACT 3888
MAP4K4_001_1239      ATCAGACAATGGGCTGGGGAGAGAAGGCCATAGAGATCCGATCTGTGGAAACTGGTCACT 3571
MAP4K4_204_1279      ATCAGACAATGGGCTGGGGAGAGAAGGCCATAGAGATCCGATCTGTGGAAACTGGTCACT 3691
                     ************************************************************

MAP4K4_202_1320      TGGATGGTGTGTTCATGCACAAAAGGGCTCAAAGACTAAAATTCTTGTGTGAACGCAATG 3948
MAP4K4_001_1239      TGGATGGTGTGTTCATGCACAAAAGGGCTCAAAGACTAAAATTCTTGTGTGAACGCAATG 3631
MAP4K4_204_1279      TGGATGGTGTGTTCATGCACAAAAGGGCTCAAAGACTAAAATTCTTGTGTGAACGCAATG 3751
                     ************************************************************

MAP4K4_202_1320      ACAAGGTGTTCTTTGCCTCTGTTCGGTCTGGTGGCAGCAGTCAGGTTTATTTCATGACCT 4008
MAP4K4_001_1239      ACAAGGTGTTCTTTGCCTCTGTTCGGTCTGGTGGCAGCAGTCAGGTTTATTTCATGACCT 3691
MAP4K4_204_1279      ACAAGGTGTTCTTTGCCTCTGTTCGGTCTGGTGGCAGCAGTCAGGTTTATTTCATGACCT 3811
                     ************************************************************

MAP4K4_202_1320      TAGGCAGGACTTCTCTTCTGAGCTGGTAGAAGCAGTGTGATCCAGGGATTACTGGCCTCC 4068
MAP4K4_001_1239      TAGGCAGGACTTCTCTTCTGAGCTGGTAG------------------------------ 3720
MAP4K4_204_1279      TAGGCAGGACTTCTCTTCTGAGCTGGTAG------------------------------ 3840
                     ****************************

MAP4K4_202_1320      AGAGTCTTCAAGATCCTGAGAACTTGGAATTCCTTGTAACTGGAGCTC 4116
MAP4K4_001_1239      -------------------------------------------------
MAP4K4_204_1279      -------------------------------------------------
```

Sense	Antisense	shRNAmir code	Position
CAAGTTAGAATCCAGCTTA	TAAGCTGGATTCTAACTTG	V2LHS_202781	Third
GCTTACATCTCCAGAGAAA	TTTCTCTGGAGATGTAAGC	V2LHS_201856	Second
AGATAAATATGCTAAAGAA	TTCTTTAGCATATTTATCT	V2LHS_68219	First
TCACCAAGGATGTAGTTCT	AGAACTACATCCTTGGTGA	V3LHS_375570	Fourth
CAGTGAAGTTTCTCCGTTA	TAACGGAGAAACTTCACTG	V2LHS_173825	N/A

Figure S4: **Sequence alignment of shRNAmirs with the MAP4K4 isoforms.** Sense sequence has been aligned against three isoforms of MAP4K4 (depicted in Fig. S3). The shaded position of each shRNAmir is depicted in the last column. One shRNAmir (173825) was not found to complement MAP4K4, and was later withdrawn from the Open Biosystems shRNAmir database. Transfection of this particular shRNAmir in HEK293T cells did not inhibit MAP4K4 RNA levels. N/A; not available

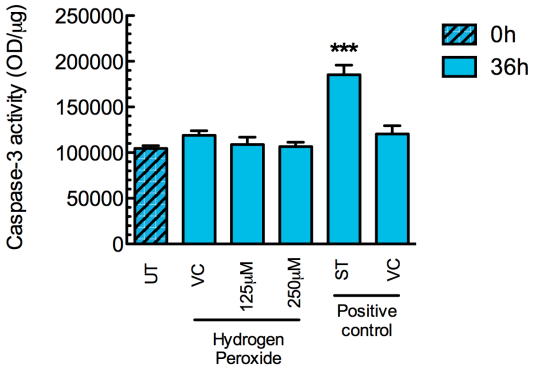


Figure S5: **Caspase-3 activation is not a late event in response to H_2O_2 in hiPSC-CMs.** Caspase-3 activation levels remained unchanged when measured at 2h 4h, 8h, 16h and 24h with H_2O_2. Caspase-3 activation did not occur as a late event at 36h. UT, untreated (N=9 wells); VC, vehicle control; ST, staurosporine; Bars represent ±SE from UT (N=9 wells) and rest (N=3 wells).

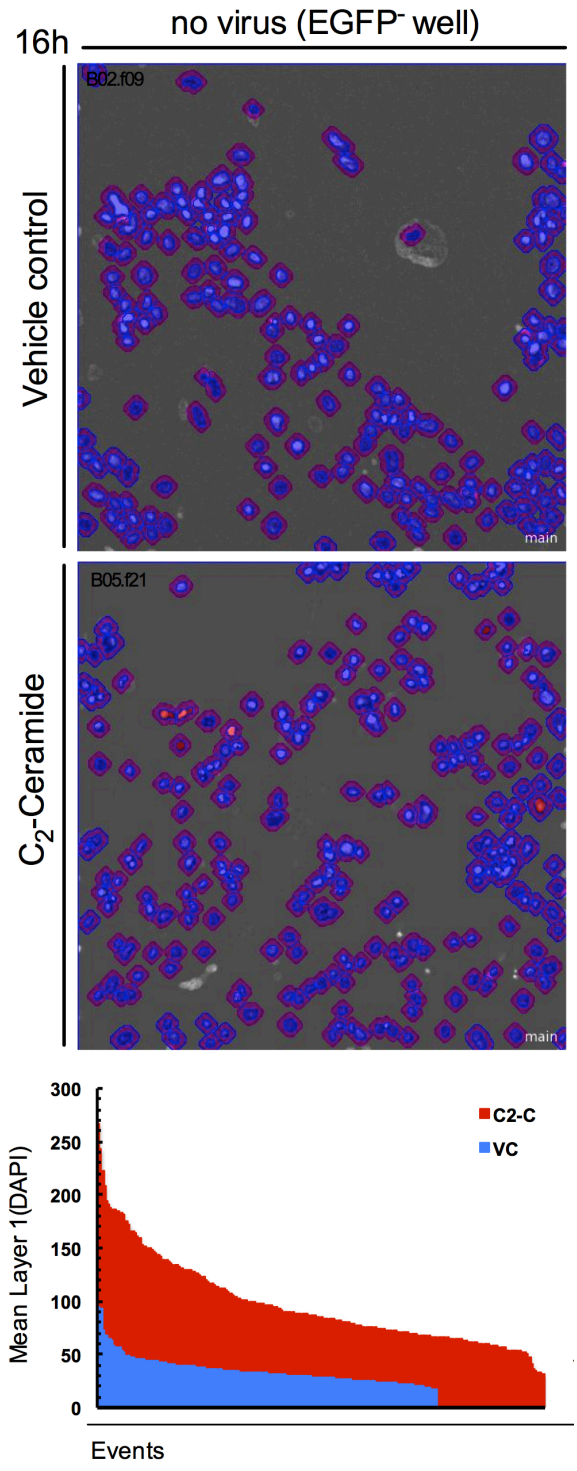


Figure S6: Algorithm for microscopy-based assays detects both apoptotic and healthy nuclei. One representative field from a c_2-ceramide-treated and a VC-treated well are shown. In summary, the algorithm can be broken down into two rounds of automatic nuclei identification based on the mean intensity after background correction, nuclei segmentation/separation, creation of a mask for the identification of RFP^+ cells and a second mask for the identification of successfully transduced hiPSC-CMs with shRNAmirs based on EGFP fluorescence. $DRAQ7^+$ or MP^- cells were extracted from the RFP^+EGFP^+ populations. The intensities between apoptotic and healthy cells are depicted in the histogram, where apoptotic cells with c_2-ceramide (C2-C) or H_2O_2 (not shown) exhibit increased intensity.

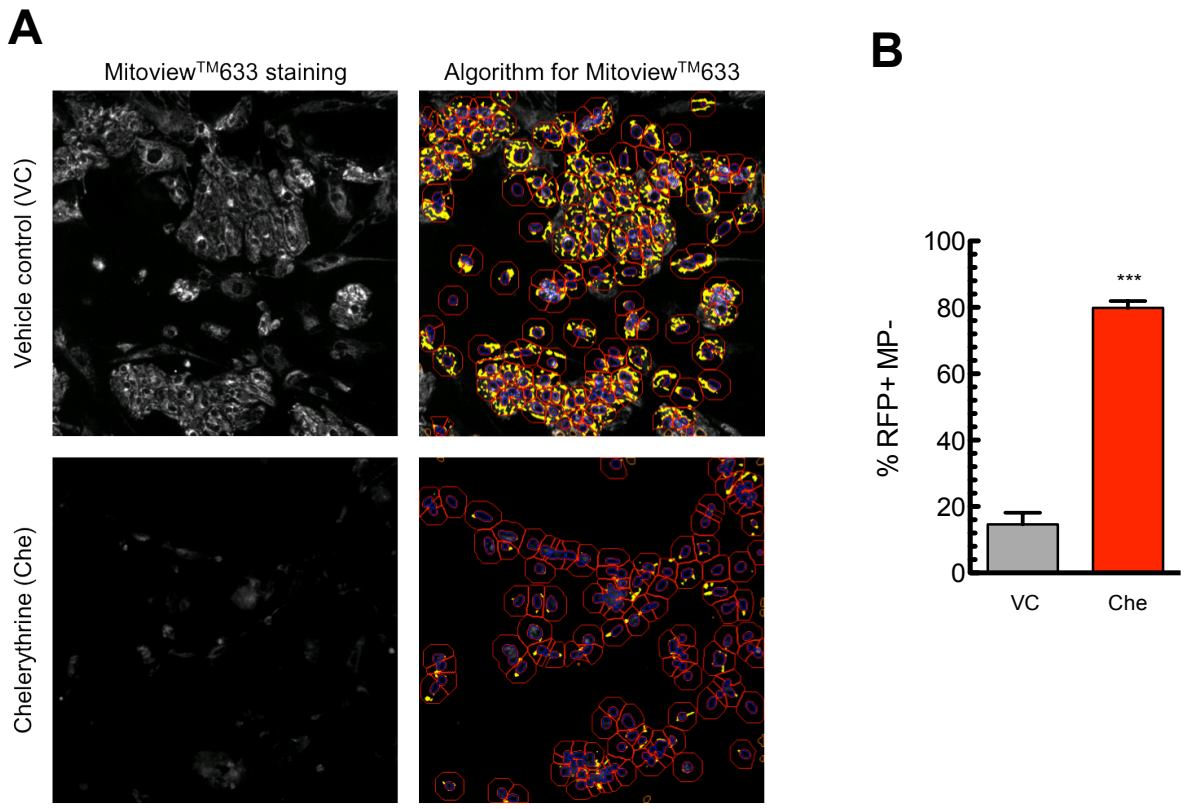


Figure S7: **Representative image for diminished mitochondrial potential in the positive control.** **(A)** The algorithm for loss of mitochondrial potential (MP^- cells) used to measure the decrease in total fluorescence of Mitoview™633 potentiometric dye at the mitochondria with **(B)** the threshold set up from chelerythrine-treated hiPSC-CMs with 10µM for 10-30min. Che, chelerythrine; VC, vehicle control. Statistical significant calculated with two-tailed t-test depicted by *** for $p<0.001$. Representative values from one experiment from N=3 wells.

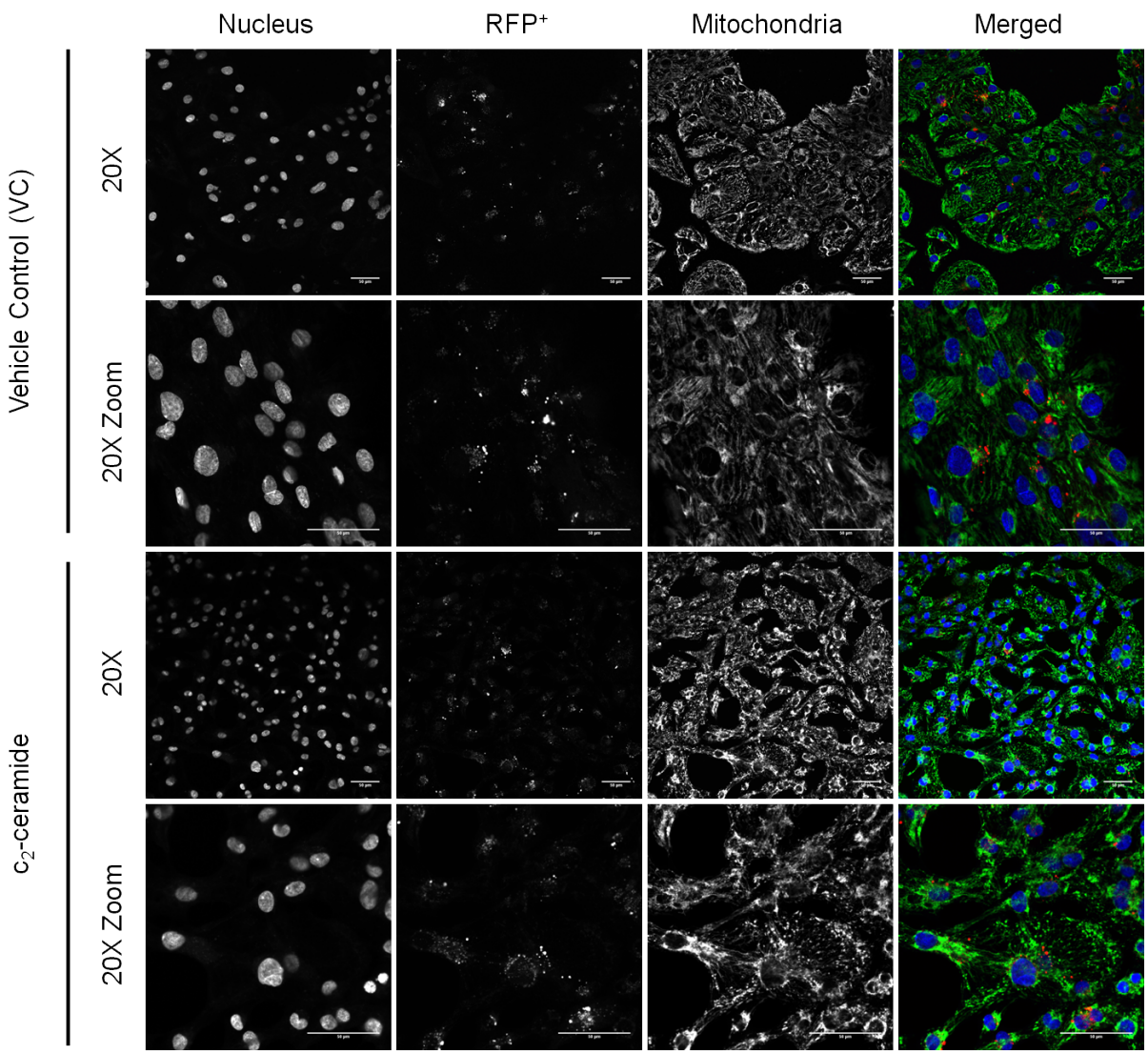


Figure S8: **Mitochondria of hiPSC-CMs exhibit mitochondria fission with c_2-ceramide.** Representative confocal microscopy images of c_2-ceramide-treated hiPSC-CMs with the vehicle control (DMSO) were captured by a 20X objective and further magnified by digital zoom. Cells were treated with 20μM c_2-ceramide for 16h.